Winter 12-15-2019

Activation and Regulation of the ALKBH3-ASCC Alkylation Repair Pathway

Josh Brickner
Washington University in St. Louis

WASHINGTON UNIVERSITY IN ST. LOUIS

Division of Biology and Biomedical Sciences
Molecular Cell Biology

Dissertation Examination Committee:
Nima Mosammaparast, Chair
Susana Gonzalo
Albert Kim
Alessandro Vindigni
Zhongsheng You
Hani Zaher

Activation and Regulation of the ALKBH3-ASCC Alkylation Repair Pathway

by
Joshua Brickner

A dissertation presented to
The Graduate School
of Washington University in
partial fulfillment of the
requirements for the degree
of Doctor of Philosophy

December 2019
St. Louis, Missouri

Table of Contents

List of Figures

Acknowledgments

I would like to thank my thesis advisor, Dr. Nima Mosammaparast, for the invaluable guidance and insight you have provided throughout graduate school. Your interactions with each lab member, your self-reflection and your willingness to always teach and help have provided a great blueprint not only on how to be an excellent scientist but also a great member with a positive environment.

A lab is only as good as its members and I luckily had an amazing lab family. Thank you to everyone who has been a member of the Mosammaparast lab. To Jennifer Soll, thank you for listening to my frustrations and ideas. To Andrea Byrum, thank you for helping me think critically about experiments and for helping out with keeping my cells alive while I would be out of town. And for keeping college rivalries alive. To Zhao Yu, thank you for being patient with me during the early learning process. To Mona Majid, your cloning was second to none. To Miranda Mudge, thank you for taking care of all the mice! To Clement Oyeniran, collaborating with you was enjoyable and an excellent learning experience. To Sheri Bagherzadeh, your kindness and cheery attitude made coming to lab easier. To Ning Tsao, your dedication and hard work are already astounding. To Brittany Townley, thank you for letting me bounce ideas off of you and for all your jokes that keep me sane in lab.

I would like to thank my thesis committee for all of their guidance and insight. To my chair, Dr. Zhongsheng You, your questions and advice always made sure to get the best out of me. To Dr. Hani Zaher, thank you for all of the advice in regard to life outside of science. Thank you to Dr.

Alessandro Vindigni, Dr. Albert Kim and Dr. Susana Gonzalo for all of your insightful comments and genuine interest in these projects.

Thank you to my family for all of your love and support. Thank you for knowing what I need in the moment, even when I do not recognize it. Thank you to all of my friends, old and new, for helping me live life to the fullest, for pushing me to experience many new things and for keeping me sane and grounded throughout this experience.

Joshua Brickner

Washington University in St. Louis

December 2019

Dedicated to my parents, Richard and Wendy

ABSTRACT OF THE DISSERTATION

Activation and Regulation of the ASCC-ALKBH3 Alkylation Repair Pathway

by

Joshua Brickner

Doctor of Philosophy in Biology and Biomedical Sciences

Molecular Cell Biology

Washington University in St. Louis, 2019

Professor Nima Mosammaparast, Chair

DNA repair is essential to prevent the cytotoxic or mutagenic effects of various types of DNA lesions. These lesions are sensed by distinct pathways to recruit repair factors specific to type of damage. In particular, the ALKBH family of proteins recognizes and repairs specific alkylated lesions, including 1-methyladenine (m1A) and 3-methylcytosine (m3C). A major outstanding question in the field is how the AlkB homologue ALKBH3 and its associated protein partners are recruited to sites of alkylation damage and how this repair activity is regulated. Understanding the upstream signaling events that mediate recognition and repair of DNA alkylation damage is particularly important as alkylation chemotherapy is one of the most widely used systemic modalities for cancer treatment and environmental chemicals may trigger DNA alkylation. Here, I demonstrate that human cells have a previously unrecognized signaling mechanism for sensing DNA damage induced by alkylation. The ALKBH3-ASCC alkylation repair complex (consisting of the dealkylase ALKBH3 and the ASCC complex subunits ASCC1, ASCC2, and ASCC3) relocalizes to distinct nuclear foci specifically upon exposure of cells to alkylation agents. These foci associate with alkylated nucleotides and are coincident with elongating RNA Polymerase II and other splicing components. Proper recruitment of the complex requires K63-polyubiquitin

recognition via the CUE (coupling ubiquitination to ER degradation) domain of the subunit ASCC2. The E3 ligase RNF113A is responsible for the upstream ubiquitin signaling necessary to recruit the repair complex. Conversely to ASCC2 and ASCC3, the subunit ASCC1 is present at nuclear speckles prior to alkylation but leaves in response to damage. Upon loss of ASCC1, ASCC3 foci significantly increase upon alkylation damage, suggesting a negative regulatory function for ASCC1. Indeed, ASCC1 appears to coordinate the proper recruitment of the ASCC complex in response to alkylation in a manner dependent on its putative RNA-binding motif. Interestingly, expression of an AlkB homologue from the blueberry scorch RNA virus containing an NLS (nuclear localization signal) fusion was sufficient to significantly reduce HA-ASCC2 foci during alkylation damage. Overexpression of the RNA-specific methyltransferase METTL8, which produces m3C on mRNA, with an NLS fusion was sufficient to induce recruitment of ASCC3 to the nucleus, and primarily the nucleolus, even in the absence of alkylating agents, suggesting that RNA alkylation is both necessary and sufficient to recruit the ALKBH3-ASCC repair complex. Together, these findings significantly contribute to the notion that human cells have specialized DNA repair mechanisms and that these mechanisms can also repair damaged RNA.

Chapter 1: Introduction

Zhao Y, Brickner JR, Majid MC, Mosammaparast N. 2014. *Trends Cell Biol*. 24: 426-434.
Brickner JR, Townley BA, Mosammaparast N. 2019. *DNA Repair (Amst)*. 102663.

1.1 Signaling Cascades in Double Strand Break Repair

Genomic integrity is constantly challenged by exposure to endogenous and exogenous damaging agents that can cause unfaithful DNA replication, which may result in mutagenesis (Fu et al., 2012; Jackson and Bartek, 2009). Many of these damaging agents also generate DNA double-strand breaks (DSBs), which are particularly cytotoxic. As such, cells have evolved multiple pathways that sense the presence of DNA damage, which activate various signaling cascades to recruit repair factors specific for the type of recognized lesion in DNA (Jackson and Durocher, 2013). In particular, the response to DNA double-stranded breaks heavily relies on post-translational modification of histones and non-chromatin proteins (Jackson and Durocher, 2013; Zhao et al., 2014). These repair mechanisms often are restricted to recognizing a specific DNA lesion. Although the signaling cascades that regulate the repair of DSBs are well characterized, whether such a "sensor-transducer-mediator" paradigm exists for specific types of DNA lesions is unknown. Regardless, understanding the various post-translational modifications that regulate DSB repair may provide insight into the upstream regulation of other DNA repair mechanisms.

1.1.1 DSB Recognition and Phosphorylation

The DSB response begins with the recognition of the double-stranded DNA break by the Mre11-Rad50-NBS1 (MRN) complex, which is thought to promote activation of signaling kinases including ATM, ATR, and DNA-PK (Sirbu and Cortez, 2013) (Figure 1.1A). These serine-threonine kinases target hundreds of proteins (Matsuoka et al., 2007) but a key target is a conserved site (serine 139) at the C-terminus of the histone variant H2A.X, which replaces the

canonical H2A in approximately 10% of the genome and is critical for orchestrating the DSB response (Celeste et al., 2002). In particular, the N-terminus of histones and histone variants are subject to post-translational modifications important for DNA repair (Gardner et al., 2011). Phosphorylated H2A.X (also known as pH2A.X) creates a ligand for MDC1, which recognizes pH2A.X via its tandem BRCT (BRCA1 C-terminal homology) domains (Reinhardt and Yaffe, 2013). MDC1 itself contains phosphorylation sites near its N-terminus that are targeted by the ATM/ATR kinases that promotes the recruitment of RNF8 via its FHA domain, which causes a feedback loop that promotes further ATM activation via RNF8 and another DSB response associated E3 ligase, CHFR (Reinhardt and Yaffe, 2013; Wu et al., 2011). Additionally, another substrate of ATM, HERC2, contains a phosphorylation site that interacts with the FHA domain of RNF8 to help assemble the RNF8-UBC13 ubiquitin ligase complex (Bekker-Jensen et al., 2010). It is therefore possible that upstream phosphorylation events regulate both the localization and enzymatic activities of proteins involved in alkylation repair.

1.1.2 Ubiquitination During DSB Repair

Ubiquitin signaling is an important cellular signaling mechanism that has been implicated in pathways ranging from targeting proteins for proteasomal degradation to promoting the DNA damage response (Komander and Rape, 2012). Ubiquitin is a small, 76 amino acid protein. There are eight primary ubiquitin chains that can be formed, dictated by linking the C-terminal of one ubiquitin monomer to either the N-terminus or one of seven lysine residues of another monomer (Komander and Rape, 2012; Pickart, 2001). Each chain acts as a unique cellular signal, though there is some overlap. While both K6- and K27-polyubiquitin chains have been implicated in DNA repair, the primary signal for repair is via K63-polyubiquitin (Wu-Baer et al., 2003; Gatti et al., 2015), while the primary signal for proteasomal degradation is K48-polyubiquitin

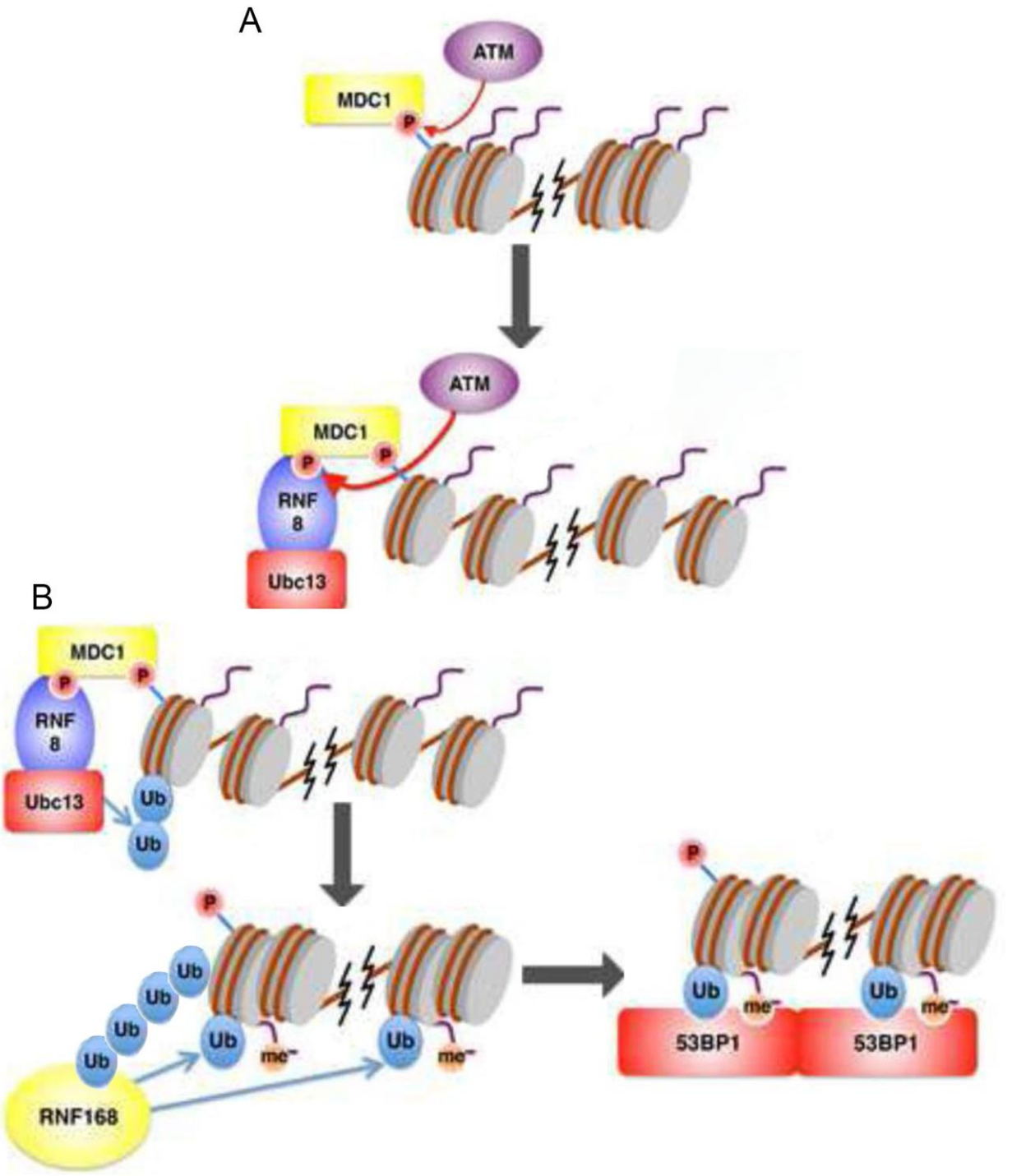

Figure 1.1. Post-Translational Modifications During DSB Repair. (A) Initially, ATM activation helps recruit MDC1 to sites of DNA damage via phosphorylation (top). MDC1 binding results in the recruitment of the RNF8-UBC13 complex. MDC1 and RNF8 coordination further activates the kinase activity of ATM and acts as a positive feedback loop to promote RNF8-mediated ubiquitination (bottom). (B) RNF8 polyubiquityates histone H1 (top), resulting in the recruitment of RNF168. RNF168 subsequently mediates mono-ubiquitination of H2A at lysine 15 near sites of DNA damage (bottom left). This mono-ubiquitination works in concert with H4K20 methylation to recruit 53BP1 via its respective tandem Tudor domains and the adjacent UDR motif (bottom right). Adapted from Zhao et. al., *Trends Cell Biol.* (2014)

(Komander and Rape, 2012). Ubiquitin conjugation occurs during a process involving an E1 activating enzyme, an E2 conjugating enzyme, and an E3 ubiquitin ligase (Schulman and Harper, 2009; Ye and Rape, 2009; Komander and Rape 2012). Substrate selectivity is dictated by the E3 ligase, which interacts with the target protein (Pickart 2001). Interestingly, different E3 ligases ubiquitinate target proteins via different mechanisms. RING E3 ligases promote the direct transfer of a ubiquitin monomer from the E2 conjugating enzyme to the substrate. Conversely, the HECT family of E3 ligases directly receive the ubiquitin monomer before ligation to the substrate (Zheng and Shabek, 2017).

The upstream phosphorylation events during DSB repair result in the recruitment of a variety of E3 ligases. In particular, phosphorylation of MDC1 recruits the E3 ligase RNF8, which ubiquitylates the histone H1 with K63-polyubiquitin chains (Huen et al., 2007; Mailand et al., 2007; Kolas et al., 2007; Thorslund et al., 2015) (Figure 1.1B). This ubiquitination event then recruits another E3 ligase, RNF168, leading to additional ubiquitination of H2A and H2A.X at lysine residues K13 and K15 (Mattiroli et al., 2012; Gatti et al., 2012). Ubiquitination at these sites is essential to recruit the repair factors 53BP1 and BRCA1 to repair these breaks (Doil et al., 2009; Stewart et al., 2009). Additionally, PCNA that becomes arrested at stalled replication forks is either mono-ubiquitinated by RAD6/RAD18, or poly-ubiquitinated by K63-linked chains by SHPRH/HLTF (Watanabe et al., 2004; Motegi et al., 2006; Motegi et al., 2008). These ubiquitin modifications result in the initiation of translesion synthesis or error-free repair, respectively (Ulrich 2009). It stands to reason that, in addition to phosphorylation, upstream ubiquitin signaling may be indispensable for recruiting the proper repair proteins during other forms of DNA damage.

1.2 The Cellular Response to Alkylation Damage

1.2.1 Characteristics of DNA Alkylation Adducts

A major class of DNA damage that threatens genomic integrity is alkylation, defined as the transfer of an alkyl group to any accepting atom on DNA. The repair of alkylated DNA is particularly critical in the context of cancer, since alkylation chemotherapy is used to treat many tumor types. While agents that cause alkylation damage are also abundant in the environment, certain physiological metabolites, such as S-adenosyl-methionine (SAM) are capable of generating alkylated lesions in DNA (Rydberg and Lindahl, 1982; Barrows and Magee, 1982). Indeed, endogenous SAM is proposed to directly methylate DNA at a rate that reflects biologically relevant damage (Eloranta 1977; Rydberg and Lindahl, 1982). To generate an alkylated base, alkylators will react with either the ring nitrogen (N) or oxygen (O) atoms via an S_N1 or S_N2 nucleophilic reaction (Fu et al., 2012; Drablos et al., 2004). Due to its high nucleophilicity, simple methylating agents primarily attack the N-atom at position 7 of guanine to generate the 7-methylguanine (m7G) adduct, which corresponds to ~75% of all observed alkylation lesions (Beranek 1990). While m7G alone is relatively well-tolerated, it can spontaneously depurinate, resulting in an abasic site (Gentil et al., 2992). Other N-lesions caused by alkylation such as 3-methyladenine (m3A), 1-methyladenine (m1A), and 3-methylcytosine (m3C), are relatively less common. However, these lesions can be highly toxic due to their ability to block the DNA polymerase and disrupt canonical Watson-Crick base pairing, resulting in DNA replication fork collapse or mutagenesis, respectively (Larson et al., 1985). Indeed, error-prone translesion polymerases can bypass these lesions (Johnson et al., 2007). Alkyl modification at the O-atom primarily produces O^6-methylguanine, which mismatch during replication, leading to mutagenesis (Warren et al., 2006: De Bont and Van Larebeke, 2004).

Due to the large variety of lesions caused by alkylating agents, even simple methylation adducts require one of three distinct pathways for their reversal. These include direct reversal by either the O^6-methylguanine DNA methyltransferase (MGMT) or the AlkB family of iron dioxygenases, as well as the multi-step base excision repair (BER) pathway (Fu et al., 2012; Soll et al., 2017). Bulkier alkylation lesions capable of helical distortion or the generation of interstrand crosslinks (ICLs) rely upon nucleotide excision repair (NER) and the Fanconi anemia (FA) pathways (Spivak 2015; Kim and D'Andrea, 2012).

1.2.2 Repair by the O^6-methylguanine DNA Methyltransferase

O^6-methylguanine (MGMT) is responsible for the direct demethylation of oxygen-linked lesions, such as O^6meG (Figure 1.2A). Demethylation occurs through the irreversible transfer of the alkyl group to a cysteine residue within the catalytic site of MGMT (Kaina et al., 2007). The alkylated protein has increased potential as a substrate for ubiquitin ligases, facilitating its degradation via the 26S proteasome (Srivenugopal et al., 1996; Xu-Welliver and Pegg, 2002; Hwang et al., 2009). As MGMT protein function is non-enzymatic and restricted to a single demethylation reaction, the repair of these lesions is dependent on the availability of MGMT. Should O^6meG avoid repair by MGMT, DNA polymerase may insert either cytosine or thymine opposite O^6meG, potentially giving rise to G:C to A:T transition mutations (Warren et al., 2006). Interestingly, MGMT expression status can be used as a predictor of how certain tumors will respond to chemotherapy. Tumors that exhibit high levels of MGMT tend to be resistant towards treatment with the alkylation chemotherapeutic temozolomide (TMZ) or other alkylating drugs (Christmann et al., 2011; Gerson 2004). Conversely, methylation of the MGMT promoter in certain tumors, such as gliomas, results in a loss of MGMT expression and better tumor response (Weller et al., 2010; Esteller et al., 2000).

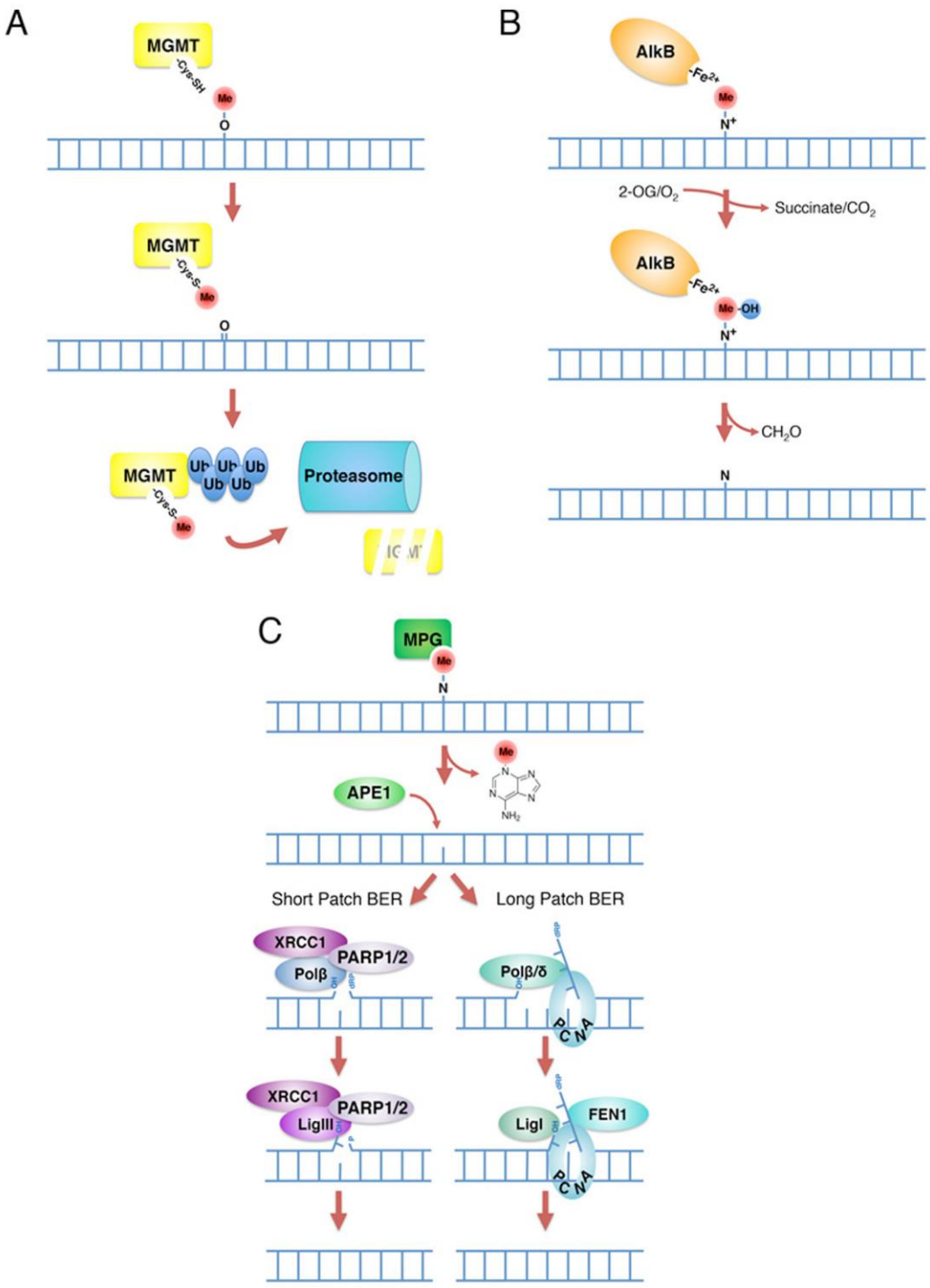

Figure 1.2. Three Distinct Mechanisms for the Repair of Alkylation Lesions. (A) Direct reversal of O-linked lesions by the methylguanine methyltransferase (MGMT). The methyl group is transferred to a catalytic cysteine. MGMT is then ubiquitinated and targeted to the proteasome. (B) AlkB-mediated demethylation of N-linked lesions. Initial oxidation of the methyl moiety leads to its hydrolysis to formaldehyde. (C) Repair of N-linked lesions by base excision repair (BER). Both pathway choices, short-patch BER (left) and long-patch BER (right) are depicted. From Soll et. al., *Trends Biochem Sci.* (2017)

1.2.3 Direct Reversal by the AlkB Family of Iron Dioxygenases

In direct contrast to MGMT, the AlkB family of iron dioxygenases serve as *bona fide* enzymes to repair N-linked alkylation adducts, such as the minor S_N2 products m1A and m3C (Fu et al., 2012) (Figure 1.2B). Mechanistically, these enzymes transfer a hydroxyl moiety to the methylated ring nitrogen of the damaged base (Sedgwick et al., 2007). This reaction consumes 2-oxoglutarate and oxygen in a 1:1 stoichiometric ratio and produces succinate and carbon dioxide as byproducts; iron serves as the catalyst for the reaction (Welford et al., 2005). Indeed, accumulation of the 2-oxoglutarate competitor, D-2-hydroxyglutarate, results in accumulation of alkylation damage, demonstrating the importance of this metabolite (Wang et al., 2015). The hydroxylated intermediate is highly unstable and will hydrolyze spontaneously, reverting the base to its original unmodified state and releasing formaldehyde as a byproduct (Falnes et al., 2002; Trewick et al., 2002). Although toxic to the cell, formaldehyde can be metabolized by cellular dehydrogenases (Sedgwick et al., 2007; Pontel et al., 2015). Alternatively, the formaldehyde-derived damage, such as ICLs, can be repaired via the Fanconi anemia pathway (Niedernhofer et al., 2005; Kee and D'Andrea, 2010).

Although nine human homologues to AlkB have been identified in humans to date, only two members of this family, ALKBH2 and ALKBH3, have definitive activity on m1A and m3C on DNA (Duncan et al., 2002; Aas et al., 2003). The presence of two repair enzymes that recognize the same lesions hints at redundancy; however, ALKBH2 preferentially dealkylates a double-stranded DNA substrate, while ALKBH3 prefers single-stranded DNA or RNA, suggesting specific roles for each repair enzyme (Aas et al., 2003). Thus, this direct reversal of DNA alkylating adducts by the ALKBH proteins prevents m1A and m3C accumulation from blocking replication events (Shrivastav et al., 2010).

1.2.4 The Base Excision Repair (BER) Pathway

While the repair mechanisms described in Chapter 1.2.2 and 1.2.3 are one-step reactions, removal of an alkylated lesion during BER involves a multi-step process that results in either short-patch BER and the removal of a single nucleotide, or long-patch BER and the removal of a small stretch of DNA (Robertson et al., 2009) (Figure 1.2C). Although BER repairs diverse damage adducts, the predominant methylated lesion resolved by this pathway is m3A. Repair for each BER pathway is initiated by recognition of the lesion by a DNA glycosylase, such as alkyladenine glycosylase (AAG) (Wyatt et al., 1999; Svilar et al., 2011). AAG cleaves the glycosidic bond, removing the base and leaving an apurinic (AP) site. The AP site is then recognized by the AP endonuclease (APE1), resulting in excision of the sugar phosphate. During short-patch BER, XRCC1/Polβ fills in the single nucleotide gap and the DNA is ligated by DNA ligase I or III (Fortini and Dogliotti, 2007). Conversely, during long-patch BER, either Polβ or Polδ/ε (in proliferating cells) fill in a several nucleotide gap. Ligation of the DNA is mediated by DNA ligase I and the remaining flap is excised by PCNA/FEN1 (Fortini and Dogliotti, 2007).

The presence of multiple pathways to repair alkylation lesions predicts that there may be some redundancy to ensure proper repair in the event that one pathway becomes defective. Indeed, loss of ALKBH2 in mice (*Alkbh2*$^{-/-}$) resulted in an accumulation of m1A, while *Alkbh3*$^{-/-}$ mice did not result in this phenotype (Ringvoll et al., 2006). While this observation suggests that ALKBH2 is the predominant demethylase for endogenous m1A, double knockout (*Alkbh2*$^{-/-}$ *Alkbh3*$^{-/-}$) mice were more susceptible to alkylation-induced tumor development relative to the single *Alkbh2*$^{-/-}$ mice (Calvo et al., 2012). Thus, both ALKBH2 and ALKBH3 contribute to alkylation resistance, albeit to different degrees. Interestingly, the *Aag*$^{-/-}$ *Alkbh2*$^{-/-}$ *Alkbh3*$^{-/-}$ triple knockout mouse exhibited a severe sensitivity to the inflammatory agents dextran sodium sulfate (DSS), resulting

in an accumulation of 1,N^6-ethanoadenine (εA) and 1,N^2-ethanoguanine (εG) in these mammals (Calvo et al., 2012). This work demonstrates the importance and redundancy of AlkB demethylases and BER proteins in repairing bulkier lesions *in vivo* (Delaney et al., 2005; Fu and Samson et al., 2012; Singer et al., 1992).

1.2.5 Regulation of Alkylation Repair Pathways by Ubiquitin Signaling

While the ubiquitin signaling events that promote double stranded break repair have been well-studied (see Chapter 1.1.2), emerging evidence exists that ubiquitin signaling may regulate alkylation damage repair. Indeed, recent studies have demonstrated that APE1 can be polyubiquitinated at several residues near its N-terminus (Meisenberg et al., 2012; Edmonds and Parsons, 2014). Polyubiquitination of APE1 by the E3 ligase UBR3 results in its proteasomal degradation (Meisenberg et al., 2012). Polβ has also been shown to be ubiquitylated on lysines at position 206 and 244 in the absence of XRCC1 in a CHIP or MULE independent manner and subsequently targeted for proteasomal degradation (Fang et al., 2014). XRCC1 is then available for K48-polyubiquitination by CHIP or protected from proteasomal degradation via direct interaction with HSP90. Thus, BER is directly regulated via ubiquitin-dependent processes.

Similarly, recent work has demonstrated that the demethylases ALKBH2 and ALKBH3 are also regulated via ubiquitin signaling. Both enzymes are modified by K48-polyubiquitin and degraded (Zhao et al., 2015). Interestingly, a deubiquitinase complex positively regulates these dealkylases by reversing the ubiquitination. A key component of this complex is the deubiquitinase OTUD4, whose catalytic activity is dispensable for the stabilization of ALKBH2 and ALKBH3. Rather, OTUD4 serves as a scaffold to promote the association of these proteins with two additional deubiquitinases: USP7 and USP9X (Zhao et al., 2015). Indeed, loss of either USP7 or USP9X destabilizes ALKBH2 and ALKBH3, resulting in hypersensitivity to alkylation

damage, dependent upon the catalytic activity of these proteins (Zhao et al., 2015). Together, these studies reveal that master regulatory mechanisms may exist for enzymes involved in repairing alkylated DNA.

1.3 The ALKBH3-ASCC Complex in Alkylation Repair

1.3.1 The ASCC3 Helicase

Our work previously showed that the repair enzyme ALKBH3 interacts with the heterotrimeric ASCC (Activating Signal Co-integrator Complex), consisting of the subunits ASCC1, ASCC2, and the ASCC3 DNA helicase. This complex was originally isolated through its physical association with ASC-1, a transcriptional coactivator (Jung et al., 2002). This original report suggested that the ASCC complex coordinates with ASC-1 to activate transcription via AP-1, NF-κB and SRF. While the individual role of each subunit remained elusive, our work demonstrated an important role for this complex in repairing alkylated DNA in various tumor cells (Dango et al., 2011). ASCC3 encodes a superfamily II tandem helicase protein that associates directly with the ALKBH3 dealkylase (Dango et al., 2011). While ASCC3 has the most homology with RNA helicases such as the spliceosomal protein BRR2, it has the ability to unwind short strands of DNA in an apparent 3'-5' direction in a manner that depends on its C-terminal ATPase domain (Dango et al., 2011). This helicase activity appears to support ALKBH3 mediated dealkylation of double-stranded DNA, expanding the substrate repertoire of ALKBH3, which strongly prefers single-stranded substrates (Aas et al., 2003). Consistently, loss of ASCC3 significantly sensitizes cells to MMS and results in accumulation of genomic m3C, particularly in cell lines which appear to overexpress this factor (Dango et al., 2011). Of note, ASCC3 and ALKBH3 are associated with each other in a sub-stoichiometric fashion, consistent with ALKBH3-independent functions of the ASCC complex.

1.3.2 ASCC1 and ASCC2

Two outstanding questions in regard to the regulation of ASCC-ALKBH3 complex are the roles of ASCC1 and ASCC2. I hypothesize that ASCC1 and ASCC2 coordinate proper complex formation and recruitment of the ASCC-AKLBH3 repair complex to modulate its activity. I further propose that ASCC1 and ASCC2 act through distinct mechanisms. Therefore, I am investigating the roles of ASCC1 and ASCC2 in regulating the recruitment and function of the ASCC-ALKBH3 complex during alkylation damage. In Chapter 2, I provide evidence that ASCC2, ASCC3 and ALKBH3 localize to nuclear speckle bodies that coincide with the m1A alkylation lesion specifically upon alkylation damage. These sites are subnuclear regions associated with active splicing and processing of RNA PolII transcripts, amongst many other functions (Spector et al., 1991; Spector and Lamond, 2011; Girard et al., 2012; Dias et al., 2010). As such, these foci are co-incident with the spliceosomal factors BRR2, PRP8 and elongating RNA PolII. Proper recruitment of this complex to alkylation-induced foci is dependent upon ubiquitin recognition by the accessory subunit ASCC2, which appears to function as an adaptor to recruit ASCC3 and ALKBH3. Consistent with dependence upon a ubiquitin signaling pathway, we identified the E3 ligase RNF113A as the key factor that produces such chains responsible for recruiting ASCC-ALKBH3 (Figure 1.3). A combination of *in vitro* and *in vivo* ubiquitination experiments demonstrated that the spliceosomal helicase BRR2 is a substrate of RNF113A. In contrast to ASCC2, ASCC1 is present at nuclear speckles prior to damage but leaves these foci in response to alkylation (Chapter 3). Loss of ASCC1 results in a dramatic increase in ASCC3 foci during alkylation damage. Interestingly, while ASCC3 and ASCC2 are primarily present in the same foci during alkylation, ASCC1 loss increases the amount of ASCC2-independent ASCC3 foci. I also demonstrate that both ASCC1 and ASCC2 are critical to promote cellular survival when challenged with alkylating agents.

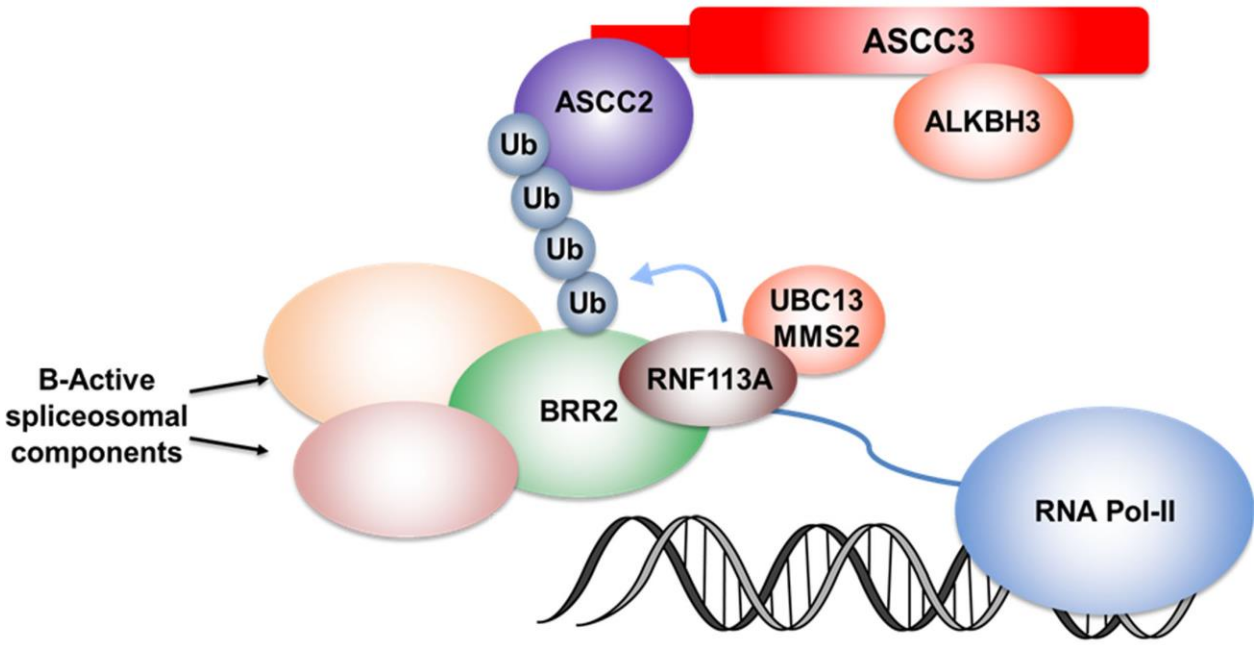

Figure 1.3. Working model for recruitment of the ALKBH3-ASCC complex through RNF113A-mediated ubiquitination. Upon alkylation, RNF113A functions with the E2 ligase UBC13-MMS2 to induce K63-linked ubiquitination chain formation on BRR2 and possibly other components of the B-active form of the spliceosome. This signaling event recruits the ALKBH3-ASCC complex via the CUE ubiquitin binding domain of ASCC2. The nature of the upstream signal to activate the pathway is currently unknown.

Together, these results suggest that ASCC1 and ASCC2 coordinate the recruitment and formation of the ASCC-ALKBH3 complex via distinct mechanisms.

1.4 The Interplay Between Transcription and DNA Damage

1.4.1 DNA Damage Responses and Transcription

A major reason why many types of damage to the genome, including alkylation, result in cytotoxicity is because of disruption to the coding capacity of DNA. Specifically, adducts that disrupt the DNA backbone or canonical Watson-Crick base pairing can affect both RNA and DNA polymerases, hindering not only DNA replication but also transcription. Canonical types of damage that are strong blocks to either process include UV damage, DNA interstrand crosslinks, and bulky alkylated adducts. Smaller adducts, such as aberrantly methylated bases, have significantly less impact on transcription. The majority of the pathways described above in Chapter 1.3, however, repair relatively simple alkylation additions, such as single methyl additions. While some evidence suggests that the AlkB enzymes may resolve bulkier N-linked lesions (Delaney et al., 2005; Li et al., 2013), larger alkylation adducts are thought to induce DNA helical distortion, which in turn activates nucleotide excision repair (NER) (Spivak et al., 2015). Indeed, MGMT-like proteins have been identified which bind to bulky lesions and activate NER, suggesting the presence of crosstalk between NER and direct alkylation reversal pathways (Tubbs et al., 2009; Latypov et al., 2012).

NER is the primary pathway that repairs bulkier adducts, which include UV lesions. Indeed, helical distortion in the DNA backbone is the major signal which activates this pathway (Hess et al., 1997; Zou et al., 2001; Sugasowa, 2001). As with BER, there are two distinct subsets of NER: global genome repair (GGR) and transcription-coupled repair (TC-NER). In global genome repair (GGR), factors such as UvrA in bacteria or XPC/Rad23 in mammals

recognize NER substrates and initiate the recruitment of excisional machinery and downstream endonucleases that cut a single-stranded region surrounding the damage site. The single-stranded gap resulting from removal of the lesion is filled in by DNA polymerases and the end is ligated by DNA ligase. However, the initial lesion recognition factors in GGR are generally limiting and RNA polymerase (RNA PolII) may encounter the lesion in a transcriptionally active gene. This encounter at actively transcribed genes initiates a specific TC-NER. TC-NER was discovered in mammalian cells, where certain silent loci within the genome were found to be relatively resistant to repair (Bohr et al., 1985). Subsequent studies demonstrated that repair of UV-induced cyclobutane dimers in CHO cells in a transcriptionally active locus is more efficient than an adjacent silent locus (Mellon et al., 1987). In fact, the transcribed strand of DNA was shown to be preferentially repaired, strongly implying a role for RNA polymerase in the early recognition events (Mellon et al., 2987).

Once an RNA polymerase molecule encounters a stalling lesion, several additional factors are recruited to promote early events unique to TC-NER, and couple it to the downstream removal of the lesion. Many of the factors involved in this pathway were initially characterized by their association with three distinct inherited syndromes, namely xeroderma pigmentosum, Cockayne syndrome, UV-sensitive syndrome, and trichothiodystrophy (XP, CS, UVSS, and TTD, respectively). Importantly, many of the severe neurological and developmental phenotypes associated with Cockayne syndrome have since been linked to general transcriptional defects that function independently of TC-NER (Apostolou et al., 2019). Accordingly, a similar phenomenon occurs in TTD, in which non-photosensitive TC-NER proficient cases feature similar phenotypes as cases with photosensitivity and TC-NER deficiency (Stefanini et al., 2010).

While to date many of the specific molecular events are not fully elucidated, a stalled RNA polymerase requires remodeling of the region to permit access to the damage site for its repair. In bacteria, the major factor that performs this function is Mfd, whose functional homologue in yeast and mammals appears to be the Rad26 and CSB proteins, respectively (Guzder et al., 1996; Selby and Sancar, 1994; Friedberg 1996). CSB is stabilized at the lesion by UVSSA-USP7, which CSB forms a complex with CSA that is thought to trigger recruitment of chromatin-remodeling factors, including the histone acetyltransferase p300 and HMGN1 (Zhang et al., 2012; Fei and Chen 2012; Fousteri et al., 2006). Subsequent to recruitment of the basal transcription factor TFIIH, the GGR and TC-NER pathways converge (Li et al., 2015). Upon recruitment of TFIIH, the helicase subunits XPD and XPB unwind the damaged DNA and replication protein A (RPA) binds to and stabilizes the undamaged strand. XPA binds the damaged site as part of a lesion verification step and RPA then directs nucleolytic cleavage of the region surrounding the lesion via ERCC1-XPF and XPG (Overmeer et al., 2011; Fagbemi et al., 2011). Upon removal of the damaged region, PCNA loading allows gap-filling DNA synthesis by one of several polymerases and subsequent DNA ligation. Notably, virtually all of these studies on TC-NER have focused on types of damage that are strong blocks to the polymerase, such as UV-induced lesions. Therefore, what happens with smaller lesions that may slow down the polymerase or otherwise negatively affect the nascent transcript is relatively unexplored.

1.4.2 Alkylated Lesions and Effects on Transcription

As stated previously, smaller adducts including methylated bases are more limited in their capacity to block transcription when they occur in DNA. Indeed, the most highly abundant adduct created when cells are treated with genotoxic methylating agents is the largely

innocuous m7G (Rinne 2005). Although prone to spontaneous depurination, m7G does not block either DNA or RNA polymerases. On the other hand, while m3A can block replicative DNA polymerases, this lesion does not significantly affect human RNA PolII elongation (Malvezzi et al., 2017). Indeed, larger 3-alkyladenine lesions are needed to block RNA PolII, and their degree of transcription inhibition appears to correlate with the size of the adduct (Malvezzi et al., 2017). m7G and m3A comprise ~90-95% of the lesions that are created using methylating agents such as MMS, consistent with the notion that global transcriptional shutdown does not occur upon treatment of human cells with this agent.

Thus, it would seem that alkylating agents, or at least simple methylating agents that do not induce bulky lesions, may not require TC-NER. However, certain alkylated lesions such as 3-methylthymine serve as strong transcriptional blocks (Xu et al., 2017). Although these N-linked lesions are thought to be exquisitely rare, they may be more pronounced in open regions of chromatin or actively transcribed regions because single-stranded DNA lacks the protection from normal base pairing. Genome-wide location analysis for these lesions will be necessary to determine their potential to impact transcription. Nevertheless, it is interesting to note that ChIP-Seq analysis of ALKBH3, one of the human AlkB homologues that has the capacity to demethylate m1A and m3C, demonstrated a strong preference for highly active genes, suggesting that the cell is poised to repair such lesions even under undamaged conditions (Liefke et al., 2015).

1.4.3 ASCC3 and Transcription

While it is unclear whether N-linked lesions that block base pairing specifically activate TC-NER, new evidence suggests that at least some of the factors that are associated with TC-NER also play a role in the cellular response to alkylation. Such potential crosstalk between repair

factors assembled in response to UV and alkylation damage has been suggested in genome-wide studies in both yeast and mammalian cells (Mathew et al., 2017; Williamson et al., 2017). A multi-omic approach to identify new factors involved in TC-NER uncovered an important role for the ASCC complex (Boeing et al., 2016). ASCC3, the largest subunit of the complex, was one of the highest scoring factors in the multi-omics TC-NER screen, becoming highly phosphorylated and ubiquitinated during UV-irradiation, and interacting with RNA PolII and CSB (Boeing et al., 2016). Interestingly, loss of ASCC3 or its interacting partner ASCC2, led to a global increase in transcription upon UV-irradiation, suggesting that ASCC may act as a suppressor of global transcription during damage (Williamson et al., 2017). Interestingly, the *ASCC3* gene encodes a short non-coding RNA which negatively regulates ASCC. Selective loss of this short isoform impedes transcriptional recovery after UV damage and increases UV-damage hypersensitivity, reminiscent of functional phenotypes associated with Cockayne syndrome (Karikkineth et al., 2017). While the mechanism of how the ASCC3 protein mediates transcriptional repression or recovery after damage is not clear, the association of ASCC3 with RNA PolII and CSB suggests a remodeling function of the polymerase holoenzyme during damage that may impinge upon proper elongation. It is tempting to speculate that the targeting of the ASCC complex may remove RNA PolII or other components of the basal transcriptional machinery during damage, as other helicases of the same family, such as DNA polymerase theta (polΘ), have the capacity to displace proteins associated with single-stranded DNA (Mateos-Gomez et al., 2017).

1.4.4 RNA Alkylation and the ASCC-ALKBH3 Repair Pathway

The same endogenous and exogenous sources of alkylation damage on DNA are also capable of alkylating RNA, which are hypothesized to disrupt RNA processing, splicing and translation

(Wurtmann and Wolin, 2009; Thapar et al., 2018). Interestingly, two modifications repaired by ALKBH2 and ALKBH3, m1A and m3C, are also products of RNA methyltransferases (Xu et al., 2017; Xiong et al., 2018). Indeed, as cells contain four to six more times the amount of RNA as compared to DNA, RNA may be more readily available for modification by alkylating agents and these modifications may also play a role in cancer progression (Feyzi et al., 2007).

In addition to reversal of DNA modifications, the AlkB family of proteins, in particular ALKBH3, have also been shown to remove modifications on RNA (Aas et al., 2003; Alemu et al., 2016). ALKBH3 exhibits equally strong preference for single-stranded RNA (ssRNA) as it does single-stranded DNA (ssDNA) (Aas et al., 2003). These observations, coupled with the data presented in Chapter 2, suggest that the ASCC-ALKBH3 repair complex may also respond to RNA alkylation. Interestingly, emerging evidence supports the notion that RNA can drive DNA damage repair (Xiang et al., 2017; Mazina et al., 2017). Thus, I propose that further upstream recruitment of the ASCC-ALKBH3 repair may be dependent upon RNA alkylation. In Chapter 4, I demonstrate that overexpression of the RNA-specific demethylase reduces ASCC3 foci during alkylation damage. This data suggests that RNA alkylation is necessary for the proper recruitment of the ASCC-ALKBH3 complex. Additionally, overexpression of an RNA methyltransferase that produces a m3C lesion, METTL8, is sufficient to induce the nucleolar localization of ASCC3. RNA-Seq experiments revealed that MMS treatment results in general transcriptional repression. Intriguingly, loss of ASCC3 led to de-repression of nearly all of these transcripts during alkylation damage, suggesting that ASCC3 serves as a negative regulator of transcription during alkylation. Additionally, I demonstrate that RNF113A autoubiquitination is not only specifically induced by alkylation damage but also by METTL8 overexpression, suggesting that upstream RNA alkylation triggers RNF113A E3 ligase activity. Taken together,

this data demonstrates that RNA alkylation is both necessary and sufficient to recruit the ASCC-ALKBH3 repair complex. These findings provide further evidence for a potential role for RNA in signaling.

Chapter 2: A Ubiquitin-Dependent Signaling Axis Specific for ALKBH-Mediated DNA Dealkylation Repair

Brickner JR, Soll JM, Lombardi PM, Vagbo CB, Mudge MC, Oyeniran C, Rabe R, Jackson J, Sullender ME, Blazosky E, Byrum AK, Zhao Y, Corbett MA, Gecz J, Field M, Vindigni A, Slupphaug G, Wolberger C, Mosammaparast N. 2017. Nature 551:389-393.

2.1 Abstract

DNA repair is essential to prevent the cytotoxic or mutagenic effects of various types of DNA lesions, which are sensed by distinct pathways to recruit repair factors specific to the damage type. Although biochemical mechanisms for repairing several forms of genomic insults are well understood, the upstream signaling pathways that trigger repair are established for only certain types of damage, such as double-stranded breaks and interstrand crosslinks (Jackson and Durocher, 2013; Sirbu and Cortez, 2013; Zhao et. al, 2014). Understanding the upstream signaling events that mediate recognition and repair of DNA alkylation damage is particularly important, since alkylation chemotherapy is one of the most widely used systemic modalities for cancer treatment and because environmental chemicals may trigger DNA alkylation (Drablos et al., 2004; Fu et al., 2012; Sedgwick et al., 2007). Here, we demonstrate that human cells have a previously unrecognized signaling mechanism for sensing damage induced by alkylation. We find that the ASCC alkylation repair complex (Dango et al., 2011) relocalizes to distinct nuclear foci specifically upon exposure of cells to alkylating agents. These foci associate with alkylated nucleotides and coincide spatially with elongating RNA polymerase II and splicing components. Proper recruitment of the repair complex requires recognition of K63-linked polyubiquitin by the CUE domain of ASCC2. Loss of this subunit impedes alkylation adduct repair kinetics and increases sensitivity to alkylating agents, but not other forms of DNA damage. We identify

RNF113A as the E3 ligase responsible for upstream ubiquitin signaling in the ASCC pathway. Cells from patients with X-linked trichothiodystrophy (TTD), which harbor a mutation in RNF113A, are defective in ASCC foci formation and are hypersensitive to alkylating agents. Together, our work reveals a heretofore unrecognized ubiquitin-dependent pathway induced specifically to repair alkylation damage, shedding light on the molecular mechanism of X-linked TTD.

2.2 Introduction

A crucial first step in DNA repair involves the recognition of the damage. After recognition, signaling pathways are activated that will recruit effectors and resolve the lesion. However, whether this "sensor-transducer-mediator" paradigm is generally applicable to pathways dedicated to repairing each distinct type of DNA lesion, such as alkylated lesions, remains unknown. Understanding the signaling events that mediate recognition and repair of DNA alkylation damage is of critical importance as alkylation chemotherapy is one of the most widely used systemic modalities for cancer treatment and because environmental chemicals may trigger DNA alkylation (Drablos et al., 2004; Fu et al., 2012).

In humans, the alkylation lesions 1-methyladenine (m1A) and 3-methylcytosine (3mC) are repaired by the dealkylases ALKBH2 and ALKBH3 (Fu et al., 2012). While ALKBH2 had been thought to be the primary enzyme responsible for reversing m1A and m3C, growing evidence suggests an important pathological role for ALKBH3. ALKBH3 is overexpressed in prostate and non-small-cell lung cancer (Konishi et al., 2005; Tasaki et al., 2011). Subsequent loss of ALKBH3 in these cell lines results in decreased cell proliferation and increased levels of m3C in genomic DNA (Dango et al., 2011), indicating a critical role for ALKBH3 in maintaining genomic stability.

One of the major outstanding questions regarding repair by ALKBH3 and the ALKBH family of proteins is the mechanism by which these repair enzymes are recruited to sites of alkylation. Previous studies have demonstrated that ALKBH3 interacts with the ASCC complex, which is comprised of the subunits ASCC1, ASCC2, and the helicase ASCC3 (Dango et al., 2011). The current model for alkylation repair by ALKBH3 suggests that ASCC3 promotes ALKBH3 repair activity by generating the preferred single-stranded substrate of ALKBH3 (Chen et al., 2010; Monsen et al., 2010). Here, we investigate the function of the uncharacterized subunit ASCC2 in promoting alkylation repair. We find that proper recruitment of the ALKBH3-ASCC repair complex to sites of alkylation lesions is dependent upon recognition of K63-polyubiquitin by the CUE domain of ASCC2. This recruitment is further promoted by the ubiquitination of BRR2 by the E3 ubiquitin ligase RNF113A. Together, our work reveals a ubiquitin-dependent pathway induced specifically to repair alkylation adducts via ALKBH3.

2.3 Results

2.3.1 The ASCC Complex Forms Nuclear Foci During Alkylation Damage

Previous studies established that the dealkylating enzyme ALKBH3 functions in concert with the ASCC helicase complex (Dango et al., 2011). We tested the subcellular localization of ASCC3 upon exposure to various DNA damaging agents. Endogenous ASCC3 formed nuclear foci upon treatment of U2OS cells with the alkylating agent methyl methanesulphonate (MMS). Strikingly, other types of DNA damaging agents did not significantly induce ASCC3 foci (Figure 2.1A-B). These genotoxins all induced pH2A.X foci, indicating that DNA damage was occurring in these cells. Knockout of ASCC3 abrogated these foci (Figure 2.1C), demonstrating that the antibody

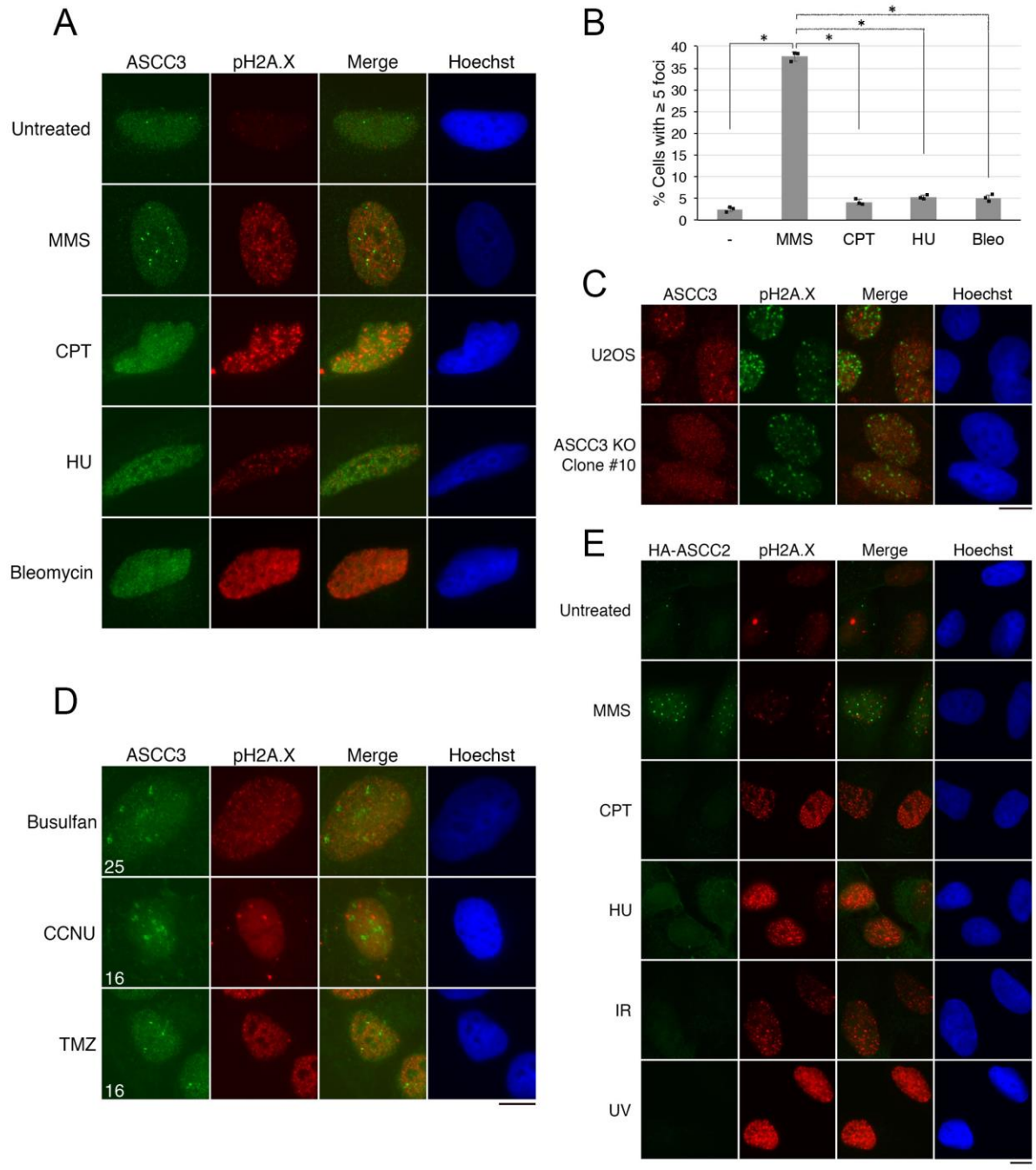

Figure 2.1. The ASCC Complex Forms Foci upon Alkylation Damage. (A) Images of ASCC3 and pH2A.X immunofluorescence after treatment with damaging agents. CPT, camptothecin; HU, hydroxyurea. (B) ASCC3 foci quantitation from (A). (n=3 biological replicates; mean ± S.D.; two-tailed *t*-test, * = $p < 0.001$). Bleo, bleomycin. (C) Images of U2OS parental cells or ASCC3-KO cells after MMS (n=3 biological replicates).. (D) Images of U2OS cells after treatment with the alkylating agents busulfan (4 mM), 1-(2-chloroethyl)-3-cyclohexyl-1-nitrosourea (CCNU; 100 μM), or temozolomide (TMZ; 1.0 mM) (n=2 biological replicates). Numbers indicate the mean percent of cells expressing five or more foci. (E) Immunofluorescence of HA-ASCC2 expressing cells after exposure to the indicated damaging agents (n=3 biological replicates). Scale bars, 10 μm.

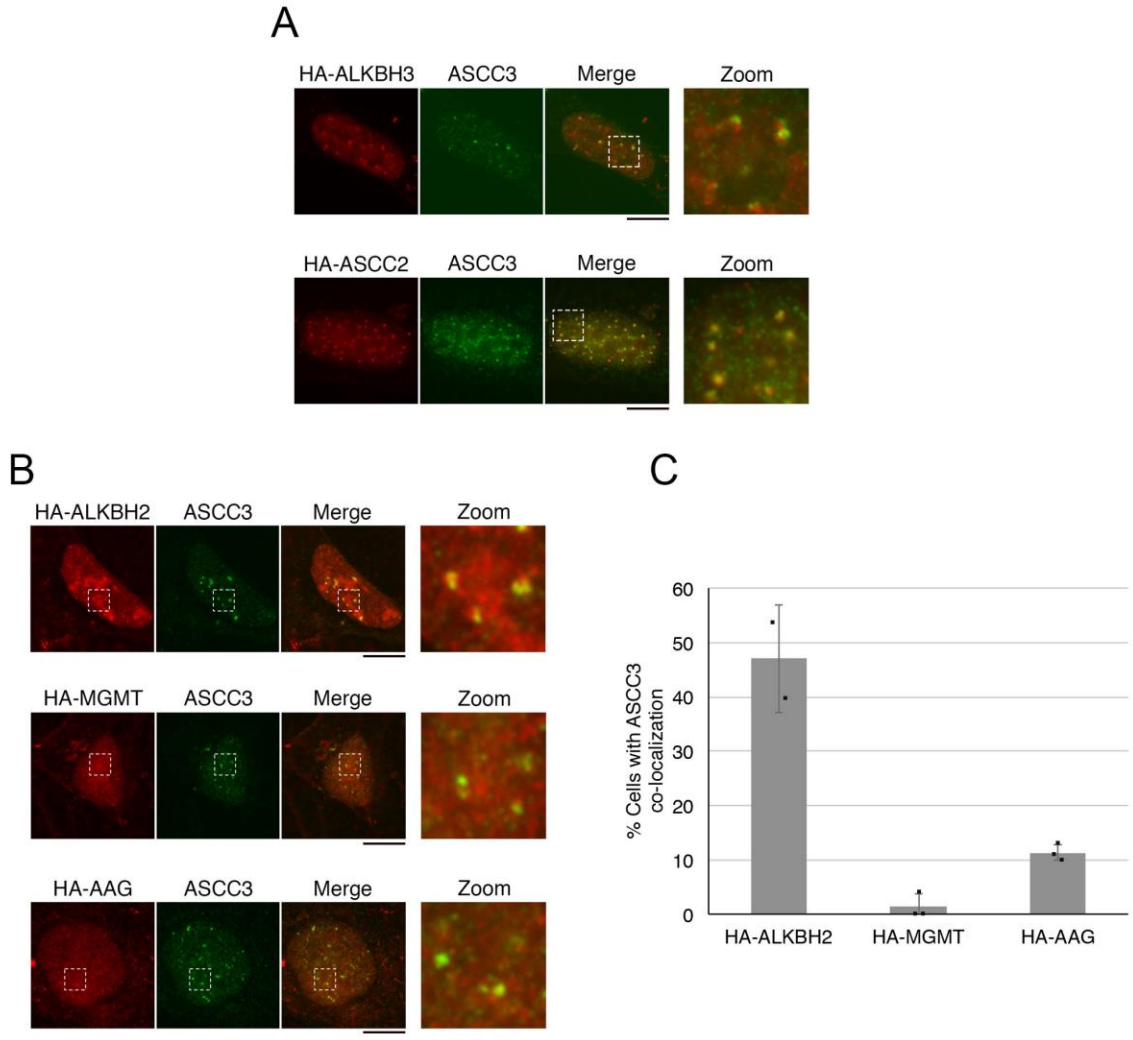

Figure 2.2. Co-localization of the ASCC Complex with Other Alkylation Repair Factors. (A) Images of cells expressing HA-ASCC2 or HA-ALKBH3 after MMS treatment (n=2 independent experiments). (B) Immunofluorescence of cells expressing HA-ALKBH2, HA-MGMT, or HA-AAG upon MMS treatment. (C) Quantitation of ASCC3 co-localization from (B) (n=3 biological replicates; mean ± S.D.). Scale bars, 10 μm.

used was specific for ASCC3. ASCC3 foci were also observed upon treatment with the alkylating agents busulfan, CCNU, and temozolomide (TMZ), all of which are used clinically in the treatment of various tumors (Figure 2.1D) (Wick and Platten, 2014). The ASCC complex subunit ASCC2 also formed foci specifically after treatment with MMS (Figure 2.1E). Consistent with their known physical association (Dango et al., 2011; Jung et al., 2002), endogenous ASCC3 co-localized with both HA-ASCC2 and the dealkylase ALKBH3 upon MMS treatment (Figure 2.2A). Interestingly, ALKBH2 also formed foci that partially co-localized with ASCC3 (Figure 2.2B-C). Conversely, two other alkylation repair factors, methylguanine methyltransferase (MGMT) and the base excision repair (BER) enzyme alkyladenine glycosylase (AAG), showed minimal co-localization with ASCC3 (Figure 2.2B-C). Taken together, this data suggests that the ASCC complex specifically forms nuclear foci in response to alkylation damage that are distinct from other alkylation repair factors.

2.3.2 The ASCC Complex Co-localizes with the Spliceosome

To provide more insight into the upstream signaling that initiates recruitment of the ASCC complex during alkylation, we asked what other DNA damage response proteins may be associated with ASCC. Surprisingly, ASCC foci did not co-localize with pH2A.X or 53BP1, demonstrating that they are distinct from double-stranded break (DSB)-induced foci (Figure 2.3A). These foci were also distinct from GFP-PCNA or BMI-1 (Figure 2.3B), indicating that these foci are not associated with replications forks or the Polycomb repressor complex (Moldovan et al., 2007; Sauvageau and Sauvageau, 2010). Indeed, HA-ASCC2 foci were largely limited to G1/early S-phase of the cell cycle (Figure 2.3C).

We thus took an unbiased proteomic approach to identify the factors associated with ASCC foci in response to alkylation damage by purifying Flag-HA-ASCC2 from HeLa-S cells using tandem

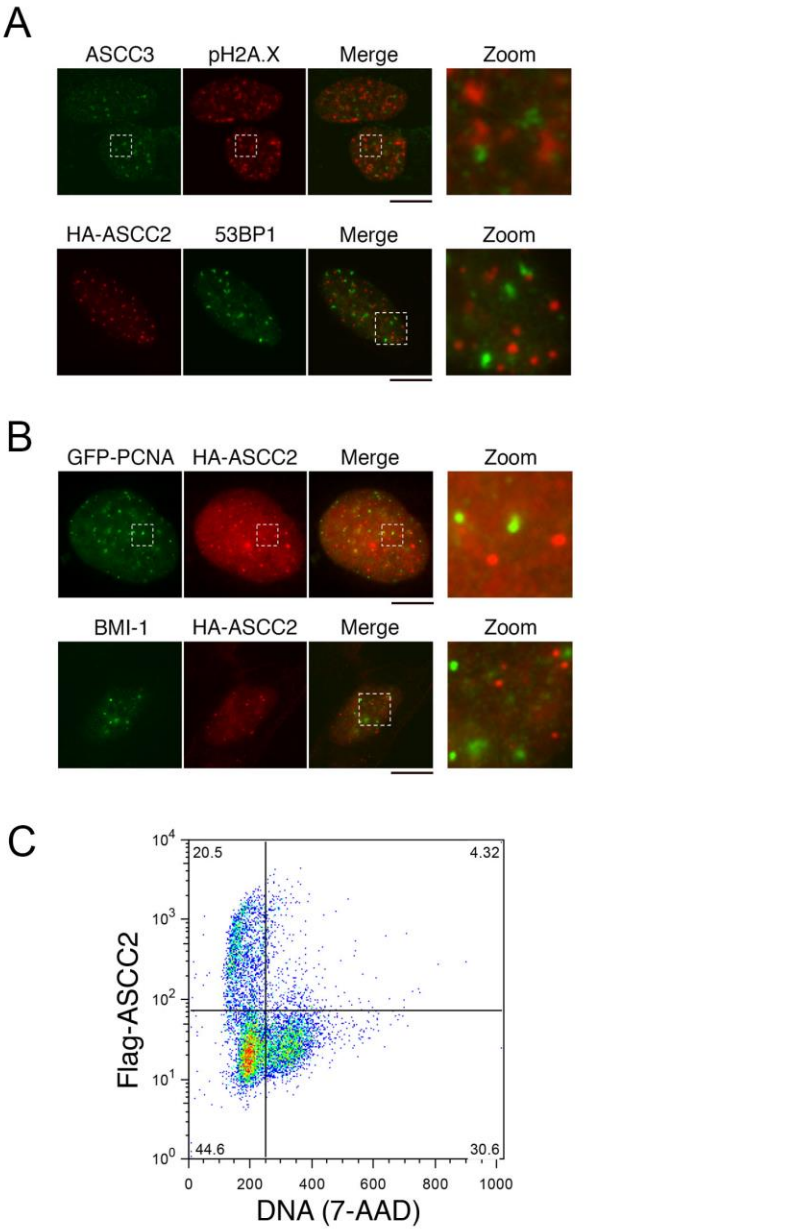

Figure 2.3. The ASCC Complex Does Not Co-localize with Canonical DDR Proteins. (A) Images of either ASCC3 and pH2A.X or HA-ASCC2 and 53BP1 immunofluorescence from U2OS cells after MMS treatment (n=3 biological replicates). (B) Images of U2OS or U2OS cells expressing the indicated vectors after MMS treatment (n=3 biological replicates). (C) Flow cytometry analysis of Flag-ASCC2 expressing cells after MMS treatment and Triton X-100 extraction. Numbers indicate the percent of total cells in each quadrant (n=2 independent experiments). Scale bars, 10 μm.

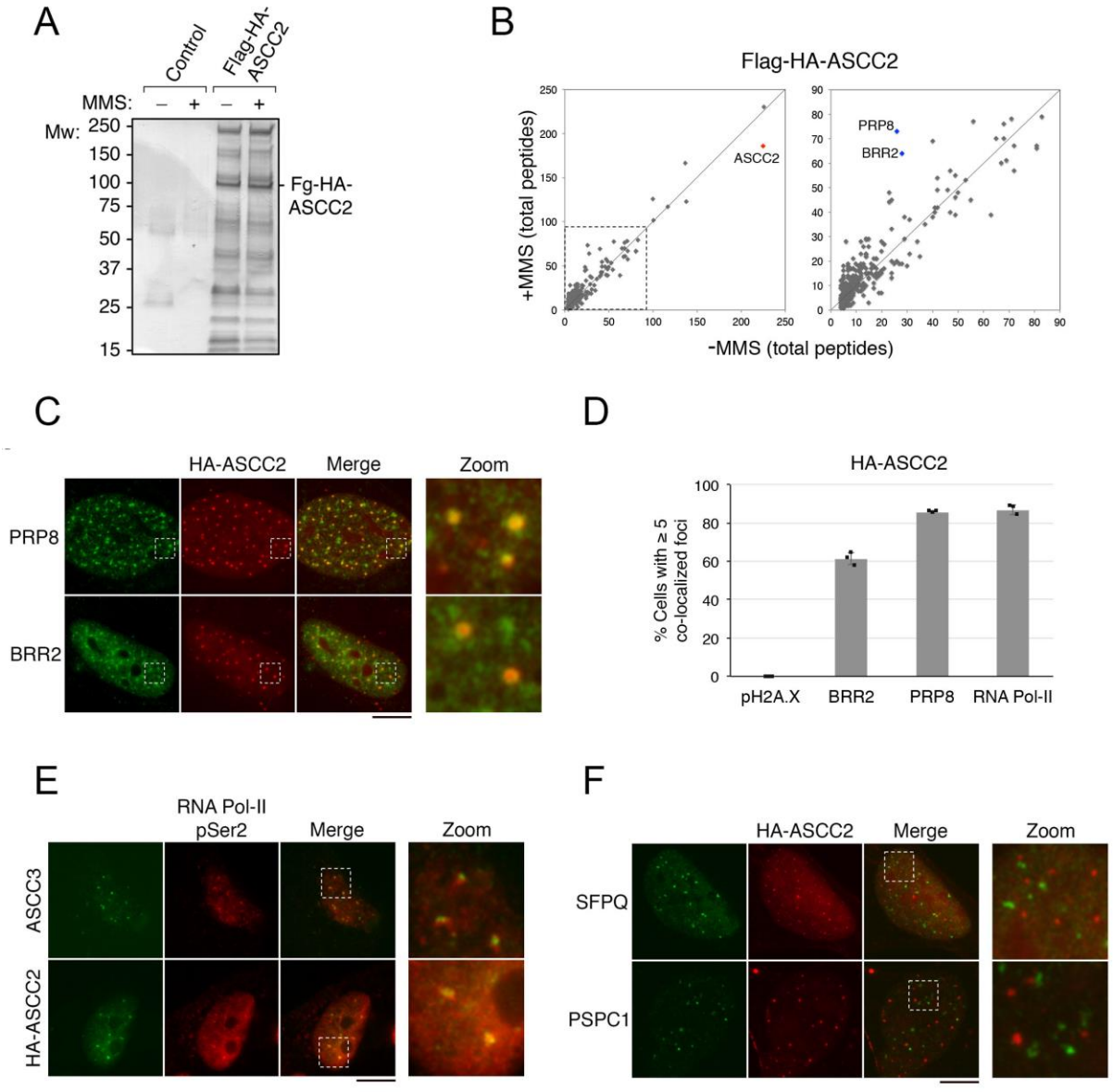

Figure 2.4. The ASCC Complex Co-localizes with the Spliceosome. (A) Silver staining of the Flag-HA-ASCC2 complex purified from HeLa-S nuclear extract separated on 4%-12% SDS-PAGE gel (n=1 independent experiment). (B) Tagged ASCC2 was purified with or without MMS and analyzed by mass spectrometry. Peptide numbers for identified proteins were plotted for each condition. Expanded view is shown on the right (n=1 independent experiment). (C) Immunofluorescence of HA-ASCC2 expressing cell treated with MMS. (D) Quantitation of MMS-induced co-localizations of HA-ASCC2 foci (n=3 biological replicates; mean ± S.D.). (E) and (F) Immunofluorescence analysis of U2OS or HA-ASCC2 expressing U2OS cells upon exposure to MMS (n=3 biological replicates). Scale bars, 10 μm.

affinity purification (Figure 2.4A) (Biancalana et al., 2004) with or without exposure to MMS. Mass spectrometric analysis of ASCC2-associated proteins revealed a constitutive association of ASCC3 and ASCC1 with ASCC2. ASCC2 also associated with many spliceosome components and basal transcription factors (Figure 2.4B). These factors, including BRR2, PRP8, and TFII-I had 2-3 fold higher total peptide numbers from cells exposed to MMS, suggesting an increased association with the ASCC complex in response to alkylation-induced damage. Focused immunofluorescence studies revealed that ASCC components co-localized with BRR2 and PRP8 upon alkylation damage (Figure 2.4C-D), confirming the results of the mass spectrometry. Furthermore, ASCC foci co-localized with elongating (Ser2 phosphorylated) RNA polymerase II, but not other transcription-associated nuclear bodies, such as paraspeckles (Figure 2.4E-F).

Due to the association of the ASCC factors with several spliceosomal factors, we next assessed the importance of proper transcription and splicing on the ability of the complex to form foci during alkylation damage. Chemical inhibition of transcription or splicing during alkylation damage significantly reduced ASCC3 foci (Figure 2.5A-B). To further assess the dependence of RNA on complex recruitment, we pre-treated samples with RNase before processing for immunofluorescence. Consistently, RNase treatment nearly completely abrogated ASCC3 foci formation (Figure 2.5C). Similarly, recombinant ASCC3 containing an N-terminal deletion (NΔ-ASCC3; residues 401-2202) bound to ssRNA *in vitro* (Figure 2.5D). Taken together, this data suggests that, while distinct from other canonical DNA repair proteins, the ASCC complex is recruited to sites of active transcription and splicing during alkylation damage. Indeed, this data is consistent with previous ChIP-Seq results finding that ALKBH3 is enriched at highly active promoters (Liefke et al., 2015).

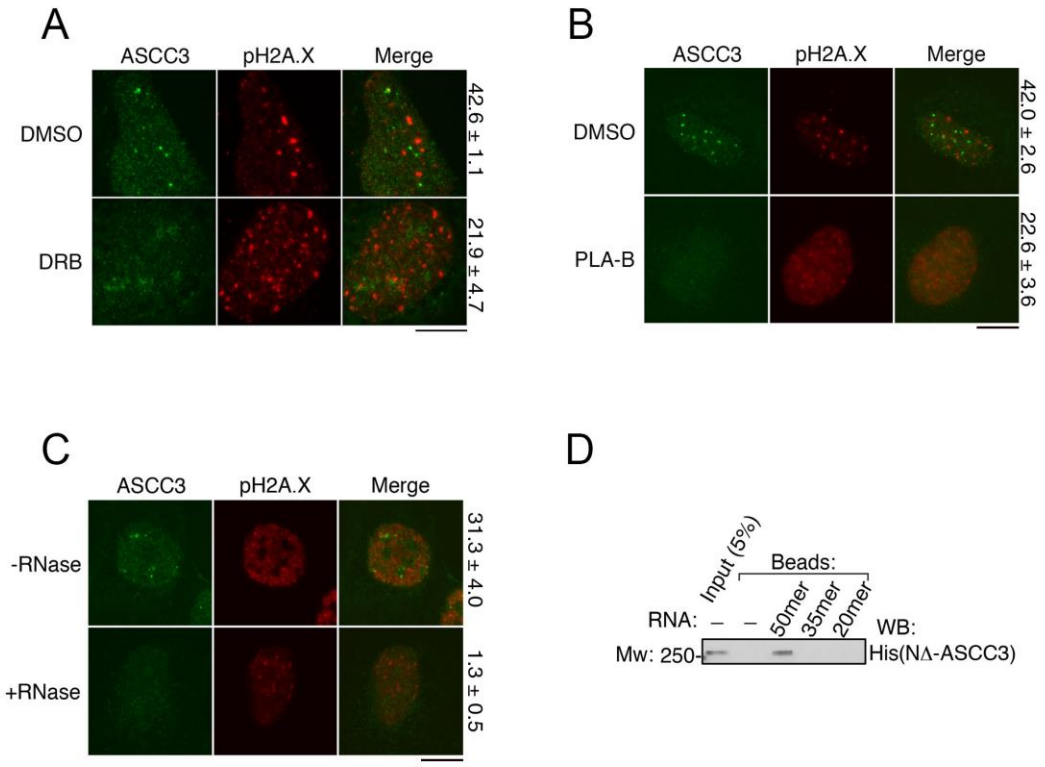

Figure 2.5. ASCC Foci Require Proper RNA Processing. Immunofluorescence images of U2OS cells treated with MMS in the presence of the RNA Pol II inhibitor DRB (A) (100 μM; n=3 biological replicates; mean ± S.D.) or the spliceosomal inhibitor PLA-B (B) (100 nM; n=3 biological replicates; mean ± S.D.). Numbers indicate the percent of cells expressing five or more ASCC3 foci. (C) U2OS cells were treated with MMS and processed for immunofluorescence with or without initial incubation with RNase A (50 nM). Numbers indicate the percent of cells expressing five or more ASCC3 foci (n=3 biological replicates; mean ± S.D.). (D) Biotinylated RNAs (20mer, 35mer, or 50mer) were immobilized and tested for binding to recombinant His-NΔ-ASCC3 (n=2 independent experiments). Scale bars, 10 μm.

2.3.3 ASCC2 Binds to K63-polyubiquitin via its CUE Domain

While recruitment of certain DNA repair complexes is dependent upon specific upstream signaling kinases (Jackson and Durocher, 2013; Sirbu and Cortez, 2013; Zhao et. al, 2014), ASCC recruitment to sites of alkylation damage seems to be independent of upstream phosphorylation events. Inhibition of ATM (ataxia-telangiectasia mutated) moderately increased ASCC3 foci formation, while ATR (ataxia-telangiectasia and Rad3 related) inhibition had no significant impact on foci formation (Figure 2.6A). We found that HA-ASCC2 foci co-localized with polyubiquitin as visualized using the FK2 antibody, suggesting that ubiquitin signaling may recruit this repair complex to sites of alkylation adducts (Figure 2.6B). Analysis of the ASCC2 protein sequence revealed a highly conserved CUE (coupling ubiquitination to ER degradation) domain (residues 467-509), which belongs to the ubiquitin binding domain superfamily (Komander and Rape, 2012) (Figure 2.7A). Previous studies focusing on CUE ubiquitin binding domains found that these domains preferably recognize K48-ubiquitin chains, which marks proteins for proteasomal degradation (Bagola et al., 2013; Shih et al., 2003). We thus assessed the capacity of ASCC2 for ubiquitin binding. Using recombinant His-ASCC2 purified from bacteria, we found that full-length ASCC2 bound K63- but not K48-linked ubiquitin chains *in vitro* (Figure 2.7B-D). Interestingly, the minimal domain necessary for *in vitro* ubiquitin binding, residues 457-525, was not sufficient to confer binding specificity to a ubiquitin chain linkage (Figure 2.7E-F), suggesting an additional region interacts with the ubiquitin monomer to provide chain specificity. Indeed, an additional conserved region adjacent to the CUE domain was necessary for specific binding to K63-linked ubiquitin (Figure 2.7E-F). Importantly, ASCC2 co-localized with K63- but not K48-linked ubiquitin foci upon MMS damage (Figure 2.7G), suggesting that K63-polyubiquitin binding may be important for its recruitment to sites of alkylation damage.

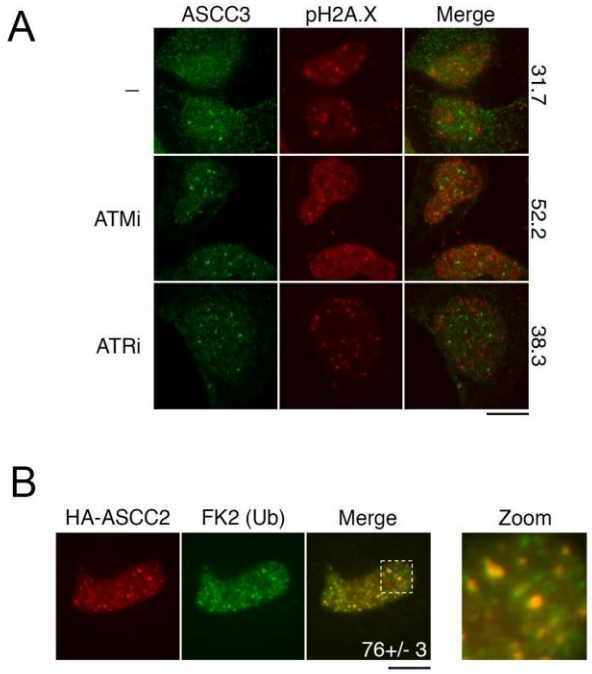

Figure 2.6. ASCC2 Foci Localize with Ubiquitin. (A) Immunofluorescence images of U2OS cells treated with MMS in the presence of the indicated damage signaling kinase inhibitor (n=2 biological replicates; mean). Numbers indicate the percent of cells expressing five or more ASCC3 foci. (B) Immunofluorescence of HA-ASCC2 and FK2 in cells after MMS (n=3 biological replicates; mean ± S.D.). Scale bars, 10 μm.

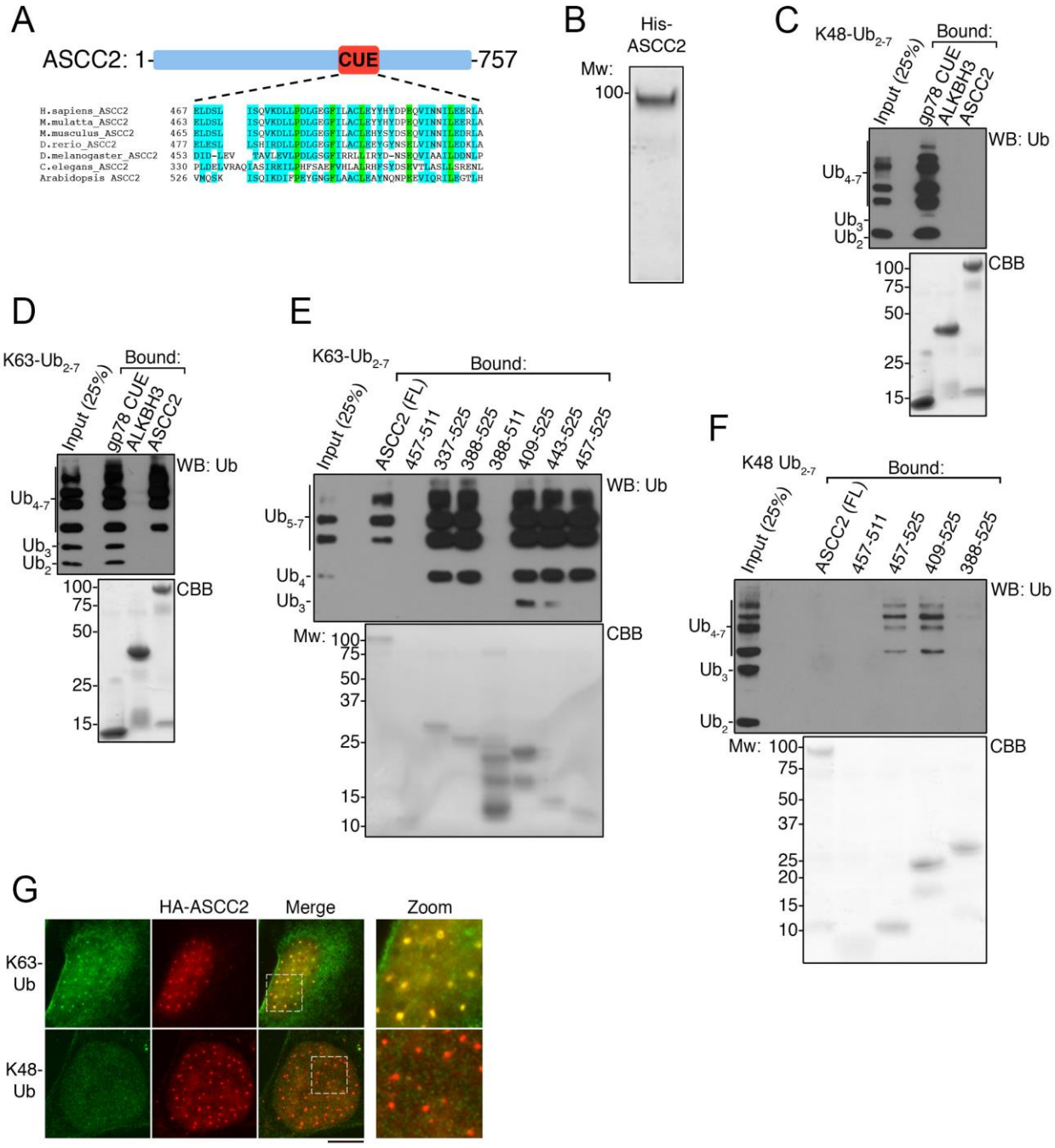

Figure 2.7. ASCC2 Binds K63-polyubiquitin. (A) ASCC2 sequence alignment. (B) His-ASCC2 was purified on Ni-NTA, separated on a 10% SDS-PAGE gel, and analyzed by Coomassie blue staining (n=2 independent experiments). (C) and (D) His-ASCC2 was immobilized and assessed for binding to K48-Ub_{2-7} (C) or K63-Ub_{2-7} (D). ALKBH3 and gp78-CUE served as controls. Bound material was analyzed by Western blot or Coomassie Blue (CBB) (n=3 independent experiments). (E) and (F) His-ASCC2 or the indicated His-ASCC2 deletions were immobilized on Ni-NTA and assessed for binding to K63-Ub_{2-7} (E) or K48-Ub_{2-7} (F) (n=3 independent experiments). (G) Immunofluorescence of HA-ASCC2 cells and K63-ubiquitin (top) or K48-ubiquitin (bottom) after MMS treatment (n=2 independent experiments). Scale bars, 10 μm.

A deposited but unpublished NMR structure of the ASCC2 CUE domain (PDB ID: 2DI0) was used to model its interaction with ubiquitin in comparison to another CUE domain from Vps9 (Figure 2.8A). While Vps9 CUE binds to ubiquitin as a dimer (Prag et al., 2003), our model predicts ubiquitin binding by a monomeric form of the ASCC2 CUE domain. Modeling of the ASCC2 CUE domain with a ubiquitin monomer alone was used to identify residues predicted to be critical for ubiquitin recognition (Figure 2.8B), and we introduced point mutations into the CUE domain at these residues. Two of these mutations, L506A and LL478-9AA, completely abrogated ubiquitin binding *in vitro*. Importantly, an introduction of a third mutation that is not predicted to be necessary for the interaction between ubiquitin and the CUE domain, P498A, had no effect on the binding capacity of the CUE domain to K63-Ub (Figure 2.8C). Isothermal titration calorimetry (ITC) experiments demonstrated that WT ASCC2 bound K63-linked di-ubiquitin chains with a K_d of 10.1 μM, which is similar to other CUE domains (Liu et al., 2012) (Figure 2.8D). In contrast, the L506A mutant showed no detectable binding (Figure 2.8E). Strikingly, both ASCC2 mutants that abrogated ubiquitin binding *in vitro* demonstrated significantly reduced foci formation upon MMS treatment (Figure 2.8F). Thus, not only does the CUE domain recognize K63-ubiquitin chains but also this recognition is critical for the recruitment of ASCC2 to sites of alkylation damage. Together, these data suggest that recruitment of ASCC2 is dependent upon upstream ubiquitin signaling events.

2.3.4 ASCC-ALKBH3 Recruitment is Dependent upon ASCC2

We reasoned that ASCC2 could act as an intermediary subunit to recruit the other components of the ASCC-ALKBH3 complex. To this end, we generated ASCC2 knockout cells using CRISPR/Cas9 (Figure 2.9A-B). Two independent ASCC2 knockout clones showed a significant reduction in ASCC3 foci formation upon MMS treatment (Figure 2.9C-D). Importantly, this

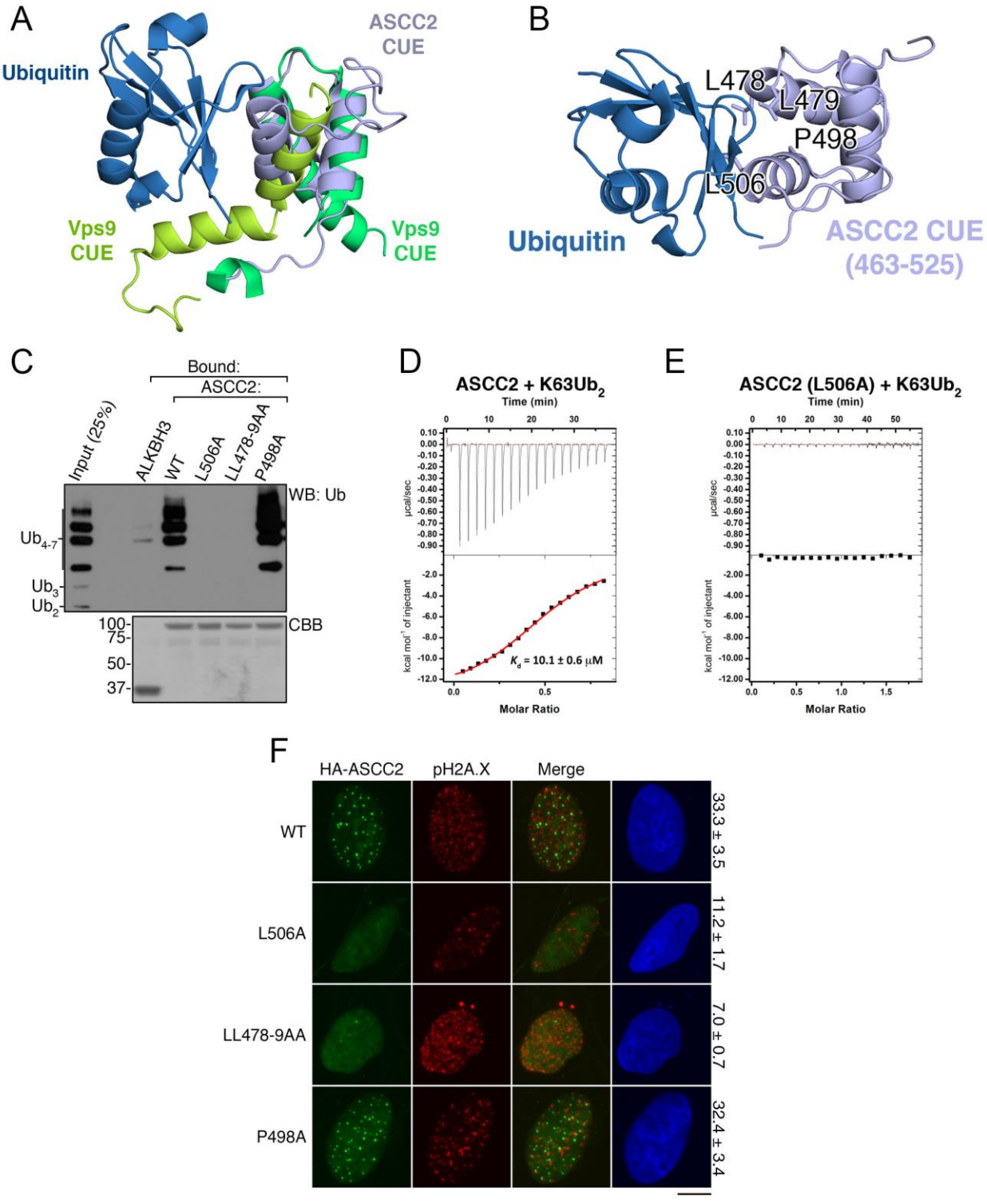

Figure 2.8. See next page for caption to Figure 2.8.

Figure 2.8. Ubiquitin Binding by ASCC2 CUE Promotes Foci Formation. (A) Structure of the ASCC2 CUE domain (PDB ID: 2DI0; grey) overlaid with the Vps9 CUE:ubiquitin complex (PDB ID: 1P3Q). (B) Interaction model between ubiquitin and the CUE domain of ASCC2 (PDB ID: 2DI0). The positions of four residues (L478, L479, P498, and L506) are shown. (C) Binding assays were performed with K63-Ub_{2-7} using WT or the mutants of His-ASCC2 (n=3 independent experiments). (D) and (E) ITC was performed with K63-Ub_2 and His-ASCC2 (D) or the L506A mutant (E) (n=1 independent experiment; mean ± S.E.). (F) Immunofluorescence images of MMS-induced foci in cells expressing various forms of HA-ASCC2. Numbers indicate the percentage of cells expressing ten or more HA-ASCC2 foci (n=3 biological replicates; mean ± S.D.). Scale bars, 10 μm.

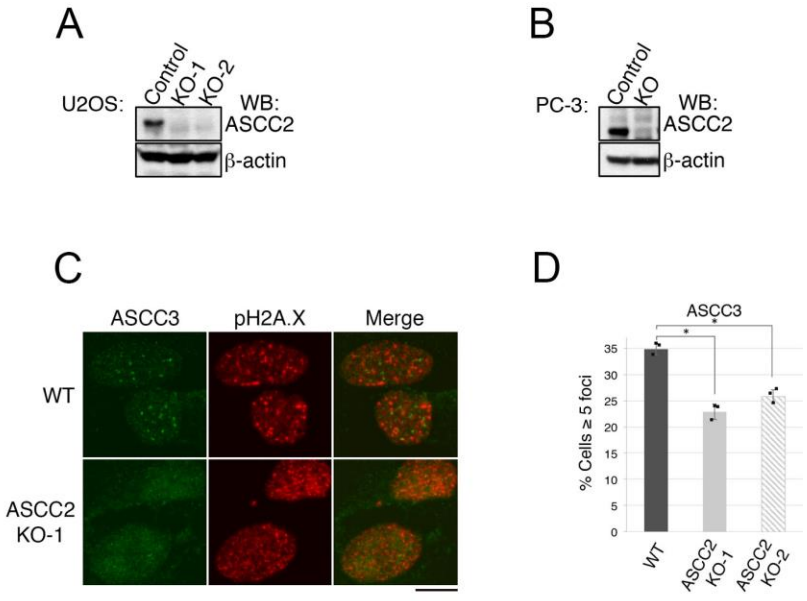

E

Cell line:	G1:	S+G2:
U2OS	48.1%	51.9%
ASCC2-KO	49.8%	50.2%

Figure 2.9. ASCC2 is Necessary for ASCC3 Foci Formation. (A) and (B) ASCC2 gene knockouts in U2OS (A) and PC-3 cells (B) were generated using CRISPR/Cas9 technology and verified by deep sequencing. Whole cell lysates of the parental and KO cells were analyzed by Western blotting as shown (n=2 independent experiments). (C) MMS-induced ASCC3 foci were assessed in WT and ASCC2-KO cells. (D) Quantitation of (C) (n=3 biological replicates; mean ± S.D.; two-tailed *t*-test, * = $p < 0.001$). (E) Flow cytometry of WT and ASCC2-KO U2OS cells after MMS treatment to determine cell cycle distribution. Scale bars, 10 μm.

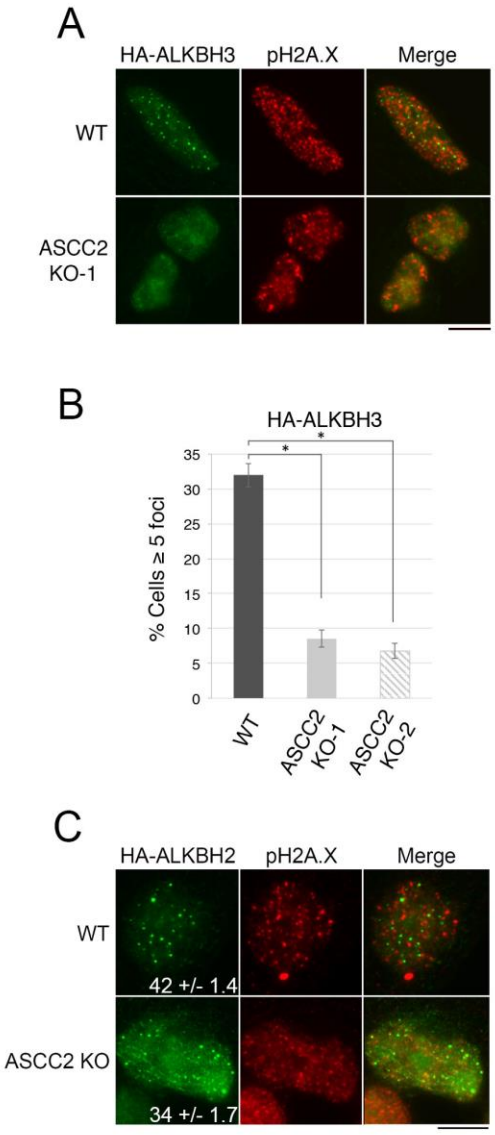

Figure 2.10. ASCC2 Recruits ALKBH3 During Alkylation Damage. (A) MMS-induced HA-ALKBH3 foci were assessed in WT and ASCC2-KO cells. (B) Quantitation of (A) (n=3 biological replicates; mean ± S.D.; two-tailed *t*-test, * = $p < 0.001$). (C) Immunofluorescence analysis of HA-ALKBH2 expressing cells after MMS. Numbers indicate the percent of cells expressing five or more HA-ALKBH2 foci (n=3 biological replicates; mean ± S.D.). Scale bars, 10 μm.

reduction was not due to a change in the population of cells in G1, as both U2OS wild-type and ASCC2 knock-out cells had similar cell cycle profiles (Figure 2.9E). Similar to ASCC3 foci, HA-ALKBH3 were also diminished in the ASCC2 KO cells (Figure 2.10A-B). Another member of the ALKBH family of proteins, HA-ALKBH2, also had reduced foci in response to MMS in the ASCC2 KO cells (Figure 2.10C). However, this loss was modest as compared to the loss observed for ASCC3 and HA-ALKBH3. Together, this data demonstrates that proper recruitment of the ASCC3-ALKBH3 repair complex is dependent upon the presence of ASCC2.

2.3.5 ASCC2 is Necessary for Alkylation Damage Resistance

To ascertain that the ASCC complex is indeed recruited to regions of the nucleus that have alkylation damage, we performed a proximity ligation assay using an antibody that recognizes m1A (PLA). In PLA, amplification of the immunofluorescence signal will only occur if the antibodies are within a certain distance of one another. We found that a specific nuclear PLA signal between 1-methyladenosine and ASCC3 is induced upon MMS damage (Figure 2.11A-C). To ensure that repair of m1A was impaired upon loss of ASCC2, we quantified the amount of remaining alkylated adducts in either U2OS WT or ASCC2 KO cells over time after exposure to MMS. DNA alkylated lesion repair kinetics was significantly slower in ASCC2 knockout cells (Figure 2.11D), suggesting that the ASCC-ALKBH3 repair complex is being recruited to sites where alkylation adducts are present. Consistent with a role in the recruitment of these factors, ASCC2-deficient PC-3 cells were hypersensitive to MMS, but not to the other damaging agents camptothecin or bleomycin. (Figure 2.12A-E). Cellular sensitivity to MMS was determined by both MTS assay as well as colony formation assay. Together, these data support the notion that ASCC2 is critical for the proper cellular response to alkylation damage.

2.3.6 ASCC2 Recruits ASCC-ALKBH3 Through K63-Ub Recognition

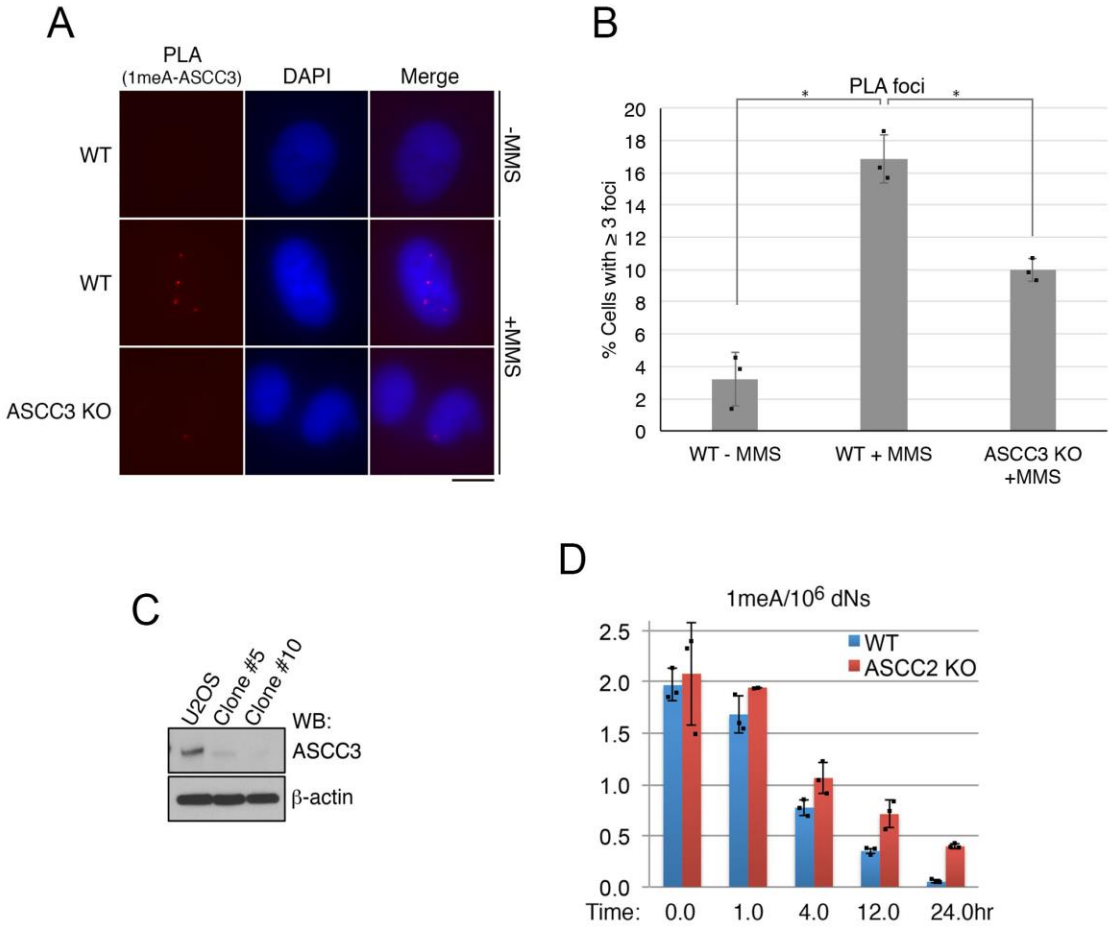

Figure 2.11. ASCC is Recruited to Sites of Alkylation Damage. (A) PLA images in control or MMS-treated cells using 1meA and ASCC3 antibodies (n=3 biological replicates). (B) PLA quantitation from (A) (n=3 biological replicates; mean ± S.D.; two-tailed *t*-test, * = $p < 0.005$). (C) ASCC3 KO cells were generated using CRISPR/Cas9 technology. Lysates were analyzed by Western blotting (n=2 independent experiments). Clone #10 was verified to be a knockout by deep sequencing. (D) 1meA quantitation in WT or ASCC2-KO cells after MMS treatment (n=3 biological replicates; mean ± S.D.). Scale bars, 10 μm.

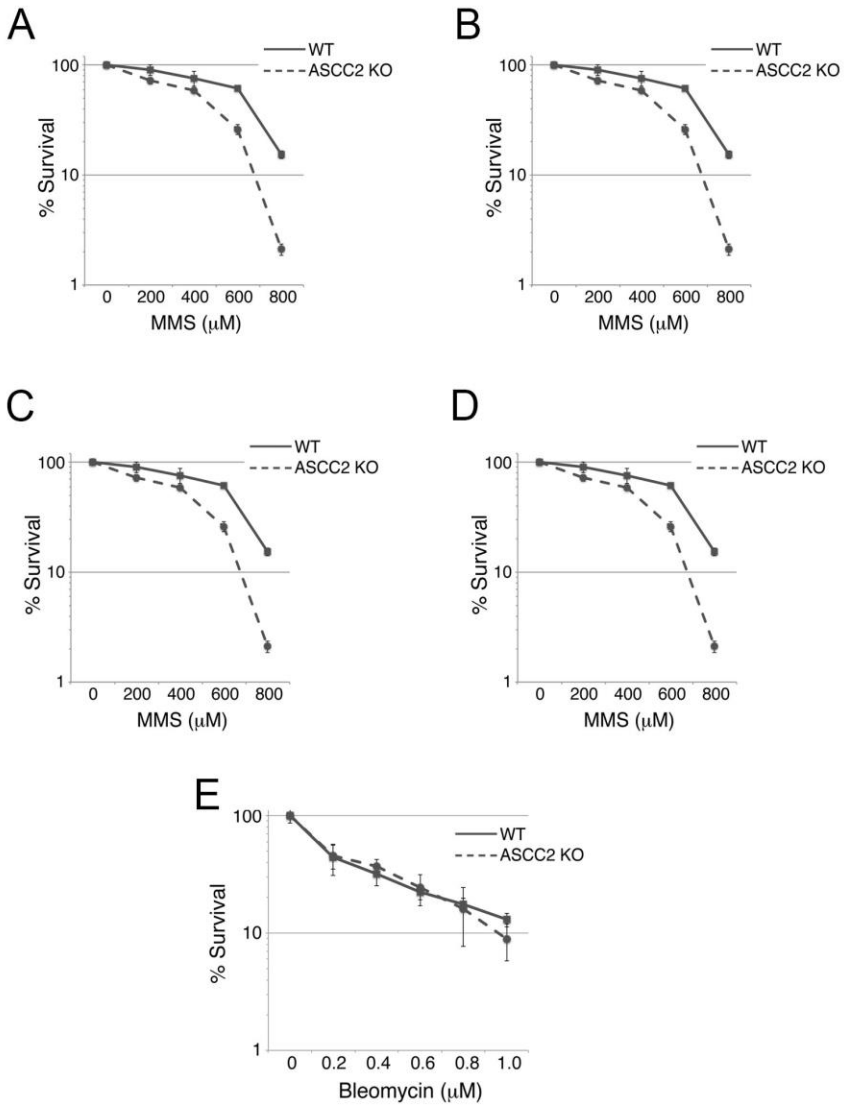

Figure 2.12. ASCC2 Loss Sensitizes Cells to MMS but not Other Damaging Agents. (A) MMS sensitivity of WT or ASCC2 KO cells using MTS assay (mean ± S.D.; n=5 biological replicates). (B-C) Sensitivity of WT and ASCC2 KO cells to MMS (B) or camptothecin (C) was assessed by clonogenic survival assay (n=4 biological replicates; mean ± S.D.). (D-E) WT PC-3 and ASCC2-KO cell sensitivity to camptothecin (D) or bleomycin (E) using the MTS assay (n=5 biological replicates; mean ± S.D.).

Due to the requirement of ubiquitin binding for ASCC2 to form foci in the presence of alkylation, we reasoned that ubiquitin recognition was necessary for the recruitment of the entire repair complex. To this end, we reconstituted ASCC2-KO cells with either wild-type or the L506A mutant version of ASCC2. WT ASCC2 but not the L506A CUE mutant restored MMS-induced HA-ALKBH3 foci formation (Figure 2.13A-C). The ubiquitin binding deficient mutant was also unable to restore ASCC3 foci in response to alkylation damage while WT ASCC2 nearly completely rescued these foci (Figure 2.13D-F). Importantly, WT ASCC2 but not the L506A mutant rescued the MMS sensitivity observed in ASCC2 knockout cells (Figure 2.14). These results strongly support the importance of ubiquitin binding to recruit not only ASCC2 but also the entire ASCC-ALKBH3 repair complex.

To ensure that mutation of the CUE domain did not disrupt the integrity of the ASCC-ALKBH3 complex, we performed co-immunoprecipitation experiments to validate proper complex formation. HA-tagged ASCC2 WT or ASCC2 L506A equally co-immunoprecipitated ASCC3 (Figure 2.15A). Further, His-ASCC3 bound to immobilized Flag-ASCC2. His-ASCC3 also bound to Flag-ALKBH3, albeit with a weaker interaction as compared to Flag-ASCC2 (Figure 2.15B). While deletion of the ASCC3 N-terminus (NΔ-ASCC3; residues 401-2202) abrogated its interaction with ASCC2, loss of the N-terminus had no effect on its capacity to bind ALKBH3 (Figure 2.15C). To further elucidate the complex conformation, binding experiments between ASCC2 and ALKBH3 were also performed. ASCC2 did not interact with recombinant ALKBH3 (Figure 2.15D). ASCC2 therefore appears to bridge ASCC3 and K63-linked ubiquitin chains, while ALKBH3 is indirectly recruited by ASCC2 through its interaction with ASCC3 (Figure 2.15E). Taken together, this data suggests that ASCC3 serves as a scaffold for the ASCC-

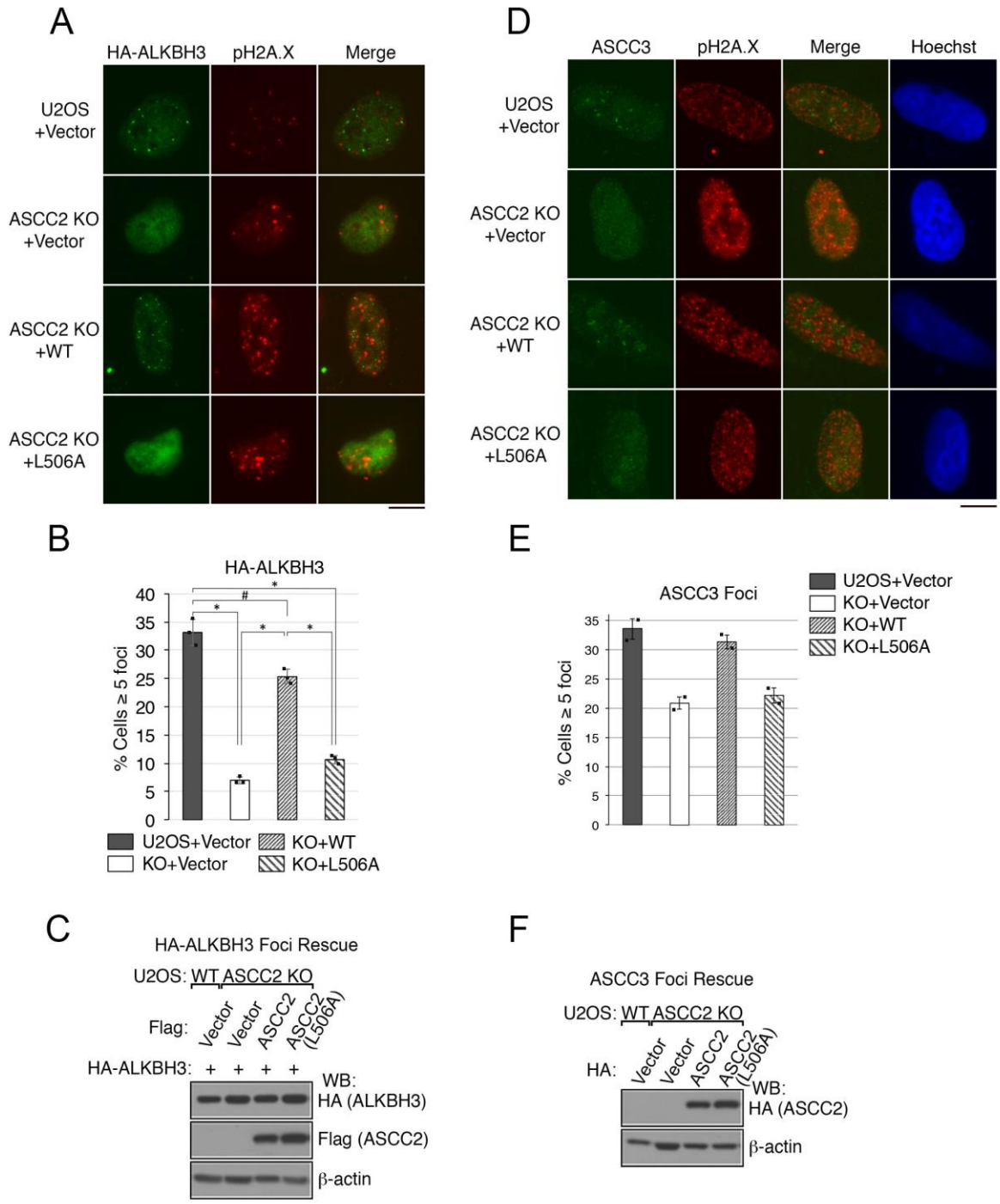

Figure 2.13. ASCC2 Ubiquitin Recognition Recruits ASCC-ALKBH3. (A) Images of WT or ASCC2-KO cells expressing indicated vectors upon MMS. (B) Quantitation of (A) (n=3 biological replicates; mean ± S.D.; two-tailed *t*-test, * = $p < 0.001$, # = $p < 0.05$). (C) Whole cell lysates from (A) were collected and expression was analyzed by Western blotting (n=2 independent experiments). (D Images of WT or ASCC2 KO cells expressing the indicated vectors after MMS exposure. (E) Quantitation of (D) (n=2 independent experiments; mean ± S.D.). (F) Whole cell lysates from Extended Data Figure 6i (left) Figure 3e (right) and (right) were collected and expression was analyzed by Western blotting (n=2 independent experiments). Scale bars, 10 μm.

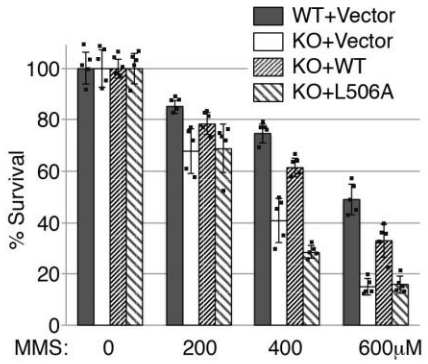

Figure 2.14. ASCC2 Ubiquitin Recognition is Necessary for Alkylation Resistance. WT or ASCC2-KO cells expressing indicated vectors were assessed for sensitivity to MMS using the MTS assay (n=5 technical replicates; mean ±S.D.).

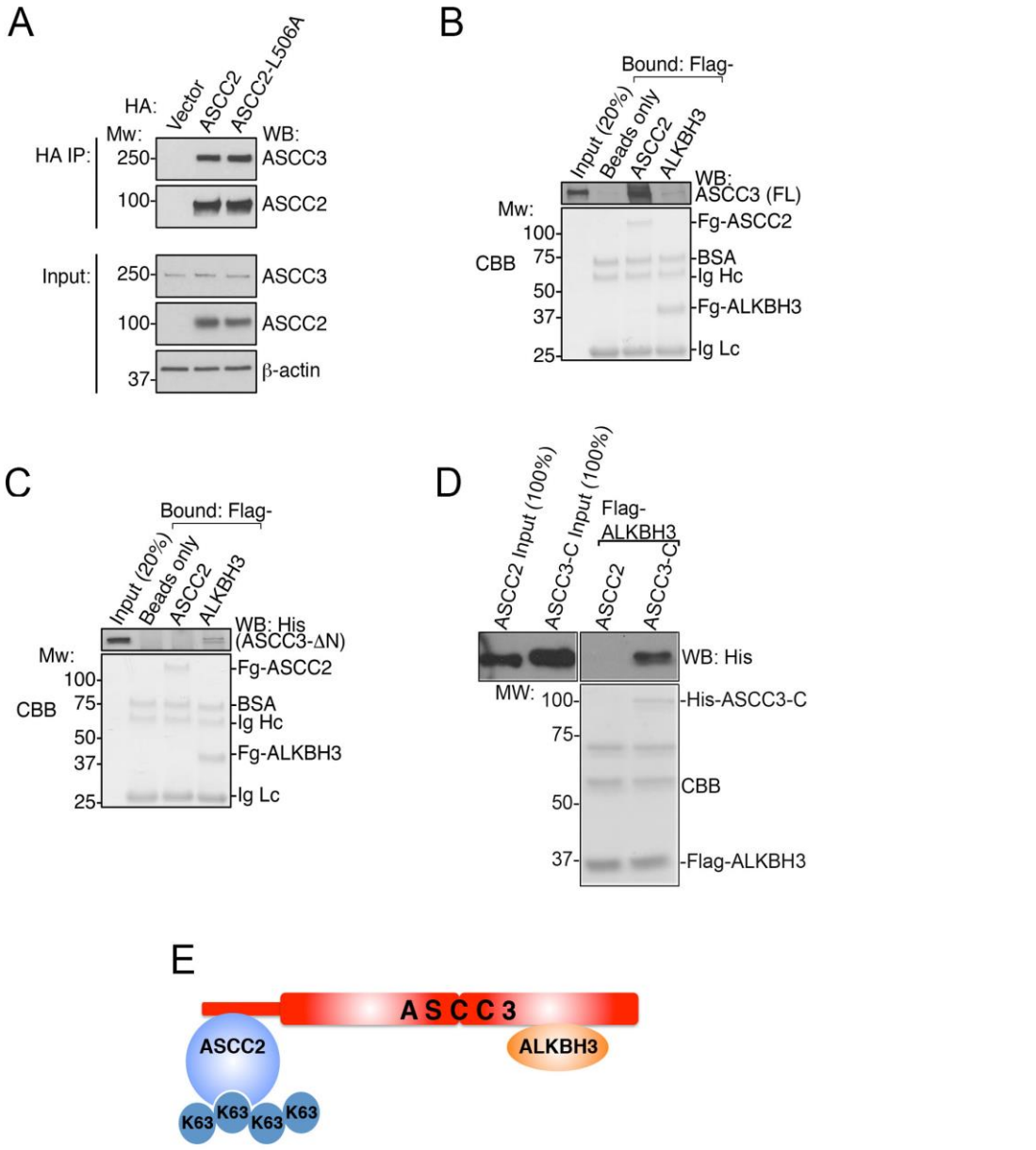

Figure 2.15. ASCC-ALKBH3 Complex Reconstitution. (A) Immunoprecipitation of HA-ASCC2 or HA-ASCC2 L506A was performed and analyzed by Western blot as shown (n=2 biological replicates). (B) Flag-ASCC2 or Flag-ALKBH3 were immobilized and tested for binding to full-length (FL) His-ASCC3. (C) Flag-ASCC2 or Flag-ALKBH3 were immobilized and tested for binding to N-terminally deleted His-ASCC3 (His-ASCC3-DN) (n=2 independent experiments). (D) Flag-ALKBH3 was immobilized and tested for binding to His-ASCC2, with His-ASCC3-C (C-terminus of ASCC3) serving as a positive control (n=2 independent experiments). (E) ASCC-ALKBH3 complex model.

ALKBH3 complex, interacting with ASCC2 near its N-terminus and with ALKBH3 near its C-terminus. This complex is then recruited to alkylation adducts via ubiquitin recognition by ASCC2.

2.3.7 The E3 Ligase RNF113A is Necessary for ASCC2 Foci Formation

As proper complex recruitment is dependent upon the recognition of upstream ubiquitin signaling by ASCC2, we next endeavored to identify the E3 ubiquitin ligase responsible for forming the ubiquitin chains recognized by ASCC2. As humans have hundreds of different E3 ligases and one E2 conjugating enzyme interacts with a specific set of E3 ligases (Hersko et al., 2000), we decided to first identify the E2 conjugating enzyme. Importantly, UBC13, a major E2 ubiquitin ligase responsible for formation of K63-linked ubiquitin chains, has previously been implicated in DNA damage response pathways (Unk et al., 2006; Zhao et al., 2007; Thorslund et al., 2015). Knockdown of UBC13 attenuated MMS-induced HA-ASCC2 foci (Figure 2.16). Importantly, knockdown of UBC13 also severely reduced 53BP1 foci (Figure 2.16A), consistent with previous reports. Interestingly, knockdown of RNF8 or RNF168, two E3 ligases involved in the double-stranded break repair (Jackson and Durocher 2013), did not affect HA-ASCC2 foci formation (data not shown), suggesting that a distinct E3 ligase functions in the alkylation pathway. To identify this E3 ligase, we performed a screen using a custom library of short-hairpin RNAs (shRNAs) that target UBC13-interacting E3 ligases or other ligases implicated in DNA repair. The screen identified RNF113A as a potential candidate, with three distinct shRNAs reducing HA-ASCC2 foci to UBC13 knockdown levels (Figure 2.17A). We confirmed that these shRNAs attenuated both RNF113A protein levels and HA-ASCC2 foci formation (Figure 2.17B-C). Importantly, MMS-induced ASCC2 foci co-localized with RNF113A (Figure 2.17D). In the absence of damage, RNF113A co-localized with PRP8 and BRR2 (Figure 2.17E),

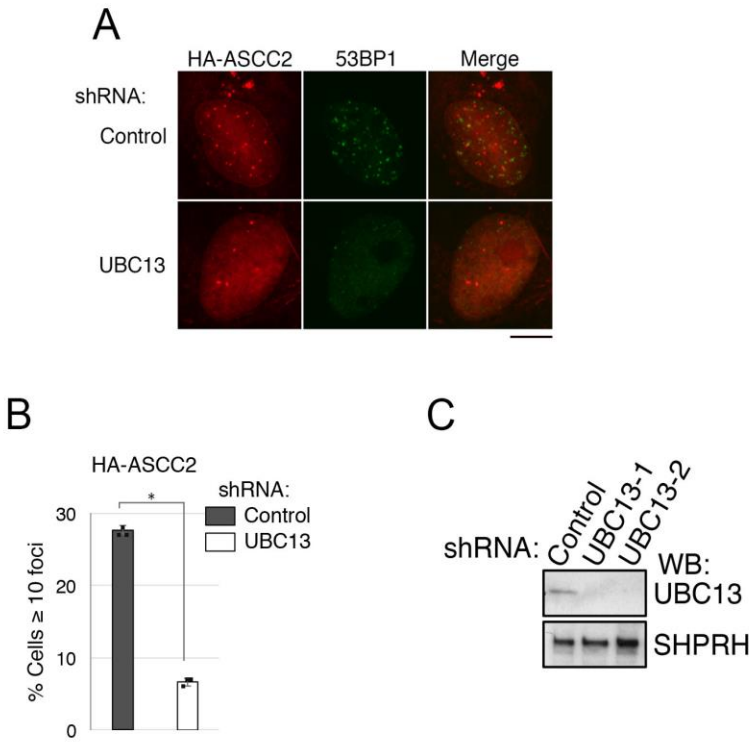

Figure 2.16. UBC13 Loss Reduces ASCC2 Foci Formation. (A) Immunofluorescence images of MMS-induced HA-ASCC2 foci in cells expressing the indicated shRNAs. (B) HA-ASCC2 foci quantitation from (A) (n=3 biological replicates; mean ± S.D.; two-tailed *t*-test, * = $p < 0.001$). (C) Whole cell lysates of U2OS cells infected with the indicated shRNAs were analyzed by Western blot. SHPRH was used as a loading control (n=1 independent experiment). Scale bars, 10 μm.

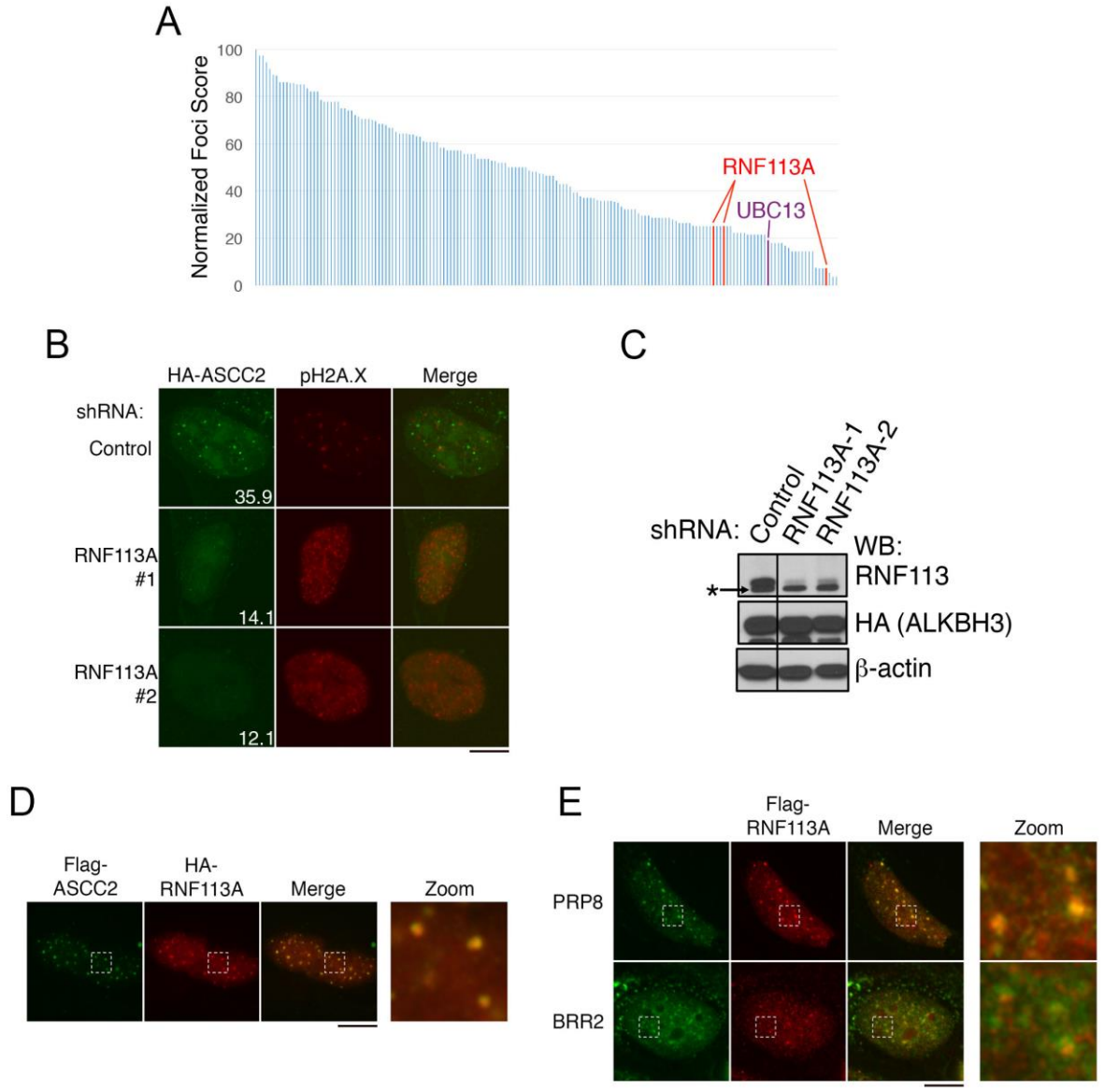

Figure 2.17. RNF113A is the E3 Ligase Implicated in the ASCC-ALKBH3 Pathway. (A Compilation of E3 ligase shRNA screen results. For each candidate, U2OS cells were transduced with HA-ASCC2 and an E3 targeting shRNA. MMS-induced HA-ASCC2 foci formation was analyzed by immunofluorescence. Results were normalized to a scrambled shRNA (normalized score = 100). UBC13 denotes the positive control (purple). Results of three different shRNA to RNF113A are indicated in red (n=1 independent experiment for each shRNA). (B) MMS-induced foci in U2OS cells expressing indicated shRNAs (n=3 technical replicates; mean). (C) Whole cell lysates of U2OS cells infected with the indicated shRNAs were analyzed by Western blot. Asterisk (*) indicates a non-specific band in the RNF113A blot (n=2 independent experiments). (D) Localization of Flag-ASCC2 and HA-RNF113A after MMS treatment (n=3 biological replicates). (E) Immunofluorescence of cells expressing Flag-RNF113A without MMS treatment (n=3 biological replicates). Scale bars, 10 μm.

which is consistent with our mass spectrometry findings that the interaction between ASCC2 and spliceosomal proteins is enriched during MMS treatment. Furthermore, this finding is consistent with previous studies suggesting that RNF113A nominally serves as a spliceosome component (Hegele et al., 2017). We then purified Flag-tagged RNF113A from HeLa-S cells to analyze its E3 ligase activity *in vitro* (Figure 2.18A). RNF113A exhibited robust E3 activity *in vitro*, which was significantly reduced with the I264A RING-finger point mutation (Figure 2.18B), which is predicted to disrupt its interaction with UBC13. Use of K63R ubiquitin abrogated chain elongation, suggesting that RNF113A may function to promote the E2 activity of UBC13 to from K63-linked ubiquitin chains (Figure 2.18C). Together, this data provides strong evidence that RNF113A is the E3 ubiquitin ligase that generates the K63-polyubiquitin recognized by ASCC2.

2.3.8 BRR2 Ubiquitylation is Critical for ASCC-ALKBH3 Recruitment

To uncover the relevant RNF113A substrate, we combined our initial proteomics screen assessing proteins enriched for their interaction with ASCC2 after MMS treatment (Figure 2.4B) with a second screen for proteins that interact preferentially with WT ASCC2 relative to the L506A mutant (Figure 2.19A). In this dataset, 295 proteins were enriched for their interaction with WT ASCC2 as compared to the L506A mutant. Of these putative substrates, only eight have been shown to be ubiquitinated by UBC13 (Thorslund et al., 2015). BRR2 was the most obvious candidate, as our previous data demonstrated that it co-localized with RNF113A and ASCC components by immunofluorescence. Indeed, BRR2 co-immunoprecipitated with RNF113A in a manner dependent upon the N-terminal domain of RNF113A (Figure 2.19B-C). Further deletion analysis revealed that the RNF113A N-terminus was also critical for its co-

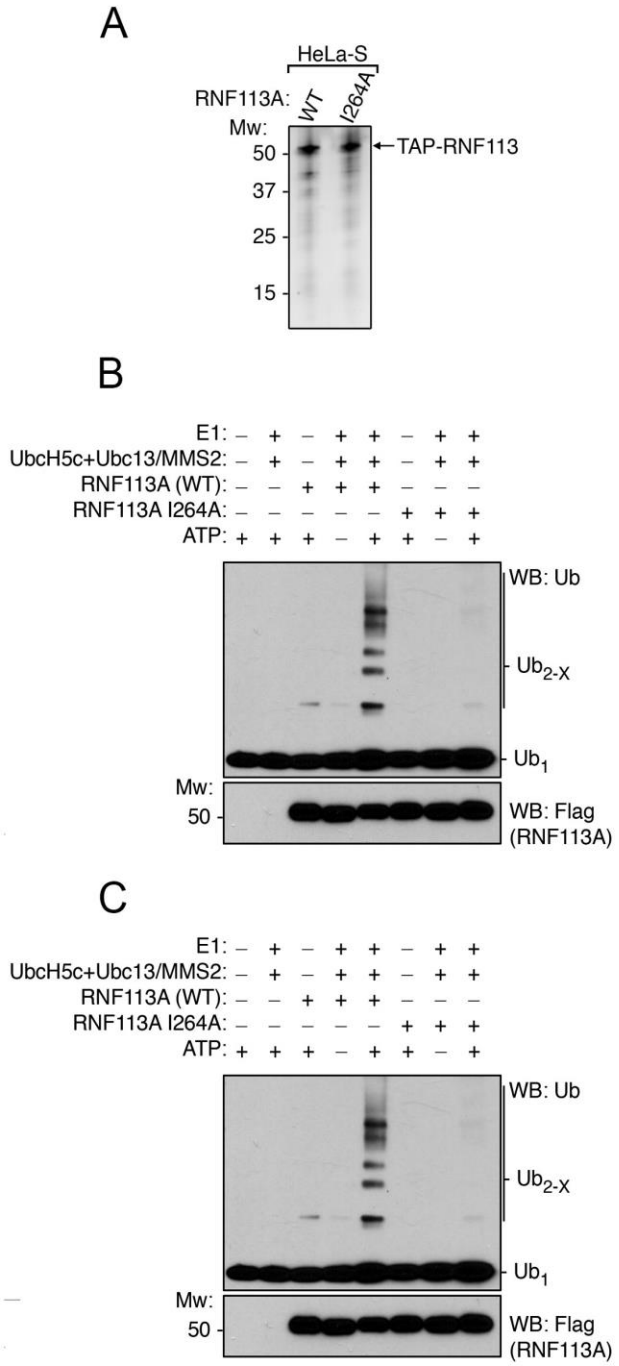

Figure 2.18. RNF113A is an Active E3 Ligase *in vitro*. (A TAP-RNF113A and the I264A RING finger mutant were stably expressed in HeLa-S cells and purified using anti-Flag resin. The eluted proteins were then analyzed by silver staining after SDS-PAGE (n=3 independent experiments). (B) Ubiquitin ligase assays using E1, E2 (UbcH5c plus Ubc13/MMS2; 50 nM each), and wildtype or I264A RNF113A. Reactions were analyzed by Western blot (n=3 independent experiments). (C) Ubiquitin ligase assays using E1, E2 (UBC13/MMS2; 250 nM), and Flag-RNF113A. K63R ubiquitin was substituted as shown (n=2 independent experiments).

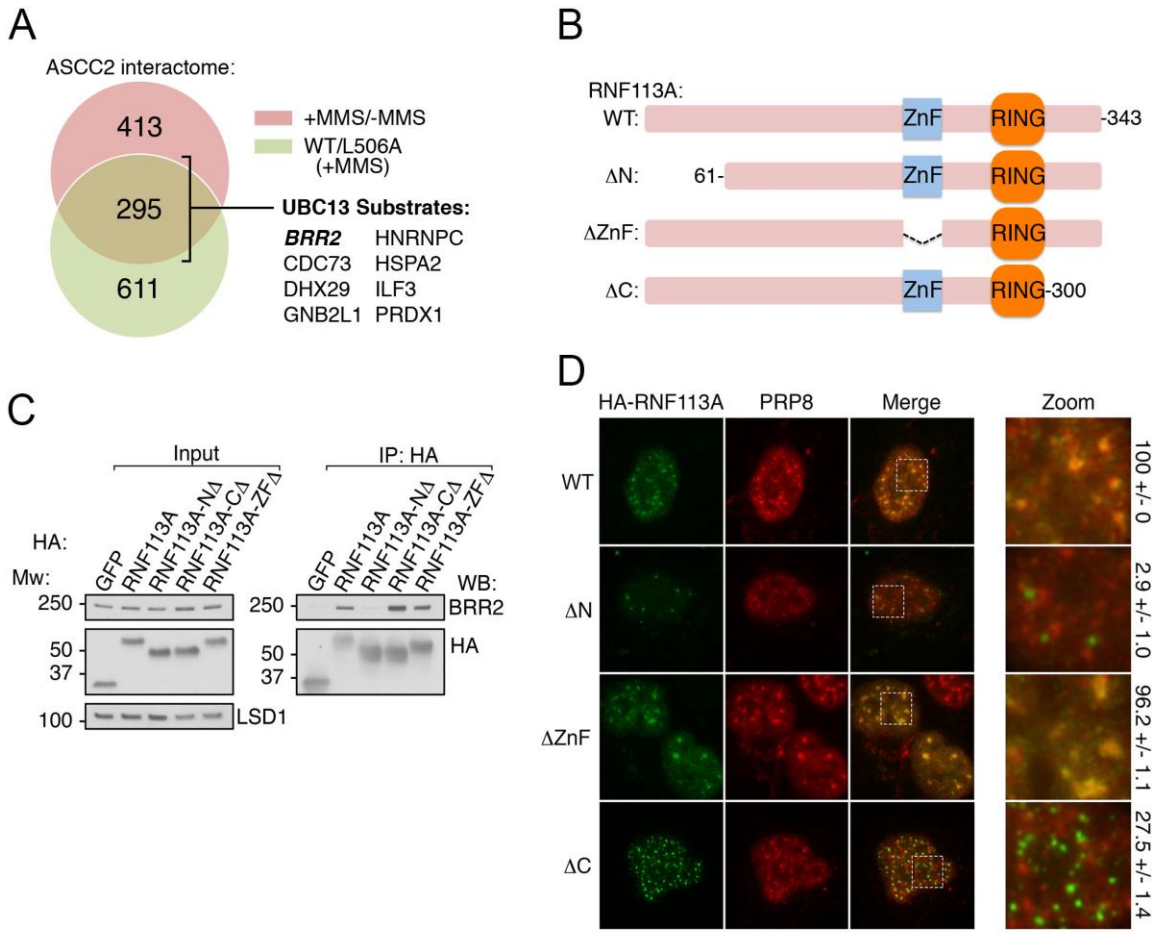

Figure 2.19. BRR2 is a Putative Substrate for RNF113A. (A) ASCC2 interactome analysis. UBC13 substrates were previously described (Thorslund et al., 2015). (B) Schematic of human RNF113A and its domain structure. The three deletion constructs used for localization analysis are also shown. (C) HA-RNF113A deletions were immunoprecipitated to analyze BRR2 interaction. (n=3 independent experiments). (D)) Images of cells expressing WT or the indicated HA-RNF113A deletion constructs. Scale bar, 10 μm. Quantitation of co-localization between each RNF113A construct and PRP8 is shown on the right (n=3 biological replicates; mean ± S.D.).

localization with PRP8 (Figure 2.19D), which is a stoichiometric partner of BRR2 (Hegele et al., 2012).

To further confirm BRR2 as a *bona fide* substrate of RNF113A, we performed an array of biochemical analyses. A denatured immunoprecipitation from cells expressing His-Ubiquitin after MMS treatment demonstrated that ubiquitin conjugation of BRR2 was significantly reduced upon loss of RNF113A (Figure 2.20A). A modified binding assay where cell lysates were added to GST-ASCC2 conjugated to Glutathione-Sepharose *in vitro* showed that RNF113A promotes BRR2 binding to ASCC2 (Figure 2.20B). BRR2 binding to ASCC2 was dependent on the RING domain of RNF113A, suggesting that ubiquitin is necessary for the interaction between ASCC2 and BRR2. Importantly, recombinant BRR2 was ubiquitinated *in vitro* by RNF113A, also in a manner dependent on its RING domain (Figure 2.20C-D). Knockdown of BRR2 or its partner PRP8 significantly reduced ASCC3 foci formation upon MMS damage (Figure 2.21 A-C). Consistently, loss of BRR2 increased sensitivity to MMS (Figure 2.21D). Thus, BRR2 likely represents at least one physiologic substrate for RNF113A in this alkylation repair pathway.

2.3.9 RNF113A Mutation is Implicated in X-linked Trichothiodystrophy

A recent study identified a nonsense mutation (Q301*) in RNF113A in two related individuals suffering from X-linked trichothiodystrophy (X-TTD) (Corbett et al., 2015). While most TTD patient cells are hypersensitive to UV damage, X-TTD cells do not have this phenotype (Corbett et al., 2015). Lymphoblastoid cell lines obtained from these two patients were hypersensitive to MMS (Figure 2.22A). U2OS cells in which RNF113A was knocked down was also hypersensitive to MMS (Figure 2.22B). Strikingly, X-TTD cells had significantly reduced ASCC3 foci formation (Figure 2.22C-D). Reconstitution of these patient cells with WT RNF113A rescued ASCC3 foci formation while the I264A mutant only partially rescued the

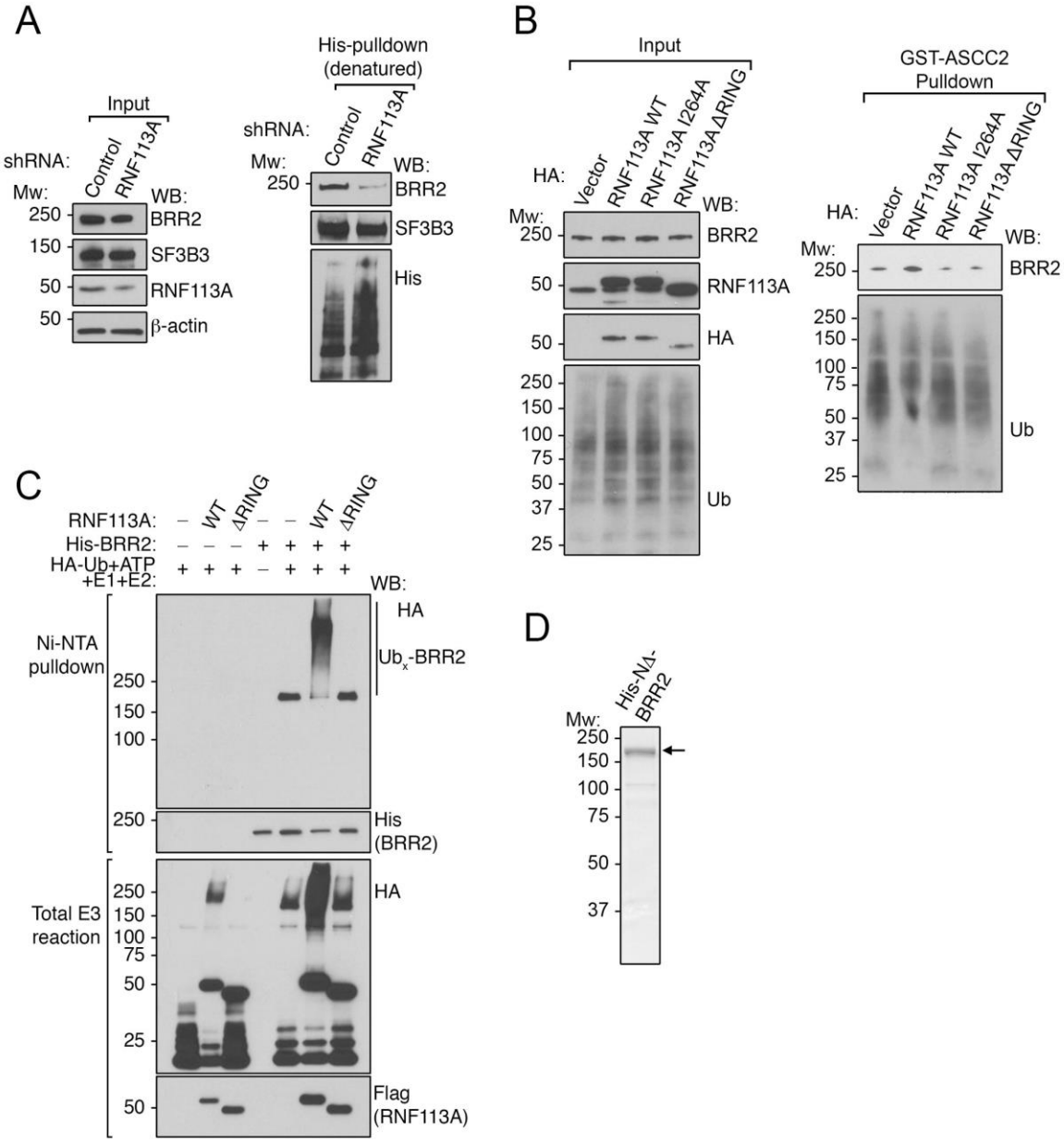

Figure 2.20. RNF113A Ubiquitylates BRR2 *in vitro*. (A) 293T cells expressing His-ubiquitin were transduced with control or RNF113A-targeting shRNAs and treated with MMS. Ubiquitinated proteins were isolated by Ni-NTA under denaturing conditions and Western blotted as shown. Input lysates were also analyzed as indicated. SF3B3, another ubiquitinated spliceosomal protein, was used as a control (n=3 independent experiments). (B) Cells expressing the indicated HA-vectors were treated with MMS as in (A). Lysates were then used for ubiquitin pulldown assays using GST-ASCC2, then blotted as shown. Input lysates were also analyzed as indicated (n=2 independent experiments). (C) and (D) His-NΔ-BRR2 was purified from Sf9 cells and analyzed by SDS-PAGE and Coomassie staining (D). This was then used as a substrate for ubiquitination assays using HA-Ub and wildtype (WT) or a RING-deletion (ΔRING) RNF113A (C) (n=2 independent experiments).

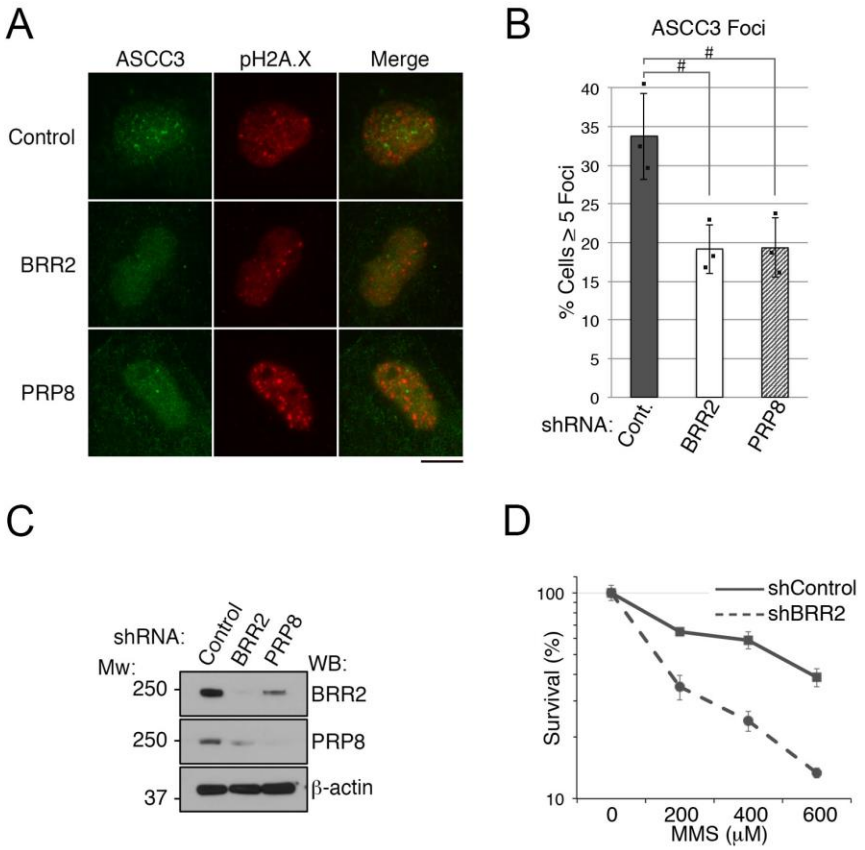

Figure 2.21. Loss of BRR2 Reduces ASCC3 Foci and Sensitizes Cells to Alkylation. (A) Images of U2OS cells expressing indicated shRNAs processed for ASCC3 immunofluorescence. (B) Quantitation of (A) (n=3 biological replicates; mean ± S.D.; two-tailed *t*-test, # = $p < 0.001$). (C) Western blot analysis of U2OS cells expressing the indicated shRNAs used for immunofluorescence analysis in Figure 4F (n=2 independent experiments). (D) MMS sensitivity of PC-3 cells expressing the indicated shRNAs was determined by MTS assay (n=5 technical replicates; mean ± S.D.). Scale bars, 10 μm.

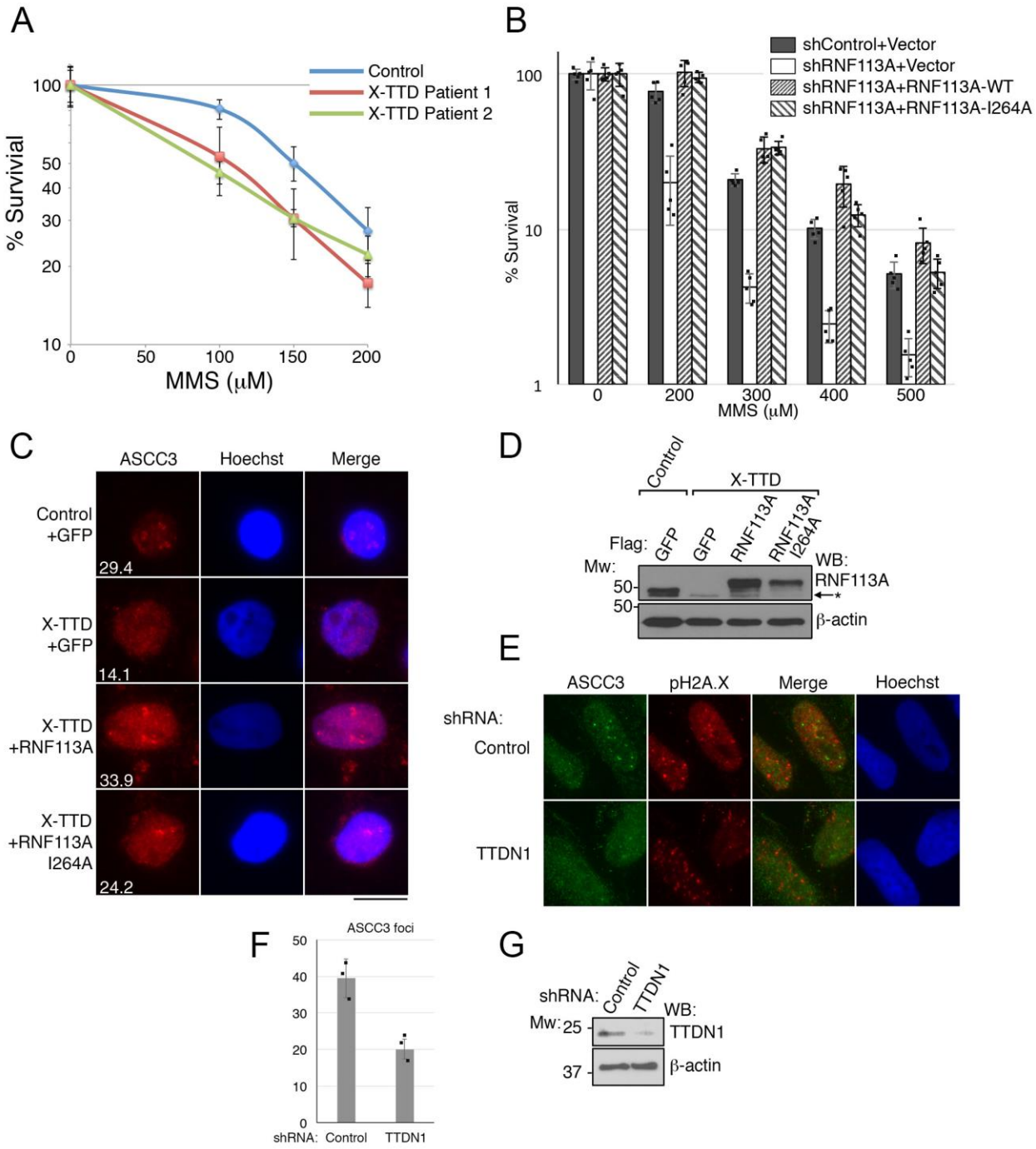

Figure 2.22. RNF113A is Implicated in X-linked Trichothiodystrophy. (A) MMS sensitivity of lymphoblasts from two X-TTD patients in comparison to an unaffected individual (n=5 biological replicates; mean ± S.D.). (B) U2OS cells expressing the indicated combination of shRNA and RNF113A rescue vector were assessed for MMS sensitivity using MTS assay (n=5 technical replicates; mean ± S.D.). (C) Images of X-TTD or control lymphoblasts expressing the indicated vectors after MMS (n=3 technical replicates; mean). (D) Whole cell lysates of control or X-TTD lymphoblasts expressing indicated vectors after selection (n=2 independent experiments). (E) Immunofluorescence analysis of U2OS cells expressing the indicated shRNAs after MMS treatment. (F) Quantification of ASCC3 foci from (E) (n=3 biological replicates; mean ± S.D.). (G) Western blot (n=2 independent experiments). Scale bars, 10 μm.

ASCC3 foci phenotype, possibly due to the small degree of remaining E3 ligase activity (Figure 2.22C). Similarly, reconstitution with U2OS cell lines with WT RNF113A but not the I264A mutant was able to restore MMS resistance in these cells (Figure 2.22B) Interestingly, loss of TTDN1, another TTD-associated gene (Nakabayahi et al., 2005), also reduced ASCC3 foci formation (Figure 2.22E-G). Together, these results demonstrate that alkylation repair is deficient in patients with X-TTD, which may contribute to the phenotypes displayed by these patients.

2.4 Discussion

Our results provide the first evidence for an alkylation-specific damage response in human cells. The ASCC complex acts as a major node in this pathway, sensing ubiquitin-dependent signaling (via ASCC2) and concomitantly recruiting alkylation repair enzymes (ALKBH3 and ASCC3). As such, ASCC2 serves as an adaptor, and may be analogous to Rap80, which recruits the BRCA1 complex to chromatin during the double-stranded break response (Jackson and Durocher, 2013). Indeed, Rap80 recognizes non-proteasomal ubiquitin chains produced by the upstream RNF8/RNF168 E3 ubiquitin ligases before BRCA1 recruitment. Here, RNF113A functions as the E3 ligase that transduces the alkylation damage signal. How alkylation damage uniquely activates RNF113A to recruit ASCC2 versus other repair complexes will be an important question for future studies. RNF113A contains a CCCH-type zinc finger, a motif known to bind RNA. Since RNA is also modified by exposure to alkylating agents, it is possible that damaged RNA serves as the initial signal to activate DNA alkylation repair. As our work strongly suggests the presence of a cellular sensor specific for alkylation damage in human cells, it may be possible to target numerous proteins in this pathway to improve tumor responses to

conventional chemotherapy. Future studies will undoubtedly clarify these critical questions regarding the upstream signals for this novel damage signaling pathway.

2.5 Materials and Methods

Data Reporting. No statistical methods were used to predetermine sample size. The experiments were not randomized and the investigators were not blinded to allocation during experiments and outcome assessment.

Plasmids. Human ALKBH3, ASCC2, ASCC3, RNF113A, BRR2, and gp78 cDNAs were isolated as previously described (Dango et al., 2011). For mammalian cell expression, cDNAs were subcloned into pHAGE-CMV-3xHA, pHAGE-CMV-Flag, or pMSCV-Flag-HA as needed by Gateway recombination (Sowa et al., 2009). The cDNA for PCNA (a kind gift of Zhongsheng You, Washington University) was subcloned into pHAGE-CMV-GFP. For recombinant protein expression, cDNAs were subcloned into pGEX-4T1, pET28a-Flag, or pDEST10. All constructs derived by PCR, including deletions and point mutations, were confirmed by Sanger sequencing.

Cell culture and cell survival assays. U2OS, PC-3, HeLa-S, and 293T cells (originally from ATCC) were cultured and maintained as previously described (Zhao et al., 2015). Cells were tested for mycoplasma at the Washington University Genome Engineering and iPSC Center and were authenticated using the ATCC human STR profiling services. Normal and X-TTD patient lymphoblastoid cell lines were kind gifts of Drs. Mark Corbett and Jozef Gecz (University of Adelaide). These cells were originally obtained after informed consent and ethical approval from the Women's and Children's Health Network Human Research Ethics Committee, as described (Corbett et al., 2015). They were maintained in RPMI 1640 media supplemented with 10% FBS and 1% penicillin-streptomycin (Corbett et al., 2015). Preparation of viruses, transfection, and

viral transduction were performed as described previously (Zhao et al., 2015). For knockout cell foci rescue experiments, cells were transduced with the pHAGE-CMV-3xHA or pHAGE-CMV-Flag lentiviral rescue vector. For knockout cell MMS sensitivity rescue experiments, cells were transduced with the pMSCV-Flag-HA retroviral rescue vector. For DNA damaging agent survival assays using PC-3 cells, 10,000 cells/well were cultured overnight in 96-well plates in 100 μl media. Cells were then exposed to medium containing the indicated concentration of methyl methanesulphonate (MMS; Sigma) for 24 hours at 37 °C. The media was then replaced with normal media, and cell viability was assessed using the MTS assay (Promega) 72 hours after initial damaging agent exposure. For experiments involving camptothecin (CPT), or bleomycin (both purchased from Sigma), cells were exposed to medium containing the indicated concentration of the damaging agent in culture medium for 72 hours at 37 °C. Viability was then processed by MTS assay as above.. For survival assays using the patient-derived cells, 10,000 cells were plated in 80 μl media. MMS-containing media was then added for a total volume of 100 μl at the indicated final concentration of MMS and incubated for 72 hours at 37 °C. MTS assay was then performed as above. All MTS-based survival experiments were carried out in quintuplicate.

CRISPR/Cas9 mediated knockouts. U2OS and PC-3 knockout cells were created using CRISPR/Cas9 genome editing at the Genome Engineering and iPSC Center (GEiC) at Washington University School of Medicine (St. Louis). PC-3 ASCC2 and ASCC3 KO clones were initially assessed by deep sequencing and confirmed by Western analysis. All other knockout clones were isolated and confirmed by Western analysis. The gRNA sequences used to generate the knockout cell line were as follows: ASCC2: 5'-GCCAAGTTACTACAGTGACCTGG-3'; ASCC3: 5'-ATGGCTTTACCTCGTCTCACAGG-

3’; RNF113A: 5’- TCTTTTGCTTCGACTCCCGGCGG-3’ and 5’-CGGGTGGTGAAGTAGGGTCCTGG-3’

Immunofluorescence microscopy. All immunofluorescence microscopy was done as previously described (Zhao et al., 2015), with minor modifications. After treatment with indicated damaging agent in complete medium at 37°C for six hours (500 μM MMS, unless indicated otherwise; 1 μM camptothecin; 10 mM hydroxyurea; 20 μM bleomycin; 5 Gy IR; or 25 J/m^2 UV), U2OS cells were extracted with 1× PBS containing 0.2% Triton X-100 and protease inhibitors (Pierce) for 10-20 minutes on ice prior to fixation with 3.2% paraformaldehyde. The cells were then washed extensively with IF Wash Buffer (1× PBS, 0.5% NP-40, and 0.02% NaN_3), then blocked with IF Blocking Buffer (IF Wash Buffer plus 10% FBS) for at least 30 minutes. Primary antibodies were diluted in IF Blocking Buffer overnight at 4°C. After staining with secondary antibodies (conjugated with Alexa Fluor 488 or 594; Millipore) and Hoechst 33342 (Sigma-Aldrich), where indicated, samples were mounted using Prolong Gold mounting medium (Invitrogen). Epifluorescence microscopy was performed on an Olympus fluorescence microscope (BX-53) using an ApoN 60X/1.49 NA oil immersion lens or an UPlanS-Apo 100X/1.4 oil immersion lens and cellSens Dimension software. Raw images were exported into Adobe Photoshop, and for any adjustments in image contrast or brightness, the levels function was applied. For foci quantitation, at least 100 cells were analyzed in triplicate, unless otherwise indicated.

Flow cytometry. Samples were prepared and flow cytometry was performed using the BrdU Flow Kit (BD Pharmingen) protocol with minor modifications. U2OS cells were transduced with pHAGE-CMV-Flag-ASCC2 lentivirus for 72 hours, treated with MMS, washed with PBS, and

extracted with Triton X-100 as for immunofluorescence. Cells were then fixed by resuspension in BD Cytofix/Cytoperm Buffer and incubated on ice for 15 minutes. Samples were washed with 1× BD Perm/Wash Buffer, resuspended with Flag antibody diluted in 1× BD Perm/Wash Buffer, incubated at room temperature for 1 hour, and washed again in the same buffer. Samples were resuspended in buffer containing Alexa Fluor 488-conjugated secondary antibody and incubated at room temperature for 20 minutes. Samples were washed and resuspended in staining buffer (1× PBS + 2% FBS) containing 7-amino-actinomycin D and processed by flow cytometry. All flow cytometry analysis was performed on the FACSCalibur Flow Cytometer using the CellQuest software. Post-acquisition analysis was performed using the FlowJo software (Tree Star).

Colony formation assay. Parental or knockout cells were trypsinized, counted, and plated at low density. After overnight incubation, the cells were treated with the indicated doses of MMS or CPT for 24 hours in complete medium. The cells were incubated for 12–14 days, fixed, and stained with crystal violet. The experiment was performed in quadruplicate for each cell line and drug dose. Colonies were counted and relative survival was normalized to untreated controls.

In situ Proximity Ligation Assay. PLA was performed using the Duolink detection kit (Sigma) following the manufacturer's instructions with minor modifications. U2OS cells were extracted and fixed as described above. The cells were washed extensively with IF Wash Buffer, then blocked with 1× Duolink blocking solution for 30 minutes at 37 °C in a pre-warmed humidifier. Primary antibodies were diluted in 1× Duolink antibody diluent and added to samples overnight at 4°C. Samples were washed with Wash Buffer A at room temperature. PLA probes anti-rabbit PLUS and anti-mouse MINUS were diluted 1:5 in 1× Duolink antibody diluent, then added to samples and incubated for 1 hour at 37 °C. Samples were again washed with Wash Buffer A at

room temperature. Duolink ligation stock and ligase were diluted 1:5 and 1:40 in pure water, respectively, and applied to samples for 30 minutes at 37°C. After washing with Wash Buffer A, Duolink amplification red probe and polymerase were diluted 1:5 and 1:80 in water and applied to samples for 100 minutes at 37°C. After a brief wash with Wash Buffer B, samples were mounted using Duolink mounting medium with DAPI and imaged as above.

Purification of TAP-ASCC2 complexes and MS/MS analysis. Affinity purification of ASCC2 was performed as previously described for ALKBH3, with minor modifications (Dango et al., 2011). Briefly, Flag-HA-ASCC2 was stably expressed after transduction of pMSCV-Flag-HA-ASCC2 retrovirus into HeLa-S cells. Nuclear extract was prepared from the stable cell line with or without prior treatment with MMS (400 μM for six hours), and the ASCC2 complex was purified using anti-Flag (M2) resin (Sigma), followed by purification using anti-HA (F-7) resin (Santa Cruz) in TAP buffer (50 mM Tris-HCl pH 7.9, 100 mM KCl, 5 mM MgCl2, 10% glycerol, 0.1% NP-40, 1 mM DTT, and protease inhibitors). For comparison of WT ASCC2 versus ASCC2 L506A, the same method was used, except that both samples were treated with MMS and the HA purification was omitted. After peptide elution, the complexes were TCA precipitated and associated proteins were identified by LC-MS/MS at the Taplin Mass Spectrometry Facility (Harvard Medical School) using an LTQ Orbitrap Velos Pro ion-trap mass spectrometer (ThermoFisher) and Sequest software (Eng et al., 1994).

Protein purification. Recombinant proteins (ALKBH3, ASCC2, ASCC3, and gp78 CUE) were purified from Rosetta (DE3) or Sf9 cells using an ÄKTA-pure FPLC (GE Healthcare). For His-tagged bacterially expressed proteins, cells were resuspended in His-lysis buffer (50 mM Tris-HCl pH 7.3, 250 mM NaCl, 0.05% Triton X-100, 3 mM β–ME, 30 mM imidazole, and protease

inhibitors) and lysed by sonication. After centrifugation and filtration, the extract was loaded onto a HisTrap HP column using a 50 ml Superloop (GE Healthcare). After extensive washing with lysis buffer, the protein was eluted using lysis buffer containing 400 mM imidazole. His-Flag-ALKBH3 was further purified on a Superdex 200 Increase 10/300 GL size exclusion column. All recombinant proteins were dialyzed into TAP buffer. Flag-tagged RNF113A was purified from HeLa-S cells by resuspension in Flag-lysis buffer (50 mM Tris-HCl pH 7.9, 150 mM NaCl, 10% glycerol 1.0% Triton X-100, 1 mM DTT, and protease inhibitors) and lysed by sonication. After incubation with Flag resin, the protein was eluted with lysis buffer containing 0.4 mg ml^{-1} Flag peptide.

Protein and RNA binding assays. All *in vitro* binding assays were performed as previously described (Drablos et al., 2004), with minor modifications. Flag (M2) agarose and Ni-NTA agarose beads were pre-blocked with 10% bovine serum albumin (BSA). For ubiquitin binding assays, 10 µg of His-ASCC2 or His-ASCC2 mutants were added to each reaction, along with 500 ng of either K48- or K63-Ub_{2-7} (Boston Biochem). The indicated proteins were added to 10 µl of beads in a total volume of 100 µl with TAP Wash Buffer. Reactions were incubated at 4 °C with rotation for 1 hour, then washed extensively with TAP Wash Buffer. A final wash was performed with 1× PBS, and bound material was eluted with 20 µl of Laemmli buffer, analyzed by SDS-PAGE, and stained with Coomassie Brilliant Blue or subjected to Western analysis as indicated. For RNA binding experiments, 0.5 nmol of each 5'-biotinylated RNA (50mer sequence: 5'-UCGAUAGUCUCUAGACAGCAUGUCCUAG CAAGCCAGAAUUCGGCAGCGUC-3'; the 35mer and 20mer removed 15 and 30 nucleotides from the 3' end of the same sequence, respectively) was immobilized on 10µl streptavidin-agarose beads. To each reaction, 1µg of His-NΔ-ASCC3 (residues 401-2202) was added in a

total volume of 100 µl in TAP Wash Buffer with RNase inhibitor (NEB). Reactions were incubated at 25°C with rotation for 30 minutes, then washed extensively with TAP Wash Buffer. A final wash was performed with 1× PBS, and bound material was eluted with 10 µl of Laemmli buffer, analyzed by SDS-PAGE and Western blotting.

Ubiquitin ligase assays. Reactions analyzing ubiquitin chain polymerization were performed in ubiquitin ligase buffer (25 mM Tris pH 7.3, 25 mM NaCl, 10 mM $MgCl_2$, 100 nM ZnCl, 1 mM mercaptoethanol) containing 5 mM ATP and 100 µM of either WT ubiquitin or K63R ubiquitin in a total volume of 20 µl. E1 activating enzyme (UBE1; Boston Biochem) was used at 500 nM, and E2 ubiquitin conjugating enzymes (Ubch5c or Ubc13/MMS2; Boston Biochem) were added at the indicated concentrations. Flag-HA-tagged-RNF113A or RNF113A I264A mutant protein purified from HeLa-S cells was added to each reaction and incubated at 37°C for 3 hours. Reactions were stopped with 20 µl of Laemmli buffer, analyzed by SDS-PAGE, and Western blotted. For ubiquitination of BRR2, 1 µg of His-NΔ-BRR2 (residues 394-2136) purified from Sf9 cells was used as a substrate for ubiquitination with Flag-RNF113A (WT and ΔRING) purified from HeLa cells. Each reaction contained E1 (50 nM), E2 (Ubch5c; 150 nM), 2 µg HA-Ub and 2 mM ATP, and were incubated at 35°C for 2 hours. An aliquot (5µl) of the total E3 reaction was saved, and the remaining reaction was used for binding to Ni-NTA beads for one hour. After extensive washing with TAP buffer, the captured His-BRR2 was eluted with Laemmli buffer, analyzed by SDS-PAGE and analyzed by SDS-PAGE, and Western blotted.

Immunoprecipitation. Immunoprecipitation of HA-tagged RNF113A was carried out by transient expression in 293T cells. The cells were resuspended in high-salt buffer (50 mM Tris-HCl pH 7.9, 300 mM NaCl, 10% glycerol 1.0% Triton X-100, 1 mM DTT, and protease

inhibitors), lysed by sonication, and centrifuged. An equal volume of buffer containing no salt was added, and the lysate was incubated with anti-HA resin. After incubation at 4°C with rotation, the beads were washed extensively with buffer containing 150 mM NaCl. Bound material was eluted with Laemmli buffer and analyzed by SDS-PAGE. Immunoprecipitation after denaturation was performed as previously described (Sowa et al., 2009) with minor modifications. Briefly, HEK293T cells were transfected with His-Ub, then transduced with the indicated shRNA lentivirus. Cells were then treated with 500 μM MMS for 6 hours and harvested. Pellets were resuspended in TBS + 1% SDS and further lysed by sonication, boiled and cleared by centrifugation. Samples were diluted to 0.1% SDS with lysis buffer (50mM Tris pH 7.9, 150 mM NaCl, 10% glycerol, 1% Triton X-100, 1mM DTT, and protease inhibitors) and incubated with Ni-NTA beads at 4°C overnight. After incubation and extensive washing with lysis buffer, the bound material was eluted with Laemmli buffer and analyzed by Western blotting.

Isothermal titration calorimetry. All reported ITC data were collected using a MicroCal iTC_{200} instrument. His-tagged ASCC2, the L506A ASCC2 mutant, and K63-Ub_2 were dialyzed in 20 mM HEPES pH 7.5, 150 mM NaCl, and 200 μM Tris(2-carboxyethyl)phosphine prior to the experiment. For the WT ASCC2 binding experiment, a 102 μM K63-Ub_2 solution in the sample cell was titrated with 435 μM ASCC2 solution using eighteen 2-μL injections. The L506A ASCC2 binding experiment was performed similarly, with 388 μM L506A ASCC2 titrated into 42 μM K63-Ub_2. Fitting was performed using Origin 7 SR4 (OriginLab, Northampton, MA).

Structural analysis. PyMOL (The PyMOL Molecular Graphics System, Version 1.8.0.5 Schrödinger, LLC.) was used to align the structure of ASCC2 residues 463-525 (PDB ID: 2DI0)

with the VSP9 CUE:ubiquitin complex structure (PDB ID: 1P3Q). Figure 2C and Extended Data Figure 3E were generated using PyMOL.

Quantification of methylated bases using LC-MS/MS. Cells were grown in DMEM (Sigma-Aldrich), supplemented with 0.03 g/L triple-deuterized L-Methionine (Sigma-Aldrich), for at least five cell divisions prior to the experiment. For each condition, 3 × 10 cm cell culture dishes were used. MMS was added to the growth medium at a final concentration of 1 mM and cells incubated further for 1 h. After a brief wash with pre-warmed PBS, new medium was added and the cells incubated further for various time spans prior to analysis. After medium removal, culture plates (60-80% confluency) were placed on ice and washed with ice cold PBS. Cells were harvested by scraping into ice cold PBS, centrifuged and the pellet washed with ice cold PBS. Dry pellets were snap frozen and stored at -80°C until further processing. Cell lysis and total DNA isolation was performed with the AllPrep DNA/RNA/Protein Mini kit (Qiagen) according to the manufacturer's instructions. DNA was hydrolyzed to nucleosides by 20 U benzonase (Santa Cruz), 0.2 U nuclease P1, and 0.1 U alkaline phosphatase (Sigma) in 10 mM ammonium acetate pH 6.0 and 1 mM magnesium chloride at 40 °C for 40 min. Three volumes of acetonitrile was added and the sample was centrifuged (16,000 g, 30 min, 4°C). The supernatants were dried and dissolved in 50 µl water for LC-MS/MS analysis of methylated and unmodified nucleosides. Chromatographic separation was performed using an Agilent 1290 Infinity II UHPLC system with an ZORBAX RRHD Eclipse Plus C18 150 x 2.1 mm ID (1.8 µm) column protected with an ZORBAX RRHD Eclipse Plus C18 5 x 2.1 mm ID (1.8 µm) guard column (Agilent). The mobile phase consisted of water and methanol (with 0.1 % formic acid) run at 0.25 ml/min, for methylated nucleosides starting with a 6-min gradient of 5-90 % methanol, followed by 4 min re-equilibration with 5 % methanol, and for unmodified nucleosides maintained isocratically with

20 % methanol. Mass spectrometric detection was performed using an Agilent 6495 Triple Quadrupole system operating in positive electrospray ionization mode, monitoring the mass transitions 282.1/150.1 (mA), 285.1/153.1 (D_3-mA), 258.1/126.1 (mC), 261.1/129.1 (D_3-mC), 298.1/166.1 (mG), 301.1/169.1 (D_3-mG), 268.1/136.1 (A), 244.1/112.1 (C), 284.1/152.1 (G), 245.1/113.1 (U), 266.1/150.1 (m(dA)), 252.1/136.1 (dA), 228.1/112.1 (dC), 268.1/152.1 (dG), and 243.1/127.1 (dT).

shRNA library and targeted E3 ligase screen. The targeted E3 ligase shRNA library was part of the TRC/pLKO.1 vector collection (Sigma). For the screen, U2OS cells were concurrently transduced with pHAGE-CMV-3xHA-ASCC2 lentivirus and individual lentiviral shRNAs. A scrambled pLKO.1 shRNA and a lentivirus targeting UBC13 (TRCN0000039435) served as the negative and positive controls, respectively. After approximately 72 hours, the cells were treated with MMS (500 μM) for six hours and processed for immunofluorescence microscopy using anti-HA and pH2A.X. At least 100 cells per sample were analyzed for HA-ASCC2 foci formation. Quantified results were normalized to the scrambled control. RNF113A was the only candidate E3 ligase with three independent shRNAs exhibiting at least a threefold reduction in MMS-induced HA-ASCC2 foci formation. For verification, U2OS cells were co-transduced with pHAGE-CMV-3xHA-ASCC2 and the candidate lentiviral shRNAs. HA-ASCC2 foci formation was assessed as above.

Statistical Analyses. All *p*-values were calculated by unpaired, two-tailed Student's *t*-test. All error bars represent the standard deviation, unless otherwise noted.

Antibodies. The antibodies and the concentration used for the given application are listed as following: 1-methyladenine (MBL Life Science; 1:500 PLA), 53BP1 (Santa Cruz; 1:1000 IF),

6x-His (Abcam; 1:2500 Western), ASCC2 (Bethyl; 1:2500 Western), ASCC3 (In house; 1:500 IF; 1:500 PLA; 1:5000 Western), BMI-1 (Millipore; 1:500 IF), BRR2 (Bethyl; 1:200 IF; 1:2500 Western), FK2 (Enzo Life Sciences; 1:1000 IF), Flag (Sigma; 1:5000 IF; 1:3000 Western; 1:200 Flow Cytometry), HA (BioLegend; 1:300 IF; 1:2500 Western), HA (Santa Cruz; 1:300 IF), K48-Ubiquitin (Millipore; 1:200 IF), K63-Ubiquitin (Millipore; 1:200 IF), LSD1 (Active Motif; 1:2500 Western), pH2A.X (Abcam; 1:2000 IF), PRP8 (Bethyl; 1:200 IF; 1:2500 Western), PSPC1 (Bethyl; 1:500 IF), RNA PolII-pS2 (Abcam; 1:200 IF), RNF113A (Sigma; 1:2000 Western), SC-35 (Abcam; 1:1000 IF), SFPQ (Bethyl; 1:200 IF), SHPRH (Abcam; 1:2500 Western), UBC13 (Cell Signaling; 1:2000 Western), Ubiquitin (Santa Cruz; 1:2500 Western), β-actin HRP (Sigma; 1:5000 Western).

Chapter 3: RNA Ligase-Like Domain in ASCC1 Regulates ASCC Complex Function during Alkylation Damage

Soll JM, Brickner JR, Mudge MC, Mosammaparast N. 2017. J. Biol. Chem. 293:13524-13533.

3.1 Abstract

Multiple DNA damage response (DDR) pathways have evolved to sense the presence of damage and recruit the proper repair factors. We recently reported a signaling pathway induced upon alkylation damage to recruit the ALKBH3– ASCC3 dealkylase–helicase repair complex (see Chapter 2). As with other DDR pathways, the recruitment of these repair factors is mediated through a ubiquitin-dependent mechanism. However, the machinery that coordinates the proper assembly of this repair complex and controls its recruitment is still poorly defined. Here, we demonstrate that the ASCC1 accessory subunit is important for the regulation of ASCC complex function. ASCC1 interacts with the ASCC complex through the ASCC3 helicase subunit. We find that ASCC1 is present at nuclear speckle foci prior to damage but leaves the foci in response to alkylation. ASCC1 loss significantly increases ASCC3 foci formation during alkylation damage. Strikingly, the majority of these foci lack ASCC2. These results suggest that ASCC1 coordinates the proper recruitment of the ASCC complex during alkylation. This function appears to depend on a putative RNA-binding motif near the ASCC1 C-terminus. Consistent with its role in alkylation damage signaling and repair, ASCC1 knockout through a CRISPR/Cas9 approach results in alkylation damage sensitivity in a manner epistatic with ASCC3. Together, our results identify a critical regulator of the ALKBH3–ASCC alkylation damage signaling pathway and suggest a potential role for RNA-interacting domains in the alkylation damage response.

3.2 Introduction

Endogenous DNA alkylation damage is caused by numerous agents that are present in the environment, as well as by cellular metabolism via the metabolite S-adenosylmethionine (Drablos et al., 2004; Fu et al., 2012; Sedgwick et al., 2007; Rydberg and Lindahl, 1982). Exogenous alkylation damage may be induced by a number of cancer chemotherapeutics. If left unrepaired, alkylated adducts can stall replication, cause mutations, and potentially lead to cell death. Due to the diverse chemical nature of alkylation damage, multiple pathways have evolved to protect the genome from alkylation damage. These include base-excision repair (BER), direct reversal by O^6-methylguanine methyltransferase (MGMT), and the AlkB family of demethylases/dealkylases (Fu et al., 2012; Sedgwick et al., 2007; Soll et al., 2017).

Although BER excises alkylated bases, it is a more general DNA repair mechanism, as this pathway also is responsible for the removal of many other forms of DNA damage, including oxidized bases, uracil and other deaminated bases (Krokan and Bjoras, 2013). Conversely, MGMT and the AlkB family of proteins appear to be dedicated solely to the direct reversal of alkylation damage (Fu et al., 2012; Sedgwick et al., 2007; Soll et al., 2017). MGMT repairs O-linked adducts, particularly O6-methylguanine, by the direct transfer of an alkyl group to a cysteine in the active site via a non-enzymatic mechanism which inactivates MGMT and signals the protein for proteasomal degradation (Xu-Welliver and Pegg, 2002; Zak et al., 1994). In contrast, AlkB proteins are *bona fide* demethylases/dealkylases that directly reverse N-linked adducts such as 1-methyladenine (m1A) and 3-methylcytosine (m3C) in an Fe(II) and 2-oxogluterate dependent reaction (Falnes et al., 2002; Trewick et al., 2002). m1A and m3C are particularly cytotoxic as both disrupt canonical base pairing, hence blocking replicative DNA polymerases (Fu et al., 2002). In humans, there are nine AlkB homologues (Gerken et al., 2007;

Kurowski et al., 2003; Sanchez-Pulido and Andrade-Navarro, 2007), but only two homologues, ALKBH2 and ALKBH3, have been shown to repair m1A and m3C on DNA with different substrate preferences (Duncan et al, 2002; Aas et al., 2003).

It is important for the cell to coordinate the various alkylation repair pathways, as there is some redundancy in the substrate binding of the numerous repair factors. This overlap in substrate preference may lead to a potential conflict during initial lesion recognition and reduce the efficiency of repair. For example, alkyl-adenine glycosylase (AAG), which is involved in the initiation step of BER, binds to the 3,N^4-ethenocytosine (ϵC) lesion but cannot excise the base (Gros et al., 2004; Lingaraju et al., 2011). ALKBH2 is capable of repairing ϵC but cannot access the lesion and is thus inhibited by the presence of AAG (Fu and Samson, 2012). Due to such competition, it is important for the cell to have a tightly controlled damage response to ensure that repair occurs in an efficient manner, while simultaneously preventing recruitment of inappropriate repair factors. In order to understand the interplay between these different repair mechanisms, it is first necessary to determine the regulation of the individual alkylation damage repair pathways. However, for alkylation damage repair, little is known about the regulation of repair factor recruitment *in vivo*.

We previously found that the ALKBH3 demethylase associates with the Activation Signal Cointegrator Complex (ASCC; also known as ASC-1) (Dango et al., 2011). This complex plays a key role in repairing alkylated DNA in cell lines overexpressing ALKBH3, such as prostate and non-small-cell lung tumor cells (Dango et al., 2011; Konishi et al., 2005; Tasaki et al., 2011). ASCC is comprised of three proteins: ASCC1 (p50), ASCC2 (p100), and ASCC3 (p200) (Jung et al., 2002). Biochemical characterization of this complex revealed that ASCC3 is a DNA helicase, whose unwinding activity is crucial for dealkylation by the ALKBH3 repair enzyme *in*

vitro (Dango et al., 2011). It is thought that ASCC3 and ALKBH3 work in concert such that ASCC3 generates the single-stranded substrate needed for ALKBH3-mediated repair. Recently, we found that ASCC2 is important for the recruitment of the ALKBH3-ASCC3 complex to nuclear speckle foci specifically during alkylation damage (Chapter 2; Brickner et al., 2017; Galganski et al., 2017; Spector and Lamond, 2011). This recruitment is dependent upon non-proteasomal K63-linked ubiquitination by the E3 ligase RNF113A (Brickner et al., 2017). The ubiquitination is recognized by the ASCC2 subunit, which is responsible for the recruitment of both ASCC3 and ALKBH3 to sites of damage. Loss of ASCC2 results in increased sensitivity to alkylating agents, strongly suggesting that ASCC2-mediated recruitment is critical for efficient repair (Brickner et al., 2017).

One of the outstanding questions remaining is how these proteins are coordinated to form an active complex and what other mechanisms are regulating its recruitment during alkylation damage. Here, we characterize ASCC1, the smallest subunit of the ASCC complex. We find that ASCC1, unlike ASCC2 or ASCC3, is constitutively present at nuclear speckle foci. In response to alkylation damage, ASCC1is removed from these nuclear regions. As a result, ASCC1 is capable of modulating ASCC3 recruitment during alkylation damage. Together, our data suggests a novel regulatory mechanism for the ALKBH3-ASCC repair pathway wherein ASCC1 modulates the localization and function of the complex components.

3.3 Results

3.3.1 ASCC1 Interacts Directly with ASCC3

We wished to determine what factors associated with the ASCC complex are involved in regulating its function in response to alkylation damage. To this end, we focused on ASCC1, a protein previously shown to co-purify with ASCC2 and ASCC3 (Dango et al., 2011; Jung et al.,

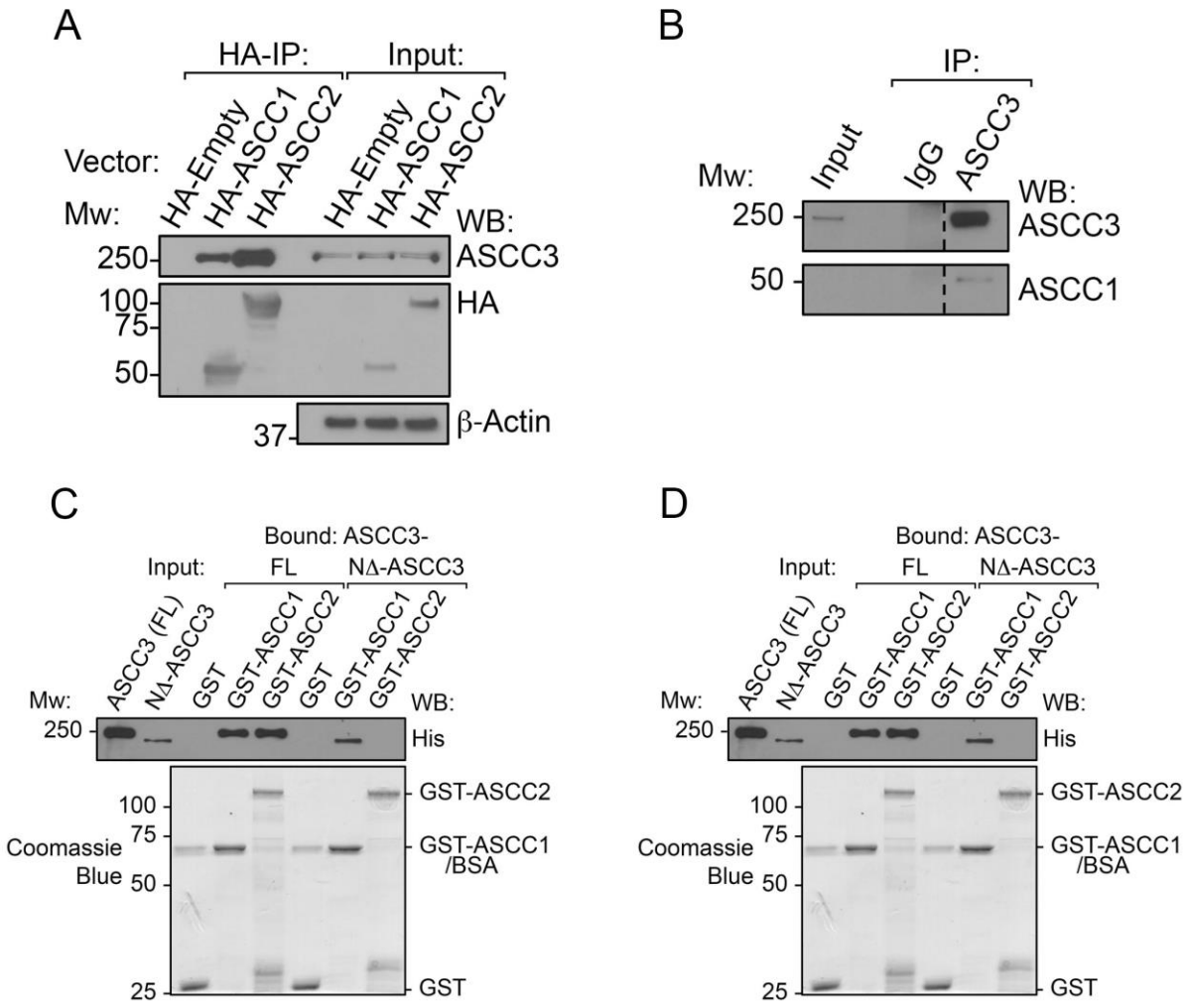

Figure 3.1. ASCC1 binds directly to ASCC3. (A) HA-tagged vector, ASCC1, or ASCC2 were expressed in 293T cells and immunoprecipitated using anti-HA resin. Immunoprecipitated (HA-IP) and input samples (1.5%) were analyzed using the indicated antibodies. The amount of ASCC3 immunoprecipitated by HA-ASCC1 was found to be 3.5% of the input, while HA-ASCC2 immunoprecpitated 8.4% of the input. Positions of molecular weight markers are shown on the left. (B) 293T whole-cell lysate was immunoprecipitated using anti-ASCC3 or IgG control antibodies, then Western blotted as shown. Input represents 2.5% of the IP samples. (C) GST, GST-ASCC1, or GST-ASCC2 were immobilized onto glutathione-Sepharose and incubated with full-length (FL) His-tagged ASCC3, or an N terminal deletion (ND-ASCC3). After washing, the bound material was analyzed by SDS-PAGE and Western blot using anti-His antibody, or by Coomassie Blue staining. (D) GST-ASCC2 was immobilized onto glutathione-Sepharose and incubated with His-ASCC1 or K63-Ub_{3-7}. After washing, the bound material was analyzed by SDS-PAGE and Western blot using anti-His antibody, anti-Ub antibody or by Coomassie Blue staining.

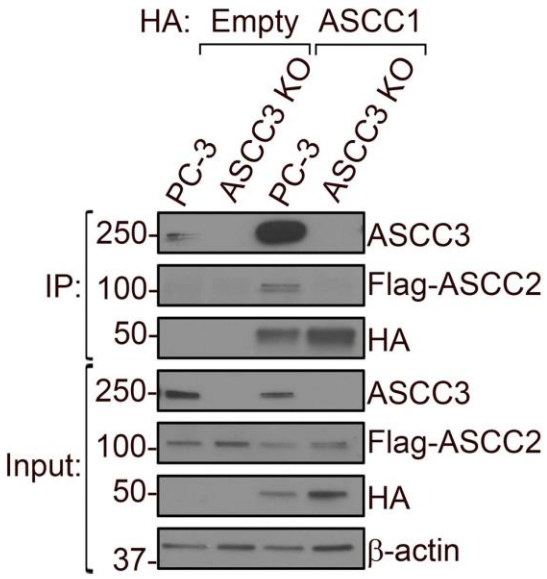

Figure 3.2. ASCC2 Interaction with ASCC1 Depends on ASCC3. HA-tagged ASCC1 was expressed in PC-3 WT or ASCC3 KO cells and immunoprecipitated using anti-HA resin. HA-IP and input samples were analyzed using the indicated antibodies.

2002). To determine how the individual complex components associate with one another, we performed immunoprecipitation of either HA-ASCC1 and HA-ASCC2 with ASCC3 (Figure 3.1A). Both of these factors co-immunoprecipitated ASCC3 from 293T cells, although a stronger interaction between HA-ASCC2 and ASCC3 was observed. Consistent with this result, immunoprecipitation of endogenous ASCC3 from 293T cell extracts yielded ASCC1, suggesting that this physical interaction is present at the endogenous level (Figure 3.1B). To test whether ASCC1 and ASCC3 interact directly, we purified all three components of the complex as recombinant proteins from *E. coli*. His-tagged ASCC3 bound to both immobilized GST-tagged ASCC1 and GST-ASCC2 but not GST alone (Figure 3.1C). An N-terminal truncation of ASCC3 (NΔ-ASCC3; residues 401-2202) abrogated the interaction with ASCC2 but did not affect ASCC1 binding (Figure 3.1C). Thus, both ASCC1 and ASCC2 can bind directly to ASCC3. These interactions are likely to be through distinct regions within ASCC3. In support of this notion, recombinant ASCC1 and ASCC2 did not interact with each other in pulldown assays (Figure 3.1D), suggesting that ASCC3 serves as a scaffold between ASCC1 and ASCC2. To test this, we knocked out ASCC3 in PC-3 cells using CRISPR/Cas9. Immunoprecipitation of HA-ASCC1 from parental PC-3 cells yielded the other two components of the complex but ASCC2 was not co-immunoprecipitated in the absence of ASCC3 (Figure 3.2). Thus, ASCC3 is required to bridge the interaction between ASCC1 and ASCC2 *in vivo*.

3.3.2 ASCC1 Forms Nuclear Foci in the Absence of Alkylation Damage

As both ASCC2 and ASCC3 form nuclear foci specifically upon alkylation damage (Brickner et al., 2017) and in light of the physical interactions between the complex components, we reasoned that ASCC1 may also form alkylation induced foci (Figure 3.3A-C). Interestingly, HA-tagged ASCC1 formed foci that co-localized with the nuclear speckle component PRP8 in the absence

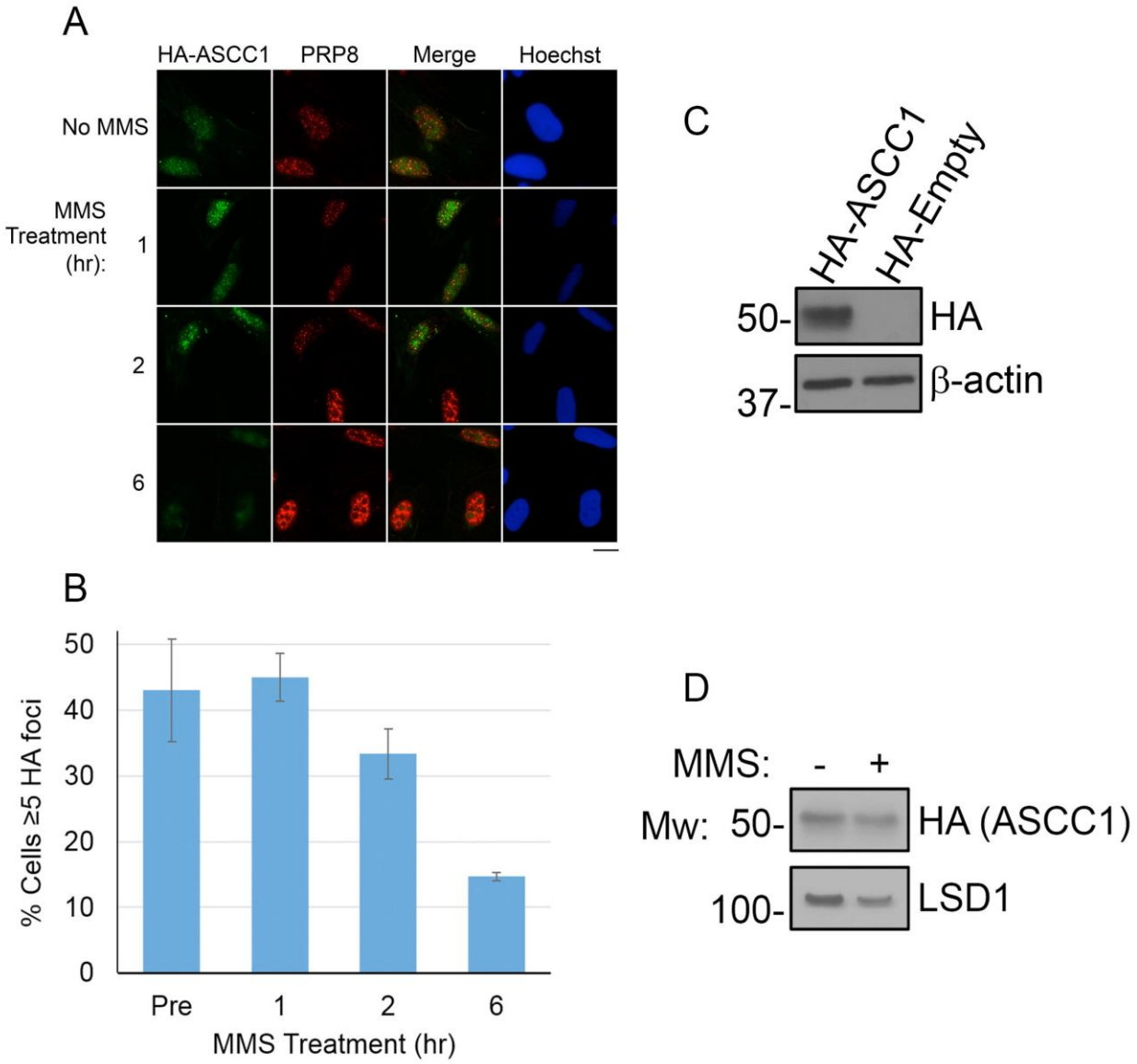

Figure 3.3. ASCC1 Forms Foci in the Absence of Alkylation Damage. (A) U2OS cells expressing HA-tagged ASCC1 were untreated or treated with MMS (0.5 mM) for 1, 2, or 6 hours as shown. Cells were processed for immunofluorescence using anti-HA and anti-PRP8 antibodies, with Hoechst used as the nuclear counterstain. Scale bar, 10 μm. (B) Quantitation of (A). N = 3 biological replicates of 100 cells for each replicate and error bars indicate +/- S.D. of the mean. (C) Whole cell lysates from U2OS WT cells expressing HA-tagged ASCC1 or empty vector were analyzed by Western blot. (D) Whole cell lysate from U2OS WT cells expressing HA-tagged ASCC1 were untreated or treated with MMS (0.5 mM) for 6 hours and analyzed by Western blotting.

of any damage, unlike the other components of the ASCC-ALKBH3 complex (Figure 3.3A-C). Surprisingly, treatment of the cells with the alkylating agent methyl methanesulphonate (MMS) significantly reduced ASCC1 co-localization with these nuclear domains in a time-dependent manner (Figure 3.3A-B). This was not due to a reduction in the expression level of the tagged ASCC1 during MMS treatment (Figure 3.3D). Taken together, these results suggest that ASCC1 is part of the ASCC complex but may perform a distinct function in response to alkylation damage.

3.3.3 ASCC1 Modulates Alkylation-Induced ASCC3 Foci Formation

We next wished to determine the role of ASCC1 in ASCC3 foci formation. To this end, we knocked out ASCC1 in U2OS cells using CRISPR/Cas9 (Figure 3.4A). Notably, loss of ASCC1 significantly increased MMS-induced ASCC3 foci formation (Figure 3.4B-C). This increase was apparent with two different knockout clones, making it unlikely that the induction of foci was due to an off-target effect of CRISPR/Cas9. These results were not attributable to an increase of ASCC3 foci at baseline (i.e., without MMS) in the ASCC1 KO cells (Figure 3.5). In time-course experiments, ASCC3 foci were still resolved in the absence of ASCC1 upon removal of MMS (Figure 3.5). These results suggested that ASCC1 modulates ASCC3 foci formation during alkylation damage.

We next asked whether ASCC1 affects the co-localization of other components of the ASCC complex. Upon MMS treatment, nearly 75% of WT cells had foci containing co-localized ASCC3 and HA-ASCC2 (Figure 3.6A-B). Under the same conditions, ASCC1 KOs had significantly fewer cells exhibiting co-localization between HA-ASCC2 and ASCC3 foci (42%). This was not due to a difference in the expression level of HA-ASCC2 in parental versus ASCC1 KO cells (Figure 3.6C). This suggested that ASCC1 may function to promote co-localization of

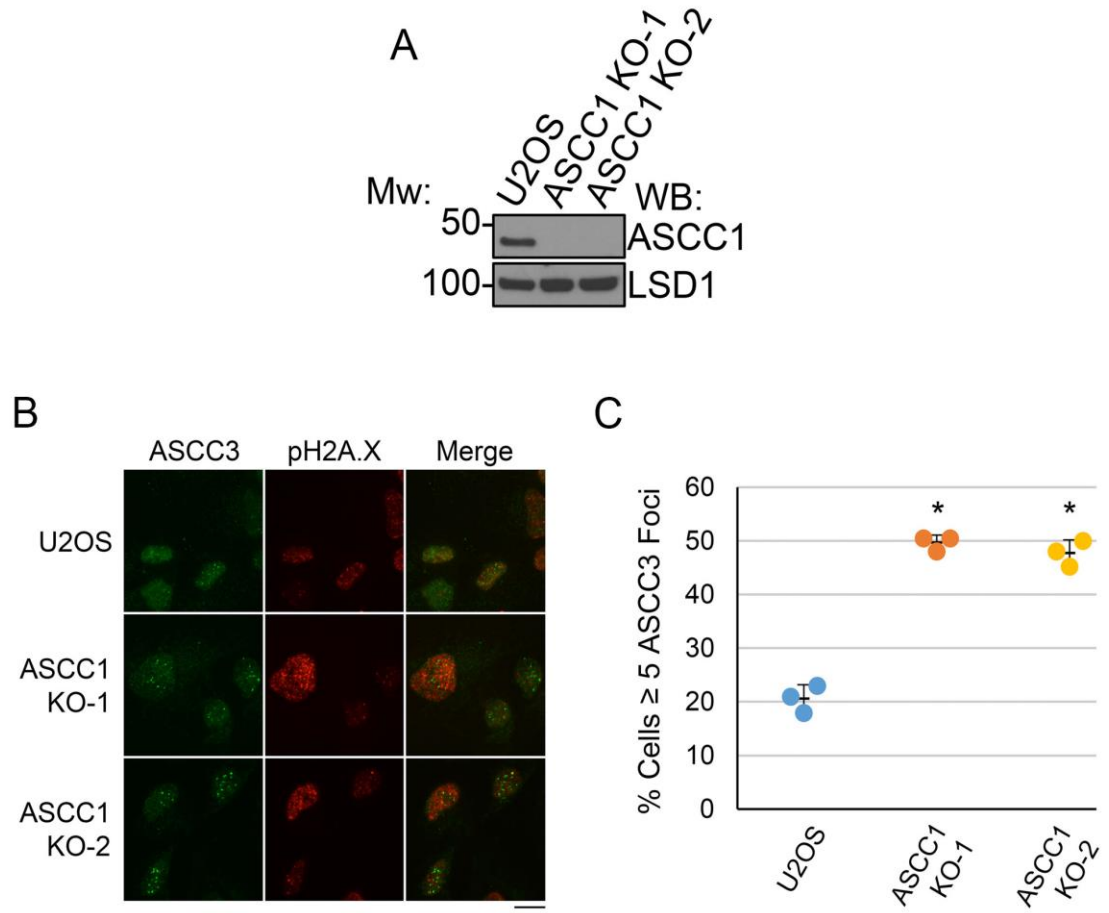

Figure 3.4. ASCC1 Modulates ASCC3 Foci Formation. (A) U2OS ASCC1 knockout was generated using CRISPR/Cas9 technology. Whole cell lysate from WT and two U2OS ASCC1 KO clones were analyzed by Western blotting. (B) U2OS WT and ASCC1 KO cells were treated with MMS (0.5 mM) for 6 hours and processed for immunofluorescence using anti-ASCC3 and anti-pH2A.X antibodies, with Hoechst as the nuclear counterstain. (C) Quantification of (B). N=3 biological replicates of 100 cells per replicate and error bars indicate +/- S.D. of the mean * = $p < 0.01$. Scale bar, 10 μm.

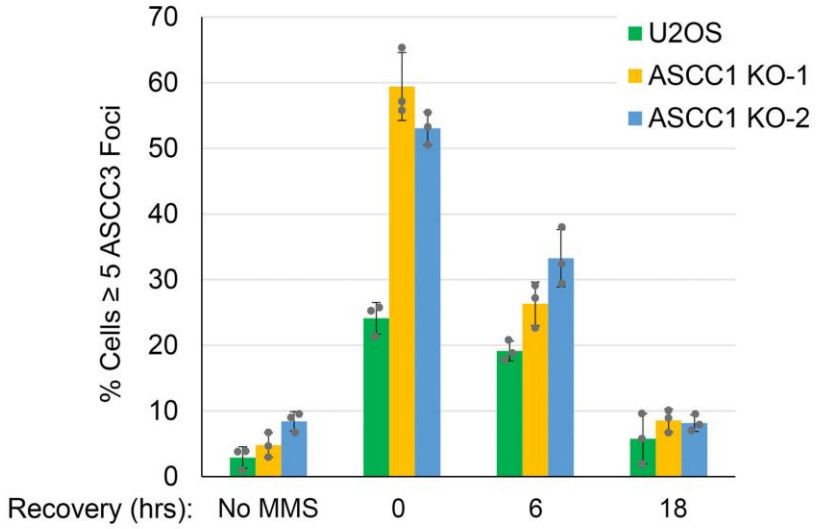

Figure 3.5. Resolution of ASCC3 Foci is Not Impaired with ASCC1 Knockout. Quantification of ASCC3 foci in WT and ASCC1 KO cells treated with MMS (0.5 mM) for 6 hours at indicated recovery times. N=3 biological replicates of 100 cells and error bars indicate +/- S.D. of the mean.

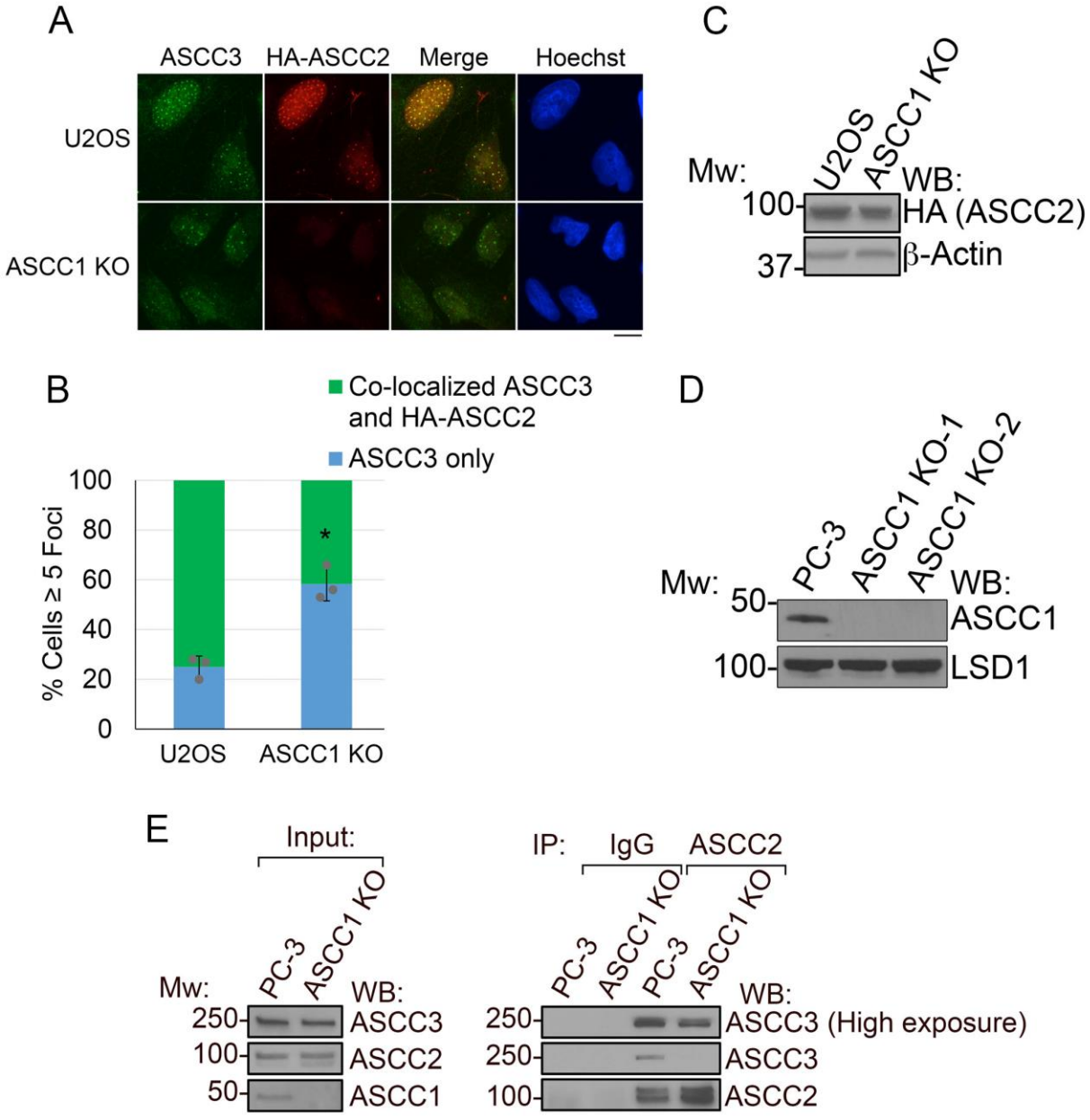

Figure 3.6. ASCC1 Coordinates ASCC Complex Formation During Alkylation Damage. (A) U2OS WT and ASCC1 KO cells expressing HA-tagged ASCC2 were treated with MMS (0.5 mM) for 6 hours. Cells were processed for immunofluorescence using anti-ASCC3 and anti-HA antibodies, with Hoechst as the nuclear counterstain. (B) Quantification of (A). Only cells with ≥ 5 ASCC3 foci were scored. N=3 biological replicates of 100 cells per replicate and error bars indicate +/- S.D. of the mean. * = $p < 0.01$ (C) Whole cell lysates from U2OS WT and ASCC1 KO cells expressing HA-tagged ASCC2 were analyzed by Western blotting. (D) Whole cell lysate from WT and two PC-3 ASCC1 KO clones were analyzed by Western blotting. (E) PC-3 WT and ASCC1 KO cells were treated with MMS (0.5 mM) for 6 hours. Whole-cell lysate was immunoprecipitated using anti-ASCC2 or IgG control antibodies, then Western blotted as shown. Inputs represent 2.5% of the IP samples. Scale bars, 10 μm.

the other two components of the complex during alkylation damage. To test this biochemically, we immunoprecipitated endogenous ASCC2 in WT versus ASCC1 knockout PC-3 cells (Figure 3.6D-E). Consistent with the diminished interaction observed by microscopy, less ASCC3 was co-immunoprecipitated with ASCC2 in ASCC1 knockout cells than in WT cells upon alkylation damage (Figure 3.6E). Thus, ASCC1 appears to coordinate the proper recruitment of the complex components during alkylation.

3.3.4 Deletion Analysis of ASCC1 Reveals Modular Functional Domains

We reasoned that distinct domains within ASCC1 may be responsible for the interaction with ASCC3 and its subsequent removal from nuclear speckle domains during damage. ASCC1 contains a KH domain adjacent to an unstructured region at its N-terminus, as well as an RNA ligase-like C-terminus, which has been postulated to be an RNA binding domain (Brown et al., 2003; Siomi et al., 1993; Valverde et al., 2008). We generated deletion mutants of ASCC1 (Figure 3.7A) and tested their individual ability to associate with ASCC3 via immunoprecipitation (Figure 3.7B). Deletion of the N-terminus of ASCC1 (ASCC1-NΔ; residues 54-357) abolished its binding to ASCC3, while deletion of the C-terminus (ASCC1-CΔ; residues 1-243) had no effect on this interaction (Figure 3.7B).

We then expressed the ASCC1-NΔ and ASCC1-CΔ constructs in ASCC1 knockout cells (Figure 3.8A) and analyzed their ability to retain localization within nuclear speckles upon MMS treatment. We utilized the ASCC1 knockout cell line to prevent possible interference from any endogenous ASCC1 may have on the localization of these constructs. Strikingly, HA-ASCC1-CΔ maintained foci formation during MMS treatment, while HA-ASCC1-NΔ behaved like WT ASCC1 (Figure 3.8B-C). This was not because ASCC1-CΔ was expressed at a higher level than

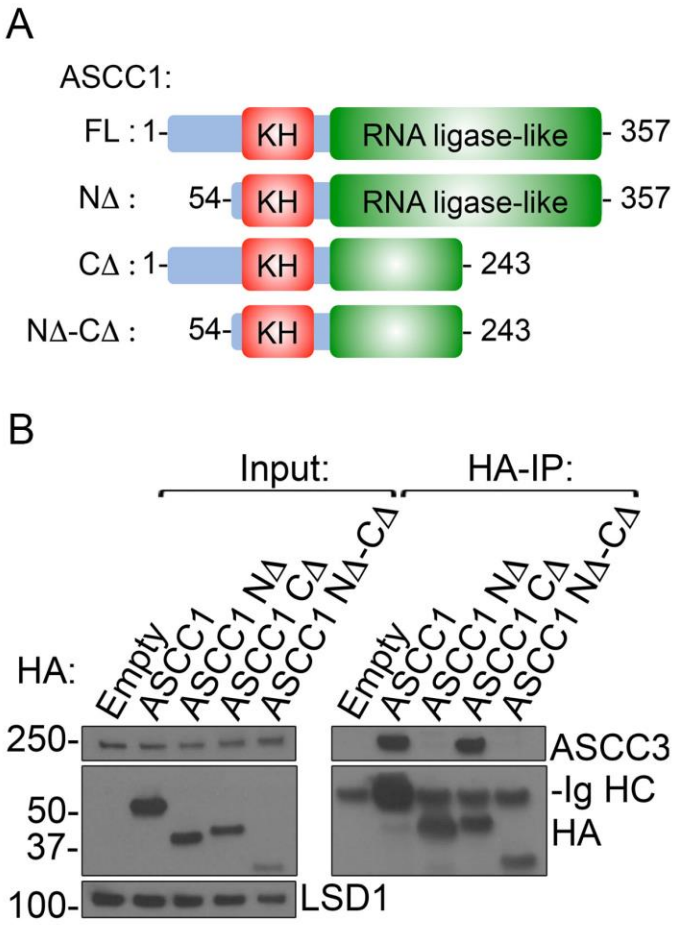

Figure 3.7. The N-terminal of ASCC1 Interacts with ASCC3. (A) Schematic of human ASCC1 domain structure and mutants (to scale). (B) HA-tagged ASCC1 FL or indicated ASCC1 deletions were expressed in 293T cells and immunoprecipitated using anti-HA resin. Immunoprecipitated HA-IP and input samples were analyzed using the indicated antibodies.

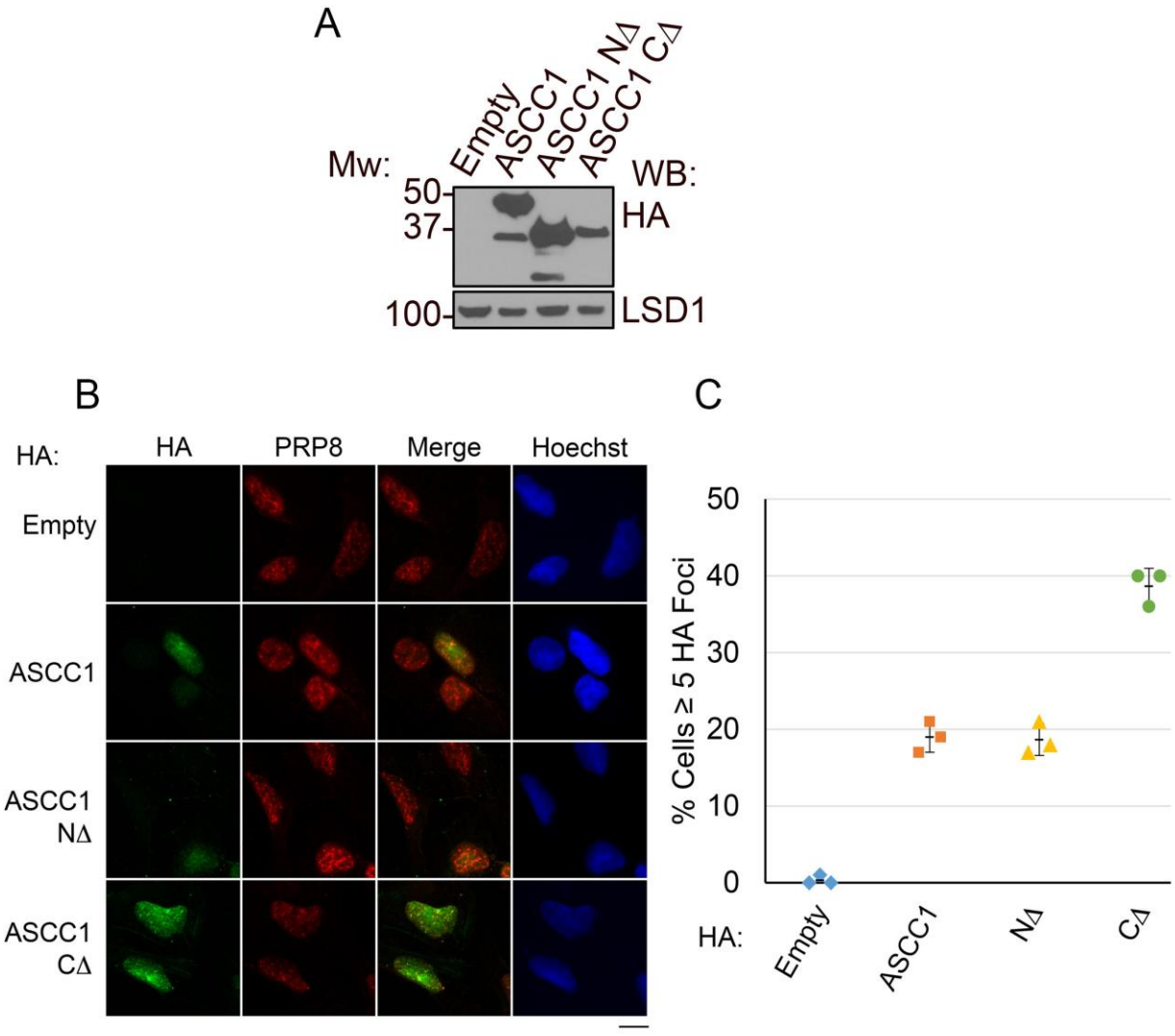

Figure 3.8. Deletion Analysis of ASCC1 Reveals Modular Functional Domains. (A) Whole cell lysates from U2OS cells expressing HA-tagged ASCC1 or indicated ASCC1 deletions were collected and expression was analyzed by Western blotting as shown. (B) U2OS ASCC1 KO cells expressing HA-tagged ASCC1 or indicated ASCC deletions were treated with MMS (0.5 mM) for 6 hours. Cells were processed for immunofluorescence using anti-HA and anti-PRP8 antibodies, with Hoechst used as the nuclear counter stain. Scale bars, 10 μm. (C) Quantification of (B). N=3 biological replicates of 100 cells per replicate and error bars indicate +/- S.D. of the mean.

WT ASCC1 or ASCC1-NΔ (Figure 3.8A). Together, these results suggest that different modular domains within ASCC1 have distinct functions during the alkylation damage response.

3.3.5 A Putative RNA-Binding Domain in ASCC1 Regulates ASCC Function

In analyzing the C-terminal RNA ligase-like domain of ASCC1, we noticed that it contains two conserved His-X-Thr (HXT) motifs, shown to be important for RNA or nucleotide binding in various proteins (Koonin and Gorbalenya, 1990). Examples of other proteins containing this motif in their nucleotide binding pocket include the 2'-5' RNA ligases from *Thermus thermophiles* and *Pyrococcus horikoshii*, as well as the AMP-binding protein AKAP18 (also known as AKAP7) (Figure 3.9A) (Koonin and Gorbalenya, 1990; Mazumder et al., 2002). Previous structural studies suggest that these HXT motifs line the substrate binding pocket and interact with the nucleotide through a pseudo 2-fold symmetry (Gold et al., 2008). We modeled this domain within ASCC1 using the Phyre2 server (Kelley et al., 2015; Kelley and Sternberg, 2009). The resulting structural analysis predicted that ASCC1 forms a similar overall structure to other members of the 2H phosphoesterase family (Figure 3.9B) (Silverman and Weiss, 2014). Furthermore, the predicted structure suggests that the conserved HXT motifs of ASCC1 are positioned such that they also line a putative nucleotide- or RNA-binding pocket similar to the aforementioned RNA ligases and AKAP18. Notably, the ASCC1 domain lacks residues critical for ligase activity (Figure 3.9C) (Doherty and Suh, 2000). We then mutated both of the HXT motifs of ASCC1 to AXA (ASCC1-AXA; $H_{179}LT \rightarrow A_{179}LA$ and $H_{277}AT \rightarrow A_{277}AA$) and analyzed its localization during MMS damage. As with ASCC1-CΔ, ASCC1-AXA retained foci under these conditions (Figure 3.10). This indicates that the HXT motifs of ASCC1 play a role in its localization during alkylation damage.

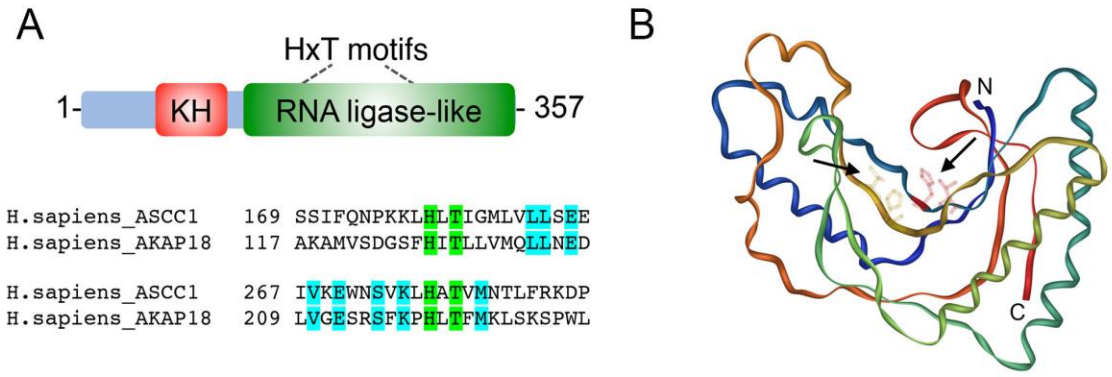

C

*h.sapiens*_ASCC1	196-	TCEMLQQCKEEFINDISGG
*h.sapiens*_DNA ligase 1	564-	TCEYKYDGQRAQIHALEGG
*t.thermophilus*_DNA ligase	114-	TVEHKVDGLSVNLYYEEGV
*e.coli*_RNA ligase	40-	VHTEKLDGENNCLNRYGVF
*e.coli*_DNA ligase	111-	CCELKLDGLAVSILYENGV

Figure 3.9. ASCC1 Contains a Putative RNA Binding Domain. (A) Schematic of the human ASCC1 protein is shown on top, with the positions of the HXT motifs (to scale). Sequence alignment with human AKAP18 is shown on bottom. The dual HXT motifs are highlighted in green, and neighboring conserved residues are highlighted in blue. (B) Predicted structure of ASCC1 (residues 132-355). The HxT motifs are indicated by arrows. This domain was modeled using the Phyre2 server. (C) Sequence alignment of conserved KxDG sequence motif found in DNA and RNA ligases. The active site lysine is shown in red.

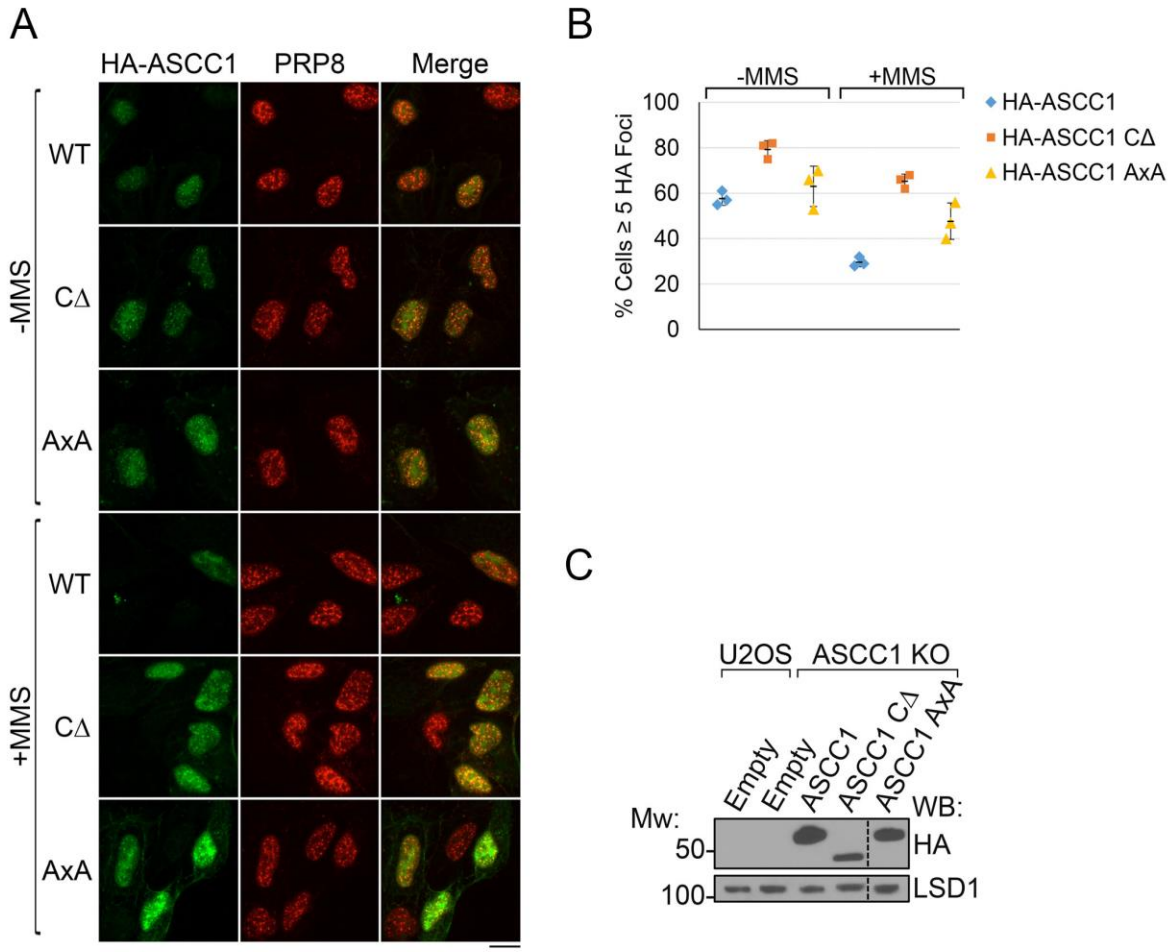

Figure 3.10. The HXT Motif has a Role in Localizing ASCC1 During Alkylation Damage. (A) U2OS ASCC1 KO cells expressing HA-tagged ASCC1 or indicated ASCC1 mutant were untreated or treated with MMS (0.5 mM) for 6 hours as indicated. Cells were processed for immunofluorescence using anti-HA and anti-PRP8 antibodies, with Hoechst as the nuclear counterstain. (B) Quantification of (A). Only cells with ≥ 5 HA foci were scored. N=3 biological replicates of 100 cells and error bars indicate +/- S.D. of the mean. (C) Whole cell lysates from U2OS WT and ASCC1 KO cells expressing HA-tagged ASCC1 FL or indicated ASCC1 mutant were analyzed by Western blotting..

Since the C-terminus of ASCC1 appeared to be critical for regulating its ability to form foci, we asked whether the RNA ligase-like domain played a role in foci formation of other complex components during alkylation damage. To address this question, we rescued ASCC1 knockout cells by expressing exogenous ASCC1 WT, ASCC1-CΔ, or ASCC1-AXA (Figure 3.11A). While the wild-type ASCC1 partially rescued HA-ASCC2/ASCC3 foci co-localization, neither ASCC1-CΔ nor ASCC1-AXA was able to rescue this phenotype (Figure 3.11B-C). Thus, this putative RNA ligase-like domain of ASCC1 plays an important role in the regulation of the ASCC complex localization upon alkylation damage.

3.3.6 ASCC1 is Important for Alkylation Resistance

The previous results suggested that ASCC1 may play a key role in modulating ASCC recruitment during alkylation damage. Therefore, we tested whether ASCC1 was functionally important for alkylation damage resistance in PC-3 prostate cancer cells. ASCC1 was knocked out in these cells using CRISPR/Cas9. Loss of ASCC1 resulted in an increase in sensitivity to MMS in these cells (Figure 3.12A). Again, this increase in sensitivity was observed with two distinct ASCC1 knockout clones. To determine whether this decrease in cell survival in response to MMS was due to the function of ASCC1 within the ASCC complex, or whether this was due to its function in another pathway, we created ASCC1-ASCC3 double knockout cells (ASCC1/3 DKO). We sequentially knocked out ASCC3 in PC-3 cells, and then knocked out ASCC1 using CRISPR/Cas9 (Figure 3.12B). MMS sensitivity of all four resulting genotypes was then tested. Consistent with our previous work, loss of ASCC3 increased sensitivity to MMS (Dango et al., 2011). However, the ASCC1/3 DKO cells did not have an increase in MMS sensitivity compared to either the single knockout cell lines of ASCC1 or ASCC3 respectively (Figure 3.12C). These results support the notion that ASCC1 has an epistatic relationship with ASCC3 in alkylation damage resistance. Taken together, our data supports a role for ASCC1 in controlling the ASCC complex recruitment and function during the cellular response to alkylation damage.

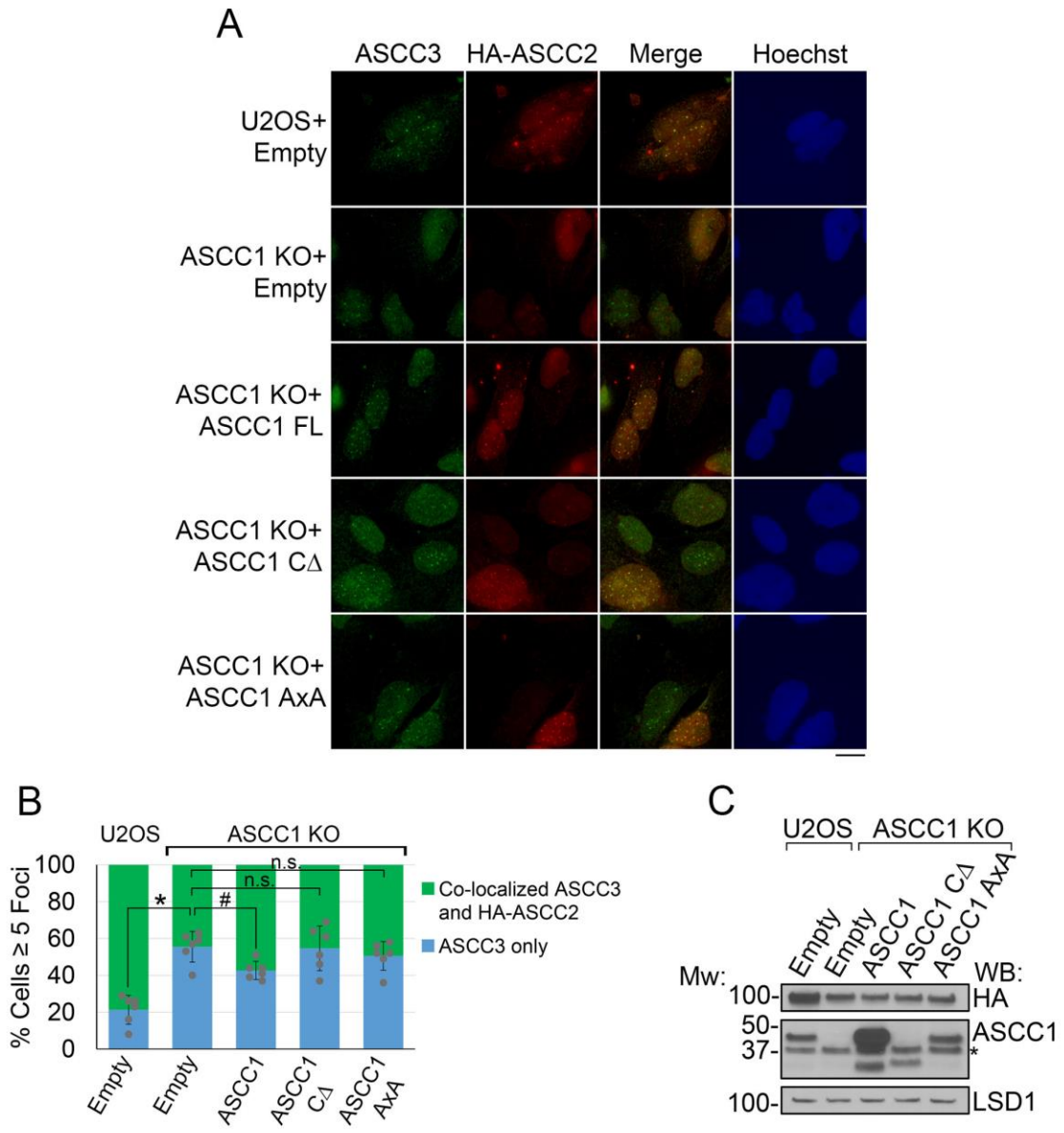

Figure 3.11. The HXT Motif Helps Coordinate ASCC2 and ASCC3 During MMS Treatment. (A) U2OS WT and ASCC1 KO cells expressing HA-tagged ASCC2 and untagged ASCC1 WT or indicated mutations were treated with MMS (0.5 mM) for 6 hours. Cells were processed for immunofluorescence using anti-HA and anti-ASCC3 antibodies, with Hoechst used as the nuclear counterstain. Scale bars, 10 μm. (B) Quantification of (A). N=6 biological replicates of 100 cells and error bars indicate +/- S.D. of the mean. * = $p < 0.001$; # = $p < 0.05$. (C) Whole cell lysates from U2OS WT and ASCC1 KO cells expressing HA-tagged ASCC2 and untagged ASCC1 FL or indicated ASCC1 mutant were analyzed by Western blotting. Asterisk (*) indicates Ig heavy chain.

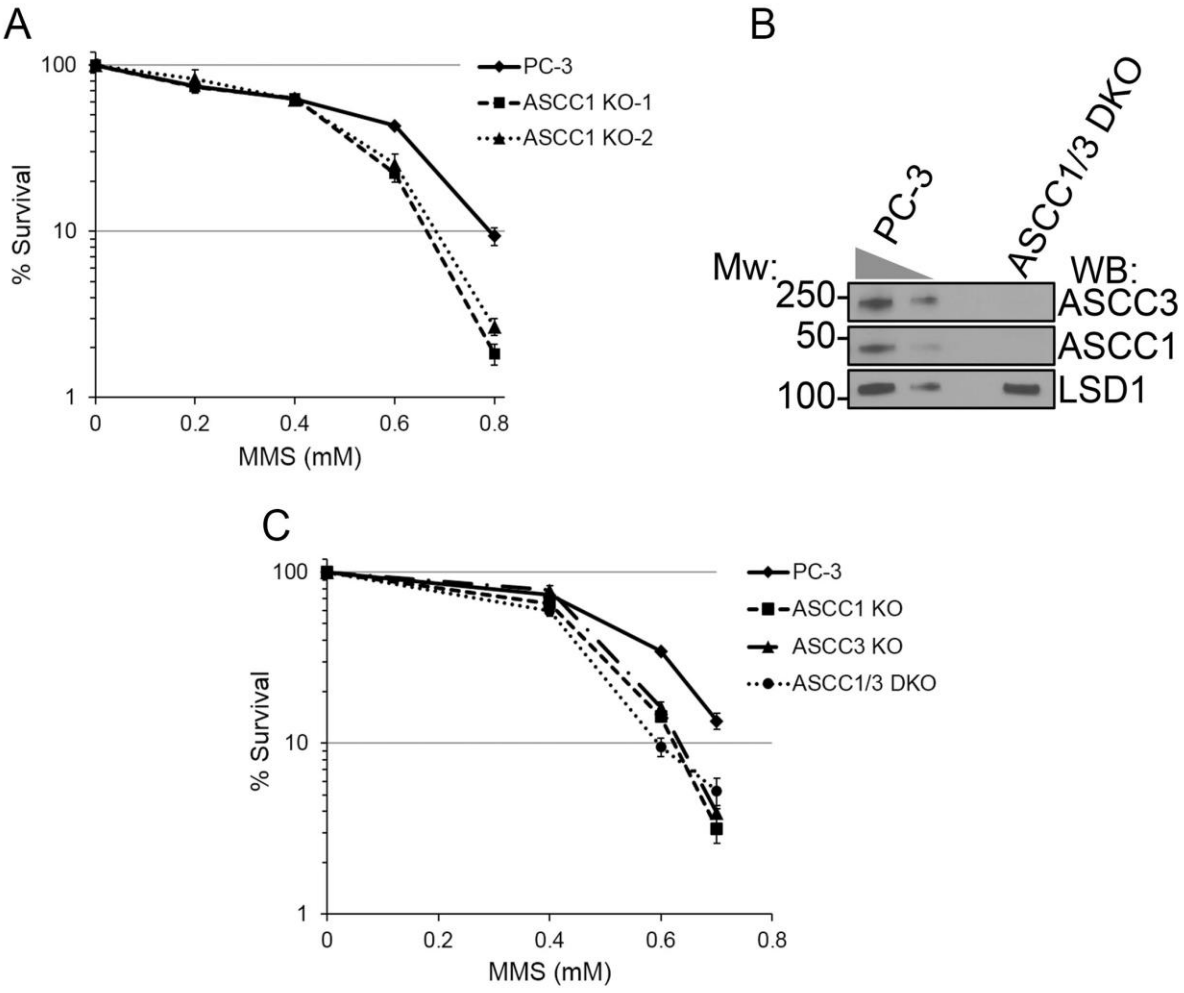

Figure 3.12. ASCC1 Confers Resistance to Alkylation Damage. (A) PC-3 ASCC1 KO cells were assessed for sensitivity to MMS relative to WT PC-3 cells. Cells survival was measured by MTS assay. N=5 and error bars indicate +/- S.D. of the mean. (B) Whole cell lysates from PC-3 cells, as well as the PC-3 ASCC1/3 double-knockout (DKO) cells, were collected and analyzed by Western blotting as shown. (C) PC-3 ASCC1 KO, ASCC3 KO, and ASCC1/3 DKO cells were assessed for sensitivity to MMS relative to WT PC-3 cells. Cells survival was measured by MTS assay. N=5 and error bars indicate +/- S.D. of the mean.

3.4 Discussion

We recently described a signaling pathway that is activated by alkylation damage to recruit the ALKBH3-ASCC complex to nuclear foci (Brickner et al., 2017). This pathway is dependent upon the RNF113A E3 ligase, which induces K63-linked ubiquitination that is then recognized by the ASCC2 subunit of the ASCC complex (Brickner et al., 2017). Here, we present evidence for additional regulation of this pathway by ASCC1. Our work suggests that ASCC1 is constitutively present at nuclear speckle foci prior to damage but leaves these foci upon MMS treatment. In addition, ASCC1 can interact directly with ASCC3 and thus modulate its localization during alkylation damage. Consistent with a role in this pathway, knockout of ASCC1 sensitizes cells to alkylation damage. Loss of ASCC1 does not further increase the sensitivity of cells that lack ASCC3, suggesting that the role of ASCC1 in the alkylation damage response is primarily through the ASCC complex.

Surprisingly, unlike ASCC2 or ASCC3, ASCC1 is already present at nuclear foci in the absence of any damage. Upon alkylation damage, ASCC1 is removed from these foci (Figure 3.3A-C). This phenomenon depends on the C-terminal domain of ASCC1, and more specifically, its HXT motifs (Figures 3.8 and 3.10). At the same time, ASCC1 can bind directly to ASCC3 via its N-terminus (Figure 3.1). This physical interaction and the dynamic localization of ASCC1 during alkylation provides the basis for the rational of our preferred model to explain the resulting phenotypes from ASCC1 deficient cells (Figure 3.13). We hypothesize that ASCC1 is acting as a specificity determinant for ASCC3 localization at these foci. In wild-type cells, we observe that the vast majority of the ASCC3 foci are positive for ASCC2 (Figure 3.6). In the ASCC1 knockout cells, although ASCC3 foci are significantly increased, the majority of these lack ASCC2. Thus, there are likely two subsets of ASCC3 foci: those that are positive for ASCC2 and

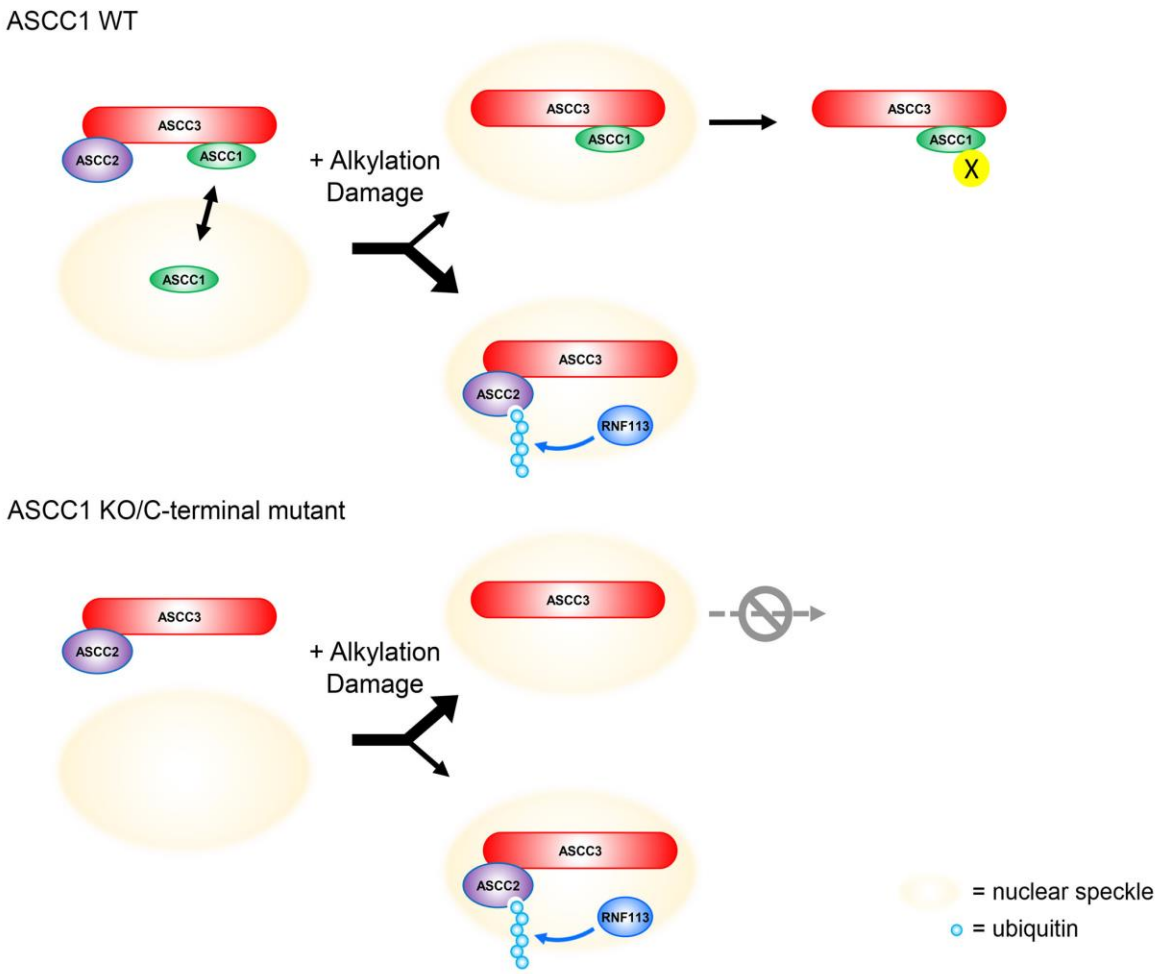

Figure 3.13. Proposed Model of ASCC Complex Localization During Alkylation Damage. Proposed model for ASCC complex localization during alkylation damage. In WT cells (36), RNF113a mediated ubiquitination is recognized by ASCC2 and recruits ASCC3 to nuclear speckle foci. Simultaneously, a fraction of ASCC3 is recruited to ASCC2 negative foci, but these are removed by ASCC1. This activity of ASCC1 is dependent upon the C-terminus RNA ligase-like domain via the engagement of an unknown ligand ("X"). In ASCC1 KO/C-terminal mutant cells (bottom), the fraction of ASCC3 foci that are independent of ASCC2 is significantly increased.

those that are negative for ASCC2. In wild-type cells, the fraction of ASCC3 present at foci without ASCC2 is likely removed in a manner dependent on ASCC1. This is consistent with the observation of increased ASCC3 foci formation in ASCC1 knockout cells. The failure of ASCC3 to be removed from these ASCC2-negative foci by ASCC1 would explain the observation that more ASCC3 foci lack ASCC2 in ASCC1 knockout cells. Our immunoprecipitation results further confirms thus notion (Figure 3.6).

Why does an increase in ASCC3 foci formation lead to increased alkylation damage sensitivity? This phenotype is potentially due to the necessary regulation of ASCC3 recruitment by ASCC1. In double-stranded break repair, the loss of the repair protein 53BP1 increases BRCA1 recruitment, but this leads to increased sensitivity to γ-irradiation, at least partly due to the recruitment of BRCA1 in the G1 phase of the cell cycle (Daley and Sung, 2014). This inappropriate recruitment and attempt at homologous recombination in G1 is thought to be deleterious in double-strand break repair. In like manner, in the absence of ASCC1, inappropriate ASCC3 recruitment may cause alkylation damage sensitivity because other repair factors are displaced, or a portion of ASCC3 needs to be removed for repair to be promptly completed. It is also possible that, in the absence of ASCC1, the complex cannot function properly, and alkylation damage sensitivity is increased despite an increase in ASCC3 recruitment.

The C-terminal RNA ligase-like domain of ASCC1, which appears to be critical for the function described here, is part of a larger 2H phosphoesterase family of enzymes that have been shown to harbor diverse activities, including *bona fide* tRNA ligases, phosphodiesterases, and putative RNA binding factors (Mazdumer et al., 2002; Silverman and Weiss, 2014). Structural studies on the phosphoesterase domain of AKAP18 initially suggested a proclivity for binding to AMP and CMP in a manner that is dependent upon its HXT motifs (Gold et al., 2008). It is intriguing that

AKAP18 binds to the same nucleotides that are the major reaction products for the ALKBH3 dealkylase activity, which primarily targets 1-methyladenine and 3-methylcytosine for demethylation. We currently do not have any direct evidence for the binding of ASCC1 to AMP or CMP. However, the importance of this domain in ASCC1 foci formation strongly implies that substrate binding through this domain, whatever its biochemical identity, plays a role in ASCC complex recruitment and function.

3.5 Materials and Methods

Plasmids. Human ASCC1 cDNA was isolated by RT-PCR from total human RNA, cloned into pENTR-3C (Invitrogen), and subcloned into pMSCV-Flag, pMSCV-Flag-HA, or pHAGE-CMV-3X-HA by Gateway recombination (Sowa et al., 2009). ASCC1 deletions and point mutations were created by PCR and cloned as above. ASCC2, ASCC3, and ALKBH3 vectors were previously described (Brickner et al., 2017). For recombinant protein expression, wild-type ASCC1, ASCC1 mutants, and ASCC2 were subcloned into pGEX-4T1 or pET28a-Flag. For expressing the 6X-His-tagged full-length ASCC3 and NΔ-ASCC3 (401-2202), the pENTR-3C vectors containing these cDNAs were subcloned into pDEST10 (Invitrogen). All constructs produced by PCR were verified by Sanger sequencing.

CRISPR/Cas9 mediated knockouts. U2OS and PC-3 KO cells were created using CRISPR/Cas9 genome editing at the Genome Engineering and iPSC Center (GEiC) at Washington University School of Medicine (St. Louis). The U2OS ASCC3 KO cells were previously described (Brickner et al., 2017). The gRNA sequences used to generate the ASCC1 KO cell lines were: 5'-AAGGATTCCGGTCTACTTTGNGG-3' and 5'- AAGTAGACCGGAATCCTTGTNGG-3'. The gRNA sequences used to generate the PC-3 ASCC3 KO cell line was 5’-

GACATTTGAAAAGGAACGCANGG-3'. All knockout clones were verified by deep sequencing or by Western blot analysis.

Cell culture, viral transduction, and cell survival assays. U2OS, PC-3, 293T, and Sf9 cells were cultured and maintained as previously described (Zhao et al., 2015). Preparation of viruses, transfection, and viral transduction were also performed as previously described (Zhao et al., 2015). For knockout cell foci rescue experiments, U2OS cells were transduced with WT ASCC1 or ASCC1 mutants using the pMSCV retroviral vector and pHAGE-CMV-3X-HA-ASCC2. For DNA damaging agent survival assays using PC-3 cells, 4,000-15,000 cells/well were cultured overnight in 96-well plates in 100µl media. Cells were then exposed to medium containing the indicated concentration of MMS (Sigma) for 24 hours at 37 °C. The media was then replaced with normal media and cell viability was assessed 72 hours after initial exposure to MMS via the MTS assay (Promega). All MTS based survival experiments were carried out in quintuplicate.

Recombinant protein purification. For purification of the 6X-His tagged ASCC3 and NΔ-ASCC3, the baculovirus vector was produced using the Bac-to-Bac expression system (ThermoFisher). Amplified baculovirus was used to infect Sf9 cells and harvested after 72 hours. The cells were resuspended in Buffer L (20 mM Tris pH 7.3, 150 mM NaCl, 8% glycerol, 0.2% NP-40, 0.1% Triton X-100, 20 mM imidazole) plus protease inhibitors and frozen -80°C. Cells were lysed by sonication and rotated for 30 minutes at 4°C. The cell extracts were then centrifuged at 10,000 rpm for 10 minutes. The supernatant was incubated with Ni-NTA beads and eluted with Buffer L containing 400 mM imidazole. His-ASCC1 and GST tagged recombinant proteins were purified from *E. coli* as described (Zhao et al., 2015). All proteins were dialyzed into TAP buffer (50 mM Tris pH 7.9, 100 mM KCl, 5 mM $MgCl_2$, 0.2 mM EDTA, 0.1% NP-40, 10% glycerol, 2 mM 2-Mercaptoethanol, 0.2 mM PMSF) after purification.

Protein binding assays. All *in vitro* GST-protein binding assays were performed as previously described (Mosammaparast et al., 2013) with minor modifications. Briefly, 5 μg of GST-tagged bait protein was incubated with 10 μl of glutathione-Sepharose beads and 250 ng of 6X-His ASCC3 FL or NΔ-ASCC3, 1 μg of 6X-His ASCC1, or 500 ng K63-Ub_{3-7} in TAP buffer containing 1% BSA in a total volume of 100 μl. After incubation at 4°C with rotation for one hour, beads were washed extensively using TAP buffer. Bound material was eluted using Laemmli buffer and analyzed by SDS-PAGE and Western blotting.

Structural model. The model for the predicted structure of ASCC1 was generated using the publicly available Phyre2 server (Kelley et al., 2015; Kelley and Sternberg, 2009).

Statistical analysis. All p-values were calculated by unpaired, two-tailed Student's t-test.

Immunofluorescence microscopy. All immunofluorescence microscopy was done as previously described (Brickner et al., 2017; Mosammaparast et al., 2013). 100 cells were analyzed at least in biological triplicate for all quantifications.

Immunoprecipitation and Western blotting. Immunoprecipitation of HA-tagged ASCC1, ASCC1 mutants, and ASCC2 were performed by transfection of constructs into 293T cells using Transit293 reagent (Mirus Bio). Cells were treated with 0.5 mM MMS as indicated, collected and washed in 1X PBS, and frozen at -80°C. Cell pellets were resuspended in IP lysis buffer (50 mM Tris pH 7.9, 300 mM NaCl, 10% glycerol, 1% Triton X-100, 1 mM DTT, and protease inhibitors), lysed by sonication, and cleared by centrifugation. An equal volume of IP lysis buffer containing no salt was added (final concentration of NaCl was 150 mM). Lysates were then incubated with anti-HA resin (Santa Cruz) for 3-4 hours at 4°C with rotation. The beads were

washed extensively with IP lysis buffer containing 150 mM NaCl and bound material was eluted with Laemmli buffer.

Preparation of viruses, transfection, and viral transduction for immunoprecipitation of HA-tagged ASCC1 or HA-empty from PC-3 WT and ASCC3 KO cells was performed as previously described (Mosammaparast et al., 2013). Cells were selected with 1 μg/ml puromycin for 24 hours. The media was then replaced with normal media for two days after which cells were transfected with Flag-ASCC2. Cells were collected and washed in 1XPBS and frozen at -80°C two days after transfection. Immunoprecipitation was then executed as described above.

Endogenous immunoprecipitation was carried out by collecting the cells and freezing at -80°C as above. Cell pellets were resuspended in TAP buffer containing 300 mM KCl, lysed by sonication, and cleared by centrifugation. IP lysis buffer containing no salt was added to bring the final concentration of KCl to 100 mM. Samples were pre-cleared by incubation with Protein A/G beads (Santa Cruz) with rotation at 4°C. After centrifugation, the supernatant was then incubated with the relevant antibodies overnight at 4°C. Protein A/G beads were then added and rotated at 4°C one hour. The samples were then centrifuged and washed extensively with TAP buffer. Bound material was eluted with Laemmli buffer and analyzed by Western blot.

Antibodies. The antibodies and the concentration used for the given application are listed as following: ASCC3 (House; 1:500 IF; 1:100 IP; 1:2500 or 1:3000 Western), 6x-His (Abcam; 1:2500 Western), ASCC1 (Abcam; 1:1250 or 1:2500 Western), ASCC2 (Bethyl; 1:200 IP; 1:2500 Western), Flag (Sigma; 1:2500 Western), HA (BioLegend; 1:250 or 1:300 IF; 1:2500 or 1:5000 Western), HA (Santa Cruz; 1:2500 Western), HA (Abcam; 1:2500 Western), IgG (Sant Cruz; 1:200 IP), LSD1 (Santa Cruz; 1:2500 Western), LSD1 (Active Motif; 1:2500 Western),

pH2A.X (Abcam; 1:2000 IF), PRPF8 (Bethyl; 1:200, 1:400 or 1:600 IF), Ub P4D1 (Santa Cruz; 1:5000 Western), β-actin HRP (Sigma; 1:2500 or 1:5000 Western).

Chapter 4: Aberrant RNA Methylation Triggers Recruitment of the ASCC-ALKBH3 Repair Complex

Brickner JR, Tsao N, Oyeniran C, Zhang L, Rodell R, Soll JM, Ganguly A, Majid MC, He C, Mosammaparast N. *In preparation*.

4.1 Abstract

DNA repair is essential to prevent the cytotoxic or mutagenic effects of various types of DNA lesions, which are sensed by distinct pathways to recruit repair factors specific to the damage type. Although the roles of the effector proteins involved in these repair pathways have been well elucidated, the importance of RNA molecules in propagating efficient DNA repair is becoming more evident, particularly for double-strand break (DSB) repair. Specifically, RNA from an actively transcribed gene is readily available for RAD52-dependent strand invasion in the presence of a DSB to act as a template during homologous recombination (HR), providing an alternative, RNA-based approach for promotion of DNA repair (Mazina et al., 2017). However, whether RNA can direct DNA repair via the regulation and activation of other DNA repair pathways remains unclear. The abundance and availability of RNA for modification by alkylating agents (Fu et al., 2012) gives credence to the notion that RNA alkylation may play a similar role during alkylation damage repair. Here, we demonstrate that RNA alkylation is necessary and sufficient to recruit the ASCC complex. Overexpression of the 3-methylcytosine RNA methyltransferase METTL8 was capable of inducing the recruitment of ASCC3, even in the absence of alkylation damage. Conversely, overexpression of an AlkB homologue from the RNA virus blueberry scorch significantly reduced ASCC foci in the presence of methyl methanesulphonate (MMS). Similar to the recruitment of the ASCC-ALKBH3 complex,

RNF113A E3 ligase activity was specifically induced upon alkylation damage. Importantly, overexpression of METTL8 was also capable of activating RNF113A E3 ligase activity, even in the absence of alkylating agents. Taken together, our results strongly suggest that alkylated RNA is an activator to initiate the alkylation damage response by ASCC-ALKBH3.

4.2 Introduction

Maintaining genomic integrity is essential for cellular survival. To counteract challenges presented by various endogenous and exogenous genotoxins, cells have developed multiple DNA repair mechanisms that are necessary to ensure faithful replication, including double strand break (DSB) repair, base excision repair (BER), and transcription-coupled nucleotide excision repair (TC-NER) (Jackson and Durocher, 2013; Soll et al., 2017; Gregersen and Svejstrup, 2018). The majority of these pathways rely upon sensor proteins to recognize the damaged lesion. These proteins then interact with various transducer proteins to propagate a signaling cascade to recruit and activate the downstream mediator proteins that resolve the lesion to avoid genomic catastrophe. Recently, we showed that this "sensor-transducer-mediator" paradigm has been shown to be important for regulating the ASCC-ALKBH3 repair complex during alkylation damage (Brickner et al., 2017).

While the majority of studies regarding DNA repair have focused on elucidating the roles of the various proteins involved in these pathways, the importance of various RNA molecules in propagating efficient DNA repair is only recently becoming more evident (Yang and Qi, 2015; Thapar 2018). RNA-directed DNA repair appears to be important for DSB repair. The first evidence for RNA-directed DNA homologous recombination (HR) demonstrated that both yeast and human cells could utilize synthetic RNA oligonucleotides as the template for HR of DNA (Storici et al., 2007; Shen et al., 2011). Interestingly, *cis*-RNA (i.e., same locus) of an actively

transcribed gene was readily available for strand invasion in the presence of a DSB in a manner dependent upon RAD52 (Keskin et al., 2014; Mazina et al., 2017), suggesting that an endogenous RNA transcript can direct HR during DSB repair.

In addition to endogenous RNA transcripts, other RNA molecules such as long non-coding RNAs (lncRNAs) and micro RNAs (miRNAs) may dictate DNA repair. Several lncRNAs have been identified as either oncogenes or tumor suppressors (Thapar 2018). A majority of these RNAs modulate DSB repair by regulating the activity and expression of p53 (Huarte et al., 2010; Mahmoudi et al., 2016). Importantly, lncRNAs also regulate the DNA damage response (DDR) by tethering chromatin remodeling factors to the damage site or by serving as a scaffold for important repair proteins such as KU70/80 and RNF169 (Wan et al., 2013; Maringele et al., 2002; Deng et al., 2019). Similar to lncRNAs, miRNAs regulate the DSB response by modulating the protein levels of DSB repair factors (Tessitore et al., 2014). Taken together, these data support the notion that the regulation of DNA repair at both the protein and template level may be mediated by RNA molecules. While the role of RNA is best characterized for HR, it remains unclear if RNA has a role in promoting other types of DNA repair.

RNA itself is subject to extensive modification, including modification by alkylating agents (Thapar et al., 2018; Fu et al., 2012). Interestingly, certain modifications induced by alkylating agents, such as 1-methyladenine (m1A) and 3-methylcytosine (m3C), also occur endogenously via methyltransferases. The RNA-specific methyltransferase METTL8 has been shown to deposit m3C on mRNA in human cells (Xu et al., 2017), although the role of this modification is unknown. The role of the m1A modification on RNA has recently become more apparent. m1A is primarily found in the 5’-UTR of mRNAs and may promote translation initiation via the m1A reader protein YTHDF3 (Dominissini et al., 2016; Dai et al., 2018). The AlkB homologue

ALKBH3 acts as the eraser of m1A and m3C on RNA (Aas et al., 2003). Intriguingly, ALKBH3 repairs m1A and m3C on DNA in concert with the ASCC complex (Dango et al., 2011; Brickner et al., 2017). Recruitment of this repair complex is strictly limited to alkylation damage and does not respond to other damaging agents (Brickner et al., 2017). However, the basis for this selectivity toward alkylation remains unknown.

As RNA is several fold more abundant than DNA in the cell and thus more readily available for modification (Vagbo et al., 2013; Thapar et al., 2018), we hypothesized that RNA alkylation may serve as an upstream activator of the ASCC-ALKBH3 repair complex. Here, we demonstrate that RNA alkylation is necessary and sufficient to recruit the ASCC-ALKBH3 complex. Overexpression of an AlkB homologue from an RNA virus significantly reduced HA-ASCC2 foci in the presence of methyl methanesulphonate (MMS). Conversely, overexpression of the RNA methyltransferase METTL8 was capable of recruiting ASCC3, even in the absence of alkylation damage. We show that alkylation damage resulted in general transcriptional repression. Strikingly, the majority of transcripts repressed during alkylation damage were de-repressed upon loss of ASCC3. Similar to the ASCC-ALKBH3 complex, RNF113A E3 ligase activity was specifically induced upon alkylation damage. Importantly, overexpression of METTL8 was also capable of activating RNF113A E3 ligase activity, even in the absence of alkylating agents. Taken together, our results strongly suggest that alkylated RNA is an activator to initiate the alkylation damage response and transcriptional repression by the ASCC complex.

4.3 Results

4.3.1 RNA Alkylation is Necessary to Mediate ASCC Recruitment

We previously reported the discovery of a nuclear ubiquitin-dependent signaling pathway that is specifically required for recruiting the ASCC complex to mediate alkylation damage

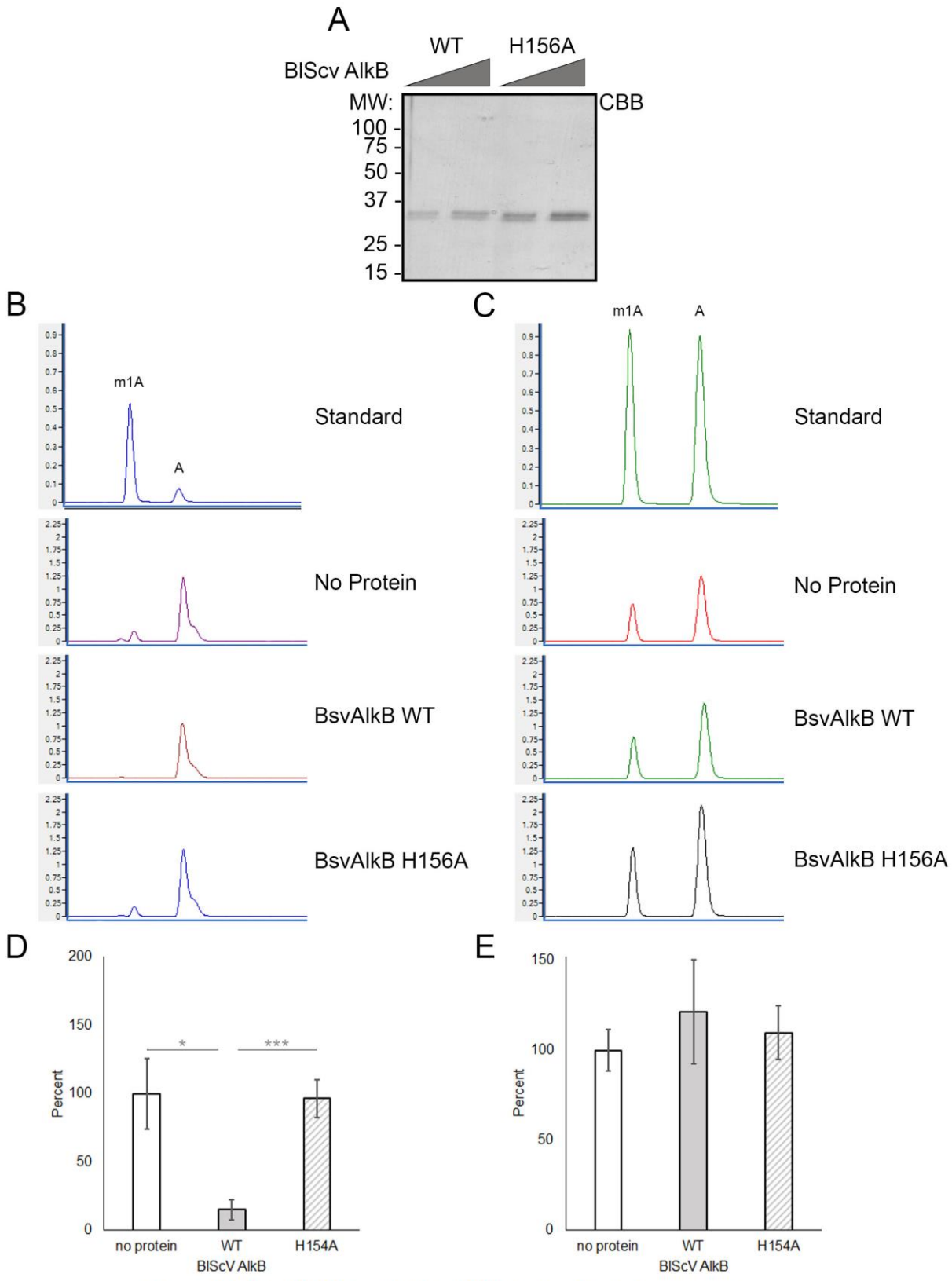

Figure 4.1. BsvAlkB Demethylates RNA *in vitro*. See below for caption.

Figure 4.1. BsvAlkB Demethylates RNA *in vitro*. (A) His-BsvAlkB was purified on Ni-NTA, separated on a 10% SDS-PAGE gel, and analyzed by Coomassie blue staining. (B) and (C) Example LC-MS chromatograms for either ssRNA (B) or ssDNA (C) containing m1A. Standards are shown at the top. A methylated RNA or DNA oligo were treated with either wild-type BsvAlkB or the H156A mutant and then processed by MS. A methylated oligo without addition of protein served as the control. Note the reduction of the m1A peak in the BsvAlkB WT sample. See Methods for oligo sequences. (D) and (E) Quantitation of 1mA/A levels on RNA (D) and DNA (E) after treatment with BsvAlkB WT or H156A protein. (n=5 biological replicates; mean ±S.D.; two-tailed *t*-test, * = $p < 0.05$, *** = $p < 0.001$.

responses (Brickner et al., 2017). However, the mechanistic basis for this alkylation damage selectivity remains unclear. We reasoned that the specificity of this pathway towards alkylation may be due to modification of RNA, consistent with the fact that RNA is more readily modified by alkylation relative to DNA (Vagbo et al., 2013; Thapar et al., 2018). To test whether RNA was necessary for the recruitment of ASCC, we cloned and expressed an AlkB homologue from blueberry scorch virus, an RNA virus (Figure 4.1A). This dealkylase was active on RNA but not DNA substrates *in vitro* (Figure 4.1B-E). Expression of BsvAlkB as an NLS-fusion targeted it to the nucleus (Figure 4.2A). Strikingly, BsvAlkB-NLS expression significantly reduced HA-ASCC2 foci formation during MMS damage (Figure 4.2B-C), suggesting that RNA alkylation is indeed necessary to recruit the ASCC-ALKBH3 complex during alkylation damage. This reduction depended on the enzymatic activity of BsvAlkB, as the H156A catalytic mutation was significantly less capable of countering ASCC2 foci formation.

4.3.2 RNA Alkylation is Sufficient to Mediate ASCC Recruitment

To test if RNA alkylation is sufficient to activate RNF113A and recruit the ASCC complex, we turned to RNA methyltransferases that produce methylated base lesions that are also created by chemical agents. We cloned the METTL8 methyltransferase, which is thought to produce 3-methylcytosine (m3C) on mRNAs (Xu et al., 2017). While the function of this modification on mRNA is unclear, it is one of the major modifications produced on RNA by MMS and is countered by the AlkB family of enzymes (Aas et al., 2003; Yan and Zaher, 2019). Flag-METTL8 is nominally cytoplasmic but was targeted to the nucleus, and particularly the nucleolus, when fused to the SV40 NLS (data not shown, Figure 4.3A). Strikingly, ectopic expression of wild-type METTL8-NLS induced recruitment of the ASCC3

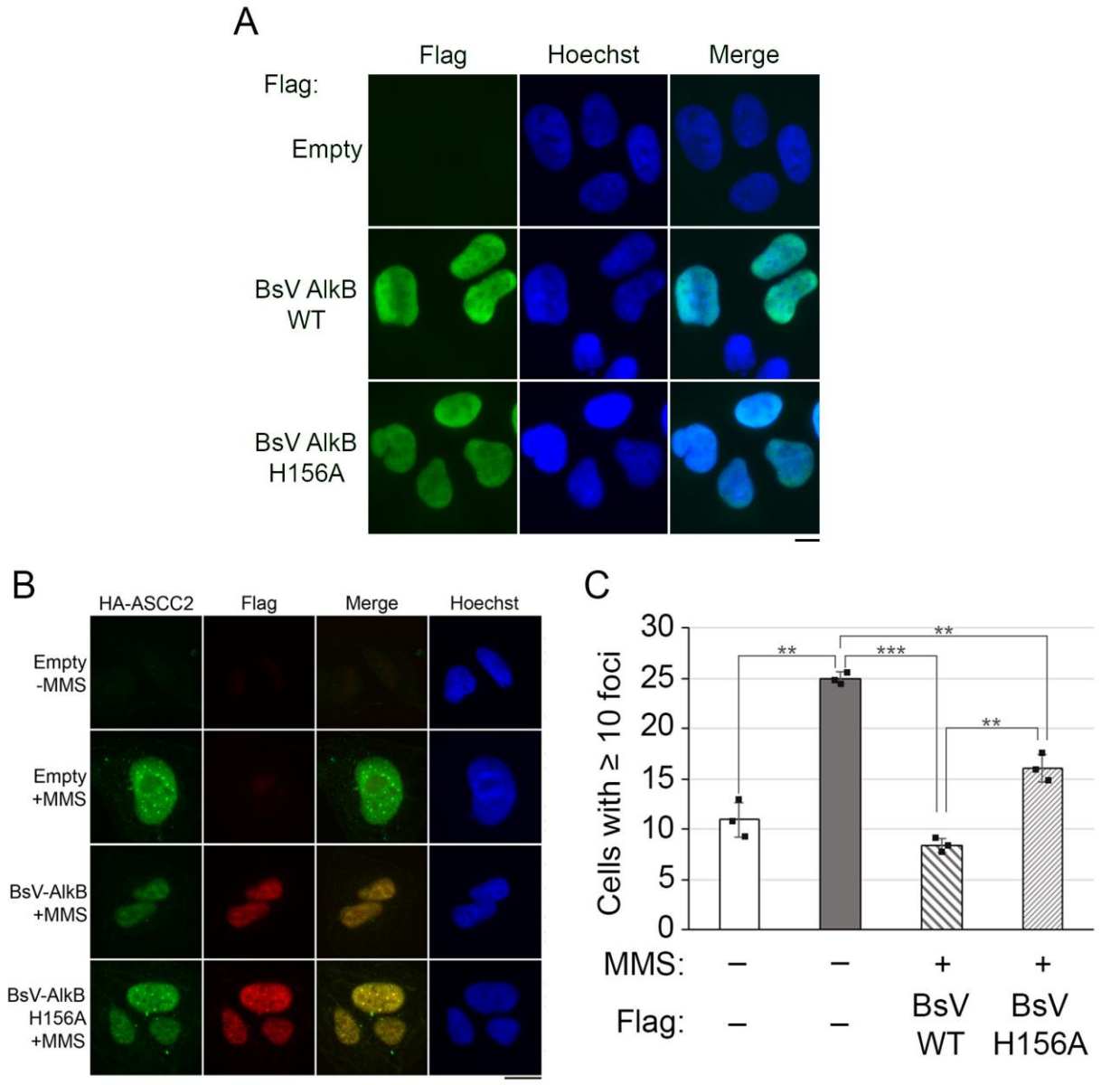

Figure 4.2. BsvAlkB Overexpression Reduces ASCC2 Foci During Alkylation Damage. (A) Images of cells expressing either Flag-BsvAlkB WT or BsvAlkB H156A. (n=3 biological replicates). (B) Representative images of HA-ASCC2 and pH2A.X in cells expressing Flag-BsvAlkB WT or H156A after MMS treatment. (C) Quantitation from (B). (n=3 biological replicates; mean ± S.D.; two-tailed *t*-test, ** = $p < 0.001$; *** = $p < 0.0001$). Scale bars, 10 μm.

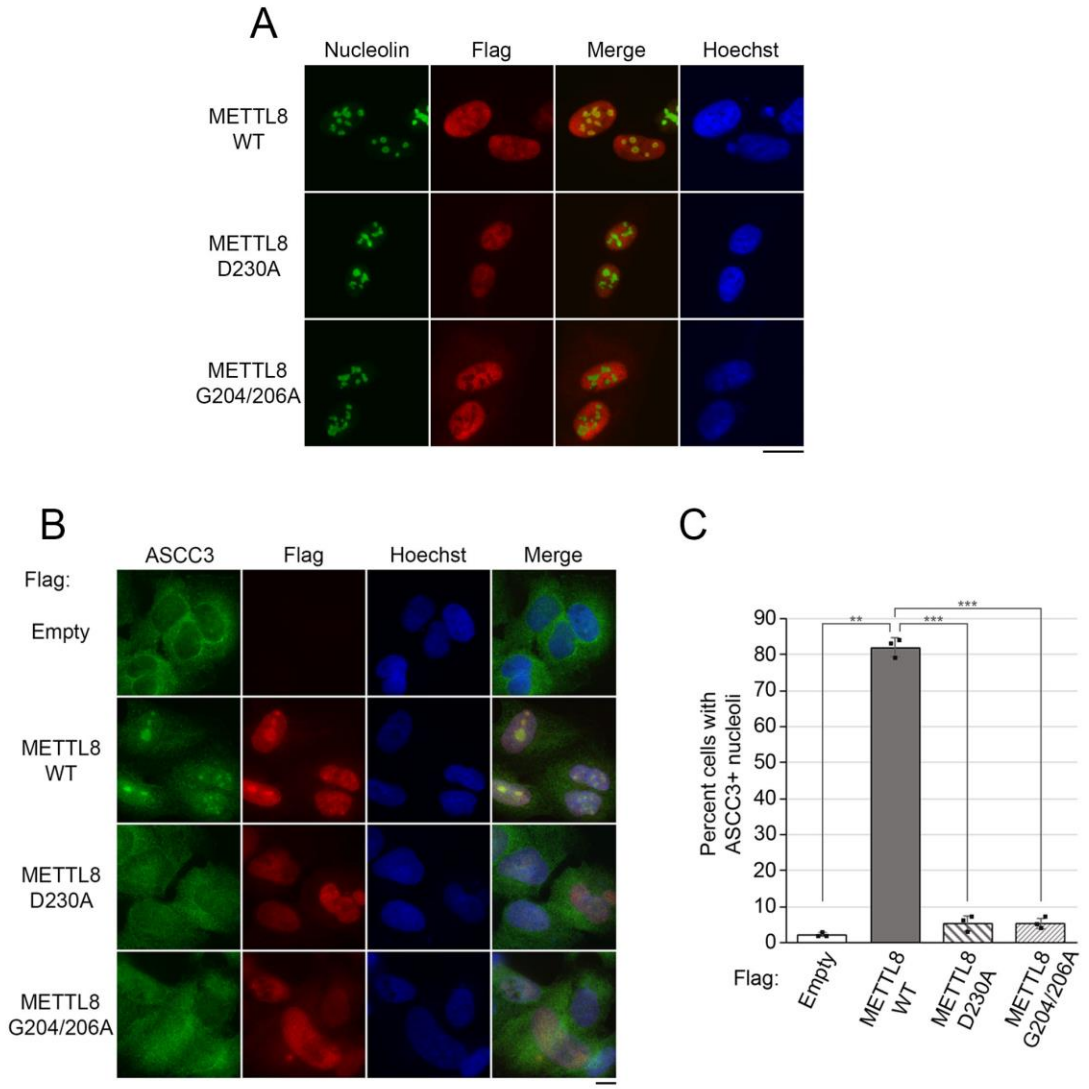

Figure 4.3. METTL8-NLS Induces Nucleolar Localization of ASCC3. (A) Images of cells expressing either Flag-METTL8 WT, the G204A/G206A mutant or the D230A mutant processed for immunofluorescence with Flag and Nucleolin. (n=3 biological replicates). (B) Representative images of ASCC3 and Flag-METTL8 in cells expressing METTL8 WT, G204A/G206A or D230A. (C) Quantitation from (B). (n=3 biological replicates; mean ± S.D.; two-tailed *t*-test, ** = $p < 0.001$; *** = $p < 0.0001$). Scale bars, 10 μm.

helicase to nucleolar regions, which coincided with the localization of the active methyltransferase (Figure 4.3B-C). Two catalytic mutations targeting the SAM-binding domain of METTL8 (G204A/G206A and D230A) (Alexandrov et al., 2005) failed to recruit ASCC3 (Figure 4.3B-C). Although the m3C activity of wild-type METTL8 was modest, the G204A/G206A mutant was in fact deficient for 3-methylcytosine RNA methyltransferase activity, as determined by MS/MS (data not shown). We noted that these mutant METTL8-NLS proteins did not localize as robustly to nucleoli compared to the wildtype counterpart (Figure 4.3B), which could alternatively explain the impairment of ASCC3 nucleolar recruitment. To address this potential concern, we utilized a single locus reporter system where we could target this methyltransferase (Shanbhag et al., 2010; Janicki et al., 2004). In this system, fusing a degron-tagged METTL8-NLS to mCherry-LacI allows for targeted recruitment of this RNA methyltransferase to the single locus (Figure 4.4A). Cells expressing either mCherry-LacI or METTL8-mCherry-LacI fused to a degron tag were recruited to this locus upon treatment with 300 nM Shield-1 (Figure 4.4B-C). As with the nucleolar targeting of ASCC3 with wildtype METTL8-NLS, we found that METTL8 induces ASCC3 recruitment to this locus in a manner dependent upon active transcription (Figure 4.4D-E). Taken together, our results support the notion that aberrant RNA methylation is necessary and sufficient to recruit the ASCC complex.

4.3.2 ASCC-mediated Transcriptional Repression in Response to Aberrant RNA Alkylation

Previous work using various genotoxins have revealed that such damage generally elicits a repressive transcriptional response, either locally or globally (Jelinsky and Samson, 1999; Silva and Ideker, 2019). We reasoned that alkylation damage may also result in transcriptional repression. Indeed, we found that MMS treatment results in a greater number of

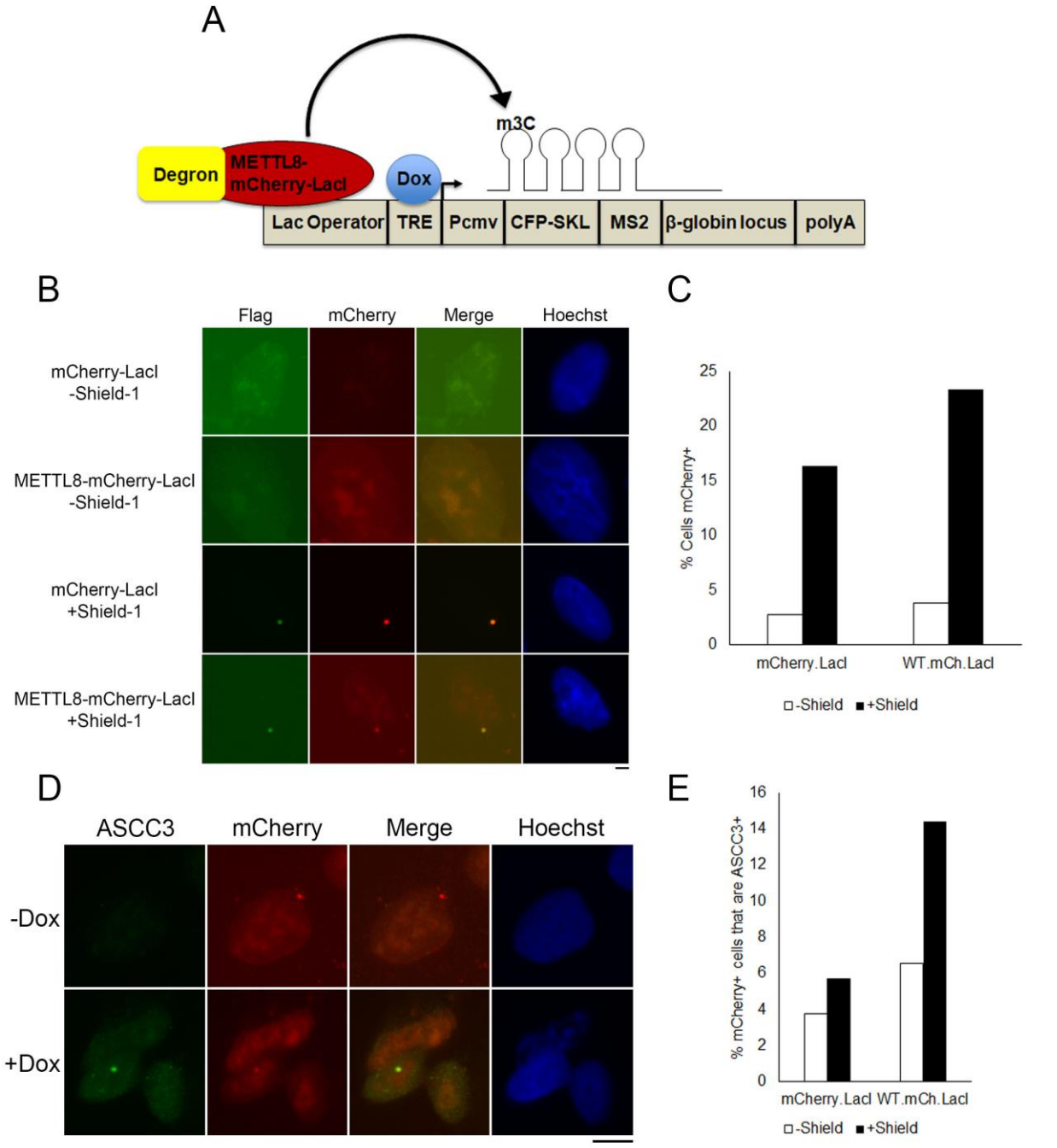

Figure 4.4. METTL8 Induces ASCC3 Localization to the Lac Operon. (A) Schematic of the Lac Operon cell line to induce targeted ASCC localization. (B) Representative images of cells expressing mCherry-LacI or METTL8-mCherry-LacI treated with 300 nM Shield-1 for 24 hours. Cells were processed for immunofluorescence with Flag. Hoechst was used as the counter stain. (C) Quantitation of (B). (n=1 biological replicate; mean). (C) Representative images of ASCC3 foci in cells expressing METTL8-mCherry-LacI with or without Dox (1ug/ml; 24 hours). Cells were processed for immunofluorescence with anti-ASCC3. Hoechst was used as the counter stain. (D) Quantitation of (E). (n=1 biological replicate; mean).

downregulated versus upregulated genes (data not shown). During alkylation treatment, 357 genes were significantly downregulated using a log2 fold change threshold. Strikingly, we found that 347 of the 357 genes (97%) repressed during alkylation are derepressed upon loss of ASCC3, again using the log2 fold change threshold. This data suggests that this complex has a major role in transcriptional repression during alkylation damage (data not shown). Together, this supports the notion that that the ASCC complex acts primarily as a transcriptional repressor during alkylation damage.

4.3.3 Selective Activation of RNF113A E3 Ligase Activity Upon Alkylation

A key factor in this pathway is the E3 ubiquitin ligase RNF113A, which we reasoned could be selectively activated during alkylation, similar to ASCC-ALKBH3 (Brickner et al., 2017). Many E3 ubiquitin ligases are autoubiquitinated when activated (Mallery et al., 2002; Ben-Saadon et al., 2006), and decided to analyze RNF113A ubiquitination status by denatured immunoprecipitation after expressing HA-RNF113A and His-Ub in HeLa cells. Indeed, we found that RNF113A is ubiquitinated in cells upon MMS treatment (Figure 4.5A). This likely represented RNF113A autoubiquitination, as inactivation of the RING domain abrogated RNF113A ubiquitination during MMS treatment (Figure 4.5B). Strikingly, other types of damaging agents, including hydroxyurea (HU), bleomycin (Bleo), or camptothecin (CPT) were not capable of inducing RNF113A autoubiquitination (Figure 4.5A), consistent with the specificity for alkylation damage observed with the ASCC-ALKBH3 repair complex. Using tandem ubiquitin binding element (TUBE) conjugated beads to isolate ubiquitinated proteins, we found that endogenous RNF113A is also autoubiquitinated, again only with MMS but not the other types of damaging agents (Figure 4.6A). These agents all induced pH2A.X, suggesting damage signaling is occurring with all of these agents (data not shown). A

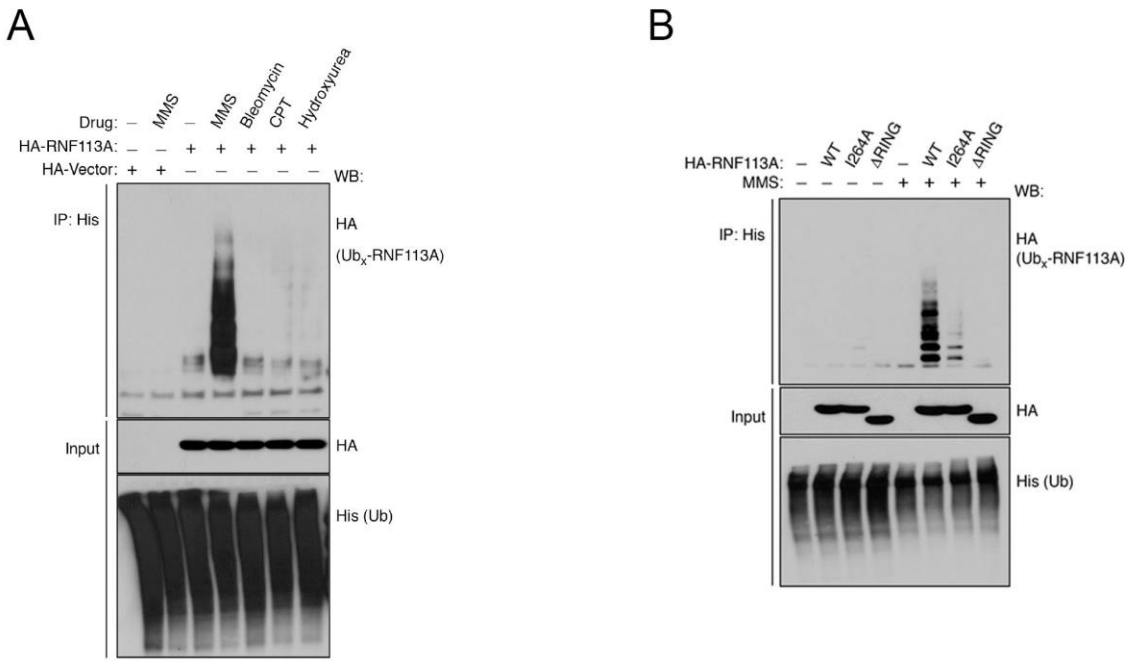

Figure 4.5. RNF113A E3 Ligase Activity is Activated by Alkylation. (A) HeLa cells expressing His-ubiquitin and HA-RNF113A were treated with various DNA damaging agents. Ubiquitinated proteins were isolated by Ni-NTA under denaturing conditions and Western blotted as shown. Input lysates were also analyzed as indicated. (n=3 independent experiments). (B) HeLa cells expressing His-ubiquitin and the indicated HA-RNF113A constructs were treated with MMS. Ubiquitinated proteins were isolated by Ni-NTA under denaturing conditions and Western blotted as shown. Input lysates were also analyzed as indicated. (n=3 independent experiments).

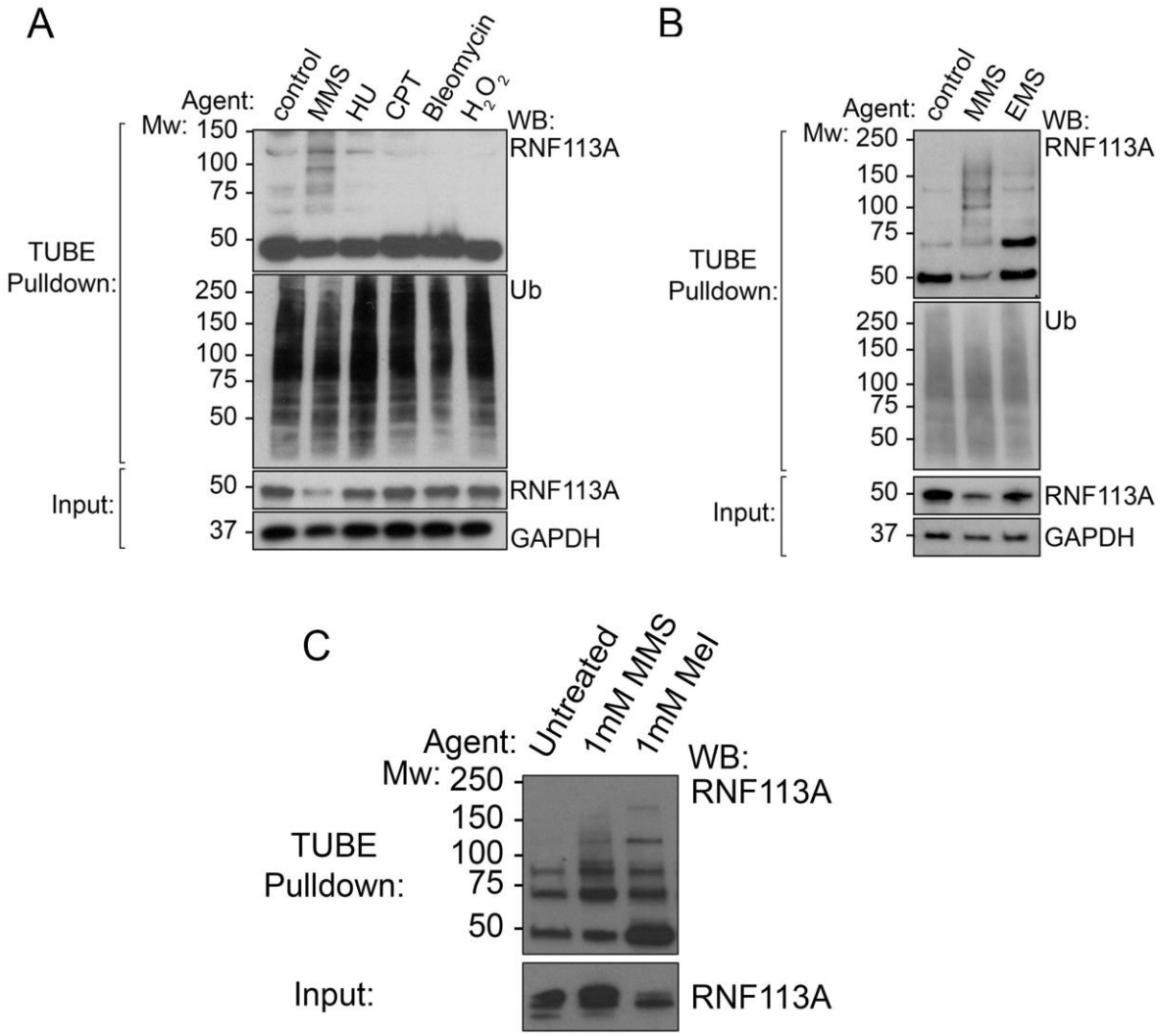

Figure 4.6. Alkylation Activates the E3 Activity of Endogenous RNF113A. (A) Endogenous ubiquitin was isolated from HeLa-S cells after treatment with various DNA damaging agents using ubiquilin TUBE beads and Western blotted for endogenous RNF113A. Input lysates were also analyzed as indicated (n=3 independent experiments). (B) Endogenous ubiquitin was isolated from HeLa-S cells after treatment with either 1mM MMS or 1mM EMS using ubiquilin TUBE beads and Western blotted for endogenous RNF113A. Input lysates were also analyzed as indicated (n=3 independent experiments). (C) Endogenous ubiquitin was isolated from HeLa-S cells after treatment with the indicated concentration of MMS or MeI using ubiquilin TUBE beads and Western blotted for endogenous RNF113A. Input lysates were also analyzed as indicated (n=1 independent experiments).

significant portion of the ubiquitin linkage associated with RNF113A during MMS treatment appeared to be K63-linked, consistent with previous findings that suggested that RNF113A functions with the K63-specific E3 ligase UBC13 (data not shown) (Brickner et al., 2017). The methylating agent methyl iodide also induced autoubiqitination of RNF113A but the ethylating agent EMS did not, suggesting that RNF113A is activated primarily by methylation (Figure 4.6B-C). This autoubiquitination of RNF113A was accompanied by increased RNF11A E3 ligase activity, as RNF113A isolated from cells treated with MMS was significantly more active than RNF113A from untreated cells (Figure 4.7). MMS-induced autoubiquitination was specific to RNF113A, as RNF8 and RNF168, two other E3 ligases involved in DNA damage signaling (Mailand et al., 2007; Doil et al., 2009), were not autoubiquitinated during alkylation (Figure 4.8). Importantly, overexpression of METTL8 in HEK293T cells was sufficient to induce similar autoubiquitination of RNF113A as compared to cells treated with MMS (Figure 4.9). Consistent with its selective activation during alkylation damage, loss of RNF113A resulted in significant sensitivity to MMS but not CPT (Figure 4.10). Together, these results suggest the specific activation of the RNF113A-ASCC pathway during alkylation damage rests with the E3 ligase activity of RNF113A.

4.4 Discussion

Our results provide the first evidence for a repair pathway mediated by aberrant RNA alkylation. RNA alkylation is sufficient to activate the E3 ligase activity of RNF113A, which in turn initiates the ubiquitin signaling cascade required to recruit the ASCC-ALKBH3 repair complex. Not only is aberrant RNA alkylation sufficient to recruit this complex but an RNA-specific demethylase is sufficient to attenuate ASCC recruitment, suggesting that RNA alkylation is also necessary for its function. How RNA alkylation acts as an activator of this pathway remains the

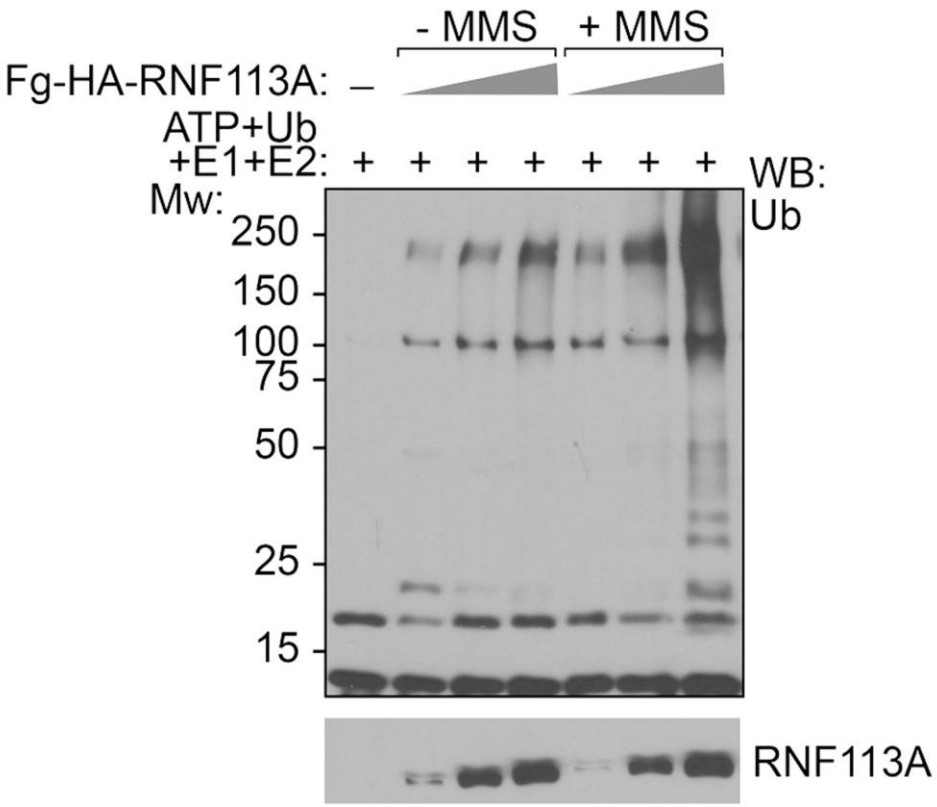

Figure 4.7. MMS Induces *in vitro* RNF113A E3 Ligase Activity. TAP-RNF113A was stably expressed in HeLa-S cells and purified using anti-Flag resin after incubation for the indicated time with 400μM MMS. The eluted proteins were then used in *in vitro* ubiquitin ligase assays using E1, E2 (UbcH5c plus Ubc13/MMS2; 50 nM each. Reactions were analyzed by Western blot (n=3 independent experiments).

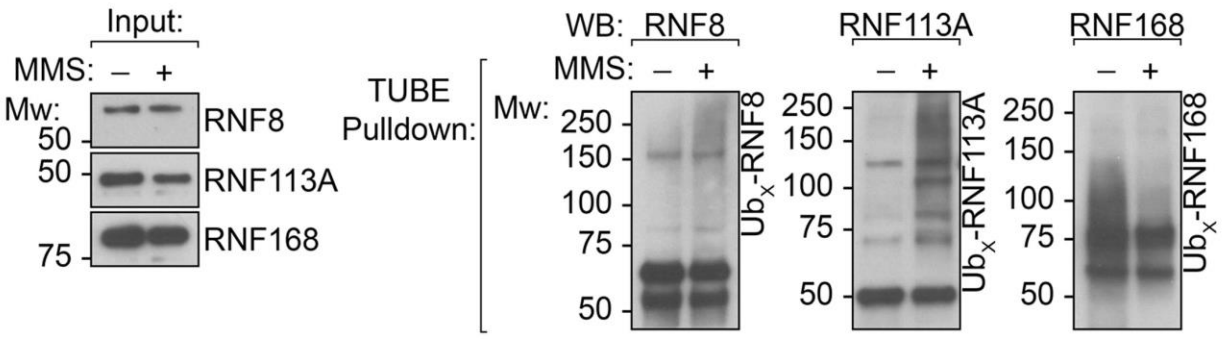

Figure 4.8. MMS Specifically Induces RNF113A Autoubiquitination. Endogenous ubiquitin was isolated from HeLa-S cells after treatment with MMS using ubiquilin TUBE beads and Western blotted for either endogenous RNF113A, RNF8 or RNF168. Input lysates were also analyzed as indicated (n=3 independent experiments).

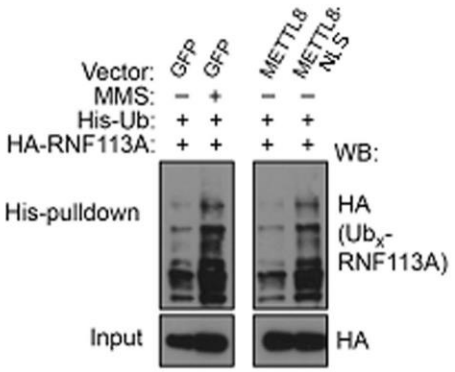

Figure 4.9. METTL8 Overexpression Induces RNF113A Autoubiquitination *in vivo*. HEK293T cells either expressing His-ubiquitin, HA-RNF113A and Flag-GFP were left untreated or treated with MMS or HEK293T expressed His-ubiquitin, HA-RNF113A and Flag-METTL8 or Flag-METTL8-NLS. Ubiquitinated proteins were isolated by Ni-NTA under denaturing conditions and Western blotted as shown. Input lysates were also analyzed as indicated. (n=1 independent experiments).

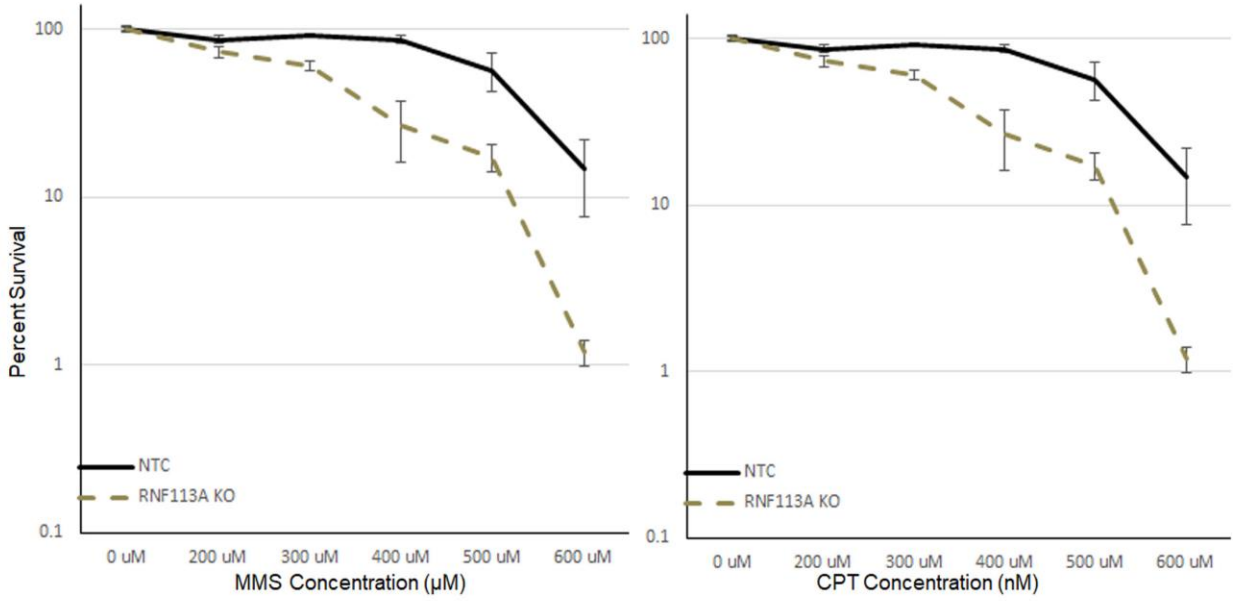

Figure 4.10. RNF113A Loss Specifically Sensitizes Cells to Alkylation. Cellular sensitivity to MMS or camptothecin (CPT) of WT U2OS cells or cells treated with a sgRNA to RNF113A using MTS assay (mean ± S.D.; n=5 biological replicates).

focus of future studies. Intriguingly, it is possible that, in addition to repairing alkylation damage on DNA, the ASCC-ALKBH3 could serve as a nuclear RNA quality control mechanism that intersects with elongating RNA Polymerase II (PolII).

Similar to epigenetic regulation in DNA, methyl-specific 'reader' proteins, such as the YTH family of proteins, recognize RNA modifications, specifically 6-methyladenine (m6A), to regulate translation initiation and elongation (Meyer and Jaffery, 2017; Wang et al., 2014; Xiao et al., 2016). Emerging evidence suggests that some of these reader proteins, such as YTHDF3 and YTHDC1, can recognize specifically damaged or alkylated RNA lesions, such as m1A (Dai et al., 2018). It is therefore plausible that after these readers engage the alkylated lesion, they initiate downstream damage signaling that is reminiscent of double-strand break repair. This signaling would activate the RNF113A E3 ligase, and ultimately result in the recruitment of the ASCC complex.

Conversely, alkylation could induce the uncoupling of RNA PolII and the RNA processing machinery. Due to the inability of RNA binding factors to recognize specific sequences on the damaged nascent transcript, such as the 5' splicing junction, splicing is inhibited, while polymerase elongation continues unperturbed. This uncoupling activates RNF113A to initiate damage signaling. Here, it is enticing to predict that RNF113A itself can serve as a 'sensor' of alkylation, as its zinc-finger domain directly interrogates the nascent pre-mRNA to identify the 5' splicing junction (Yan et al., 2016). Future studies will undoubtedly clarify these critical questions regarding the signaling cascade initiated by aberrant RNA alkylation in activating this repair pathway.

4.5 Materials and Methods

Data Reporting. No statistical methods were used to predetermine sample size. The experiments were randomized and the investigators were single-blinded to allocation during experiments and outcome assessment.

Plasmids. Human METTL8 and RNF113A cDNAs were isolated as previously described (Dango et al., 2011). Humanized BsvAlkB DNA was ordered as a gene block from IDT. For mammalian cell expression, cDNAs were subcloned into pHAGE-CMV-3xHA, pHAGE-CMV-Flag, pLVX-PTuner, or pMSCV-Flag-HA as needed by Gateway recombination (Sowa et al., 2009). For recombinant protein expression, cDNAs were subcloned into pET28a-Flag. All constructs derived by PCR, including deletions and point mutations, were confirmed by Sanger sequencing.

Cell culture. U2OS, HeLa-S, HeLa, and 293T cells (originally from ATCC) were cultured and maintained as previously described (Zhao et al., 2015). Cells containing the lac operon reporter system were a generous gift from Roger Greenberg and maintained as previously described (Shanbhag et al., 2010). Cells were tested for mycoplasma at the Washington University Genome Engineering and iPSC Center and were authenticated using the ATCC human STR profiling services. Preparation of viruses, transfection, and viral transduction were performed as described previously (Zhao et al., 2015). For cell foci experiments, cells were transduced with pHAGE-CMV-3xHA-ASCC2 and pHAGE-CMV-Flag-BsvAlkB WT or H156A lentiviral vectors or the pHAGE-CMV-Flag-METTL8-NLS or pLVX-PTuner-METTL8-NLS lentiviral vectors.

Cell survival assays. For DNA damaging agent survival assays using HeLa cells, 2,000 cells-3,000 cells/well were cultured overnight in 96-well plates in 100 μl media. Cells were then

exposed to medium containing the indicated concentration of methyl methanesulphonate (MMS; Sigma) or camptothecin (CPT; Sigma) for 24 or 72 hours at 37 °C, respectively. The media was then replaced with normal media, and cell viability was assessed using the MTS assay (Promega) 72 hours after initial damaging agent exposure. All MTS-based survival experiments were carried out in quintuplicate.

CRISPR/Cas9 mediated knockouts. U2OS ASCC3 knockout cells were created using CRISPR/Cas9 genome editing at the Genome Engineering and iPSC Center (GEiC) at Washington University School of Medicine (St. Louis). ASCC3 KO clones were initially assessed by deep sequencing and confirmed by Western analysis. ASCC3: 5'-ATGGCTTTACCTCGTCTCACAGG-3'. For pooled RNF113A knockout, HeLa or U2OS cells were infected with pLentiV2-CRISPR-Cas9 lentivirus and selected for infection with 1μg/ml puromycin. Knockout of RNF113A was confirmed by Western analysis. RNF113A: 5'-GTAGCGACGAAGGCTGCACT-3'.

Immunofluorescence microscopy. All immunofluorescence microscopy was done as previously described (Zhao et al., 2015), with minor modifications. After treatment with 500 μM MMS in complete medium at 37°C for six hours or incubation with 300 nM Shield-1 ligand for 24 hours, U2OS cells were extracted with 1× PBS containing 0.2% Triton X-100 and protease inhibitors (Pierce) for 20 minutes on ice prior to fixation with 3.2% paraformaldehyde. The cells were then washed extensively with IF Wash Buffer (1× PBS, 0.5% NP-40, and 0.02% NaN_3), then blocked with IF Blocking Buffer (IF Wash Buffer plus 10% FBS) for 30 minutes. Primary antibodies were diluted in IF Blocking Buffer overnight at 4°C. After staining with secondary antibodies (conjugated with Alexa Fluor 488 or 594; Millipore) and Hoechst 33342 (Sigma-Aldrich), where

indicated, samples were mounted using Prolong Gold mounting medium (Invitrogen). Epifluorescence microscopy was performed on an Olympus fluorescence microscope (BX-53) using an UPlanS-Apo 100X/1.4 oil immersion lens and cellSens Dimension software. Raw images were exported into Adobe Photoshop and for any adjustments in image contrast or brightness, the levels function was applied. For foci quantitation, at least 100 cells were analyzed in triplicate, unless otherwise indicated.

Purification of Flag-RNF113A complexes. Affinity purification of RNF113A was performed as previously described, with minor modifications (Brickner et al., 2017). Briefly, Flag-RNF113A was stably expressed after transduction of pMSCV-Flag-RNF113A retrovirus into HeLa-S cells. Flag-tagged RNF113A was purified from HeLa-S cells by resuspension in Flag-lysis buffer (50 mM Tris-HCl pH 7.9, 150 mM NaCl, 10% glycerol 1.0% Triton X-100, 1 mM DTT, and protease inhibitors) with or without prior treatment with MMS (400 μM for 30, 60, 120, or 240 minutes) and lysed by sonication. After incubation with anti-Flag (M2) resin (Sigma), the protein was eluted in TAP buffer (50 mM Tris-HCl pH 7.9, 100 mM KCl, 5 mM MgCl2, 10% glycerol, 0.1% NP-40, 1 mM DTT, and protease inhibitors) containing 0.4 mg ml^{-1} Flag peptide.

Protein purification. Recombinant BsvAlkB WT or H156A proteins were purified from Rosetta (DE3) cells using an ÄKTA-pure FPLC (GE Healthcare). For His-tagged bacterially expressed proteins, cells were resuspended in His-lysis buffer (50 mM Tris-HCl pH 7.3, 250 mM NaCl, 0.05% Triton X-100, 3 mM β–ME, 30 mM imidazole, and protease inhibitors) and lysed by sonication. After centrifugation and filtration, the extract was loaded onto a HisTrap HP column using a 50 ml Superloop (GE Healthcare). After extensive washing with lysis buffer, the protein was eluted using lysis buffer containing 400 mM imidazole and dialyzed into TAP buffer.

Ubiquitin ligase assays. Reactions analyzing ubiquitin chain polymerization were performed in ubiquitin ligase buffer (25 mM Tris pH 7.3, 25 mM NaCl, 10 mM $MgCl_2$, 100 nM ZnCl, 1 mM mercaptoethanol) containing 5 mM ATP and 100 μM of ubiquitin in a total volume of 20 μl. E1 activating enzyme (UBE1; Boston Biochem) was used at 500 nM, and E2 ubiquitin conjugating enzymes (Ubch5c or Ubc13/MMS2; Boston Biochem) were added at 250 nM. Flag-HA-tagged-RNF113A protein purified from HeLa-S cells was added to each reaction and incubated at 37°C for 1 hour. Reactions were stopped with 20 μl of Laemmli buffer, analyzed by SDS-PAGE and Western blotted.

Immunoprecipitation. Immunoprecipitation after denaturation was performed as previously described (Sowa et al., 2009) with minor modifications. Briefly, HEK293T cells were transfected with His-Ub, the indicated RNF113A construct and either Flag-GFP or Flag-METTL8 or Flag-METTL8-NLS simultaneously. then transduced with the indicated RNF113A WT or lentivirus. Cells were then treated with 500 μM MMS for 6 hours and harvested. Pellets were resuspended in TBS + 1% SDS and further lysed by sonication, boiled and cleared by centrifugation. Samples were diluted to 0.1% SDS with lysis buffer (50mM Tris pH 7.9, 150 mM NaCl, 10% glycerol, 1% Triton X-100, 1mM DTT, and protease inhibitors) and incubated with Ni-NTA beads at 4°C overnight. After incubation and extensive washing with lysis buffer, the bound material was eluted with Laemmli buffer and analyzed by Western blotting. For analysis of RNF113A autoubiquitination after exposure to various DNA damaging agents for 6 hours (500 μM MMS, 10mM HU, 20 μM bleomycin, 1 μM CPT), HeLa cells stably expressing Flag-HA-RNF113A WT or ΔRING protein were transduced with His-Ub and His-Ub was immunoprecipitated after denaturation as described previously (Gajjar et al., 2012; Xirodimas et al., 2001).

TUBE pulldown assays. Endogenous ubiquitination of RNF113A was assessed as described previously, with minor modifications. HeLa-S cells were diluted to 350,000 cells/ml and grown in completed medium at 37°C overnight. Cells were then treated with the indicated genotoxin (1mM MMS, 250 μM hydrogen peroxide, 20 μM bleomycin, 1 μM camptothecin, 10 mM hydroxyurea, 1mM ethyl methanesulphonate, or 1 mM methyl iodide) for 4 hours. After pelleting, cells were incubated in Lysis Buffer (50 mM Tris-HCl pH 7.5, 1 mM EGTA, 1 mM EDTA, 1% Triton X-100, 0.25M Sucrose +protease inhibitors) at 4°C for 1 hour. Cell debris was cleared by tandem centrifugation at 6500 rpm for 30 minutes, then again at 5000 rpm for 5 minutes. The supernatant was added to ubiquilin TUBE2 beads (AM-130; Boston Biochem) with overnight rotation at 4°C. After extensive washing with High Salt TAP Buffer (50 mM Tris-HCl pH7.9, 300 mM KCl, 5 mM $MgCl_2$, 0.2 mM EDTA, 0.1% NP-40, 10% glycerol, protease inhibitors) then Low Salt TAP Buffer (see above; 0 mM KCl), bound material was eluted with Laemmli Buffer and analyzed by Western blotting.

In vitro BsvAlkB Demethylase Assay. 60 pmol of ssRNA or ssDNA substrate was incubated with 20 pmol of either BsvAlkB WT or H156A recombinant protein in demethylase reaction buffer (50 mM HEPES-KOH pH 7.5, 2 mM ascorbate, 100 μM 2-oxoglutarate, 40 μM $FeSO_4$, and 1 μl RNAse inhibitor) for 1 hour at 37°C. Reactions were digested with S1 nuclease (Sigma) overnight at 37°C, then incubated with alkaline phosphatase (NEB) for 1 hour at 37°C. Chromatographic separation was performed using an Agilent 1290 Infinity II UHPLC system with an ZORBAX RRHD Eclipse Plus C18 150 x 2.1 mm ID (1.8 μm) column protected with an ZORBAX RRHD Eclipse Plus C18 5 x 2.1 mm ID (1.8 μm) guard column (Agilent). The mobile phase consisted of water and methanol (with 0.1 % formic acid) run at 0.25 ml/min, for methylated nucleosides starting with a 6-min gradient of 5-90 % methanol, followed by 4 min re-

equilibration with 5 % methanol, and for unmodified nucleosides maintained isocratically with 20 % methanol. Mass spectrometric detection was performed using an Agilent 6495 Triple Quadrupole system operating in positive electrospray ionization mode, monitoring the mass transitions 282.1/150.1 (mA), 268.1/136.1 (A), 266.1/150.1 (m(dA)) and 252.1/136.1 (dA).

Quantification of RNA methylated bases using LC-MS/MS. HEK293T cells were transfected with METTL8 WT or G204A/G206A mutant and grown in DMEM (Sigma-Aldrich), supplemented with 0.03 g/L triple-deuterized L-Methionine (Sigma-Aldrich). Cells were harvested and total RNA was extracted according to the manufacturer's directions (Qiagen) using TRIzol (Rio et al., 2010; Su et al., 2014; Thuring et al., 2016). Chromatographic separation was performed using an Agilent 1290 Infinity II UHPLC system with an ZORBAX RRHD Eclipse Plus C18 150 x 2.1 mm ID (1.8 μm) column protected with an ZORBAX RRHD Eclipse Plus C18 5 x 2.1 mm ID (1.8 μm) guard column (Agilent). The mobile phase consisted of water and methanol (with 0.1 % formic acid) run at 0.25 ml/min, for methylated nucleosides starting with a 6-min gradient of 5-90 % methanol, followed by 4 min re-equilibration with 5 % methanol, and for unmodified nucleosides maintained isocratically with 20 % methanol. Mass spectrometric detection was performed using an Agilent 6495 Triple Quadrupole system operating in positive electrospray ionization mode, monitoring the mass transitions 258.1/126.1 (mC), and 244.1/112.1 (C).

RNA-Seq. 5 million U2OS WT or ASCC3 KO cells were plated onto a 10cm plate and grown under standard conditions. Cells were treated with 500 μM MMS for 8 hours and total RNA was extracted using the miRNeasy Kit (Qiagen) following the manufacturer's directions. Library preparation, reads, and data analysis were performed by the Genome Technology Access Center in the Department of Genetics at Washington University School of Medicine.

Statistical Analyses. All *p*-values were calculated by unpaired, two-tailed Student's *t*-test. All error bars represent the standard deviation, unless otherwise noted.

Antibodies. The antibodies and the concentration used for the given application are listed as following: 6x-His (Abcam; 1:2500 Western), ASCC3 (In house; 1:500 IF; 1:5000 Western), Flag (Sigma; 1:1000 IF; 1:3000 Western), GAPDH (Abcam; 1:3500 Western), HA (BioLegend; 1:300 IF; 1:2500 Western), Nucleolin (Bethyl; 1:200 IF), pH2A.X (Active Motif; 1:1000 IF), RNF113A (Sigma; 1:2000 Western), RNF8 (Abcam; 1:2500 Western), RNF168 (Abcam; 1:2500 Western), Ubiquitin (Santa Cruz; 1:2500 Western)

Chapter 5: Conclusion and Future Directions

Although ALKBH2 is the primary dealkylase responsible for repairing m1A and m3C lesions (Ringvoll et al., 2006), ALKBH3 is overexpressed in certain subsets of cancer, such as non-small cell lung carcinoma and prostate adenocarcinoma (Konishi et al., 2005; Tasaki et al., 2011). As alkylating agents represent a large class of clinically used chemotherapeutic drugs, ALKBH3 may be required to repair such lesions in these subsets of cancer (Duncan et al., 2002). Previous studies demonstrated that ALKBH3 co-precipitates with the ASCC complex, which is comprised of the helicase ASCC3 and the undefined accessory proteins ASCC1 and ASCC2. Interestingly, *in vitro* studies of ALKBH3 have also identified ssRNA as a substrate for this enzyme (Aas et al., 2003). As RNA has been shown to direct DNA repair of DSBs (Keskin et al., 2014), it is enticing to envision RNA alkylation as another mechanism by which ALKBH3 repair is activated.

The research presented here provides insight into how ASCC1 and ASCC2 regulate the recruitment of the ASCC-ALKBH3 repair complex during alkylation damage. We find that ASCC1 coordinates complex assembly, while ASCC2 is critical for proper recruitment of the complex to alkylation lesion sites. Additionally, we demonstrate that aberrant RNA alkylation is both necessary and sufficient to induce the recruitment of this repair complex. Together, this knowledge expands upon the understanding of DNA alkylation repair and provides further evidence of RNA-mediated DNA repair.

5.1 Ubiquitin Recognition by ASCC2 in Alkylation Repair

5.1.1 Conclusions

The role of the DNA helicase ASCC3 in generating single-stranded DNA, the preferred substrate of ALKBH3, has been well-elucidated (Dango et al., 2011; Falnes et al., 2002; Trewick et al., 2002; Duncan et al., 2002). However, the mechanistic basis for regulating the recruitment of the ASCC-ALKBH3 repair complex to m1A and m3C adducts remained elusive. Here, we describe an essential role for ASCC2 in regulating the recruitment of this complex to sites of alkylation damage.

Interestingly, the several components of the ASCC-ALKBH3 repair complex, ASCC2, ASCC3 and ALKBH3, form nuclear foci specifically upon induction of damage with alkylating agents (Figures 2.1 and 2.2). While these foci did not co-localize with canonical DSB repair factors or replication factors, ASCC2 and ASCC3 co-localized with the spliceosomal proteins BRR2 and PRP8, as well as with elongating RNA PolII (Figures 2.3 and 2.4). These results were confirmed by mass spectrometry. Perturbation of both splicing and transcription significantly reduced ASCC3 foci formation, while inhibiting the canonical DSB kinases ATR and ATM had no effect on complex recruitment (Figures 2.4 and 2.5). This data suggests that the ASCC-ALKBH3 complex may be associated with regions of active transcription and may be necessary to repair lesions at or near genes with high transcriptional activity via a mechanism that is distinct from DSB repair.

We hypothesized that proper recruitment of this complex may be mediated by ASCC2, which contains a CUE ubiquitin binding motif (residues 467-509). ASCC2 co-localized with the general ubiquitin antibody FK2 as well as with K63-Ub upon alkylation damage (Figures 2.6 and 2.8). We found that ASCC2 bound to K63-linked ubiquitin chains but not K48-linked ubiquitin

chains (Figure 2.7). While CUE domains have previously been shown to recognize K48-linked ubiquitin chains (Shih et al., 2002), an upstream and downstream region to the CUE domain (residues 388-525) provided the specificity for K63-linked ubiquitin (Figure 2.7E-F). Mutational analysis of ASCC2 identified a leucine mutation in the ubiquitin recognition motif, L506A, that abrogated its *in vitro* ubiquitin binding and severely diminished ASCC2 foci formation (Figure 2.8). Thus, ASCC2 recruitment to sites of alkylation damage is mediated by recognition of K63-polyubiquitin via its CUE domain.

Strikingly, ASCC2 also mediated the recruitment of both ASCC3 and ALKBH3. Loss of ASCC2 significantly reduced both ASCC3 and ALKBH3 foci formation in response to alkylation damage (Figure 2.9 and 2.10). Proximity ligation experiments (PLA) revealed that the ASCC-ALKBH3 complex is being recruited to alkylated bases (Figure 2.11). Importantly, loss of ASCC2 caused cells to become hypersensitive to alkylating agents but not to other types of genotoxins and impaired m1A repair kinetics on both RNA and DNA (Figures 2.11 and 2.12). Reconstitution of ASCC2 KO cells with wild-type ASCC2 was able to restore foci formation of both complex components. Conversely, the L506A mutant ASCC2 was incapable of restoring ASCC3 and ALKBH3 foci (Figure 2.13). Similar to the foci experiments, reconstitution of ASCC2 KO cells with WT ASCC2 was able to restore cellular survival during exposure to alkylation damage while the L506A mutant reconstituted cells remained hypersensitive (Figure 2.14). Thus, proper complex recruitment is dependent upon K63-polyubiquitin recognition by the ASCC2 subunit.

As the above work suggests that ASCC2 is upstream to both ASCC3 and ALKBH3, we then analyzed the physical interactions between the different complex components. Utilizing *in vitro* recombinant protein binding assays as well as *in vivo* immunoprecipitation experiments, we

found that ASCC3 serves as a scaffold for this repair complex, with ASCC2 and ALKBH3 interacting with distinct regions of ASCC3 (Figure 2.15). ASCC2 binds to the N-terminus of ASCC3, while ALKBH3 binds to the helicase cassettes of ASCC3. ASCC2 and ALKBH3 did not directly interact with one another. This supports the conclusion that ASCC2 bridges the interaction between K63-polyubiquitin and ASCC3 and that ALKBH3 is recruited via its interaction with ASCC3.

To further unveil the mechanistic regulation of this repair complex, we next sought to identify the E2 conjugating enzyme and E3 ubiquitin ligase responsible for forming the chains recognized by ASCC2. Knockdown of the E2 conjugating enzyme UBC13 significantly decreased ASCC2 foci formation (Figure 2.16), suggesting that this enzyme is critical for complex recruitment. Using this knowledge as the basis for identifying the E3 ligase, we performed a shRNA screen of E3 ligases known to interact with UBC13. From this screen, we identified RNF113A as the E3 ligase of this pathway, as knockdown of RNF113A using several different shRNA attenuated ASCC2 foci formation (Figure 2.17). RNF113A consistently co-localized with PRP8 and BRR2, suggesting that this enzyme is the *bona fide* E3 ligase of this pathway.

In vitro ubiquitin ligase assays confirmed that RNF113A purified from human cells is an active E3 ligase that predominantly forms K63-linked ubiquitin chains (Figure 2.18). Through further analysis of the mass spectrometry-based ASCC2 interactome, we identified BRR2 as one of the substrates of RNF113A. RNF113A was able to ubiquitinate recombinant BRR2 *in vitro*. Furthermore, immunoprecipitation of RNF113A pulled down BRR2, demonstrating that these proteins interact *in vivo* (Figures 2.19 and 2.20). Like RNF113A, loss of BRR2 or its stoichiometric partner PRP8 resulted in reduced ASCC2 foci in response to alkylation damage

(Figure 2.21). These cells were also hypersensitive to alkylation damage. Thus, these data implicate BRR2 as being the target of RNF113A ubiquitination during alkylation damage.

Surprisingly, recent studies have identified mutations RNF113A as for X-linked trichothiodystrophy (X-TTD) (Corbett et al., 2015). Lymphoblasts from patients with a Q301* mutation were hypersensitive to alkylation damage and exhibited reduced ASCC3 foci upon MMS treatment (Figure 2.22). Complementation of these cells with WT RNF113A was able to completely rescue ASCC3 foci, while the I264A mutant, which has impaired interaction with the E2 conjugating enzyme (Zheng and Shabek, 2017), only partially rescued ASCC3 foci formation. This data suggests that a sensitivity to alkylation damage may be contributing to the phenotypes exhibited by X-TTD patients.

Taken together, this data describes a function for ASCC2 in which it promotes alkylation repair by recruiting the ASCC-ALKBH3 repair complex to sites of alkylation damage. This recruitment is dependent upon ubiquitin recognition by ASCC2. Additionally, BRR2 both co-localizes with ASCC2 and is upstream in the recruitment of the complex, suggesting that there may be an intersection between active transcription, splicing, and alkylation repair by the ASCC-ALKBH3 complex *in vivo.*

5.1.2 Future Directions

Additional future studies could focus on the alternative mechanisms by which recruitment of the ASCC-ALKBH3 repair complex during alkylation damage is regulated. In the absence of damage, ASCC2 is primarily contained within the cytoplasm (Figure 5.1A). After alkylation damage, ASCC2 remains primarily cytoplasmic until four hours post-treatment (Figure 5.1A-B). Importantly, pre-treatment of U2OS cells with leptomycin B, an inhibitor of nuclear export (Kudo et al., 1998), causes ASCC2 to be retained in the nucleus (Figure 5.1C). Taken together,

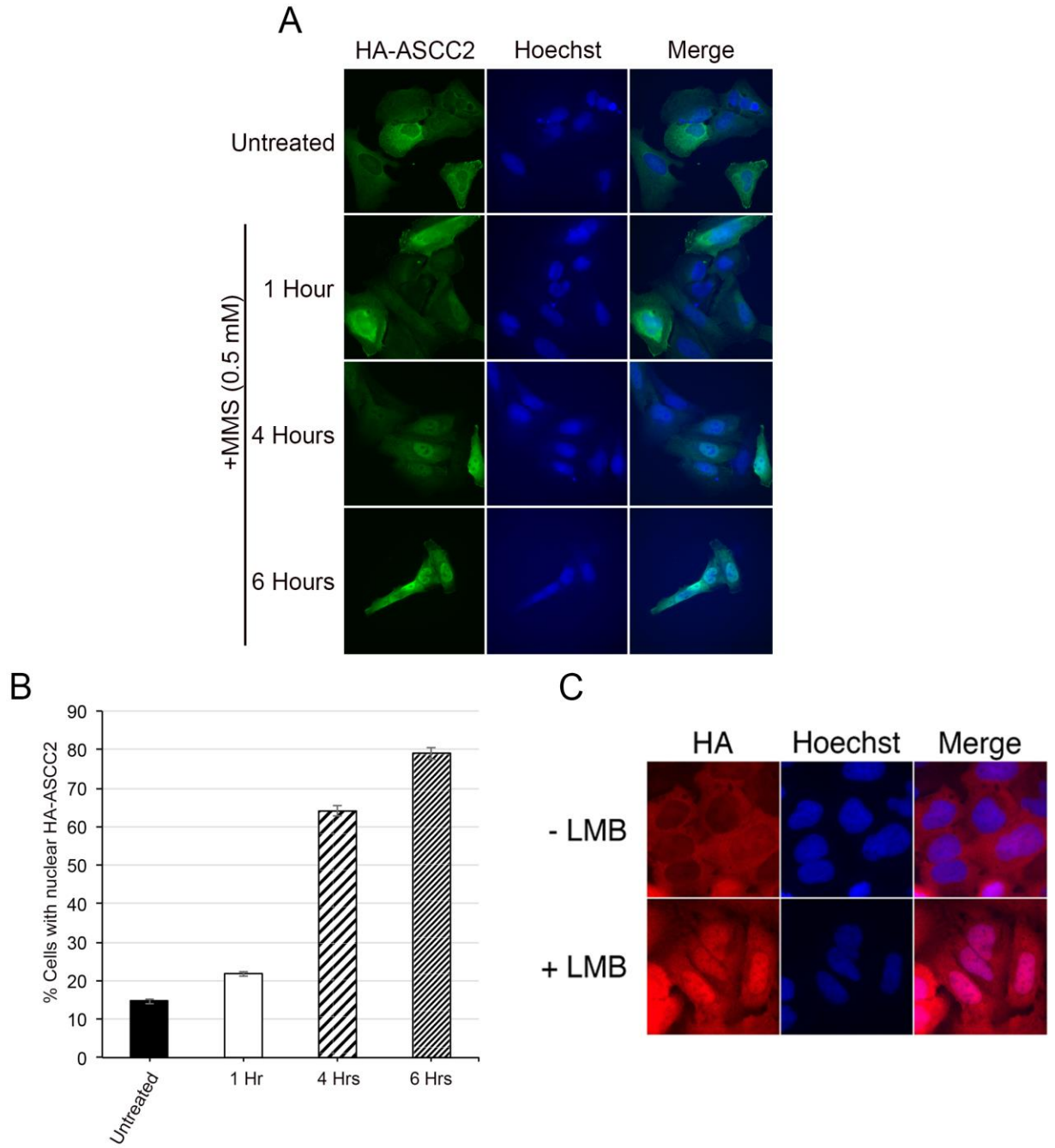

Figure 5.1. ASCC2 is Cytoplasmic in the Absence of Damage. (A) Representative images of HA-ASCC2 localization after different incubation times with 500 μM MMS. Cells were processed for immunofluorescence with HA. (B) Quantitiation of (B)) (n=3 biological replicates; mean ± S.D.). (C) Representative images of HA-ASCC2 localization with or without leptomycin B treatment. Cells were processed for immunofluorescence with HA. Scale bars, 10 μm.

these data suggest that ASCC2 is actively imported into the nucleus during alkylation damage. Future experiments could focus on the effect of importins and the nuclear export proteins RanGAP/CRM1 on ASCC2 localization during alkylation damage (Cook et al., 2007; Fukuda et al., 1997; Bohnsack et al., 2002). Like ASCC-ALKBH3 complex recruitment is dependent upon ubiquitin recognition of ASCC2, the complex localization could be similarly dictated by ASCC2. More in-depth analysis of the ASCC2 protein sequence could provide insight into the presence of either a nuclear localization signal (NLS) or nuclear export signal (NES) in ASCC2. Conversely, the ASCC-ALKBH3 complex could be shuttled as passenger complex for another protein or protein complex. A genome-wide CRISPR/Cas9 screen could identify chaperone proteins that are needed for the nuclear localization of the ASCC-ALKBH3 complex. ASCC2 localization during MMS treatment would be used as the read-out for the screen. Intriguingly, recent studies have shown that inhibitors for importins, RanGAP or CRM1 are promising anticancer targets (Lapalombella et al., 2012; Miyake et al., 2015; Kim et al., 2016). Thus, targeting the nuclear transport of ASCC2 could be another mechanism by which to inhibit ALKBH3 in certain cancer types.

In addition to the nuclear transport of ASCC-ALKBH3, the data presented in Figure 5.1 suggests that this complex has a cytoplasmic function. As such, future experiments could be performed to elucidate the cytoplasmic role of ASCC. I predict that ASCC-ALKBH3 serves as an RNA quality control mechanism, similar to nonsense-mediated decay. To identify factors that could be involved in ASCC-ALKBH3-mediated RNA quality control, Flag-HA-ASCC2 could be purified from cells in the presence or absence of alkylation damage from the cytoplasmic fraction. Additionally, the levels of the alkylation lesions m1A and m3C on mature mRNA can be determined by mass spectrometry. The levels of methylated RNA can be quantified for both PC-

3 and U2OS control, ASCC2 KO, ASCC3 KO, RNF113A knock-down, and ALKBH3 KO cell lines by purifying mRNA by TRIzol extraction (Rio et al., 2010). Mature mRNA can be further purified by polyA enrichment. This RNA can then be digested with S1 nuclease (Sigma) and FastAP alkaline phosphatase (ThermoFisher Scientific) and analyzed by liquid chromatography-tandem mass spectrometry (LC-MS/MS) to quantify m1A and m3C lesions (Su et al., 2014; Thuring et al., 2016). I predict that m1A and m3C will be enriched on mRNA upon loss of all of these factors.

Alternatively, ASCC-ALKBH3 could be an alternative mechanism to prevent ribosome stalling and escape no-go decay (Simms et al., 2017). PC-3 control or ASCC2 KO cells in the presence or absence of MMS will be resuspended in lysis buffer and lysed. Cell lysate will then be layered over a sucrose gradient, fractionated and analyzed by Northern blotting to determine the localization of the polysomes on the transcript. I hypothesize that there will be more polysomes on transcripts in the ASCC2 KO cells, suggesting impaired translation kinetics and increased no-go decay during alkylation damage. These experiments will establish a role for the ASCC-ALKBH3 in translation and cytoplasmic RNA quality control.

RNF113A is a key component of the activated spliceosome and binds directly with the 5’ splice sites of the nascent mRNA, suggesting a link with RNA splice site selection and maturation (Wu et al., 2017). While most cases are not due to *RNF113a* mutations, nearly half of all TTD cases are non-photosensitive (NP-TTD), strongly suggesting the core molecular defect in TTD is not necessarily due to a defect with UV-induced TCR (Faghri et al., 2008). Mutations in *RNF113a* are associated with a non-photosensitive form of TTD (NP-TTD), linking ASCC complex recruitment to a disease connected with TC-NER (Corbett et al., 2015). Exome sequencing revealed an H279R variant in *RNF113A*, along with severely skewed X-chromosome

inactivation (Figure 5.2A-B). The histidine residue mutated in this patient is essential for coordinating one of the zinc ions in the RING domain, which is necessary for catalytic activity (Figure 5.2C) (Deshaies et al., 2009). This patient also did not present the "tiger-tail" banding pattern as seen on hair polarizing light microscopy that is common in TTD patients (Figure 5.2D). This point mutation disrupted its E3 ubiquitin ligase activity *in vitro* (Figure 5.3). Importantly, the H279R mutation did not affect the localization of RNF113A with the spliceosomal components PRP8 or BRR2 (Figure 5.4A-D). Complementation of RNF113A knock-down cells with the H279R mutant RNF113A reduced ASCC foci formation during alkylation damage (Figure 5.4E-F) and increased alkylation damage hypersensitivity (Figure 5.5). Together, these data suggest that an inability to recruit the ASCC complex may be a key molecular defect in non-photosensitive TTD.

Interestingly, loss of TTDN1, a more commonly mutated factor associated with NP-TTD, appears to reduce ASCC3 foci formation during alkylation damage (Figure 2.22). Similar to RNF113A, proteomic studies have revealed interactions between TTDN1 and the RNA splicing machinery, such as the debranching enzyme DBR1 (data not shown). It is possible, therefore, that a major molecular defect in NP-TTD is the inability to recruit the ASCC complex when transcription goes awry, which may happen during UV as well as alkylation damage. During UV damage, the polymerase is stalled on the chromatin template, while it may not be during alkylation damage. However, alkylation of the RNA still requires remodeling of the elongating polymerase and its associated machinery, which may thus require the RNF113A-induced recruitment of the ASCC complex. Interestingly, the shared commonality between Xeroderma pigmentosum (XP), Cockayne syndrome (CS) and TTD seems to be an underlying transcriptional defect. It is also possible that what goes awry in TTD may be aberrant signaling

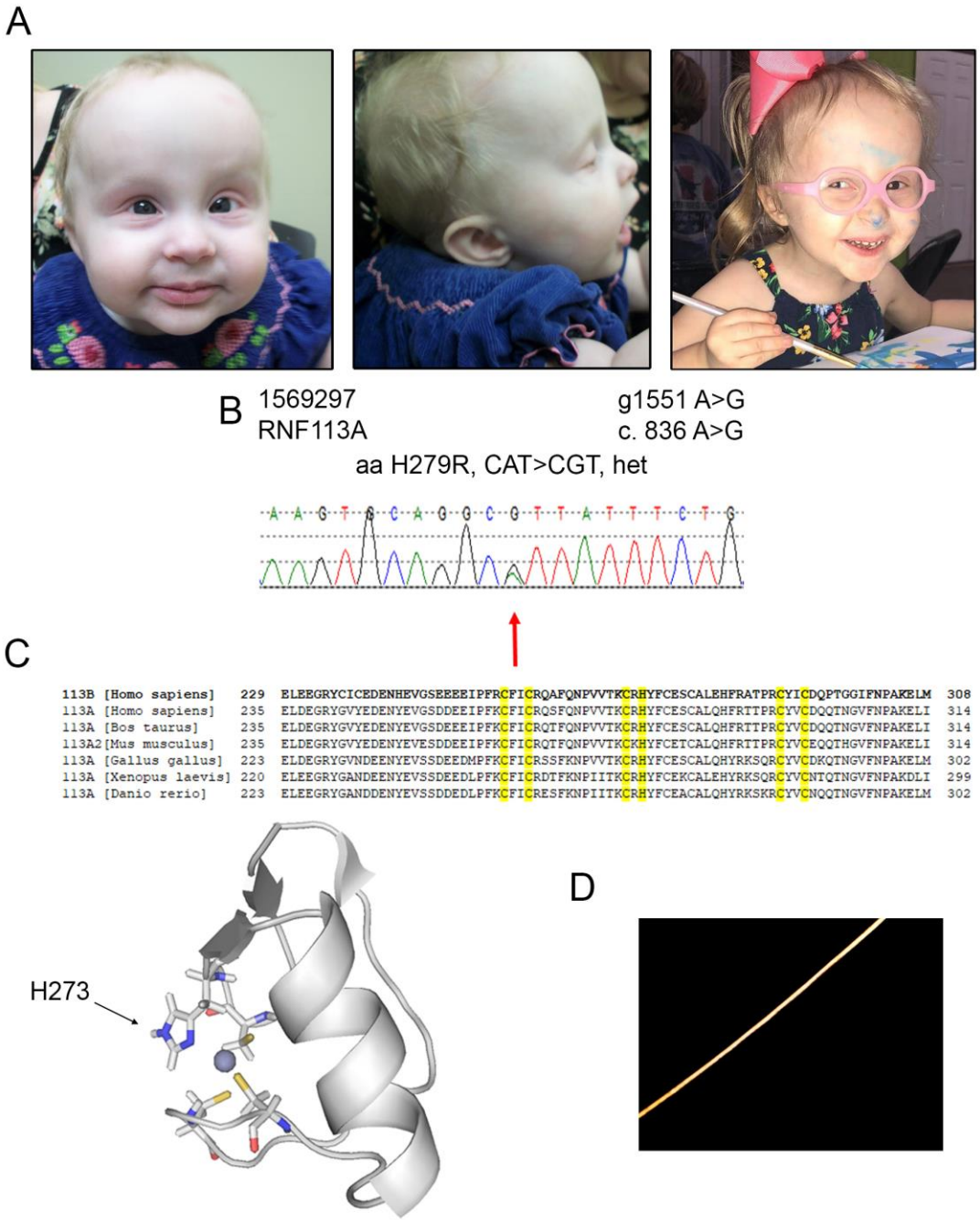

Figure 5.2. Phenotypic Characterization of a Trichothiodystrophy-like Syndrome. (A) Patient images at 11 months and 3 years of age. She has facial dysmorphisms including upslanting palpebral fissures, sparse eyebrows, smooth philtrum, low-hanging columella, and micrognathia but with prominent appearance of the chin in frontal view. She has growth restriction (<1st%ile for all growth parameters), cutis marmorata, and ocular manifestations (nystagmus and retinal pigmentary deficiency). (B) Sanger sequencing identifying a heterozygous A>G mutation in the patient. This mutation results in an H279R point mutation. (C) Sequence alignment of RNF113A or the homolog RNF113B from various species (top) and the structure of the human RNF113B RING domain (bottom). Residues highlighted in yellow are critical for coordinating the zinc cations. The red arrow denotes the location of the conserved histidine residue. Note that H273 in RNF113B sequence and structure aligns with H279 in RNF113A. (D) The patient's normal polarized light evaluation of the hair.

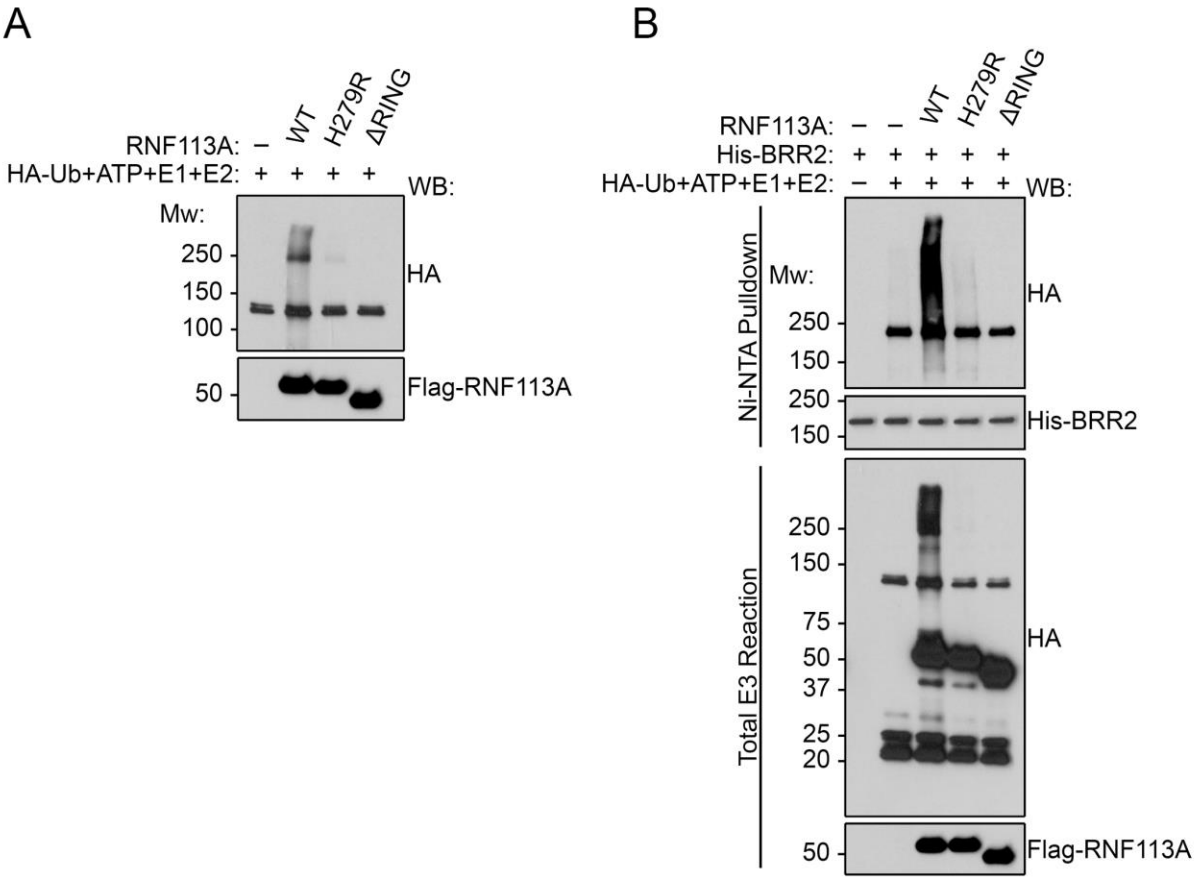

Figure 5.3. The H279R Mutation Disrupts RNF113A E3 Ligase Activity. (A) Ubiquitin ligase assay of Flag-HA-RNF113A WT or the indicated mutants using E1 (50 nM), E2 (UbcH5c; 150 nM) and HA-Ub. The samples were incubated at 35°C for 2 hours, boiled in Laemmli buffer and analyzed by Western blotting. (B) Ubiquitin ligase assay as in (A) in the presence of His-ΔN-BRR2. After incubation at 35°C, samples were bound to Ni-NTA beads. Samples were then eluted with Laemmli buffer and analyzed by Western blotting.

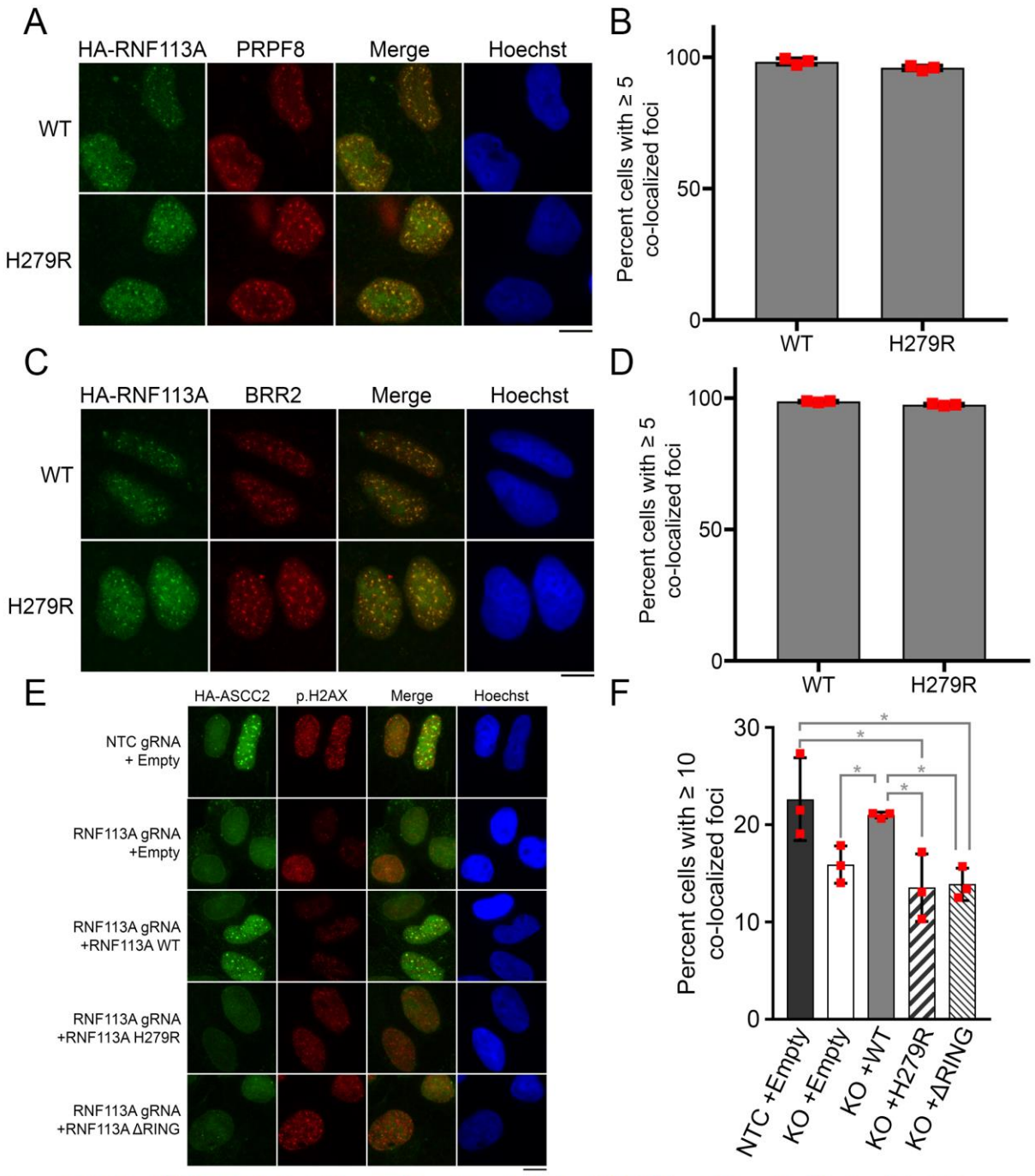

Figure 5.4. The H279R Mutation Disrupts Recruitment of the ASCC Repair Complex During Alkylation Damage. U2OS cells expressing HA-RNF113A WT or H279R were processed for immunofluorescence using anti-HA and either anti-PRPF8 (A) or anti-BRR2 (C) antibodies. Hoechst was used as the nuclear stain. (B) and (D) Quantitation of (A) or (C), respectively. N=3 biological replicates of ≥ 200 cells, bar graphs indicate the mean, and error bars represent ± S.D. of the mean. Red boxes mark the individual experiments. (E) U2OS cells expressing either non-targeting (NTC) or RNF113A guide RNA with Cas9, HA-ASCC2, and Flag-RNF113A WT or the indicated mutants were treated with 500 μM MMS for 6 hours. Cells were then processed for immunofluorescence using the indicated antibodies. (F) Quantitation of (C). N=3 biological replicates of ≥ 200 cells, bar graphs indicate the mean and error bars represent ± S.D. of the mean. Statistics were calculated using a two-tailed student's *t*-test. * = $p < 0.05$. Red boxes mark the individual replicates. Scale bars, 10 mm.

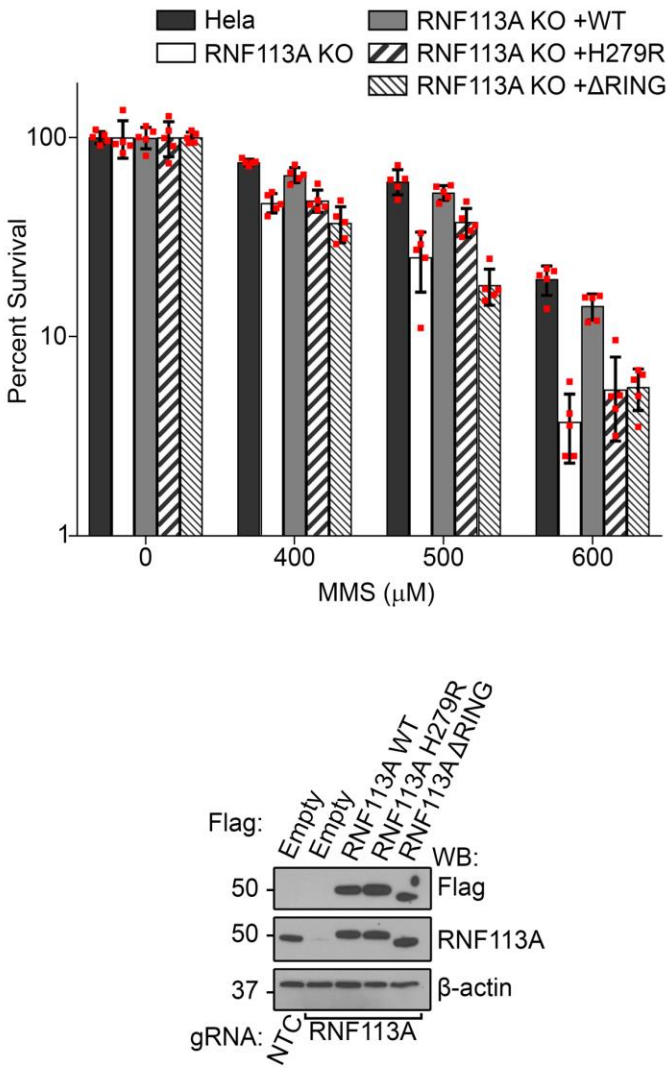

Figure 5.5. The H279R Mutation Sensitizes Cells to Alkylation. (Top) Wild-type or RNF113A KO Hela cells expressing the indicated vectors were assessed for sensitivity to MMS using the MTS assay. N=5, bar graphs indicate the mean, and error bars indicate ± S.D. of the mean. Red boxes denote the individual replicates. (Bottom) Whole cell lysates from HeLa cells expressing either a non-targeting control gRNA or a RNF113A-specific gRNA, and either Flag-RNF113A WT or the indicated mutants were analyzed by Western blotting.

between TFIIH and the later RNA processing machinery in TC-NER after the RNA PolII has been repositioned for lesion repair on the DNA template. Notably, TFIIH mutations that cause TTD selectively disrupt the overall complex integrity of TFIIH without necessarily altering its helicase or ATPase, unlike XP or CS associated mutations (Fan et al., 2008). Thus, determining whether TTD-associated TFIIH mutations, as opposed to XP or CS associated mutations, selectively disrupt RNF113A activation and ASCC recruitment during alkylation and elucidating the interplay between alkylation repair, RNA processing and TC-NER requires further examination.

5.2 ASCC-ALKBH3 Complex Coordination by ASCC1

5.2.1 Conclusions

Chapter 2 establishes that ALKBH3, ASCC2 and ASCC3 all form nuclear foci in response to alkylation damage and establishes a role for ubiquitin-dependent signaling mediated by ASCC2 in complex recruitment (Brickner et al., 2017). In contrast to the other complex components, ASCC1 forms nuclear foci in the absence of alkylation damage (Figure 3.3). These foci did co-localize with the spliceosomal factor PRP8, indicating that ASCC1 is also associated with areas of active transcription in the absence of damage. However, this indicates that ASCC1 has a distinct role in the alkylation response in comparison to other complex components.

In vitro binding assays demonstrated that recombinant ASCC1 and ASCC3 interact directly (Figure 3.1). Co-immunoprecipitation studies indicated that, like ASCC2 and ALKBH3, ASCC1 and ASCC2 interaction is mediated by ASCC3 (Figure 3.2), suggesting that ASCC3 serves as a scaffold for the entire ASCC-ALKBH3 complex. Due to the interaction between ASCC1 and ASCC3, we decided to determine the effect of ASCC1 depletion on ASCC3 recruitment during alkylation damage. Surprisingly, there was an increase in ASCC3 foci in the ASCC1 KO cells as

compared to control cells in response to alkylation (Figure 3.4). While there was an increase in the initial number of ASCC3 foci, foci resolution was not altered (Figure 3.5), suggesting that the recruitment but not repair kinetics are altered in ASCC1 KO cells. Together, these data suggest that ASCC1 may negatively regulate ASCC3 foci formation.

We then asked if ASCC1 affects complex assembly at sites of alkylation damage. During alkylation damage, the majority of ASCC3 foci in the wild-type cells co-localized with HA-ASCC2 (Figure 3.6A-B). Upon loss of ASCC1, there was a reduction in co-localization between these two factors and many ASCC3 foci were HA-ASCC2 independent. Consistent with this result, ASCC2 immunoprecipitation from ASCC1 KO cells pulled down less ASCC3 as compared to their wild-type counterpart. Therefore, while ASCC2 and ASCC3 interact directly, their *in vivo* co-localization and recruitment to foci appears to be dependent upon ASCC1.

ASCC1 contains two putative RNA-binding domains: a KH domain and a C-terminal ligase domain. Within the latter domain are two conserved His-X-Thr motifs (Mazumder et al., 2002), which are found in members of the 2H phosphoesterase family (Silverman and Weiss, 2014). Previous data has demonstrated that these motifs are important for nucleotide binding activity of proteins containing this motif. Therefore, we wished to determine which domains within ASCC1 were necessary for its removal from nuclear speckle domains during alkylation damage. ASCC1-NΔ, ASCC1-CΔ and ASCC1-AXA were expressed in ASCC1 KO cells and foci formation was analyzed after MMS treatment. Interestingly, HA-ASCC1-CΔ and ASCC1-AXA still formed foci during alkylation damage, while HA-ASCC1-NΔ were reduced after MMS treatment, similar to WT ASCC1 (Figures 3.8 and 3.10). Consistent with the immunofluorescence experiments, ASCC1 WT but not ASCC1-CΔ or ASCC1-AXA could partially rescue HA-

ASCC2 and ASCC3 co-localization during damage (Figure 3.11). Together, the putative RNA ligase-like domain regulates ASCC1 removal from foci during MMS treatment.

To date, ASCC2, ASCC3 and ALKBH3 have been shown to promote resistance to alkylation damage as assessed by MTS assay and clonogenic survival assay (Brickner et al., 2017; Dango et al., 2011). We demonstrated that ASCC1 also confers resistance to alkylation damage using the MTS assay. PC-3 knockout cells lacking either ASCC1, ASCC3 or both ASCC1 and ASCC3 were hypersensitive to MMS, with ASCC1 being epistatic to ASCC3 (Figure 3.12).

Taken together, this data supports a model whereby ASCC1 acts as a specificity determinant for ASCC3 localization at sites of alkylation damage and as such acts as a regulator of this complex. As the majority of ASCC3 foci in wild-type cells were ASCC2 positive but the majority of these foci in ASCC1 KO cells were ASCC2 independent, we hypothesize that two distinct populations of ASCC3 foci exist. In wild-type cells, RNF113A-mediated ubiquitination of BRR2 is recognized by ASCC2, which recruits ASCC3-ALKBH3 to nuclear speckle foci. Simultaneously, a fraction of ASCC3 is recruited to ASCC2-negative foci by an independent mechanism. These foci are removed by ASCC1 in a manner dependent upon the activity of the C-terminal RNA ligase-like domain, likely via the engagement of an unknown ligand. Thus, in ASCC1 KO cells, the fraction of ASCC3 foci that are ASCC2 independent is significantly increased (Figure 3.13).

5.2.2 Future Directions

There remains much to be discovered about the enzymatic activity of ASCC1. Future research should focus on determining the structure of the RNA ligase-like domain and characterizing its potential catalytic activity. Indeed, in collaboration with the Tainer lab, we are working to solve the structure of the RNA ligase-like domain. Their group has solved the X-ray crystal structure

of this domain to 2.8A resolution (Thapar, unpublished). This structure indicates that the HXT motifs are positioned in a manner similar to the 2H phosphodiesterase family member AKAP18 (Figure 3.9) (Song et al., 2010). AKAP18 degrades 2'-5' oligoadenylate (OA) (Gold et al., 2008; Gusho et al., 2014). Due to the sequence and structural similarities of ASCC1 to AKAP18, I predict that ASCC1 is a *bona fide* phosphodiesterase. Furthermore, I predict that ASCC1 will bind to methylated RNA substrates, particularly m1A and m3C adducts on RNA (Dominissini et al., 2016; Koivisto et al., 2004; Roundtree et al., 2017).

To further identify the exact substrate of ASCC1, RNA immunoprecipitation coupled with mass spectrometry (RIP-MS) could be performed. In this experiment, Flag-ASCC1 WT and Flag-ASCC1 AXA would be immunoprecipitated and RNA will subsequently be extracted by TRIzol reagent (Rio et al., 2010). The RNA will be digested and analyzed by mass spectrometry to determine the preferred RNA modification or sequence motif of ASCC1. Once the substrate is identified, solving the crystal structure of ASCC1 in complex with the ligand would provide valuable insight into the activity of ASCC1.

Lastly, comparing RNA-Seq data from wild-type or ASCC1 KO cells in the presence or absence of MMS could provide insight into global transcriptome changes. In addition to giving information about changes in gene expression during alkylation, these RNA-Seq experiments could provide insight into regulation of alternative splicing during alkylation damage (Kukurba and Montgomery, 2015). Together, these experiments would provide a better understanding of the role of ASCC1 in the overall cellular response to alkylation damage extending beyond the ASCC-ALKBH3 repair pathway.

5.3 Aberrant RNA Alkylation is Necessary and Sufficient for ASCC Complex Recruitment

5.3.1 Conclusions

Emerging evidence provides support for the notion that RNA plays a role in propagating efficient DNA repair, particularly for homologous recombination (HR). Specifically, RNA from an actively transcribed gene is readily available for RAD52-dependent strand invasion to act as a template during HR (Mazina et al., 2017). Previously, we demonstrated that RNA processing events, such as splicing and active transcription, are important for proper recruitment of the ASCC complex during alkylation damage (Brickner et al., 2017). Whether RNA plays a role in promoting other types of DNA repair besides DSB repair remains unclear. Here, we describe a role for aberrant RNA alkylation in recruiting the ASCC complex.

To assess the effect of aberrant RNA alkylation on the recruitment of the ASCC complex, we first analyzed whether aberrant RNA alkylation was necessary for complex recruitment to sites of alkylation damage. Recombinant BsvAlkB, a dealkylase purified from the RNA virus blueberry scorch, dealkylated a ssRNA substrate but not a ssDNA substrate *in vitro*, suggesting that this protein is active towards alkylated ssRNA (Figure 4.1). Overexpression of BsvAlkB in U2OS cells during exposure to MMS resulted in significantly reduced HA-ASCC2 foci formation (Figure 4.2). This was dependent upon the catalytic activity of BsvAlkB (Figure 4.2). Together, these data suggest that aberrant RNA alkylation is necessary to recruit the ASCC complex to sites of alkylation damage.

In addition to being necessary for ASCC recruitment, we hypothesized that RNA alkylation would also be sufficient to recruit this complex. To assess whether RNA alkylation is sufficient for complex recruitment, we overexpressed the 3-methylcytosine (m3C) RNA methyltransferase

METTL8 in U2OS cells. METTL8 was fused to the SV40 NLS to force its nuclear localization and ensure that it is primarily alkylating nuclear RNAs. Importantly, m3C modifications on RNA are reversed by ALKBH3 *in vitro* (Aas, et al., 2003), suggesting that the ASCC complex should respond to aberrant RNA alkylation by METTL8. Strikingly, overexpression of METTL8 was sufficient to induce ASCC3 nuclear recruitment, even in the absence of alkylation damage (Figure 4.3). ASCC3 recruitment was dependent upon the catalytic activity of METTL8, as expression of two different point mutations in the SAM binding domain, D230A and G204A/G206A (Alexandrov et al., 2005), was insufficient for ASCC3 recruitment (Figure 4.3).

Notably, while wild-type METTL8 localized to the nucleolus, neither METTL8 mutant co-localized with the nucleolar protein nucleolin (Figure 4.3A). To ensure that this difference in METTL8 localization was not responsible for the lack of ASCC recruitment with the catalytic mutants, we utilized a single locus reporter system where we could target this methyltransferase to a specific locus by fusing it to LacI (Figure 4.4A) (Shanbhag et al., 2010; Janicki et al., 2004). Fusion of a degron-tagged METTL8 to mCherry protein and LacI was sufficient to localize wild-type METTL8 to this locus in the presence of the ligand Shield-1, which stabilizes the degron-tagged protein and protects it from degradation (Figure 4.4B) (Banaszynski et al., 2006). The addition of doxycycline can also control transcription at this locus (Figure 4.4A). METTL8 expression induced the localization of ASCC3 to this locus in a manner dependent on active transcription (Figure 4.4C). Together, these data suggest that aberrant RNA alkylation is sufficient to recruit the ASCC complex.

Our previous work demonstrated that the ASCC-ALKBH3 complex was specifically recruited during alkylation damage in a manner dependent upon RNF113A ubiquitin signaling (Brickner et al., 2017). We therefore hypothesized that RNF113A E3 ligase activity may also be

specifically activated upon alkylation. Thus, we assessed RNF113A E3 ligase activity via RNF113A autoubiquitination. Denatured pulldown of His-ubiquitin revealed that RNF113A undergoes robust autoubiquitination during MMS treatment. In contrast to MMS, other DNA damaging agents did not induce RNF113A autoubiquitination (Figure 4.5A). RNF113A ubiquitination status was dependent upon the RING domain of RNF113A (Figure 4.5B), suggesting that assessing RNF113A autoubiquitination measures RNF113A ligase activity.

To ensure that the observed autoubiquitination was not an artifact of the experiment, we utilized the tandem ubiquitin binding element (TUBE) method to assess autoubiquitination of endogenous RNF113A. As with the denatured pulldown, only MMS was sufficient to induce autoubiquitination of endogenous RNF113A (Figure 4.6A). Strikingly, the alkylating agent ethyl methanesulphonate (EMS) did not induce RNF113A autoubiquitination but the agent methyl iodide (MeI) did (Figure 4.6B-C). Induction of E3 ligase activity due to alkylation damage was specific to RNF113A, as MMS failed to alter the activity of two other E3 ligases involved in DNA damage signaling (Figure 4.8) (Mailand et al., 2007; Doil et al., 2009). Together, these data suggest that RNF113A activity is activated primarily by methylation.

To further underscore the importance of aberrant RNA alkylation for recruiting the ASCC complex, we asked whether METTL8 was capable of activating RNF113A activity. Strikingly, overexpression of METTL8 in HEK293T cells induced RNF113A autoubiquitination (Figure 4.9). This autoubiquitination was comparable to the autoubiquitination induced by MMS. Consistent with its selective activation during alkylation damage, loss of RNF113A resulted in significant sensitivity to MMS but not CPT (Figure 4.10), suggesting that RNF113A is important for the response to alkylation damage. Taken together, these results suggest the

specific activation of the RNF113A-ASCC pathway during alkylation damage rests with the E3 ligase activity of RNF113A.

5.3.2 Future Directions

This work details an E3 ligase whose activity is specifically activated upon alkylation. Interestingly, previous work has demonstrated that the activity of E3 ligases and deubiquitinases (DUBs) are regulated by post-translational modifications like phosphorylation (Khosravi et al., 1999; Wertz et al., 2015; Zhao et al., 2018). Thus, future experiments analyzing the post-translational modifications that regulate RNF113A would be of particular importance. Intriguingly, preliminary studies from our lab suggest that pre-treatment of Flag-RNF113A purified from HeLa-S cells with either the CIP phosphatase or λ-phosphatase drastically reduces *in vitro* RNF113A ligase activity (Figure 5.6), suggesting that phosphorylation may regulate RNF113A E3 ligase activity.

To identify the phosphorylation site on RNF113A, Flag-HA-RNF113A was purified from HeLa-S cells after MMS treatment. The complex was run on a Coomassie gel after elution and the RNF113A band was isolated for phosphorylation-specific mass spectrometry. The mass spectrometry data revealed four sites that were phosphorylated: S6, S84, S85, and S253 (data not shown), which are detailed in Figure 5.7A. Additionally, we generated the RNF113A N5 mutant (S6A, S43A, S45-47A), the N7 mutant (S6A, S43, S45-47A, and S84-85A) or the C9 mutant (T168A, S169A, S174-175A, T192A, S253A, S268A, and T292-293A) constructs containing mutations of putative phosphorylation sites (Figure 5.7A). Mutation of S6 to alanine significantly attenuated RNF113A ligase activity *in vitro*, while the S84A/S85A and S253A had no appreciable effect on its activity (Figure 5.7B). The RNF113A S6A mutant also demonstrated decreased autoubiquitination activity, as did the S84A/S85A mutant. Conversely, the S253A

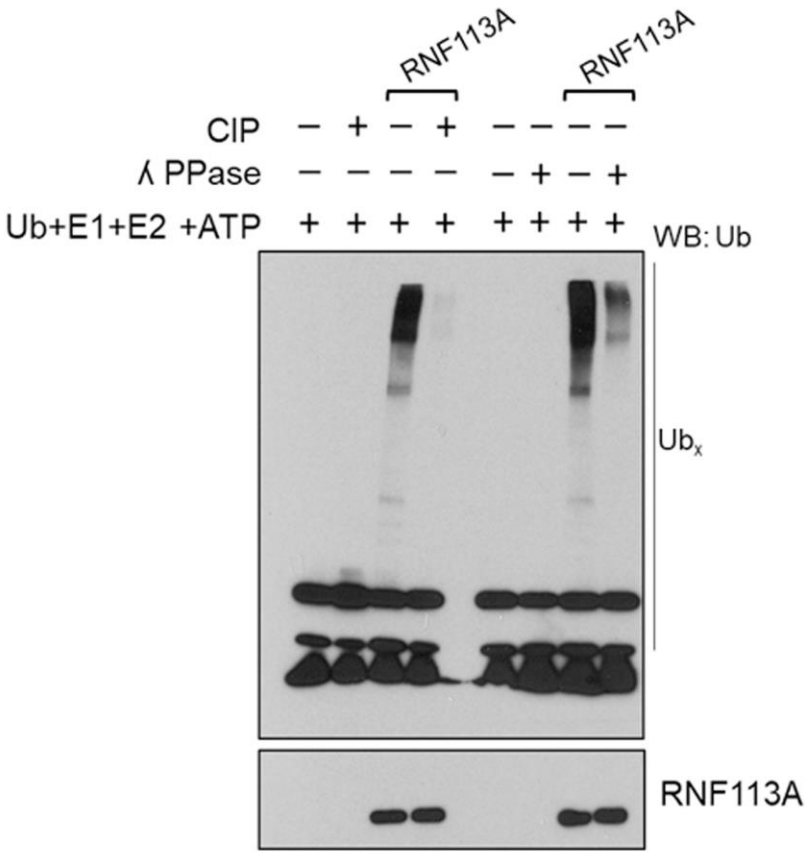

Figure 5.6. Phosphatase Treatment Reduces RNF113A Activity *in vitro*. Flag-RNF113A was purified from HeLa-S cells. Protein was pre-treated with either CIP phosphatase or λ phosphatase for 1 hour at 37C. This protein was then used in ubiquitin ligase assays using E1 (500 nM), and E2 (UbcH5c 250 nM each). Reactions were analyzed by Western blot (n=3 independent experiments).

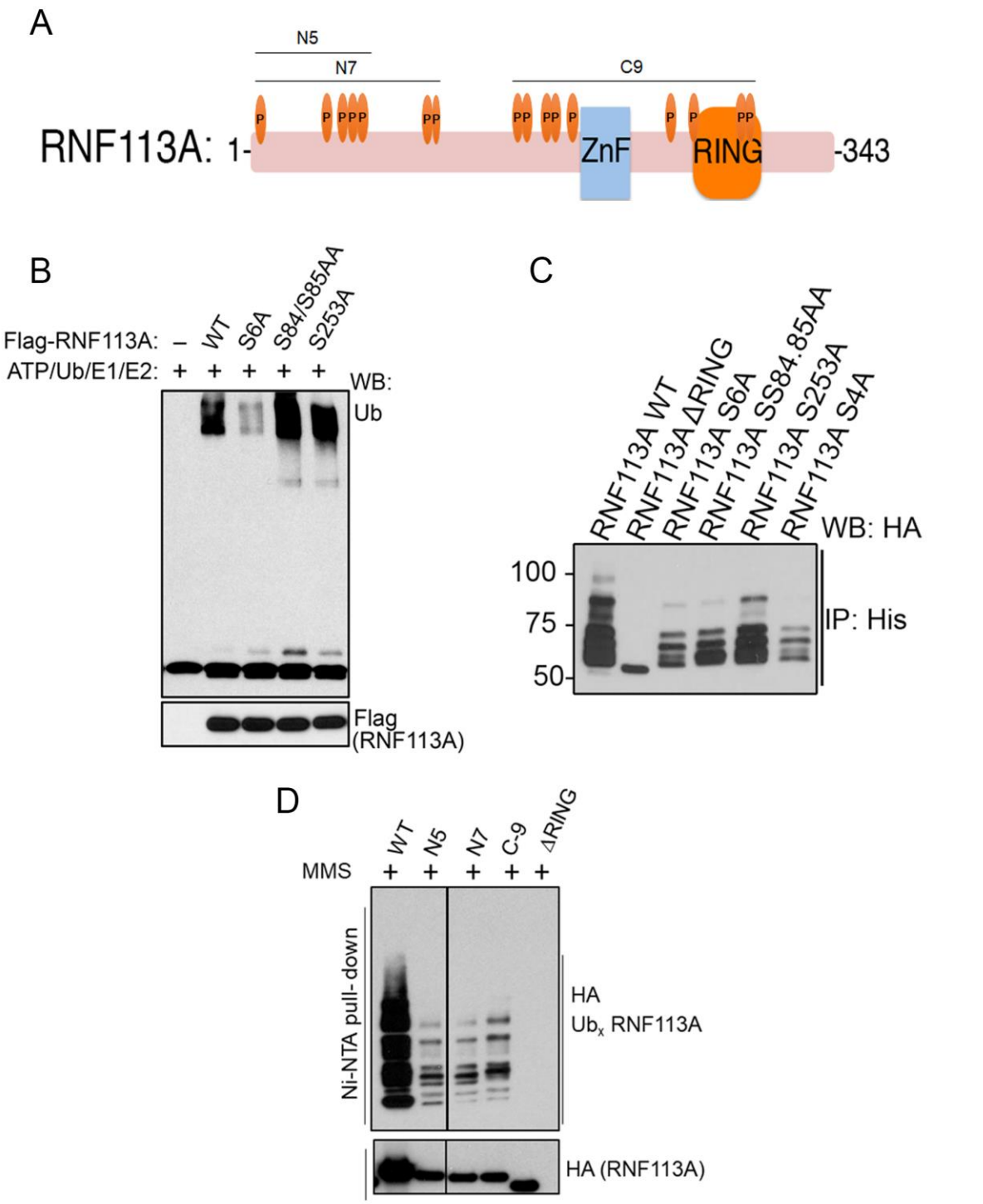

Figure 5.7. Mutational Analysis of RNF113A Phosphorylation Mutants. (A) Schematic of potential phosphorylation sites in RNF113A. (B) Flag-RNF113A mutants were purified from HeLa-S cells and then used in ubiquitin ligase assays using E1 (500 nM), and E2 (UbcH5c 250 nM each). Reactions were analyzed by Western blot (n=3 independent experiments). (C) and (D) 293T cells expressing His-ubiquitin were transduced with Flag-HA-RNF113A variants and treated with MMS. Ubiquitinated proteins were isolated by Ni-NTA under denaturing conditions and Western blotted as shown. Input lysates were also analyzed as indicated (n=3 independent experiments).

mutation had less effect on RNF113A autoubiquitination (Figure 5.7C). Each of these RNF113A mutant, however, was more active than RNF113A WT protein purified in the absence of alkylation damage (data not shown), suggesting that these single mutants are not sufficient to abrogate RNF113A E3 ligase activity. The RNF113A N5, N7 and C9 mutants also reduced but did not abrogate RNF113A autoubiquitination (Figure 5.7). The RNF113A N5 and N7 mutants co-localized with PRP8 to similar levels as wild-type RNF113A (Figure 5.8A-B). Conversely, the RNF113A C9 mutant did not express (data not shown). Interestingly, both the RNF113A N5 and N7 mutants reduced HA-ASCC2 foci during alkylation damage (Figure 5.8C), suggesting that phosphorylation near the N-terminus of RNF113A regulates is E3 ligase activity and thus regulates ASCC complex recruitment. Taken together, this data suggests that a post-translational phosphorylation modification regulates RNF113A ligase activity.

While the data described above provides the groundwork for identifying the phosphorylation site, future experiments could help further elucidate the specific phosphorylation site. TUBE pulldown assays using various RNF113A phosphorylation mutants could identify which mutants reduce RNF113A autoubiquitination. These mutants could then be used to complement RNF113A KO cells in both U2OS and HeLa cells. The effect of these phosphorylation mutants on ASCC2/ASCC3 foci formation and sensitivity to MMS could be assessed, respectively. Additionally, rather than mutating the serine or threonine residue(s) to alanine, the same experiments could be performed using RNF113A mutants where the serine or threonine has been mutated to aspartate or glutamate, generating phospho-mimetic mutants. Using these mutants will determine whether the change in protein charge or the actual phosphate is responsible for activation of RNF113A ligase activity. Together, this work will help further elucidate the mechanism by which the ASCC-ALKBH3 repair pathway is regulated.

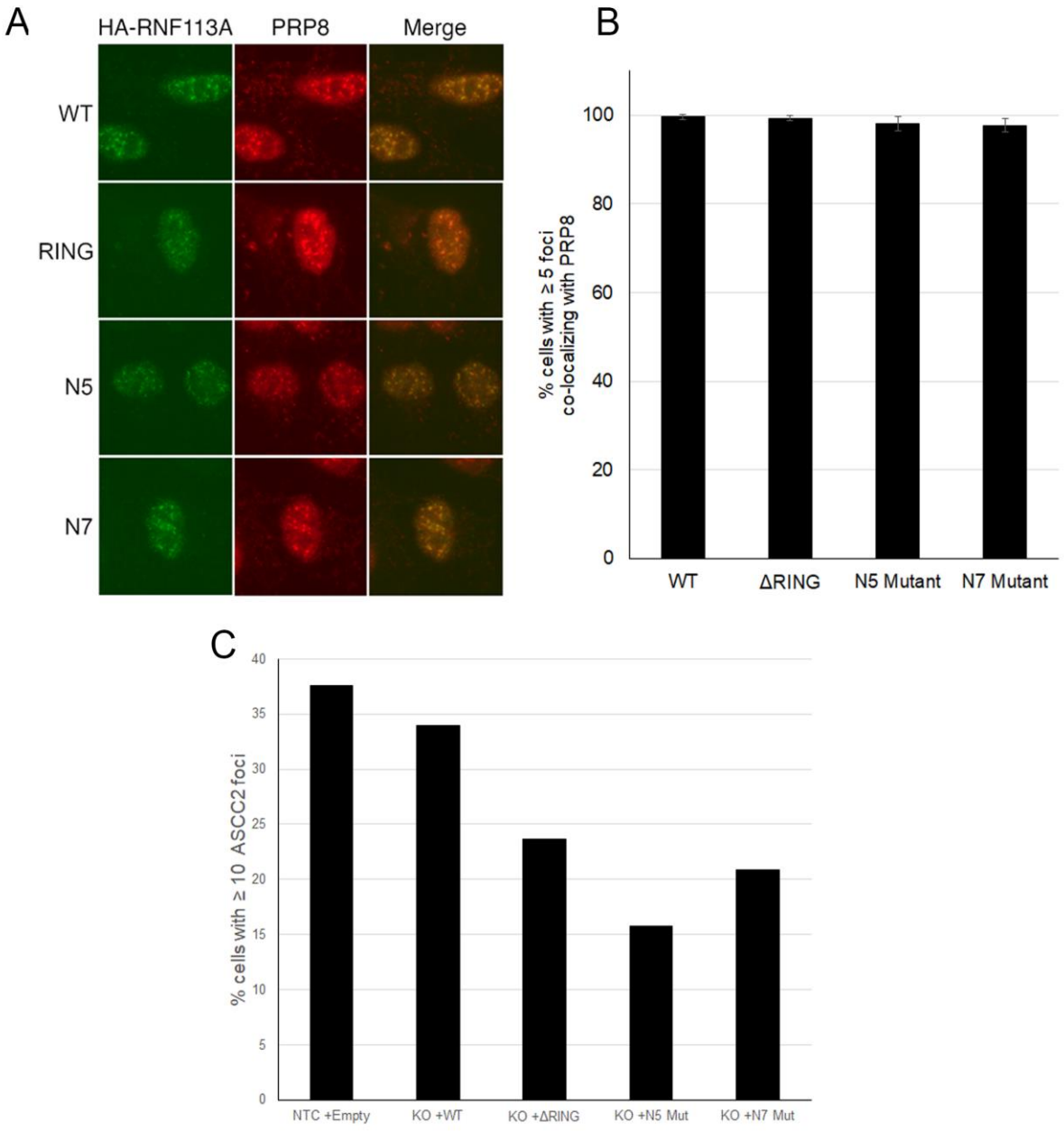

Figure 5.8. RNF113A Phospho-Mutants Reduce ASCC2 Foci Formation. (A) Images of cells expressing WT or the indicated HA-RNF113A phosphorylation mutant constructs. Scale bar, 10 μm. (B) Quantitation of co-localization between each RNF113A construct and PRP8 (n=3 biological replicates; mean ± S.D.). (C) Quantitation of HA-ASCC2 foci in RNF113A knockdown U2OS cells expressing the indicated RNF113A mutant constructs after MMS treatment (n=1 biological replicate; mean).

In addition to identifying the phosphorylation site that regulates RNF113A activity, future experiments could also focus on the kinase responsible for the phosphorylation. Analysis of the RNF113A interactome as determined by tandem mass spectrometry revealed several kinases that interact with RNF113A (Figure 5.9A). Of particular interest are the kinases CDK12 and CDK13, as each of these kinases phosphorylate the CTD domain of RNA PolII to initiate the switch from an initiation complex to an elongation complex (Bartkowiak et al., 2010; Liang et al., 2015). As ASCC2 and ASCC3 co-localize with elongating RNA PolII during alkylation damage (Figure 2.4), it is probable that one of these kinases are responsible for phosphorylating RNF113A. Interestingly, S6 is a canonical CDK target site, providing further support for the notion that this may be the site of phosphorylation. Knockdown of CDK12 and its associated partner Cyclin K reduced ASCC2 foci during alkylation damage (Figure 5.9B), while knockdown of CDK13 had a much less significant effect. Strikingly, inhibition of CDK12 using the CDK12/CDK13-specific inhibitor THZ531 (Zhang et al., 2016) attenuated RNF113A autoubiquitination as assessed by the TUBE assay (Figure 5.10). Taken together, these data suggest that RNF113A may be a substrate of CDK12.

To further elucidate the role of CDK12 in recruiting the ASCC-ALKBH3 complex, CDK12 knockdown cells or cells treated with THZ531 could be assessed for sensitivity to MMS. The knockdown cells could then be complemented with wild-type or mutant versions of CDK12. To distinguish between the role of CDK12 and CDK13, the MMS sensitivity phenotype of CDK12 knockdown cells could be compared to the MMS sensitivity displayed by CDK12 knockdown cells. I predict that CDK12 but not CDK13 loss will result in hypersensitivity to MMS.

The interplay between RNA alkylation and CDK12-mediated activation by can be further determined by overexpressing METTL8 in cells. After transducing cells with METTL8,

A

	MWT(kDa)	Unique Untreated	Total Untreated	Unique Treated	Total Treated	Intensity: UT	Intensity: 30min
CDK11A	91.31	0	0	2	2	0.0	1.0
CDK13	164.82	0	0	2	2	0.0	1.0
CDK12	164.05	0	0	2	2	0.0	1.0

B

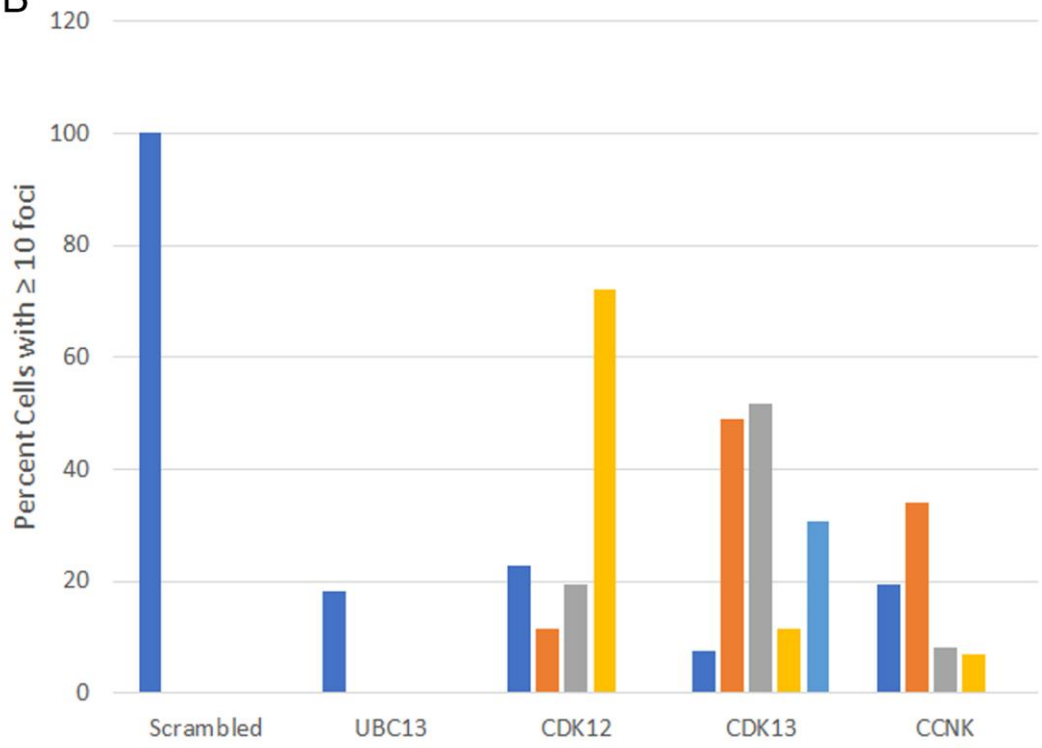

Figure 5.9. CDK12 May Regulate ASCC2 Foci Formation. (A) Kinase peptides found identified in the mass spectrometry data analyzing the RNF113A interactome. (B) Quantitation of HA-ASCC2 foci in U2OS cells transduced with shRNA to CDK12, CDK13 or Cyclin K. UBC13 was used as the positive control and a Scrambled sequence as the negative control (n=1 biological replicate).

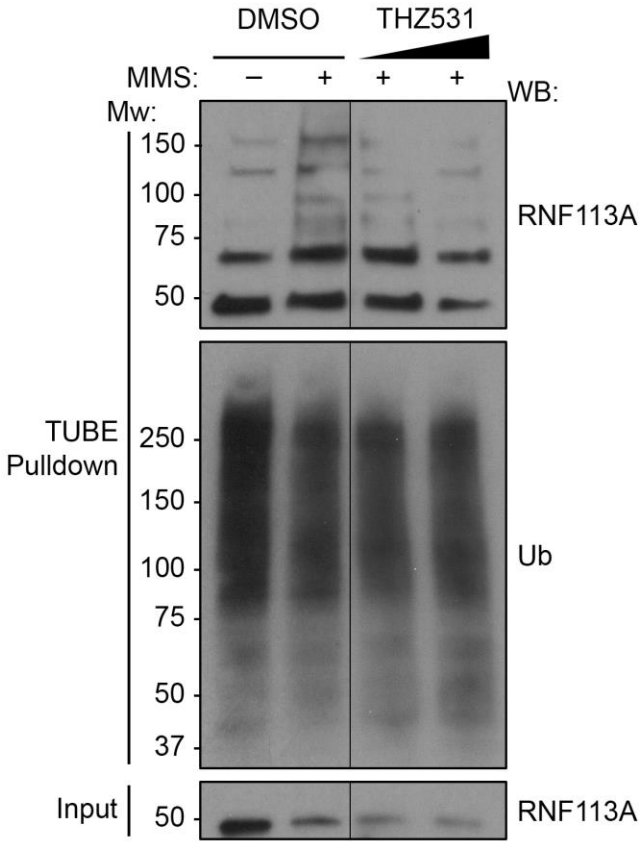

Figure 5.10. CDK12 Inhibition Reduces RNF113A Autoubiquitination. Cells were pre-treated with THZ531 (200 or 400 μM) for 1 hour, then treated with 500 μM MMS for 4 hours. Endogenous ubiquitin was isolated from HeLa-S cells using ubiquilin TUBE beads and Western blotted for endogenous RNF113A. Input lysates were also analyzed a indicated (n=2 independent experiments).

RNF113A autoubiquitination can be assessed by the TUBE assay in the presence or absence of THZ531. I predict that, like MMS treatment, THZ531 inhibition will result in a decrease in RNF113A autoubiquitination during METTL8 expression. Additionally, m1A and m3C levels on both DNA and RNA could be measured upon inhibition of CDK12 after alkylation. I predict that m1A and m3C levels will be elevated on both RNA and DNA upon inhibition of CDK12 with THZ531. Together, these studies will provide further evidence that CDK12 is part of the mechanism regulating ASCC-ALKBH3-mediated alkylation repair.

In collaboration with the Reynoird lab, preliminary experiments have also identified RNF113A as a substrate for the protein methyltransferase SMYD3 (Figure 5.11A-B). Previous work described a mechanism by which methylation of the SMYD3 substrate MAP3K2 inhibits the interaction between MAP3K2 and the PP2A phosphatase complex, thus promoting MAP3K2 kinase activity (Mazur et al., 2014). Thus, a potential model for RNF113A activation during alkylation suggests that RNF113A remains in an equilibrium between being phosphorylated by CDK12 and de-phosphorylated by an unknown phosphatase. During alkylation damage, methylation by SMYD3 may inhibit the interaction between RNF113A and this phosphatase, promoting RNF113A phosphorylation and resulting in an active RNF113A enzyme (Figure 5.11C). Future experiments could focus on identifying the phosphatase in this pathway. To identify the phosphatase, a panel of shRNAs targeting the different phosphatases could be co-transduced with HA-ASCC2 into cells. Spontaneous ASCC2 foci formation in the absence of damage could then be assessed, serving as a read-out for hyperactive RNF113A and thus revealing the putative phosphatase. Alternatively, RNF113A autoubiquitination after knockdown of these phosphatases could also be measured to identify the putative kinase. The effect of a loss of the phosphatase on MMS sensitivity could also be assessed. I predict that loss of the

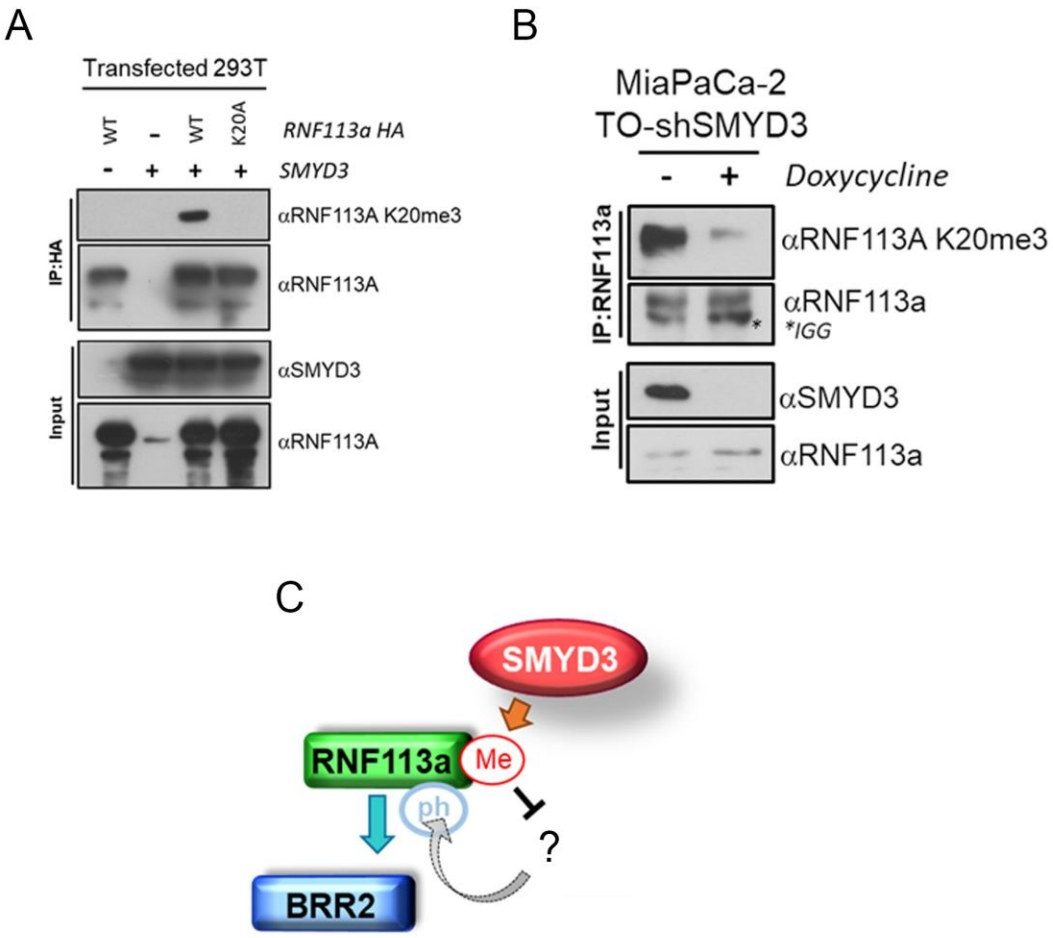

Figure 5.11. RNF113A is a Substrate of SMYD3. (A) The indicated HA-RNF113A constructs and SMYD3 were transfected in HEK293T cells. HA-RNF113A was immunoprecipitated from cells and the eluate was analyzed by Western blot for the indicated antibodies. (B) MiaPaCa cells were treated with doxycycline to induce expression of SMYD3 shRNA. Endogenous RNF113A was immunoprecipitated from cells and eluate was analyzed by Western blot with the indicated antibodies. (C) Potential model for regulation of RNF113A activity by SMYD3.

phosphatase would result in hyper-resistance of these cells to MMS as compared to their wild-type counterparts. These cells could be complemented with wild-type and catalytic mutant versions of the phosphatase and reassessed for MMS sensitivity. These experiments will shed insight into another mode of regulation for this pathway.

The role of RNA modification in regulating translation, RNA processing, and DNA repair is becoming more apparent (Thapar 2018; Thapar et al., 2018). Similar to DNA damage repair, this regulation involves RNA readers, writers, and erasers (Jonkhout et a., 2017). While evidence of a 'reader' protein for alkylation damage adducts on pre-mRNA remains speculative, m6A on mature mRNA is recognized by multiple proteins, including YTHDF2 (Meyer and Jaffrey, 2017; Wang et al., 2014; Xiao et al., 2016). Interestingly, recent work suggests that a subset of these m6A readers may recognize m1A, making it plausible that readers of alkylated lesions could exist (Dai et al., 2018).

As such, future work could also focus on identifying these reader proteins of pre-mRNA alkylation lesions. Of particular interest would be YTHDF3 and YTHDC2, both of which have been shown to be nuclear (Sigma Protein Atlas). Our preliminary studies also suggest that loss of YTHDF3 and YTHDC2 reduce ASCC2 foci formation during alkylation (data not shown), suggesting that these proteins may be *bona fide* readers of alkylation adducts on RNA that promote ASCC complex recruitment. To verify that these proteins bind to m1A and m3C adducts, RIP-MS experiments could be performed. YTHDF3 and YTHDC2 would be purified from cells after alkylation damage and the RNA will be subsequently isolated using TRIzol extraction (Rio et al., 2010). The resulting RNA can then be digested to the nucleoside and analyzed by mass spectrometry to identify the modification recognized by these proteins, respectively. Additionally, knockout cell lines of these proteins could be generated and ASCC

foci formation, RNF113A autoubiquitination and MMS sensitivity could be determined. I predict that loss of these proteins would result in reduced ASCC foci formation and RNF113A autoubiquitination in response to alkylation damage. These cells would also be hypersensitive to MMS as compared to their wild-type counterpart. Taken together, these experiments would identify novel readers of alkylation damage occurring on RNA and provide further support for the idea that ASCC complex recruitment depends upon RNA alkylation.

Lastly, further exploration into the transcriptional repression function of this complex is required. To demonstrate that the ASCC complex represses transcription in response to RNA alkylation, global RNA-Seq experiments can be performed. Here, RNA will be isolated from cells expressing METTL8-NLS protein and transcript levels will be analyzed by sequencing. As a control, a separate population of cells will be treated with MMS. Changes in transcription can be compared between the MMS-treated samples and the METTL8-NLS overexpression cells. I hypothesize that these two cell populations will have a similar expression profiles. As an additional control, RNA will be isolated from ASCC3 KO cells expressing METTL8-NLS and sequenced. As loss of ASCC3 de-repressed the majority of transcripts that were repressed upon alkylation, I predict that overexpressing METTL8 in an ASCC3 KO background will mimic this de-repression phenotype.

Additionally, it would particularly interesting to map the m3C landscape on RNA during METTL8 overexpression. In collaboration with the Chuan He lab, RNA has been isolated from cells overexpressing METTL8-NLS and the m3C landscape is being profiled (Zhang et al., 2019). Concurrent ChIP-Seq of ASCC3 would demonstrate that the ASCC complex is being recruited to sites of RNA modification by METTL8. Here, ASCC3 will be immunoprecipitated from cells. Crosslinking would be reversed, the RNA or DNA isolated, and sequenced. I

hypothesize that the m3C landscape will overlap with the reads from ASCC3 ChIP-Seq, suggesting that ASCC3 is being recruited to sites of METTL8 RNA methylation. Additionally, I predict that these sites will correspond to regions of active transcription, providing further support for RNA-driven recruitment of the ASCC complex.

Together, these studies will provide invaluable insight into the increasingly complex mechanisms by which ASCC complex recruitment is regulated. Importantly, a more complete understanding of ASCC complex regulation could provide multiple potential novel therapeutic targets for inhibitors to re-sensitize cancers to chemotherapy. Additionally, these studies will provide a better understanding of how RNA alkylation impacts the recruitment of the ASCC complex and elucidate the transcriptional responses dictated by the ASCC complex and beyond.

References

Aas, P.A., Otterlei, M., Falnes, P.O., Vagbo, C.B., Skorpen, F., Akbari, M., Sundheim, O., Bjoras, M., Slupphaug, G., Seeberg, E., *et al.* (2003). Human and bacterial oxidative demethylases repair alkylation damage in both RNA and DNA. Nature *421*, 859-863.

Alemu, E.A., He, C., and Klungland, A. (2016). ALKBHs-facilitated RNA modifications and de-modifications. DNA Repair *44*, 87-91.

Alexandrov, A., Grayhack, E.J., and Phizicky, E.M. (2005). tRNA m7G methyltransferase Trm8p/Trm82p: evidence linking activity to a growth phenotype and implicating Trm82p in maintaining levels of active Trm8p. RNA *11*, 821-830.

Apostolou, Z., Chatzinikolaou, G., Stratigi, K., and Garinis, G.A. (2019). Nucleotide excision repair and transcription-associated genome instability. BioEssays *41*, 1800201.

Bagola, K., von Delbruck, M., Dittmar, G., Scheffner, M., Ziv, I., Glickman, M.H., Ciechanover, A., and Sommer, T. (2013). Ubiquitin binding by a CUE domain regulates ubiquitin chain formation by ERAD E3 ligases. Mol Cell *50*, 528-539.

Banaszynski, L.A., Chen, L.C., Maynard-Smith, L.A., Ooi, A.G.L., and Wandless, T.J.A. (2006). A rapid, reversible, and tunable method to regulate protein function in living cells using synthetic small molecules. Cell *126*, 995-1004.

Barrows, L.R., and Magee, P.N. (1982). Nonenzymatic methylation of DNA by S-adenosylmethionine in vitro. Carcinogenesis *3*, 349-351.

Bartkowiak, B., Liu, P., Phatnani, H.P., Fuda, N.J., Cooper, J.J., Price, D.H., Adelman, K., Lis, J.T., and Greenleaf, A.L. (2010). CDK12 is a transcription elongation-associated CTD kinase, the metazoan ortholog of yeast Ctk1. Genes Dev *24*, 2303-2316.

Ben-Saadon, R., Zaaroor, D., Ziv, T., and Ciechanover, A. (2006). The polycomb protein Ring1B generates self atypical mixed ubiquitin chains required for its in vitro histone H2A ligase activity. Mol Cell *24*, 701-711.

Bekker-Jensen, S., Rendtlew Danielson, J., Fugger, K., Gromova, I., Nerstedt, A., Lukas, C., Bartek, J., Lukas, J., and Mailand, N. (2010). HERC2 coordinates ubiquitin-dependent assembly of DNA repair factors on damaged chromosomes. Nat Cell Biol *12*, 80-86.

Beranek, D.T. (1990). Distribution of methyl and ethyl adducts following alkylation with monofunctional alkylating agents. Mutat Res *231*, 11-30.

Biancalana, V., Beldjord, C., Taillandier, A., Szpiro-Tapia, S., Cusin, V., Gerson, F., Philippe, C., and Mandel, J.L. (2004). Five years of molecular diagnosis of Fragile X syndrome (1997-2001): a collaborative study reporting 95% of the activity in France. Am J Med Genet A *129A*, 218-224.

Boeing, S., Williamson, L., Encheva, V., Gori, I., Saunders, R.E., Instrell, R., Aygun, O., Rodriguez-Martinez, M., Weems, J.C., Kelly, G.P., Conaway, J.W., Conaway, R.C., Stewart, A.,

Howell, M., Snijders, A.P., and Svejstrup, J.Q. (2016). Multiomic analysis of UV-induced DNA damage response. Cell Rep *15*, 1597-1610.

Bohnsack, M.T., Regener, K., Schwappach, B., Saffrich, R., Paraskeva, E., Hartmann, E., and Gorlich, D. (2002). Exp5 exports eEF1A via tRNA from nuclei and synergizes with other transport pathways to confine translation to the cytoplasm. EMBO J *21*, 6205-6215.

Bohr, V.A., Smith, C.A., Okumoto, D.S., and Hanawalt, P.C. (1985). DNA repair in an active gene: removal of pyrimidine dimers from the DHFR gene of CHO cells is much more efficient than in the genome overall. Cell *40*, 359-369.

Brickner, J.R., Soll, J.M., Lombardi, P.M., Vagbo, C.B., Mudge, M.C., Oyeniran, C., Rabe, R., Jackson, J., Sullender, M.E., Blazosky, E., *et al.* (2017). A ubiquitin-dependent signalling axis specific for ALKBH-mediated DNA dealkylation repair. Nature *551*, 389-393.

Brown, R.L., August, S.L., Williams, C.J., and Moss, S.B. (2003). AKAP7gamma is a nuclear RI-binding AKAP. Biochem Biophys Res Commun *306*, 394-401.

Calvo, J.A., Meira, L.B., Lee, C.Y., Moroski-Erkul, C.A., Abolhassani, N., Taghizadeh, K., Eichinger, L.W., Muthupalani, S., Nordstrand, L.M., Klungland, A., *et al.* (2012). DNA repair is indispensable for survival after acute inflammation. J Clin Invest *122*, 2680-2689.

Celeste, A., Petersen, S., Romanienko, P.J., Fernandez-Capetillo, O., Chen, H.T., Sedelnikova, O.A., Reina-San-Martin, B., Coppola, V., Meffre, E., Difilippantonio, M.J., Redon, C., Pilch, D.R., Olaru, A., Eckhaus, M., Camerini-Otero, R.D., Tessarollo, L., Livak, F., Manova, K., Bonner, W.M., Nussenzweig, M.C., and Nussenzweig, A. (2002). Genomic instability in mice lacking H2AX. Science *296*, 922-927.

Christmann, M., Verbeek, B., Roos, W.P., and Kaina, B. (2011). O(6)-Methylguanine-DNA methyltransferase (MGMT) in normal tissues and tumors: enzyme activity, promoter methylation and immunohistochemistry. Biochim Biophys Acta *1816*, 179-190.

Cook, A., Bono, F., Jinek, M., and Conti E. (2007). Structural biology of nucleocytoplasmic transport. Annu Rev Biochem *76*, 647-671.

Corbett, M.A., Dudding-Byth, T., Crock, P.A., Botta, E., Christie, L.M., Nardo, T., Caliguiri, G., Hobson, L., Boyle, J., Mansour, A., Friend, K.L., Crawford, J., Jackson, G., Vandeleur, L., Hackett, A., Tarpey, P., Stratton, M.R., Turner, G., Gecz, J., and Field, M. (2015). A novel X-linked trichothiodystrophy associated with a nonsense mutation in RNF113A. J Med Genet *52*, 269-274.

Dai, X., Wang, T., Gonzalez, G., and Wang, Y. (2018). Identification of YTH domain-containing proteins as the readers for N1-methyladenosine in RNA. Anal Chem *90*, 6380-6384.

Daley, J.M., and Sung, P. (2014). 53BP1, BRCA1, and the choice between recombination and end joining at DNA double-strand breaks. Mol Cell Biol *34*, 1380-1388.

Dango, S., Mosammaparast, N., Sowa, M.E., Xiong, L.J., Wu, F., Park, K., Rubin, M., Gygi, S., Harper, J.W., and Shi, Y. (2011). DNA unwinding by ASCC3 helicase is coupled to ALKBH3-dependent DNA alkylation repair and cancer cell proliferation. Mol Cell *44*, 373-384.

de Bont, R., and Van Larebeke, N. (2004). Endogenous DNA damage in humans: a review of quantitative data. Mutagenesis *19*, 169-185.

Delaney, J.C., Smeester, L., Wong, C., Frick, L.E., Taghizadeh, K., Wishnok, J.S., Drennan, C.L., Samson, L.D., and Essigmann, J.M. (2005). AlkB reverses etheno DNA lesions caused by lipid oxidation in vitro and in vivo. Nat Struct Mol Biol *12*, 855-860.

Deng, B., Xu, W., Wang, Z., Liu, C., Lin, P., Li, B., Huang, Q., Yang, J., Zhou, H., and Qu, L. (2019). An LTR retrotransposon-derived lncRNA interacts with RNF169 to promote homologous recombination. EMBO Rep, e47650.

Deshaies, R.J., and Joazeiro, C.A. (2009). RING domain E3 ubiquitin ligases. Annu Rev Biochem *78*, 399-434.

Dias, A.P., Dufu, K., Lei, H., and Reed, R. (2010). A role for TREX components in the release of spliced mRNA from nuclear speckle domains. Nat Commun *1*, 97.

Doherty, A.J., and Suh, S.W. (2000). Structural and mechanistic conservation in DNA ligases. Nucleic Acids Res *28*, 4051-4058.

Doil, C., Mailand, N., Bekker-Jensen, S., Menard, P., Larsen, D.H., Pepperkok, R., Ellenberg, J., Panier, S., Durocher, D., Bartek, J., Lukas, J., and Lukas. C. (2009). RNF168 binds and amplifies ubiquitin conjugates on damaged chromosomes to allow accumulation of repair proteins. Cell *136*, 435-446.

Dominissini, D., Nachtergaele, S., Moshitch-Moshkovitz, S., Peer, E., Kol, N., Ben-Haim, M.S., Dai, Q., Di Segni, A., Salmon-Divon, M., Clark, W.C., *et al.* (2016). The dynamic N(1)-methyladenosine methylome in eukaryotic messenger RNA. Nature *530*, 441-446.

Drablos, F., Feyzi, E., Aas, P.A., Vaagbo, C.B., Kavli, B., Bratlie, M.S., Pena-Diaz, J., Otterlei, M., Slupphaug, G., and Krokan, H.E. (2004). Alkylation damage in DNA and RNA--repair mechanisms and medical significance. DNA repair *3*, 1389-1407.

Duncan, T., Trewick, S.C., Koivisto, P., Bates, P.A., Lindahl, T., and Sedgwick, B. (2002). Reversal of DNA alkylation damage by two human dioxygenases. Proc Natl Acad Sci U S A *99*, 16660-16665.

Edmonds, M.J., and Parsons, J.L. (2014). Regulation of base excision repair proteins by ubiquitylation. Exp Cell Res *329*, 132-138.

Eloranta, T.O. (1977). Tissue distribution of S-adenosylmethionine and S-adenosylhomocysteine in the rat. Effect of age, sex and methionine administration on the metabolism of S-adensoylmethionine, S-adenosylhomocysteine and polyamines. Biochem J *166*, 521-529.

Eng, J.K., McCormack, A.L., and Yates, J.R. (1994). An approach to correlate tandem mass spectral data of peptides with amino acid sequences in a protein database. J Am Soc Mass Spectrom *5*, 976-989.

Esteller, M., Garcia-Foncillas, J., Andion, E., Goodman, S.N., Hidalgo, O.F., Vanaclocha, V., Baylin, S.B., and Herman, J.G. (2000). Inactivation of the DNA-repair gene MGMT and the clinical response of gliomas to alkylating agents. N Engl J Med *343*, 1350-1354.

Fagbemi, A.F., Orelli, B., and Scharer, O.D. (2011). Regulation of endonuclease activity in human nucleotide excision repair. DNA Repair (Amst) *10*, 722-729.

Faghri S., Tamura, D., Kraemer, K.H., and Digiovanna, J.J. (2008). Trichothiodystrophy: a systematic review of 112 published cases characterises a wide spectrum of clinical manifestations. J Med Genet *45*, 609-621.

Falnes, P.O., Johansen, R.F., and Seeberg, E. (2002). AlkB-mediated oxidative demethylation reverses DNA damage in Escherichia coli. Nature *419*, 178-182.

Fan, L., Fuss, J.O., Cheng, Q.J., Arvai, A.S., Hammel, M., Roberts, V.A., Cooper, P.K., and Tainer, J.A. (2008). XPD helicase structures and activities: insights into the cancer and aging phenotypes from XPD mutations. Cell *133*, 789-800.

Fang, Q., Inanc, B., Schamus, S., Wang, X.H., Wei, L., Brown, A.R., Svilar, D., Sugrue, K.F., Goellner, E.M., Zeng, X., *et al.* (2014). HSP90 regulates DNA repair via the interaction between XRCC1 and DNA polymerase beta. Nat Commun *5*, 5513.

Fei, J., and Chen, J. (2012). KIAA1530 protein is recruited by Cockayne syndrome complementation group A (CSA) to participate in transcription-coupled repair (TCR). J Biol Chem *287*, 35118-35126.

Feyzi, E., Sundheim, O., Westbye, M.P., Aas, P.A., Vagbo, C.B., Otterlei, M., Slupphaug, G., and Krokan, H.E. (2007). RNA base damage and repair. Curr Pharm Biotechnol *8*, 326-331.

Fortini, P., and Dogliotti, E. (2007). Base damage and single-strand break repair: mechanisms and functional significance of short- and long-patch repair subpathways. DNA Repair (Amst) *6*, 398-409.

Fousteri, M., Vermeulen, W., van Zeeland, A.A., and Mullenders, L.H.F. (2006). Cockayne syndrome A and B proteins differentially regulate recruitment of chromatin remodeling and repair factors to stalled RNA polymerase II in vivo. Mol Cell *23*, 471-482.

Friedberg, E.C. (1996). Relationships between DNA repair and transcription. Annu Rev Biochem *65*, 15-42.

Fu, D., Calvo, J.A., and Samson, L.D. (2012). Balancing repair and tolerance of DNA damage caused by alkylating agents. Nat Rev Cancer *12*, 104-120.

Fu, D., and Samson, L.D. (2012). Direct repair of 3,N(4)-ethenocytosine by the human ALKBH2 dioxygenase is blocked by the AAG/MPG glycosylase. DNA Repair (Amst) *11*, 46-52.

Fukuda, M., Asano, S., Nakamura, T., Adachi, M., Yoshida, M., Yanagida, M., and Nishida, E. (1997). CRM1 is responsible for intracellular transport mediated by the nuclear export signal. Nature *390*, 308-311.

Gajjar, M., Candeias, M.M., Malbert-Colas, L., Mazars, A., Fujita, J., Olivares-Illana, V., and Fahraeus, R. (2012). The p53 mRNA-Mdm2 interaction controls Mdm2 nuclear trafficking and is required for p53 activation following DNA damage. Cancer Cell *21*, 25-35.

Gardner, K.E., Allis, C.D., and Strahl, B.D. (2011). Operating on chromatin, a colorful language where context matters. J Mol Biol *409*, 36-46.

Gatti, M., Pinato, S., Maspero, E., Soffientini, P., Polo, S., and Penengo, L. (2012). A novel ubiquitin mark at the N-terminal tail of histone H2As targeted by the RNF168 ubiquitin ligase. Cell Cycle *11*, 2538-2544.

Gatti, M., Pinato, S., Maiolica, A., Rocchio, F., Prato, M.G., Aebersold, R., and Penengo, L. (2015). RNF168 promotes noncanonical K27 ubiquitination to signal DNA damage. Cell Reports *10*, 226-238.

Gentil, A., Cabral-Neto, J.B., Mariage-Samson, R., Margot, A., Imbach, J.L., Rayner, B., and Sarasin, A. (1992). Mutagenicity of a unique apurinic/apyrimidinic site in mammalian cells. J Mol Biol *227*, 981-984.

Gerken, T., Girard, C.A., Tung, Y.C., Webby, C.J., Saudek, V., Hewitson, K.S., Yeo, G.S., McDonough, M.A., Cunliffe, S., McNeill, L.A., *et al.* (2007). The obesity-associated FTO gene encodes a 2-oxoglutarate-dependent nucleic acid demethylase. Science *318*, 1469-1472.

Gerson, S.L. (2004). MGMT: its role in cancer aetiology and cancer therapeutics. Nat Rev Cancer *4*, 296-307.

Girard, C., Will, C.L., Peng, J., Makarov, E.M., Kastner, B., Lemm, I., Urlaub, H., Hartmuth, K., Luhrmann, R. (2012). Post-transcriptional spliceosomes are retained in nuclear speckles until splicing completion. Nat Commun *3*, 994.

Gold, M.G., Smith, F.D., Scott, J.D., and Barford, D. (2008). AKAP18 contains a phosphoesterase domain that binds AMP. J Mol Biol *375*, 1329-1343.

Gregersen, L.H., and Svejstrup, J.Q. (2018). The cellular response to transcription-blocking DNA damge. Trends Biochem Sci *43*, 327-341.

Gros, L., Maksimenko, A.V., Privezentzev, C.V., Laval, J., and Saparbaev, M.K. (2004). Hijacking of the human alkyl-N-purine-DNA glycosylase by 3,N4-ethenocytosine, a lipid peroxidation-induced DNA adduct. J Biol Chem *279*, 17723-17730.

Gusho, E., Zhang, R., Jha, B.K., Thornbrough, J.M., Dong, B., Gaughan, C., Elliott, R., Weiss, S.R., and Silverman, R.H. (2014). Murine AKAP7 has a 2',5'-phosphodiesterase domain that can complement an inactive murine coronavirus ns2 gene. MBio *5*, e01312-01314.

Guzder, S.N., Habraken, Y., Sung, P., Prakash, L., and Prakash, S. (1996). RAD26, the yeast homolog of human cockayne's syndrome group B gene, encodes a DNA-dependent ATPase. J Biol Chem *271*, 18314-18317.

Hegele, A., Kamburov, A., Grossmann, A., Sourlis, C., Wowro, S., Weimann, M., Will, C.L., Pena, V., Luhrmann, R., and Stelzl, U. (2012). Dynamic protein-protein interaction wiring of the human spliceosome. Mol Cell *45*, 567-580.

Hershko, A., Ciechanover, A., and Varshavsky, A. (2000). Basic medical research award. The ubiquitin system. Nat Med *6*, 1073-1081.

Hess, M.T., Schwitter, U., Petretta, M., Giese, B., and Naegeli, H. (1997). Bipartite substrate discrimination by human nucleotide excision repair. PNAS *94*, 6664-6669.

Huarte, M., Guttman, M., Feldser, D., Garber, M., Koziol, M.J., Kenzelmann-Broz, D., Halil, A.M., Zuk, O., Amit, I., Rabani, M., Attardi, L.D., Regev, A., Lander, E.S., Jacks, T., and Rinn, J.L. (2010). A large intergenic noncoding RNA induced by p53 mediates global gene repression in the p53 response. Cell *142*, 409-419.

Huen, M.S., Grant, R., Manke, I., Minn, K., Yu, X., Yaffe, M.B., and Chen, J. (2007). RNF8 transduces the DNA-damage signal via histone ubiquitylation and checkpoint protein assembly. Cell *131*, 901-914.

Hwang, C.S., Shemorry, A., and Varshavsky, A. (2009). Two proteolytic pathways regulate DNA repair by cotargeting the Mgt1 alkylguanine transferase. PNAS *106*, 2142-2147.

Jackson, S.P. and Bartek, J. (2009). The DNA-damage response in human biology and disease. Nature *551*, 1071/1078.

Jackson, S.P., and Durocher, D. (2013). Regulation of DNA damage responses by ubiquitin and SUMO. Mol Cell *49*, 795-807.

Janicki, S.M., Tsukamoto, T., Salghetti, S.E., Tansey, W.P., Sachidanandam, R., Prasanth, K.V., Ried, T., Shav-Tal, Y., Bertrand, E., Singer, R.H., and Spector D.L. (2004). From silencing to gene expression: real-time analysis in single cells. Cell *116*, 683-698.

Jelinsky, S.A., and Samson, L.D. (1999). Global response of Sccharomyces cerevisiae to an alkylating agent. PNAS *96*, 1486-1491.

Johnson, R.E., Yu, S.L., Prakash, S., and Prakash, L. (2007). A role for yeast and human translesion synthesis DNA polymerases in promoting replication through 3-methyl adenine. Mol Cell Biol *27*, 7198-7205.

Jonkhout, N., Tran, J., Smith, M.A., Schonrock, N., Mattick, J.S., and Novoa, E.M. (2017). The RNA modification landscape in human disease. RNA *23*, 1754-1769.

Jung, D.J., Sung, H.S., Goo, Y.W., Lee, H.M., Park, O.K., Jung, S.Y., Lim, J., Kim, H.J., Lee, S.K., Kim, T.S., *et al.* (2002). Novel transcription coactivator complex containing activating signal cointegrator 1. Molecular and cellular biology *22*, 5203-5211.

Kaina, B., Christmann, M., Naumann, S., and Roos, W.P. (2007). MGMT: key node in the battle against genotoxicity, carginogenicity and apoptosis induced by alkylating agents. DNA Repair (Amst) *6*, 1079-1099.

Karikkineth, A.C., Scheibye-Knudsen, M., Fivenson, E., Croteau, D.L., and Bohr, V.A. (2017). Cockayne syndrome: clinical features, model systems and pathways. Ageing Res Rev *33*, 3-17.

Kee, Y., and D'Andrea, A.D. (2010). Expanded roles of the Fanconi anemia pathway in preserving genomic stability. Genes Dev *24*, 1680-1694.

Kelley, L.A., Mezulis, S., Yates, C.M., Wass, M.N., and Sternberg, M.J. (2015). The Phyre2 web portal for protein modeling, prediction and analysis. Nat Protoc *10*, 845-858.

Kelley, L.A., and Sternberg, M.J. (2009). Protein structure prediction on the Web: a case study using the Phyre server. Nat Protoc *4*, 363-371.

Keskin, H., Shen, Y., Huang, F., Patel, M., Yang, T., Ashley, K., MAzin, A.V., and Storici, F. (2014). Transcript-RNA-templated DNA recombination and repair. Nature *515*, 436-439.

Kim, H., and D'Andrea, A.D. (2012). Regulation of DNA cross-link repair by the Fanconi anemia/BRCA pathway. Genes Dev *26*, 1393-1408.

Kim, J., McMillan, E., Kim, H.S., Venkateswaran, N., Makkar, G., Rodriguez-Canales, J., Villalobos, P., Neggers, J.E., Mendiratta, S., Wei, S., Landesman, Y., Senapedis, W., Baloglu, E., Chow, C.B., Frink, R.E., Gao, B., Roth, M., Minna, J.D., Daelemans, D., Wistuba, I.I., Posner, B.A., Scaglioni, P.P., and White, M.A. (2016). XPO1-dependent nuclear export is a druggable vulnerability in KRAS-mutant lung cancer. Nature *538*, 114-117.

Khosravi, R., Maya, R., Gottlieb, T., Oren, M., Shiloh, Y., and Shkedy, D. (1999). Rapid ATM-dependent phosphorylation of MDM2 precedes p53 accumulation in repsonse to DNA damage. PNAS *96*, 14973-14977.

Kolas, N.K., Chapman, J.R., Nakada, S., Ylanko, J., Chahwan, R., Sweeney, F.D., Panier, S., Mendez, M., Wildenhain, J., Thomson, T.M., Pelletier, L., Jackson, S.P., and Durocher, D. (2007). Orchestration of the DNA-damage response by the RNF8 ubiquitin ligase. Science *318*, 1637-1640.

Komander, D., and Rape, M. (2012). The ubiquitin code. Annu Rev Biochem *81*, 203-229.

Konishi, N., Nakamura, M., Ishida, E., Shimada, K., Mitsui, E., Yoshikawa, R., Yamamoto, H., and Tsujikawa, K. (2005). High expression of a new marker PCA-1 in human prostate carcinoma. Clinical cancer research : an official journal of the American Association for Cancer Research *11*, 5090-5097.

Koonin, E.V., and Gorbalenya, A.E. (1990). Related domains in yeast tRNA ligase, bacteriophage T4 polynucleotide kinase and RNA ligase, and mammalian myelin 2',3'-cyclic nucleotide phosphohydrolase revealed by amino acid sequence comparison. FEBS Lett *268*, 231-234.

Krokan, H.E., and Bjoras, M. (2013). Base excision repair. Cold Spring Harb Perspect Biol *5*, a012583.

Kudo, N., Wolff, B., Sekimoto, T., Schreiner, E.P., Yoneda, Y., Yanagida, M., Horinouchi, S., and Yoshida, M. (1998). Leptomycin B inhibition of signal-mediated nuclear export by direct binding to CRM1. Exp Cell Res *242*, 540-547.

Kurowski, M.A., Bhagwat, A.S., Papaj, G., and Bujnicki, J.M. (2003). Phylogenomic identification of five new human homologs of the DNA repair enzyme AlkB. BMC Genomics *4*, 48.

Lapalombella, R., Sun, Q., Williams, K., Tangeman, L., Jha, S., Zhong, Y., Goettl, V., Mahoney, E., Berglund, C., Gupta, S., Farmer, A., Mani, R., Johnson, A.J., Lucas, D., Mo, X., Daelemans, D., Sandanayaka, V., Shechter, S., McCauley, D., Shacham, S., Kauffman, M., Chook, Y.M., and Byrd, J.C. (2012). Selective inhibitors of nuclear export show that CRM1/XPO1 is a target in chronic lymphocytic leukemia. Blood *120*, 4621-4634.

Larson, K., Sahm, J., Shenkar, R., and Strauss, B. (1985). Methylation-induced blocks to in vitro DNA replication. Mutat Res *150*, 77-84.

Latypov, V.F., Tubbs, J.L., Watson, A.J., Marriott, A.S., McGown, G., Thorncroft, M., Wilkinson, O.J., Senthong, P., Butt, A., Arvai, A.S., *et al.* (2012). Atl1 regulates choice between global genome and transcription-coupled repair of O(6)-alkylguanines. Mol Cell *47*, 50-60.

Li, D., Fedeles, B.I., Shrivastav, N., Delaney, J.C., Yang, X., Wong, C., Drennan, C.L., and Essigmann, J.M. (2013). Removal of N-alkyl modifications from N2-alkylguanine and N4-alkylcytosine in DNA by the adaptive response protein AlkB. Chem Res Toxicol *26*, 1182-1187.

Li, C.L., Golebiowski, F.M., Onishi, Y., Samara, N.L., Sugasawa, K., and Yang, W. (2015). Tripartite DNA lesion recognition and verification by XPC, TFIIH, and XPA in nucleotide excision repair. Mol Cell *59*, 1025-1034.

Liang, K., Gao, X., Gilmore, J.M., Florens, L., Washburn, M.P., Smith, E., and Shilatifard, A. (2015). Characterization of human cyclin-dependent kinase 12 (CDK12) and CDK13 complexes in C-terminal domain phosphorylation, gene transcription, and RNA processing. Mol Cell Biol *35*, 928-938.

Liefke, R., Windhof-Jaidhauser, I.M., Gaedcke, J., Salinas-Riester, G., Wu, F., Ghadimi, M., and Dango, S. (2015). The oxidative demethylase ALKBH3 marks hyperactive gene promoters in human cancer cells. Genome Med *7*, 66.

Lingaraju, G.M., Davis, C.A., Setser, J.W., Samson, L.D., and Drennan, C.L. (2011). Structural basis for the inhibition of human alkyladenine DNA glycosylase (AAG) by 3,N4-ethenocytosine-containing DNA. J Biol Chem *286*, 13205-13213.

Liu, S., Chen, Y., Li, J., Huang, T., Tarasov, S., King, A., Weissman, A.M., Byrd, R.A., and Das, R. (2012). Promiscuous interactions of gp78 E3 ligase CUE domain with polyubiquitin chains. Structure *20*, 2138-2150.

Mahmoudi, S., Henriksson, S., Corcoran, M., Mendez-Vidal, C., Wiman, K.G., and Farnebo, M. (2016). Wrap53, a natural p53 antisense transcript required for p53 induction upon DNA damage. Mol Cell *64*, 1009.

Mailand N., Bekker-Jensen, S., Faustrup, H., Melander, F., Bartek, J., Lukas, C., and Lukas, J. (2007). RNF8 ubiquitylates histones at DNA double-strand breaks and promotes assembly of repair proteins. Cell *131*, 887-900.

Mallery, D.L., Vandenberg, C.J., and Hiom, K. (2002). Activation of the E3 ligase function of the BRCA1/BARD1 complex by polyubiquitin chains. EMBO J *21*, 6755-6762.

Malvezzi, S., Farnung, L., Aloisi, C.M.N., Angelov, T., Cramer, P., and Sturla, S.J. (2017). Mechanism of RNA polymerase II stalling by DNA alkylation. PNAS *114*, 12172-12177.

Maringele, L., and Lydall, D. (2002). EXO1-dependent single-stranded DNA at telomeres activates subsets of DNA damage and spindle checkpoint pathways in budding yeast yku70Delta mutants. Genes Dev *16*, 1919-1933.

Mathew, V., Tam, A.S., Milbury, K.L., Hofmann, A.K., Hughes, C.S., Morin, G.B., Loewen, J.R., and Stirling, P.C. (2017). Selective aggregation of the splicing factor Hsh155 suppresses splicing upon genotoxic stress. J Cell Biol *216*, 4027.

Matsuoka, S., Ballif, B.A., Smogorzewska, A., McDonald, E.R., Hurov, K.E., Luo, J., Bakalarski, C.E., Zhao, Z., Solimini, N., Lerenthal, Y., Shiloh, Y., Gygi, S.P., and Elledge, S.J. (2007). ATM and ATR substrate analysis reveals extensive protein networks responsive to DNA damage. Science *316*, 1160-1166.

Mateos-Gomez, P.A., Kent, T., Deng, S.K., McDevitt, S., Kashkina, E., Hoang, T.M., Pomerantz, R.T., and Sfeir, A. (2017). The helicase domain of Polθ counteracts RPA to promote alt-NHEJ. Nat Struct Mol Biol *24*, 1116-1123.

Mattiroli, F., Vissers, J.H., van Dijk, W.J., Ikpa, P., Citterio, E., Vermeulen, W., Marteijn, J.A., and Sixma, T.K. (2012). RNF168 ubiquitinates K13-15 on H2A/H2AX to drive DNA damage signaling. Cell *150*, 1182-1195.

Mazina, O.M., Keskin, H., Hanamshet, K., Storici, F., and Mazin, A.V. (2017). Rad52 inverse strand exchange drives RNA-templated DNA double-strand break repair. Mol Cell *67*, 19-29.

Mazumder, R., Iyer, L.M., Vasudevan, S., and Aravind, L. (2002). Detection of novel members, structure-function analysis and evolutionary classification of the 2H phosphoesterase superfamily. Nucleic Acids Res *30*, 5229-5243.

Mazur, P.K., Reynoird, N., Khatri, P., Jansen, P.W., Wilkinson, A.W., Liu, S., Barbash, O., Van Aller, G.S., Huddleston, M., Dhanak, D., Tummino, P.J., Kruger, R.G., Garcia, B.A., Butte, A.J., Vermeulen, M., Sage, J., and Gozani, O. (2014). SMYD3 links lysine methylation of MAP3K2 to Ras-driven cancer. Nature *510*, 283-287.

Meisenberg, C., Tait, P.S., Dianova, I.I., Wright, K., Edelmann, M.J., Ternette, N., Tasaki, T., Kessler, B.M., Parsons, J.L., Kwon, Y.T., and Dianov, G.L. (2012). Ubiquitin ligase UBR3

regulates cellular levels of the essential DNA repair protein APE1 and is required for genome stability. Nucleic Acids Res *40*, 701-711.

Mellon, I., Spivak, G., and Hanawalt, P.C. (1987). Selective removal of transcription-blocking DNA damage from the transcribed strand of the mammalian DHFR gene. Cell *51*, 241-249.

Meyer, K.D., and Jaffrey, S.R. (2017). Rethinking m6A readers, writers, and erasers. Annu Rev Cell Dev Biol *33*, 319-342.

Miyake, T., Pradeep, S., Wu, S.Y., Rupaimoole, R., Zand, B., Wen, Y., Gharpure, K.M., Nagaraja, A.S., Hu, W., Cho, M.S., Dalton, H.J., Previs, R.A., Taylor, M.L., Hisamatsu, T., Kang, Y., Liu, T., Shacham, S., McCauley, D., Hawke, D.H., Wiktorowicz, J.E., Coleman, R.L., and Sood, A.K. (2015). XPO1/CRM1 inhibiton causes antitumor effects by mitochondrial accumulation of eIF5A. Clin Cancer Res *21*, 3286-3297.

Moldovan, G.L., Pfander, B., and Jentsch, S. (2007). PCNA, the maestro of the replication fork. Cell *129*, 665-679.

Mosammaparast, N., Kim, H., Laurent, B., Zhao, Y., Lim, H.J., Majid, M.C., Dango, S., Luo, Y., Hempel, K., Sowa, M.E., *et al.* (2013). The histone demethylase LSD1/KDM1A promotes the DNA damage response. J Cell Biol *203*, 457-470.

Motegi, A., Sood, R., Moinova, H., Markowitz, S.D., Liu, P.P., and Myung, K. (2006). Human SHPRH suppresses genomic instability through proliferating cell nuclear antigen polyubiquitination. J Cell Biol *175*, 703-708.

Motegi A., Liaw, H.J., Lee, K.Y., Roest, H.P., Maas, A., Wu, X., Moinova, H., Markowitz, S.D., Ding, H., Hoeijmakers, J.H., and Myung, K. (2008). Polyubiquitination of proliferating cell nuclear antigen by HLTF and SHPRH prevents genomic instability from stalled replication forks. PNAS *105*, 12411-12416.

Nakabayashi, K., Amann, D., Ren, Y., Saarialho-Kere, U., Avidan, N., Gentles, S., MacDonald, J.R., Puffenberger, E.G., Christiano, A.M., Martinez-Mir, A., Salas-Alanis, J.C., Rizzo, R., Vamos, E., Raams, A., Les, C., Seboun, E., Jaspers, N.G.J., Beckmann, J.S., Jackson, C.E., and Scherer, S.W. (2005). Identification of C7orf11 (TTDN1) gene mutations and genetic heterogeneity in nonphotosensitive trichothiodystrophy. Am J Hum Genet *76*, 510-516.

Niedernhofer, L.J., Lalai, A.S., and Hoeijmakers, J.H. (2005). Fanconi anemia (cross)linked to DNA repair. Cell *123*, 1191-1198.

Overmeer, R.M., Moser, J., Volker, M., Kool, H., Tomkinson, A.E., van Zeeland, A.A., Mullenders, L.H.F., and Fousteri, M. (2011). Replication protein A safeguards genome integrity by controlling NER incision events. J Cell Biol *192*, 401-415.

Pickart, C.M. (2001). Mechanisms underlying ubiquitination. Annu Rev Biochem *70*, 503-533.

Prag, G., Misra, S., Jones, E.A., Ghirlando, R., Davies, B.A., Horazdovsky, B.F., and Hurley, J.H. (2003). Mechanism of ubiquitin recognition by the CUE domain of Vps9p. Cell *113*, 609-620.

Pontel, L.B., Rosado, I.V., Burgos-Barragan, G., Garaycoechea, J.I., Yu, R., Arends, M.J., Chandrasekaran, G., Broecker, V., Wei, W., Liu, L., Swenberg, J.A., Crossan, G.P., and Patel, K.J. (2015). Endogenous formaldehye is a hematopoietic stem cell genotoxin and metabolic carcinogen. Mol Cell *60*, 177-188.

Reinhardt, H.C., and Yaffe, M.B. (2013). Phospho-Ser/Thr-binding domains: navigating the cell cycle and DNA damage response. Nat Rev Mol Cell Biol *14*, 563-580.

Ringvoll, J., Nordstrand, L.M., Vagbo, C.B., Talstad, V., Reite, K., Aas, P.A., Lauritzen, K.H., Liabakk, N.B., Bjork, A., Doughty, R.W., *et al.* (2006). Repair deficient mice reveal mABH2 as the primary oxidative demethylase for repairing 1meA and 3meC lesions in DNA. EMBO J *25*, 2189-2198.

Rinne, M.L. (2005). N-methylpurine DNA glycosylase overexpression increases alkylation sensitivity by rapidly removing non-toxic 7-methylguanine adducts. Nucleic Acids Res *33*, 2859-2867.

Rio, D.C., Ares, M., Jr., Hannon, G.J., and Nilsen, T.W. (2010). Purification of RNA using TRIzol (TRI reagent). Cold Spring Harb Protoc *2010*, pdb prot5439.

Robertson, A.B., Klungland, A., Rognes, T., and Leiros, I. (2009). DNA repair in mammalian cells: Base excision repair: the long and short of it. Cell Mol Life Sci *66*, 981-993.

Roundtree, I.A., Evans, M.E., Pan, T., and He, C. (2017). Dynamic RNA Modifications in Gene Expression Regulation. Cell *169*, 1187-1200.

Rydberg, B., and Lindahl, T. (1982). Nonenzymatic methylation of DNA by the intracellular methyl group donor S-adenosyl-L-methionine is a potentially mutagenic reaction. The EMBO journal *1*, 211-216.

Sauvageau, M., and Sauvageau, G. (2010). Polycomb group proteins: multi-faceted regulators of somatic stem cells and cancer. Cell Stem Cell *7*, 299-313.

Sanchez-Pulido, L., and Andrade-Navarro, M.A. (2007). The FTO (fat mass and obesity associated) gene codes for a novel member of the non-heme dioxygenase superfamily. BMC Biochem *8*, 23.

Schulman R.A., and Harper, J.W. (2009). Ubiquitin-like protein activation by E1 enzymes: the apex for downstream signalling pathways. Nat Rev Mol Cell Biol *10*, 319-331.

Sedgwick, B., Bates, P.A., Paik, J., Jacobs, S.C., and Lindahl, T. (2007). Repair of alkylated DNA: recent advances. DNA repair *6*, 429-442.

Selby, C.P., and Sancar, A. (1994). Mechanisms of transcription-repair coupling and mutation frequency decline. Microbiol Rev *58*, 317-329.

Shanbhag, N.M., Rafalska-Metcalf, I.U., Blane-Bolivar, C., Janicki, S.M., and Greenberg, R.A. (2010). ATM-dependent chromatin changes silence transcription in cis to DNA double-strand breaks. Cell *14*, 970-981.

Shen, Y., Nandi, P., Taylor, M.B., Stuckey, S., Bhadsavle, H.P., Weiss, B., and Storici, F. (2011). RNA-driven genetic changes in bacteria and human cells. Mutat Res *717*, 91-98.

Shih, S.C., Prag, G., Francis, S.A., Sutanto, M.A., Hurley, J.H., and Hicke, L. (2003). A ubiquitin-binding motif required for intramolecular monoubiquitylation, the CUE domain. EMBO J *22*, 1273-1281.

Shrivastav, N., Li, D., and Essigmann, J.M. (2010). Chemical biology of mutagenesis and DNA repair: cellular responses to DNA alkylation. Carcinogenesis *31*, 59-70.

Silva, E., and Ideker, T. (2019). Transcriptional responses to DNA damage. DNA Repair (Amst) *79*, 40-49.

Silverman, R.H., and Weiss, S.R. (2014). Viral phosphodiesterases that antagonize double-stranded RNA signaling to RNase L by degrading 2-5A. J Interferon Cytokine Res *34*, 455-463.

Simms, C.L., Yan, L.L., and Zaher, H.S. (2017). Ribosome collision is critical for quality control during no-go decay. Mol Cell *68*, 361-373.

Singer, B., Antoccia, A., Basu, A.K., Dosanjh, M.K., Fraenkel-Conrat, H., Gallagher, P.E., Kusmierek, J.T., Qiu, Z.H., and Rydberg, B. (1992). Both purified human 1,N6-ethenoadenine-binding protein and purified human 3-methyladenine-DNA glycosylase act on 1,N6-ethenoadenine and 3-methyladenine. Proc Natl Acad Sci U S A *89*, 9386-9390.

Siomi, H., Matunis, M.J., Michael, W.M., and Dreyfuss, G. (1993). The pre-mRNA binding K protein contains a novel evolutionarily conserved motif. Nucleic Acids Res *21*, 1193-1198.

Sirbu, B.M., and Cortez, D. (2013). DNA damage response: three levels of DNA repair regulation. Cold Spring Harb Perspect Biol *5*, a012724.

Spivak, G. (2015). Nucleotide excision repair in humans. DNA Repair (Amst) *36*, 13-18.

Soll, J.M., Sobol, R.W., and Mosammaparast, N. (2017). Regulation of DNA Alkylation Damage Repair: Lessons and Therapeutic Opportunities. Trends Biochem Sci *42*, 206-218.

Song, E.J., Werner, S.L., Neubauer, J., Stegmeier, F., Aspden, J., Rio, D., Harper, J.W., Elledge, S.J., Kirschner, M.W., and Rape, M. (2010). The Prp19 complex and the Usp4Sart3 deubiquitinating enzyme control reversible ubiquitination at the spliceosome. Genes Dev *24*, 1434-1447.

Sowa, M.E., Bennett, E.J., Gygi, S.P., and Harper, J.W. (2009). Defining the human deubiquitinating enzyme interaction landscape. Cell *138*, 389-403.

Spector, D.L., Fu, X.D., and Maniatis, T. (1991). Associations between distinct pre-mRNA splicing components and the cell nucleus. EMBOJ *10*, 3467-3481.

Spector, D.L., and Lamond, A.I. (2011). Nuclear speckles. Cold Spring Harb Perspect Biol *3*.

Srivenugopal, K.S., Yuan, X.H., Friedman, H.S., and Ali-Osman, F. (1996). Ubiquitin-dependent proteolysis of O6-methylguanine-DNA methyltransferase in human and murine tumor cells

following inactivation with O6-benzylguanine or 1,3-bis(2-chloroethyl)-1-nitrosourea. Biochemistry *35*, 1328-1334.

Stefanini, M., Botta, E., Lanzafame, M., and Orioli, D. (2010). Trichothiodystrophy: from basic mechanisms to clinical applications. DNA Repair (Amst) *9*, 2-10.

Stewart, G.S., Panier, S., Townsend, K., Al-Hakim, A.K., Kolas, N.K., Miller, E.S., Nakada, S., Ylanko, J., Olivarius, S., Mendez, M., Oldreive, C., Wildenhain, J., Tagliaferro, A., Pelletier, L., Taubenheim, N., Durandy, A., Byrd, P.J., Stankovic, T., Taylor, A.M., and Durocher, D. (2009). The RIDDLE syndrome protein mediates a ubiquitin-dependent signaling cascade at sites of DNA damage. Cell *136*, 420-434.

Storici F., Bebenek, K., Kunkel, T.A., Gordenin, D.A., and Resnick, M.A. (2007). RNA-templated DNA repair. Nature *447*, 338-341.

Su, D., Chan, C.T., Gu, C., Lim, K.S., Chionh, Y.H., McBee, M.E., Russell, B.S., Babu, I.R., Begley, T.J., and Dedon, P.C. (2014). Quantitative analysis of ribonucleoside modifications in tRNA by HPLC-coupled mass spectrometry. Nat Protoc *9*, 828-841.

Sugasawa, K., Okamoto, T., Shimizu, Y., Masutani, C., Iwai, S., and Hanaoka, F. (2001). A multistep damage recognition mechanism for global genomic nucleotide excision repair. Genes Dev *15*, 507-521.

Svilar, D., Goellner, E.M., Almeida, K.H., and Sobol, R.W. (2011). Base excision repair and lesion-dependent subpathways for repair of oxidative DNA damage. Antioxid Redox Signal *14*, 2491-2507.

Tasaki, M., Shimada, K., Kimura, H., Tsujikawa, K., and Konishi, N. (2011). ALKBH3, a human AlkB homologue, contributes to cell survival in human non-small-cell lung cancer. British journal of cancer *104*, 700-706.

Tessitore, A., Cicciarelli, G., Del Vecchio, F., Gaggiano, A., Verzella, D., Fischietti, M., Vecchiotti, D., Capece, D., Zazzeroni, F., and Alesse, E. (2014). MicroRNAs in the DNA damage/repair network and cancer. Int J Genomics *2014*, 820248.

Thapar, R. (2018). Regulation of DNA double-strand break repair by non-coding RNAs. Molecules *23*, E2789.

Thapar, R., Bacolla, A., Oyeniran, C., Brickner, J.R., Chinnam, N.B., Mosammaparast, N., and Tainer, J.A. (2018). RNA Modifications: reversal mechanisms and cancer. Biochemistry *58*, 312-329.

Thorslund, T., Ripplinger, A., Hoffmann, S., Wild, T., Uckelmann, M., Villumsen, B., Narita, T., Sixma, T.K., Choudhary, C., Bekker-Jensen, S., *et al.* (2015). Histone H1 couples initiation and amplification of ubiquitin signalling after DNA damage. Nature *527*, 389-393.

Thuring, K., Schmid, K., Keller, P., and Helm, M. (2016). Analysis of RNA modifications by liquid chromatography-tandem mass spectrometry. Methods *107*, 48-56.

Trewick, S.C., Henshaw, T.F., Hausinger, R.P., Lindahl, T., and Sedgwick, B. (2002). Oxidative demethylation by Escherichia coli AlkB directly reverts DNA base damage. Nature *419*, 174-178.

Tubbs, J.L., Latypov, V., Kangula, S., Butt, A., Melikishvili, M., Kraehenbuehl, R., Fleck, O., Marriott, A., Watson, A.J., Verbeek, B., McGown, G., Thorncroft, M., Santibanez-Koref, M.F., Millington, C., Arvai, A.S., Kroeger, M.D., Peterson, L.A., Williams, D.M., Fried, M.G., Margison, G.P., Pegg, A.E., and Tainer, J.A. (2009). Flipping of alkylated DNA damage bridges base and nucleotide excision repair. Nature *459*, 808-813.

Ulrich, H.D. (2009). Regulating post-translational modifications of the eukaryotic replication clamp PCNA. DNA Repair (Amst) *8*, 461-469.

Unk, I., Hajdu, I., Fatyol, K., Szakal, B., Blastyak, A., Bermudez, V., Hurwitz, J., Prakash, L., Prakash, S., and Haracska, L. (2006). Human SHPRH is a ubiquitin ligase for Mms2-Ubc13-dependent polyubiquitylation of proliferating cell nuclear antigen. Proc Natl Acad Sci U S A *103*, 18107-18112.

Vagbo, C.B., Svaasand, E.K., Aas, P.A., and Krokan, H.E. (2013). Methylation damage to RNA induced in vivo in Escherichia coli is repaired by endogenous AlkB as part of the adaptive response. DNA Repair (Amst) *12*, 188-195.

Valverde, R., Edwards, L., and Regan, L. (2008). Structure and function of KH domains. FEBS J *275*, 2712-2726.

Wan, G., Hu, X., Liu, Y., Han, C., Sood, A.K., Calin, G.A., Zhang, X., and Lu, X. (2013). A novel non-coding RNA lncRNA-JADE connects DNA damage signalling to histone H4 acetylation. EMBO J *32*, 2833-2847.

Wang, X., and He, C. (2014). Reading RNA methylation codes through methyl-specific binding proteins. RNA Biol *11*, 669-672.

Wang, P., Wu, J., Ma, S., Zhang, L., Yao, J., Hoadley, K.A., Wilkerson, M.D., Perou, C.M., Guan, K.L., Ye, D., *et al.* (2015). Oncometabolite D-2-Hydroxyglutarate Inhibits ALKBH DNA Repair Enzymes and Sensitizes IDH Mutant Cells to Alkylating Agents. Cell Rep *13*, 2353-2361.

Watanabe, K., Tateishi, S., Kawasuji, M., Tsurimoto, T., Inoue, H., and Yamaizum, M. (2004). Rad18 guides poleta to replication stalling sites through phsyical interaction and PCNA monoubiquitination. EMBO J *23*, 3886-3896.

Warren, J.J., Forsberg, L.J., and Beese, L.S. (2006). The structural basis for the mutagenicity of O(6)-methyl-guanine lesions. Proc Natl Acad Sci U S A *103*, 19701-19706.

Welford, R.W., Kirkpatrick, J.M., McNeill, L.A., Puri, M., Oldham, N.J., and Schofield, C.J. (2005). Incorportation of oxygen into the succinate co-product of iron(II) and 2-oxoglutarate dependent oxygenases from bacteria, plants and humans. FEBS Lett *579*, 5170-5174.

Weller, M., Stupp, R., Reifenberger, G., Brandes, A.A., van den Bent, M.J., Wick, W., and Hegi, M.E. (2010). MGMT promoter methylation in malignant gliomas: ready for personalized medicine? Nat Rev Neurol *6*, 39-51.

Wertz, I.E., Newton, K., Seshasayee, D., Kusam, S., Lam, C., Zhang, J., Popovych, N., Helgason, E., Schoeffler, A., Jeet, S., Ramamoorthi, N., Kategaya, L., Newman, R.J., Horikawa, K., Dugger, D., Sandoval, W., Mukund, S., Zindal, A., Martin, F., Quan, C., Tom, J., Fairbrother, W.J., Townsend, M., Warming, S., DeVoss, J., Liu, J., Dueber, E., Caplazi, P., Lee, W.P., Goodnow, C.C., Balazs, M., Yu, K., Kolumam, G., and Dixit, V.M. (2015). Phosphorylation and linear ubiquitin direct A20 inhibition of inflammation. Nature *528*, 370-375.

Wick, W., and Platten, M. (2014). Understanding and targeting alkylator resistance in glioblastoma. Cancer Discov *4*, 1120-1122.

Williamson, L., Saponaro, M., Boeing, S., East, P., Mitter, R., Kantidakis, T., Kell, G.P., Lobley, A., Walker, J., Spencer-Dene, B., Howell, M., Stewart, A., and Svejstrup, J.Q. (2017). UV irradiation induces a non-coding RNA that functionally opposes the protein encoded by the same gene. Cell *168*, 843-855.

Wu, J., Chen, Y., Lu, L.Y., Wu, Y., Paulsen, M.T., Ljungman, M., Ferguson, D.O., and Yu, X. (2011). Chfr and RNF8 synergistically regulate ATM activation. Nat Struct Mol Biol *18*, 761-768.

Wu, T.P., Wang, T., Seetin, M.G., Lai, Y., Zhu, S., Lin, K., Liu, Y., Byrum, S.D., Mackintosh, S.G., Zhong, M., *et al.* (2016). DNA methylation on N(6)-adenine in mammalian embryonic stem cells. Nature *532*, 329-333.

Wu, N.Y., Chung, C.S., and Cheng, S.C. (2017). Role of Cwc24 in the first catalytic step of splicing and fidelity of 5' splice site selection. Mol Cell Biol *37*, e00580-16

Wu-Baer, F., Lagrazon, K., Yuan, W., and Baer, R. (2003). The BRCA1/BARD1 heterodimer assembles polyubiquitin chains through an unconventional linkage involving lysine residue K6 of ubiquitin. J Biol Chem *278*, 34743-34746.

Wurtmann, E.J., and Wolin, S.L. (2009). RNA under attack: cellular handling of RNA damage. Crit Rev Biochem Mol Biol *44*, 34-49.

Wyatt, M.D., Allan, J.M., Lau, A.Y., Ellenberger, T.E., and Samson, L.D. (1999). 3-methyladenine DNA glycosylases: structure, function and biological importance. BioEssays *21*, 668-676.

Xiang, Y., Laurent, B., Hsu, C.H., Nachtergaele, S., Lu, Z., Sheng, W., Xu, C., Chen, H., Ouyang, J., Wang, S., Ling, D., Hsu, P.H., Zou, L., Jambheker. A., He, C., and Shi, Y. (2017). RNA m(6)A methylation regulates the ultraviolet-induced DNA damage response. Nature *543*, 573-576.

Xiao, C.L., Zhu, S., He, M., Zhang, Q., Chen, Y., Yu, G., Liu, J., Xie, S.Q., Luo, F., Liang, Z., Wang, D.P., Bo, X.C., Gu, X.F., Wang, K., and Yan, G.R. (2018). N(6)-methyladenine DNA modification of the human genome. Mol Cell *71*, 306-318.

Xiong, X., Li, X., and Yi, C. (2018). N(1)-methyladenosine methylome in messenger RNA and non-coding RNA. Curr Opin Chem Biol *45*, 179-186.

Xirodimas, D., Saville, M.K., Edling, C., Lan, D.P., and Lain, S. (2001). Different effects of p14ARF on the levels of ubiquitinated p53 and Mdm2 in vivo. Oncogene *20*, 4972-4983.

Xu, L., Wang, W., Wu, J., Shin, J.H., Wang, P., Unarta, I.C., Chong, J., Wang, Y., and Wang, D. (2017). Mechanism of DNA alkylation-induced transcriptional stalling, lesion bypass, and mutagenesis. PNAS *114*, E7082-E7091.

Xu, L., Liu, X., Sheng, N., Oo, K.S., Liang, J., Chionh, Y.H., Xu, J., Ye, F., Gao, Y.G., Dedon, P.C., and Fu, X.Y. (2017). Three distinct 3-methylcytidine (m(3)C) methyltransferases modify tRNA and mRNA in mice and humans. J Biol Chem *292*, 14695-14703.

Xu-Welliver, M., and Pegg, A.E. (2002). Degradation of the alkylated form of the DNA repair protein, O(6)-alkylguanine-DNA alkyltransferase. Carcinogenesis *23*, 823-830.

Yan, C., Wan, R., Bai, R., Huang, G., and Shi, Y. (2016). Structure of a yeast activated spliceosome at 3.5A resolution. Science *353*, 904-911.

Yan, L.L., and Zaher, H.S. (2019). How do cells cope with RNA damage and its consequences? J Biol Chem *294*, 15158-15171.

Yang, Y.G., and Qi, Y. (2015). RNA-directed repair of DNA double-strand breaks. DNA Repair (Amst) *32*, 82-85.

Ye, Y., and Rape, M. (2009). Building ubiquitin chains: E2 enzymes at work. Nat Rev Mol Cell Biol *10*, 755-764.

Zak, P., Kleibl, K., and Laval, F. (1994). Repair of O6-methylguanine and O4-methylthymine by the human and rat O6-methylguanine-DNA methyltransferases. J Biol Chem *269*, 730-733.

Zhang, T., Kwiatkowski, N., Olson, C.M., Dixon-Clarke, S.E., Abraham, B.J., Greifenberg, A.K., Ficarro, S.B., Elkins, J.M., Liang, Y., Hannett, N.M., Manz, T., Hao, M., Bartkowiak, B., Greenleaf, A.L., Marto, J.A., Geyer, M., Bullock, A.N., and Gray, N.S. (2016). Covalent targeting of remote cysteine residues to develop CDK12 and CDK13 inhibitors. Nat Chem Biol *12*, 876-884.

Zhang, X., Horibata, K., Saijo, M., Ishigami, C., Ukai, A., Kanno, S., Tahara, H., Neilan, E.G., Honma, M., Nohmi, T., Yasui, A., and Tanaka, K. (2012). Mutations in UVSSA cause UV-sensitive syndrome and destabilize ERCC6 in transcription-coupled DNA repair. Nat Genet *44*, 593-597.

Zhang, Z., Chen, L.Q., Zhao, Y.L., Yang, C.G., Roundtree, I.A., Zhang, Z., Ren, J., Xie, W., He, C., and Luo, G.Z. (2019). Single-base mapping of m6A by an antibody-independent method. Sci Adv *5*, eaax0250

Zhao, G.Y., Sonoda, E., Barber, L.J., Oka, H., Murakawa, Y., Yamada, K., Ikura, T., Wang, X., Kobayashi, M., Yamamoto, K., *et al.* (2007). A critical role for the ubiquitin-conjugating enzyme Ubc13 in initiating homologous recombination. Mol Cell *25*, 663-675.

Zhao, Y., Brickner, J.R., Majid, M.C., and Mosammaparast, N. (2014). Crosstalk between ubiquitin and other post-translational modifications on chromatin during double-strand break repair. Trends Cell Biol.

Zhao, Y., Majid, M.C., Soll, J.M., Brickner, J.R., Dango, S., and Mosammaparast, N. (2015). Noncanonical regulation of alkylation damage resistance by the OTUD4 deubiquitinase. EMBO J *34*, 1687-1703.

Zhao, Y., Mudge, M.C., Soll, J.M., Rodrigues, R.B., Byrum, A.K., Schwarzkopf, E.A., Bradstreet, T.R., Gygi, S.P., Edelson, B.T., and Mosammaparast, N. (2018). OTUD4 is a phospho-activated K63 deubiquitinase that regulates MyD88-dependent signaling. Mol Cell *69*, 505-516.

Zheng, N., and Shabek, N. (2017). Ubiquitin Ligases: Structure, Function, and Regulation. Annu Rev Biochem *86*, 129-157.

Zou, Y., Luo, C., and Geacintov, N.E. (2001). Hierarchy of DNA damage recognition in Escherichia coli nucleotide excision repair. Biochemistry *40*, 2923-2931.